A CONTINUUM APPROACH TO MODELING PORE STRUCTURE OF HOMOGENEOUS POROUS MEDIA

by

Ravi J. Suman

A Thesis
Submitted to the Faculty of Graduate Studies
in Partial Fulfillment of the Requirements
for the Degree of

DOCTOR OF PHILOSOPHY

Department of Mechanical and Industrial Engineering
University of Manitoba
Winnipeg, Manitoba R3T 2N2 Canada

ISBN 0-315-86072-3

Name RAVI TEE SUMAN

Dissertation Abstracts International is arranged by broad, general subject categories. Please select the one subject which most nearly describes the content of your dissertation. Enter the corresponding four-digit code in the spaces provided.

[redacted] [redacted] CIVIL

SUBJECT TERM

0	5	4	3

SUBJECT CODE

UMI

Subject Categories

THE HUMANITIES AND SOCIAL SCIENCES

COMMUNICATIONS AND THE ARTS

Architecture 0729
Art History 0377
Cinema 0900
Dance 0378
Fine Arts 0357
Information Science 0723
Journalism 0391
Library Science 0399
Mass Communications 0708
Music 0413
Speech Communication 0459
Theater 0465

EDUCATION

General 0515
Administration 0514
Adult and Continuing 0516
Agricultural 0517
Art 0273
Bilingual and Multicultural 0282
Business 0688
Community College 0275
Curriculum and Instruction 0727
Early Childhood 0518
Elementary 0524
Finance 0277
Guidance and Counseling 0519
Health 0680
Higher 0745
History of 0520
Home Economics 0278
Industrial 0521
Language and Literature 0279
Mathematics 0280
Music 0522
Philosophy of 0998
Physical 0523
Psychology 0525
Reading 0535
Religious 0527
Sciences 0714
Secondary 0533
Social Sciences 0534
Sociology of 0340
Special 0529
Teacher Training 0530
Technology 0710
Tests and Measurements 0288
Vocational 0747

LANGUAGE, LITERATURE AND LINGUISTICS

Language
- General 0679
- Ancient 0289
- Linguistics 0290
- Modern 0291

Literature
- General 0401
- Classical 0294
- Comparative 0295
- Medieval 0297
- Modern 0298
- African 0316
- American 0591
- Asian 0305
- Canadian (English) 0352
- Canadian (French) 0355
- English 0593
- Germanic 0311
- Latin American 0312
- Middle Eastern 0315
- Romance 0313
- Slavic and East European 0314

PHILOSOPHY, RELIGION AND THEOLOGY

Philosophy 0422
Religion
- General 0318
- Biblical Studies 0321
- Clergy 0319
- History of 0320
- Philosophy of 0322

Theology 0469

SOCIAL SCIENCES

American Studies 0323
Anthropology
- Archaeology 0324
- Cultural 0326
- Physical 0327

Business Administration
- General 0310
- Accounting 0272
- Banking 0770
- Management 0454
- Marketing 0338

Canadian Studies 0385
Economics
- General 0501
- Agricultural 0503
- Commerce-Business 0505
- Finance 0508
- History 0509
- Labor 0510
- Theory 0511

Folklore 0358
Geography 0366
Gerontology 0351
History
- General 0578
- Ancient 0579
- Medieval 0581
- Modern 0582
- Black 0328
- African 0331
- Asia, Australia and Oceania 0332
- Canadian 0334
- European 0335
- Latin American 0336
- Middle Eastern 0333
- United States 0337

History of Science 0585
Law 0398
Political Science
- General 0615
- International Law and Relations 0616
- Public Administration 0617

Recreation 0814
Social Work 0452
Sociology
- General 0626
- Criminology and Penology 0627
- Demography 0938
- Ethnic and Racial Studies 0631
- Individual and Family Studies 0628
- Industrial and Labor Relations 0629
- Public and Social Welfare 0630
- Social Structure and Development 0700
- Theory and Methods 0344

Transportation 0709
Urban and Regional Planning 0999
Women's Studies 0453

THE SCIENCES AND ENGINEERING

BIOLOGICAL SCIENCES

Agriculture
- General 0473
- Agronomy 0285
- Animal Culture and Nutrition 0475
- Animal Pathology 0476
- Food Science and Technology 0359
- Forestry and Wildlife 0478
- Plant Culture 0479
- Plant Pathology 0480
- Plant Physiology 0817
- Range Management 0777
- Wood Technology 0746

Biology
- General 0306
- Anatomy 0287
- Biostatistics 0308
- Botany 0309
- Cell 0379
- Ecology 0329
- Entomology 0353
- Genetics 0369
- Limnology 0793
- Microbiology 0410
- Molecular 0307
- Neuroscience 0317
- Oceanography 0416
- Physiology 0433
- Radiation 0821
- Veterinary Science 0778
- Zoology 0472

Biophysics
- General 0786
- Medical 0760

EARTH SCIENCES

Biogeochemistry 0425
Geochemistry 0996
Geodesy 0370
Geology 0372
Geophysics 0373
Hydrology 0388
Mineralogy 0411
Paleobotany 0345
Paleoecology 0426
Paleontology 0418
Paleozoology 0985
Palynology 0427
Physical Geography 0368
Physical Oceanography 0415

HEALTH AND ENVIRONMENTAL SCIENCES

Environmental Sciences 0768
Health Sciences
- General 0566
- Audiology 0300
- Chemotherapy 0992
- Dentistry 0567
- Education 0350
- Hospital Management 0769
- Human Development 0758
- Immunology 0982
- Medicine and Surgery 0564
- Mental Health 0347
- Nursing 0569
- Nutrition 0570
- Obstetrics and Gynecology 0380
- Occupational Health and Therapy 0354
- Ophthalmology 0381
- Pathology 0571
- Pharmacology 0419
- Pharmacy 0572
- Physical Therapy 0382
- Public Health 0573
- Radiology 0574
- Recreation 0575
- Speech Pathology 0460
- Toxicology 0383

Home Economics 0386

PHYSICAL SCIENCES

Pure Sciences

Chemistry
- General 0485
- Agricultural 0749
- Analytical 0486
- Biochemistry 0487
- Inorganic 0488
- Nuclear 0738
- Organic 0490
- Pharmaceutical 0491
- Physical 0494
- Polymer 0495
- Radiation 0754

Mathematics 0405
Physics
- General 0605
- Acoustics 0986
- Astronomy and Astrophysics 0606
- Atmospheric Science 0608
- Atomic 0748
- Electronics and Electricity 0607
- Elementary Particles and High Energy 0798
- Fluid and Plasma 0759
- Molecular 0609
- Nuclear 0610
- Optics 0752
- Radiation 0756
- Solid State 0611

Statistics 0463

Applied Sciences

Applied Mechanics 0346
Computer Science 0984
Engineering
- General 0537
- Aerospace 0538
- Agricultural 0539
- Automotive 0540
- Biomedical 0541
- Chemical 0542
- Civil 0543
- Electronics and Electrical 0544
- Heat and Thermodynamics 0348
- Hydraulic 0545
- Industrial 0546
- Marine 0547
- Materials Science 0794
- Mechanical 0548
- Metallurgy 0743
- Mining 0551
- Nuclear 0552
- Packaging 0549
- Petroleum 0765
- Sanitary and Municipal 0554
- System Science 0790

Geotechnology 0428
Operations Research 0796
Plastics Technology 0795
Textile Technology 0994

PSYCHOLOGY

General 0621
Behavioral 0384
Clinical 0622
Developmental 0620
Experimental 0623
Industrial 0624
Personality 0625
Physiological 0989
Psychobiology 0349
Psychometrics 0632
Social 0451

A CONTINUUM APPROACH TO MODELING PORE STRUCTURE OF HOMOGENEOUS POROUS MEDIA

BY

RAVI J. SUMAN

A thesis submitted to the Faculty of Graduate Studies of the University of Manitoba in partial fulfillment of the requirements of the degree of

DOCTOR OF PHILOSOPHY

ABSTRACT

The microscopic information about the geometry of the solid-fluid interface inside a porous medium is "hidden" in such macroscopic transport properties as permeability, Klinkenberg's gas-slippage factor and formation factor. In this study, explicit integral expressions are derived for these properties by comparing the volume averaged microscopic conservation equations (mass and momentum for permeability and gas permeability with slip, and electric charge for formation factor) to the corresponding phenomenological laws (Darcy's law for permeability and gas permeability with slip, and Ohm's law at macroscopic level for formation factor). The expression for each property consists of two terms which involve integrals of the related microscopic thermodynamic variables.

Idealized porous media, consisting of networks of tubes, are employed to validate the expressions for permeability and formation factor, and to interpret the terms in them. It is found that the first term in the expression for permeability (formation factor), called the "viscous term" ("current term"), accounts for the fluid (electric) flow in the macroscopic flow direction, whereas the second term, called the "pressure term" ("potential term"), accounts for the fluid (current) flow in the directions normal to the macroscopic flow direction. Interestingly, the magnitude of the pressure term (potential term), which represents the flow in the directions normal to the macroscopic flow direction, depends on the variation of the hydraulic conductances (electrical conductances) of the tubes in the macroscopic flow direction. The results show that the pressure and potential terms are directly responsible for the value of tortuosity exceeding 1. In the presence of microscopic cross flow (microscopic flow normal to the macroscopic flow direction), it is shown that the classical definition of tortuosity as a ratio of geometric lengths is simplistic. The study suggests two types of tortuosities, one accounting for the sinuousness of the individual flow channels (classical definition) and the other accounting for the cross flow. An exact relation between the formation factor and tortuosity is presented. In the presence of cross flow, the equivalence of

hydraulic and electrical tortuosities is shown to be invalid.

Based on the integral expressions, explicit relations of permeability, permeability with slip and formation factor to the statistical parameters characterizing the pore space of parallel and serial capillary models are developed. With the help of nonlinear regression, similar relations, based on the integral expressions, are also determined for the permeability and formation factor of a three-dimensional cubic network model. It is observed that the absence of the "networking effect" in the parallel and serial capillary models results in these models showing opposite behaviors, whereas, its presence in the network model results in an intermediate behavior representative of the real porous media. These relations are shown to be valid for a considerably larger range of coefficient of variation of tube diameter distribution (which represents the breadth of the distribution) as compared to the relations based on the effective-medium approximation (Nicholson et al., 1988).

A methodology for modeling the pore structure of homogeneous porous media, based on the explicit relations of the transport properties of the models to their pore structure parameters, is outlined. A preliminary study of this methodology is conducted on five sandstone samples and a limestone sample. It is found that for the same sample the values of the pore structure parameters predicted by the network model are intermediate between those predicted by the parallel and serial capillary models. Except for one sandstone sample, all the three models satisfactorily predicted the plateau portion of the drainage capillary pressure curves of the rest of the sandstone samples. However, the models did not accurately predict the drainage capillary pressure curve of these samples near the irreducible wetting phase saturation. The present models are found to be inappropriate for modeling the pore structure of non-uniform porous media such as limestones. Incorporation of features such as assignment of volume to junctions and size correlations between the neighboring tubes are recommended to improve the capillary pressure curve predictions of the models near the irreducible wetting phase for the sandstone samples.

To my parents

ACKNOWLEDGMENTS

I sincerely thank Dr. Douglas W. Ruth for supervising this research and for his continual support and helpful suggestions. I also thank committee members Dr. Ram S. Azad, Dr. Alan C. Trupp and Dr. Allan D. Woodbury for their suggestions. I am highly appreciative of the external examiner Dr. William G. Gray for his invaluable comments and suggestions. Computer assistance provided by Mr. David Young is also gratefully acknowledged.

I highly appreciate the financial support provided by the Department of Mechanical and Industrial Engineering during the course of this work.

Finally, I wish to thank my parents, brothers and sister, and my friends whose constant encouragement and moral support were significant catalysts for the successful completion of this research.

TABLE OF CONTENTS

CHAPTER PAGE

CHAPTER PAGE

CHAPTER PAGE

LIST OF FIGURES

LIST OF TABLES

NOMENCLATURE

A	area
A_c	coefficient in approximate expression for T_c of network model
A_e	coefficient in approximate expression for T_e of network model
A_k	cross-sectional area of REV normal to k direction
A_p	coefficient in approximate expression for T_p of network model
A_v	coefficient in approximate expression for T_v of network model
A_β	$A_{\sigma\beta} + A_{\beta e}$
$A_{\beta e}$	interfacial area between the β phase inside and outside of the REV
$A_{\beta 1}$	effective cross-sectional area of REV open to flow in $k = 1$ direction
$A_{\sigma\beta}$	interfacial area between the σ and β phases contained within the REV
a_i	gravitational acceleration
a_S	σ_S/μ_S
a_δ	σ_δ/μ_δ
B	coefficient in expression for g
B_e	coefficient in approximate expression for T_e of network model
B_p	coefficient in approximate expression for T_p of network model
b	Klinkenberg coefficient
C_1	macroscopic current in the $k = 1$ direction
c	constant in expression for gas flow rate in a tube (with slip)
c_I	current in the Ith tube
E_i	electric field intensity
e	electric potential
e_h	electric potential at the upstream side of the REV
e_I	electric potential at the Ith junction
e'_I	$N_2^P N_3^P e_I/(R_w C_1)$
e_l	electric potential at the downstream side of the REV
F	formation factor
F^n	formation factor of network model

F^p	formation factor of parallel capillary model
F_s	formation factor of a standard RUC
f_I	fraction of macroscopic fluid flow rate in the Ith tube ($= q_I/C_1$)
f_I'	$N_2^P N_3^P q_I/Q_1$
f_I^c	fraction of macroscopic current in the Ith tube ($= c_I/C_1$)
$f_I^{c'}$	$N_2^P N_3^P c_I/C_1$
g	conductance of a tube ($= B\delta^\epsilon/S$)
g_I	$\pi\delta_I^4/(128\,\mu\,S_I)$
g_I^c	$\pi\delta_I^2/(4\,R_w\,S_I)$
g_m	conductance of a network based on the EMA
$\mathbf{h}$	oriented distance
J_i	current density
k_{a1}	Klinkenberg permeability in the $k = 1$ direction
k_s	permeability of a standard RUC
k_1	permeability in the $k = 1$ direction
k_1^n	permeability of network model
k_1^p	permeability of parallel capillary model
L_e	effective length in the definition of tortuosity
L_k	characteristic length of the REV in k direction
L^*	characteristic length of macroscopic domain
l	diameter of spherical REV of volume V_b (also $l_{\min}$, $l_{\max}$)
m	hydraulic mean radius
N_A	N_T/A_1 for parallel capillary model, N_{ch}/A_1 for serial capillary model and $N_2^P N_3^P/A_1$ for network model
N_{ch}	number of flow paths in serial capillary model
N_P	total number of junctions in a model
N_P'	number of junctions/flow path in serial capillary model
N_T	total number of tubes in a pore structure model
N_1^P, N_2^P, N_3^P	number of columns, rows and tiers in network model (Figure 5.3)
N_1^T	number of tubes in the macroscopic flow direction, $k = 1$

n_k	unit outwardly normal vector
P_m	$(p_h + p_l)/2$
p	pressure
p_I	pressure at a junction
p'_I	$N_2^P N_3^P p_I/(\mu Q_1)$
p_h	pressure at the upstream side of the REV
p_{Ia}, p_{Ib}	pressures at the two ends of Ith tube
p_l	pressure at the downstream side of the REV
p_m^I	$(p_{Ia} + p_{Ib})/2$
Q_1	macroscopic (bulk) fluid flow rate in REV in the $k = 1$ direction
$\overline{Q}_1$	macroscopic gas flow rate in REV in the $k = 1$ direction (with slip)
q_I	volumetric fluid flow rate in the Ith tube
$\overline{q}_I$	gas flow rate in the Ith tube (with slip)
R	gas constant
R_o	resistivity of REV saturated with an electrically conductive fluid
R_w	resistivity of electric conductor saturating the REV
r_k	coordinate on the microscopic scale
S_I	length of the Ith tube
s	coordinate along the axis of a tube
T	absolute temperature
T_c	current term
T_e	potential term
T_p	pressure term
$\overline{T}_p$	slip pressure term
T_v	viscous term
$\overline{T}_v$	slip viscous term
t	time
u_o	slip velocity at the wall
V	volume
V_b	total volume of the REV

V_β	volume of the fluid phase inside REV
v_1	macroscopic velocity in the $k = 1$ direction
w_k	microscopic velocity of the fluid
w_s^I	microscopic velocity inside the Ith tube
x_k , $\mathbf{x}$	coordinates on the macroscopic scale
$Z^{k_1}(a_\delta)$	function in expression of k_1 of network model (Appendix E)
$Z^F(a_\delta)$	function in expression of F of network model (Appendix E)

Greek Letters

γ_m	normalized effective-medium conductance
Δp_I	$p_{Ia} - p_{Ib}$
δ	tube diameter
$\delta_a, \delta_b, \delta_c$	tube diameters used in RUC 1
δ_I	diameter of the Ith tube
δ_{uI}, δ_{dI}	diameters of the tubes in the $k = 1$ direction, upstream and downstream of Ith junction, for network model
ϵ	exponent on δ in expression for g
ζ	$(\delta/\mu_\delta)^\epsilon - 1$
η	average coordination number
κ	$\delta/\mu_\delta - 1$
$\gamma(\mathbf{x})$	characteristic function of void space
Λ	$1/\eta$
λ	average mean free path of flowing gas
μ	dynamic viscosity of the fluid
μ_S	mean of tube length distribution
μ_δ	mean of tube diameter distribution
ξ_k	areosity in k direction
ρ	density of the fluid
σ_S	standard deviation of tube length distribution

σ_δ	standard deviation of tube diameter distribution
τ	μ_S/L_1 for parallel capillary model, $N'_P\mu_S/L_1$ for serial capillary model and $N_1^P\mu_S/L_1$ for network model
τ_G	tortuosity (general definition)
τ_a, τ_b	two types of tortuosity in fluid flow
τ'_a, τ'_b	two types of tortuosity in electric flow
τ_h	hydraulic tortuosity
ϕ	porosity
ψ, ψ'	general variables
$\omega(g)$	probability density function of g

Symbols

$\langle\ \rangle$	phase average over V_b
$\langle\ \rangle^\alpha$	intrinsic phase average over V_b
$\langle\ \rangle^{\mathrm{EN}}$	ensemble average
$\tilde{}$	deviation from intrinsic phase average
$E(\ ), E[\ ]$	expected value of ( ), [ ]

Subscripts

α	a general phase
β	the fluid phase
σ	the solid phase

CHAPTER 1

INTRODUCTION

Transport phenomena in porous media are encountered in many fields of engineering. To mention a few, the flow of oil, water and gas through hydrocarbon reservoirs is studied in petroleum engineering, the flow of water and transport of pollutants in aquifers is studied in civil engineering, the movement of moisture through soil and grain is studied in agricultural engineering and the chemical reactions in packed-bed columns are studied in chemical engineering. The familiar conservation equations (e.g., mass, momentum, energy, electric charge) can, in principle, be employed to describe the transport phenomena in porous media associated with these topics. It may also be possible to state the boundary conditions, for example, the no-slip condition at the solid surface in the case of momentum transport. These equations describe the transport phenomena at the microscopic level, however, their solutions are not generally sought at this level. There are two important reasons for such a choice: One, our inability to observe and describe the complex geometry of the solid-fluid interface at the microscopic level precludes any direct solutions to these equations and two, one is not usually interested in knowing the details of transport at the microscopic level. Instead the solutions of the averaged conservation equations, which represent the behavior of relatively large portions of porous media, are sought. This is called the macroscopic level or continuum description of transport phenomena in porous media.

The macroscopic level description circumvents the need for microscopic information about the solid-fluid interface. This information is lumped into coefficients that

arise as a result of moving from the microscopic to the macroscopic level, and is therefore "hidden" in such macroscopic transport properties as absolute permeability (Darcy, 1856), gas-slippage factor (Klinkenberg, 1941) and formation factor (Archie, 1942). These transport properties are generally determined by conducting controlled physical experiments in the laboratory or in the field. In other fields of science, where the continuum approach is also applied, attempts have been made at theoretically predicting the corresponding coefficients and many times with good accuracy. For example, in the kinetic theory of gases, the coefficients (e.g., mass diffusion coefficient, dynamic viscosity, thermal conductivity) are predicted with accuracy by returning to the molecular scale and modeling the behavior of the individual molecules (Hirschfelder et al., 1954). In the case of porous media, much of the effort has been spent on developing the theory of averaging, estimating the size of the averaging volume for which representative results may be statistically meaningful and deriving the macroscopic conservation equations (Anderson and Jackson, 1967; Marle, 1967; Whitaker, 1967, 1969; Gray, 1975; Gray and O'Neill, 1976; Hassanizadeh and Gray, 1979a, 1979b, 1980; Bachmat and Bear; 1986, Bear and Bachmat, 1986; Bear and Bachmat, 1991).

In the present study, an approach to modeling the macroscopic transport properties of homogeneous porous media is outlined. The properties considered are absolute permeability (referred to as simply permeability hereafter), gas-slippage factor (referred to as Klinkenberg coefficient hereafter) and formation factor. Volume averaging, which is one of the methods used for achieving transition from the microscopic to the macroscopic level, is employed to derive macroscopic conservation equations from the microscopic conservation equations. By comparing the macroscopic conservation equations (mass and momentum for permeability and gas permeability with slip, and electric charge for formation factor) to the corresponding phenomenological laws (Darcy's law for permeability and permeability with slip, and Archie's expres-

sion for formation factor), explicit expressions are derived for these properties. These expressions involve integrals of the microscopic field variables over the solid-fluid interface—formalisms that represent exactly the information lost in the averaging process.

Idealized porous media are employed to validate the integral expressions and to interpret the terms in these expressions. This study provides a clear understanding of the macroscopic transport property of porous media known as tortuosity and its relations to permeability and formation factor. Based on the integral expressions, explicit relations of permeability and formation factor to the statistical parameters characterizing the pore space of parallel capillary, serial capillary and three-dimensional cubic network models of porous media (e.g., means and standard deviations of the diameters and lengths of the tubes constituting the models) are developed. Similar relations are also developed for the Klinkenberg permeability (and consequently for the Klinkenberg coefficient) of the parallel and serial capillary models. A comparison is made between these relations and similar relations based on the effective-medium approximation (EMA) (Nicholson et al., 1988).

Since their introduction by Fatt (1956), network models have been found to be realistic representations of the pore structure. Most of the work on network models has been related to mercury porosimetry (Van Brakel, 1975; Tsakiroglou and Payatakes, 1990, 1991). The emphasis has been laid on extracting enough pore structure information from the capillary pressure curves so that a unique network model can be constructed to replace a given porous medium. However, less effort seems to have been spent on deriving the pore structure information from single phase transport properties. These transport properties also contain important information about the pore structure which can complement the information derived through mercury porosimetry. In the present study, a methodology to model the pore structure of porous media, based on the relations of the transport properties of the parallel capillary, serial capil-

lary and three-dimensional cubic network models to their statistical parameters, mentioned earlier, is outlined. This methodology can be employed to study other transport phenomena and to predict complex properties such as capillary pressure curves and relative permeabilities. Following is the philosophy behind this methodology: If N statistical parameters are required to describe a porous medium according to a given pore structure model, then N transport properties can be determined experimentally on a sample of a porous medium and N equations for these N properties can be written. These equations can then be inverted to determine the N statistical parameters. Once the statistical parameters are known, the complex properties may be predicted explicitly or with the help of computer simulations. The experiments for measuring single phase properties of a porous medium are simple and less time consuming as compared to those for complex properties such as capillary pressures and relative permeabilities; therefore this methodology can be very useful in estimating values of the complex properties, and studying other transport phenomena. In the present work, a preliminary study based on this methodology is conducted on five sandstone samples and one limestone rock sample, all of which are selected from the existing literature. A comparison is made between the drainage capillary pressure curves predicted by the methodology and those observed experimentally.

Based on the discussion above, the motivation and objectives of the present research are summarized as follow:

1.1 Motivation

1. Most of the work related to the continuum description of transport phenomena in porous media has been directed toward: Development of mathematical concepts related to the quantification of REV size, development

of averaging rules, interpretation of the various terms in the averaged equations and derivation of the phenomenological laws from first principles. It will be very useful and interesting to employ this approach to study the relations of the macroscopic transport properties of porous media such as permeability, Klinkenberg permeability, formation factor and tortuosity, to various features of pore structure.

2. Relative permeability and capillary pressure are perhaps the most important data required for predicting the performance of oil reservoirs. However, experimentation for determining such properties on samples of the reservoir is tedious and time consuming. A quick and dependable way to predict these properties can be very helpful. An ordinary sandstone core sample used for laboratory experimentation, can, for all practical purposes be assumed as homogeneous, therefore the methodology outlined in the previous section can be very useful in this regard.

1.2 Objectives

1. To derive explicit integral expressions for permeability, Klinkenberg permeability and formation factor by comparing appropriate averaged conservation equations to the corresponding phenomenological laws.

2. To validate and interpret the integral expressions for permeability and formation factor with the help of idealized porous media and to study the transport property tortuosity and its relations to permeability and formation factor.

3. Based on the integral expressions derived in 1, to develop explicit relations of permeability and formation factor to the statistical parameters characterizing the pore space of parallel capillary, serial capillary and three-

dimensional cubic network models of porous media. Also, to derive similar relations for the Klinkenberg coefficient of the parallel and serial capillary models. To compare the present relations to those based on the effective-medium approximation (EMA).

4. To outline a methodology for modeling the pore structure of homogeneous porous media, based on the relations for the macroscopic transport properties developed in 3. Also, to compare the drainage capillary pressure curves of real porous media samples predicted by the methodology to the those observed experimentally.

1.3 Layout of the Dissertation

This dissertation is composed of seven chapters. An extensive literature review and its relevance to the present research is discussed in Chapter 2. The volume averaging method and the derivation of integral expressions for permeability, formation factor and Klinkenberg permeability are presented in Chapter 3. Validation and interpretation of the integral expressions and the study of tortuosity based on simple idealized porous media is conducted in Chapter 4. The relations of permeability, formation factor and Klinkenberg permeability of the pore structure models to the statistical parameters characterizing their pore space are developed in Chapter 5. This chapter also includes a comparison of these relations to those based on the effective-medium approximation. The methodology to model the pore structure of porous media is outlined in Chapter 6. Finally, conclusions are presented in Chapter 7.

CHAPTER 2

REVIEW OF THE LITERATURE

As mentioned at the beginning of Chapter 1, the study of transport phenomena in porous media is covered in many fields of engineering and science, and therefore, the information is widely scattered. Here, in order to form a clear picture of the background for the present work, relevant literature from all possible sources which the author has come across during the period of this study, is reviewed.

2.1 Scope of the Review

The review presented here is limited to pore structure models and other means employed to study the relations of permeability, formation factor, Klinkenberg permeability, tortuosity and capillary pressure of a porous medium to different aspects of its pore structure. The review includes the relations of these properties to the microscopic pore structure parameters and the correlations between two or more properties proposed in the literature. The experimental techniques for measuring these properties are not relevant to the present study and therefore are not reviewed. The review is confined to studies at the core level (laboratory scale) and studies at larger scales, such as reservoir level, are not considered. Different topics related to the continuum description of transport phenomena are briefly discussed in Section 2.2. The study related to tortuosity forms a significant part of the present work and therefore, the literature related to it is reviewed separately in Section 2.3. In Section 2.4, the literature related to permeability, Klinkenberg permeability and formation factor is reviewed. This section also includes a brief review of the work related to the effective-medium

approximation (EMA) (Kirkpatrick, 1973), relevant to the present study. The literature covered under permeability, formation factor and tortuosity overlaps slightly. The current thrusts in research related to mercury porosimetry and capillary pressure modeling are reviewed in Section 2.5. Finally, the relevance of the present research is discussed in the light of the reviewed literature in Section 2.6.

2.2 Continuum Description of Transport Phenomena in Porous Media

As pointed out in Chapter 1, our inability to observe and describe the solid-fluid interface inside a porous medium necessitates a continuum description of transport phenomena in porous media. The continuum description primarily consists of deriving the conservation equations for the extensive quantities with appropriate boundary conditions at the macroscopic level from the corresponding conservation equations and boundary conditions at the microscopic (or pore) level. Volume averaging, statistical averaging and homogenization are the three methods usually employed to derive the macroscopic conservation equations. The volume averaging is the only method of interest to the present work; therefore, only literature related to it is reviewed. The review is confined to the applications of volume averaging method for studying single phase flow in porous media, however some recent studies related to two-phase flow are briefly mentioned. The literature related to the applications of volume averaging method for studying other transport phenomena in porous media (e.g., heat, mass, diffusion and dispersion) is not considered.

A preliminary discussion of the volume averaging method is presented in Chapter 3. This chapter also includes brief introductions to the statistical averaging and homogenization methods, and to the techniques generally employed for solving the averaged conservation equations. For detailed information on the statistical aver-

aging method and the techniques for solving the averaged conservation equations, the reader is referred to Beran (1968) and Dagan (1989). An introduction to the homogenization method is given in Ene (1990).

In essence, the volume averaging method involves the following steps: Criteria for selection of the averaging volume size, definitions of average quantities, enunciation of averaging rules, deterministic derivations of macroscopic or averaged conservation equations, closure schemes for the macroscopic thermodynamic quantities, theoretical expressions for various macroscopic transport properties of porous media such as permeability, formation factor, Klinkenberg coefficient and inertial coefficient (when Forchheimer effects are considered), and solutions of the averaged conservation equations.

The main theory behind the volume averaging method has been developed over the last thirty years and the contributions to this development have been reported in a variety of journals. Important contributions include the works of Anderson and Jackson (1967), Marle (1967), Slattery (1967, 1969), Whitaker (1967, 1969), Gray (1975), Gray and O'Neill (1976), Gray and Lee (1977), Hassanizadeh (1979), Hassanizadeh and Gray (1979a, 1979b, 1980), Bachmat and Bear (1986), Bear and Bachmat (1986) and Bear and Bachmat (1991).

By invoking some statistical concepts Bachmat and Bear (1986) (also in Bear and Bachmat, 1991) gave a systematic development of the universal criteria for the selection of the upper and lower bounds on the size of the averaging volume. This size of the averaging volume is usually known as representative elementary volume (abbreviated as REV). The key mathematical theorem which relates the average of a gradient of a microscopic quantity to the gradient of the averaged quantity was presented independently by Anderson and Jackson (1967), Marle (1967), Slattery (1967) and Whitaker (1967). Gray (1975) presented a modified version of this theorem. Veverka (1981) questioned whether the volume average is differential; Howes and Whitaker

(1985) re-examined the derivation and confirmed its correctness. Mls (1987) demonstrated the existence of the first derivative of the volume average everywhere in a three-dimensional Euclidean vector space. Based on an order of magnitude analysis, Carbonell and Whitaker (1984) showed that for the averaged quantities to be single valued, the radius of the averaging volume (REV) should be very small as compared to the macroscopic dimension of the problem. Gray (1975) defined the deviation of a microscopic quantity from its macroscopic value within an REV. Hassanizadeh and Gray (1979a) gave the explicit dependence of various quantities in this definition on the microscopic and macroscopic coordinate systems. The averaging rules were summarized by Bachmat and Bear (1986).

In the averaged conservation equations, quantities of the form $\langle \tilde{w}_i \, \tilde{w}_j \rangle^\beta$ are encountered (see Chapter 3). Here w_k are the microscopic velocities, $\langle \ \rangle^\beta$ denotes the intrinsic phase average which is evaluated over a single phase in the REV and the tilde denotes the deviation of a microscopic quantity from its intrinsic phase average value. This term is the dispersive flux of momentum (per unit mass) in the fluid phase. Expressions for such quantities in terms of the average values are required for the solution of the averaged conservation equations. Closure is also required for the interfacial integral terms which arise in the averaged equations (see Chapter 3). These integrals contain the information about the micro-structure of porous media and as will be shown in Chapter 3, they are related to the macroscopic transport properties such as permeability. Hassanizadeh and Gray (1980) and Shapiro (1981) incorporated the dispersive flux term with the macroscopic viscous stress tensor and formed a constitutive relation for the combined quantity. Gray and O'Neill (1976) and Bear and Bachmat (1986) developed a separate constitutive relation for $\langle \tilde{w}_i \, \tilde{w}_j \rangle^\beta$. Slattery (1969, 1981) developed a constitutive relation for combined viscous and pressure integral terms. This relation expresses the combined quantity as a linear function of the intrinsic phase average velocity, the coefficient of which was determined by

using the Buckingham–Pi theorem. Constitutive relations for these terms were also presented by Gray and O'Neill (1976), Hassanizadeh and Gray (1980) and Bear and Bachmat (1986). For Stokes flow in porous media, Whitaker (1986a) developed a scheme to transform the closure problem into a boundary value problem of the deviation quantities. This scheme did not require any constitutive assumptions.

The failure of Darcy's law at high flow rates in porous media led to the development of the Forchheimer equation (Forchheimer, 1901). Recently, many articles have been published which have tried to link the nonlinear effects to various terms in the averaged momentum conservation equations. Barak and Bear (1981) studied physical models with variable degrees of complexity and derived relationships between pressure gradient and velocity; Du Plessis and Masliyah (1988), Coulaud et al. (1988) and Barak (1987) associated the nonlinear effects to the microscopic inertial forces. The explanation for such a conclusion was that at increasing pore Reynolds number, vorticities are generated inside the pores resulting in tortuous streamlines. Cvetkovič (1986) associated the nonlinear effects with the dispersion flux and concluded that this term contains most of the information related to microscopic inertial effects. However, Du Plessis and Masliyah (1988) obtained macroscopic inertial effects even when the dispersion term was neglected. Hassanizadeh and Gray (1987) concluded that the microscopic viscous drag is responsible for the nonlinear effects. Barak's comments (Barak, 1987) on the paper by Hassanizadeh and Gray (1987) contended that the microscopic viscous drag is not the fundamental reason for the nonlinear effects; the microscopic inertial effects (the change of streamlines due to generation of vorticities) is the fundamental cause and increase in the microscopic drag is a consequence of that. Hassanizadeh and Gray (1988) in their reply to Barak's comments (Barak, 1987) agreed with Barak's view. However, the authors stressed that in studies of porous media flow for large-scale applications, interest should not be focused on the micro-scale phenomena rather on their manifestations at the macro-scale, and there-

fore it is not necessary to study the change in streamlines at the microscopic level at high velocities. By examining flow in some very simple tube models of porous media, Ruth and Ma (1992) demonstrated that the averaged microscopic inertial terms are not responsible for nonlinear effects. The authors postulated that the Forchheimer effects are due to the distortions of the microscopic velocity and pressure fields which result in changes in the integral terms in the averaged equations.

The volume averaging method has also been employed to study phenomenological relations (e.g., the permeability in Darcy's law and the inertial coefficient in Forchheimer's equation). By ignoring the convective and inertial terms in the general macroscopic conservation equations for slow flow in an anisotropic porous medium, Gray and O'Neill (1976) derived the Darcy's law. Hassanizadeh and Gray (1980) showed that Darcy's law can be recovered by neglecting the inertial and macroscopic viscous effects (Brinkman effects) in the macroscopic fluid-phase momentum conservation equations. However, both of these studies did not associate any explicit dependence of the permeability in the Darcy's law to the micro-pore geometry. Whitaker (1986a) presented a theoretical derivation of Darcy's law for Stokes flow in porous media and provided means for direct theoretical determination of the permeability tensor. However, explicit relation of permeability to the microscopic pore structure parameters is not possible with this method. Also, the solution of the final equations depends on finding simpler representative pore structure cells. The relevance of the the present work concerning the study of permeability, in the light of the works by Whitaker (1986a) and Hassanizadeh and Gray (1980), will be discussed in Chapter 3. Barrere et al. (1992) showed that Whitaker's (1986a) solution of the closure problem in terms of an integro-differential equation can be transformed into a set of Stokes-like equations. They found that the solutions of these equations were in good agreement with the experimental data. Du Plessis and Masliyah (1988) evaluated the various terms in the averaged momentum conservation equations by

assuming developed flow inside a square duct of a cubic representative cell which was considered as model of sponge-like porous media. For creeping flows they derived an expression for the permeability. The limitations of this expression will be discussed in Section 2.4.1. Du Plessis and Masliyah (1991) performed an analysis similar to their previous work (Du Plessis and Masliyah, 1988), on a porous medium consisting of a stationary swarm of separate granules. Du Plessis (1991) carried out a similar study on a two-dimensional idealized porous medium.

Whitaker (1986b, 1986c) applied the volume averaging method to derive the relevant macroscopic conservation equations for Stokes flow of two immiscible fluids through a rigid porous medium and Stokes flow of a single fluid in a deformable porous medium. Recently, Quintard and Whitaker and their coworkers, in a series of papers (Quintard and Whitaker, 1987, 1988, 1990a, 1990b; Bertin et al., 1990), have reported their work on the applications of volume averaging method for studying two-phase flow in heterogeneous porous media. The authors introduced and applied the concept of large-scale averaging to two-phase flow in heterogeneous porous media. At this point, the difference between local volume averaging and large-scale volume averaging may be stated. Local volume averaging is the method in which the familiar microscopic conservation equations with appropriate boundary conditions are averaged to get the macroscopic conservation equations. The work of Whitaker (1986a) in which Stokes equations with appropriate boundary conditions were averaged to produce the familiar Darcy-level equations is an example of the local volume averaging. For heterogeneous porous media, the local volume averaging closure problem becomes exceedingly complex (Quintard and Whitaker, 1988). To by-pass this difficulty, large-scale averaging is considered in which the Darcy-scale equations are averaged over a region that is large compared to the length of the heterogeneities (Quintard and Whitaker, 1988).

Kalaydjian (1987) pointed out some drawbacks of the volume averaging method.

In particular, the author argued that it is not sure whether a common REV size can be determined for all the properties and field variables associated with a transport process which is a requirement for the application of the volume averaging method. Also, it may not be possible to determine the size of the REV experimentally. He employed a weighted function method to define the properties at the macroscopic level. This method was applied to derive macroscopic mass, momentum, energy and entropy balance equations. The author, however, opined that the volume averaging and weighted function methods are very similar and lead to similar results when applied for deriving macroscopic balance equations.

Kalaydjian and Legait (1987) performed a quantitative estimation of the coupling terms for the two-phase flow in square cross-section capillary tubes and found that these terms are not negligible with respect to the usual terms. Kalaydjian (1990) described an experimental approach to study the origin and to quantify the viscous coupling for two-phase flow in porous media at the pore level as well as at the macroscopic level.

Hassanizadeh and Gray, in a series of papers (Hassanizadeh and Gray 1989a, 1989b, 1990; Gray and Hassanizadeh, 1989), have reported their recent work on transport of interface properties in multi-phase flow in porous media. In these papers, the authors have laid down a frame work for forming the macroscopic equations for interface properties in multi-phase flows. According to the authors, these equations must complement the macroscopic equations for the bulk phases to complete the mathematical description of a well-posed problem. In the light of this study, the authors, in their latest work (Gray and Hassanizadeh, 1991a, 1991b), pointed out some paradoxes in the currently practiced unsaturated flow theory (simultaneous flow of air and water in porous media) and presented a theory that includes interfacial phenomena.

2.3 Tortuosity of Porous Media

Because the properties of a porous medium like porosity, permeability, formation factor and capillary pressure are different manifestations of the same microscopic pore structure, attempts have been made to relate them to one another or in groups. Because porosity and permeability were among the first such properties to be introduced and studied, earlier attempts were aimed at relating these two properties. In fact, until the early part of the twentieth century, no distinction was made between permeability and porosity in the oil industry. The permeability and porosity are related because a medium with zero porosity will also have zero permeability. However, a general correlation between the two is not possible. A review of various attempts at directly relating permeability to porosity is presented in Scheidegger (1974). This review clearly points out that it not possible to arrive at a universal relationship between permeability and porosity. Exploration of the possibility that permeability and porosity can be related by introducing additional parameters which contain more information about the pore structure was the obvious next step and tortuosity is one such parameter.

The tortuosity of a porous medium is defined as the ratio of the average length of the flow path to the corresponding macroscopic length. It was introduced by Carman (1937, 1938) to achieve agreement between the values of permeability predicted by the familiar Carman-Kozeny equation and those observed experimentally. A detailed derivation of the Carman-Kozeny equation was given by Wyllie and Spangler (1952). This derivation is summarized as follows: The average velocity in a circular pipe under a pressure gradient according to the Hagen-Poiseuille law is

$$v_1 = \frac{\delta^2}{32\,\mu}\,\frac{p_h - p_l}{L_e}\,, \tag{2.1}$$

where v_1 is the average velocity of a fluid with viscosity μ in a pipe of diameter δ and length L_e, and $p_h - p_l$ is the pressure drop across the pipe. For non-circular cross

sections, this equation is modified to

$$v_1 = \frac{m^2}{c'\mu}\,\frac{p_h - p_l}{L_e}\,, \tag{2.2}$$

where c' is the shape factor and m is the mean hydraulic radius defined as the ratio of the volume of the pipe to the area of the wetted surface. The essential part of the Carman-Kozeny theory lies in the application of Equation (2.2) to porous media. To do that, the void space inside a porous medium is conceptualized as a pipe with arbitrary cross-sectional area and length greater than the straight bulk length. It is argued that the average velocity within the porous medium must be greater than the velocity given by Q_1/A_1 (where Q_1 is the volumetric flow rate in the macroscopic flow direction, $k = 1$ and A_1 is the bulk area normal to it). Two reasons are cited in favor of this argument: one, the area available for flow in the macroscopic flow direction is less because of blockage due to the solid matrix; this area is taken to be ϕA_1 instead of A_1, where ϕ is the porosity of the medium; two, because of the tortuous nature of the flow paths inside a porous medium, the average path length, L_e, is greater than the corresponding bulk length, L_1, therefore the average velocity is faster by a factor of L_e/L_1. If these concepts are considered, the average velocity in a porous medium (equivalent to v_1 in Equation (2.2)) is $(Q_1 L_e)/(\phi A_1 L_1)$. The increased effective length also affects the pressure gradient, that is, the pressure gradient is $(p_h - p_l)/L_e$ instead of $(p_h - p_l)/L_1$. Therefore the equation for average velocity in porous media, analogous to Equation (2.2) for average velocity in a pipe, is:

$$\frac{Q_1}{A_1}\,\frac{L_e}{L_1}\,\frac{1}{\phi} = \frac{m^2}{c'\mu}\,\frac{p_h - p_l}{L_e}\,. \tag{2.3}$$

If Equation (2.3) is compared to Darcy's law in the form

$$\frac{Q_1}{A_1} = \frac{k_1}{\mu}\,\frac{p_h - p_l}{L_1}\,, \tag{2.4}$$

then the permeability, k_1, in the macroscopic flow direction, $k = 1$ is

$$k_1 = \frac{\phi m^2}{c'\tau_{ck}^2}\,. \tag{2.5}$$

Here $\tau_{ck}^2 = (L_e/L_1)^2$ is the Carman-Kozeny definition of tortuosity. In the present study, Equation (2.5) will be called the Carman-Kozeny equation. Equation (2.5) can also be written in the form

$$k_1 = \frac{\phi^3}{c' \tau_{ck}^2 S_o^2 (1-\phi)^2} , \tag{2.6}$$

where S_o is the surface area of the porous medium per unit solid volume. Several authors have given estimations of the shape factor c' and the tortuosity factor τ_{ck}. By considering the probable shape of the flow paths in unconsolidated porous media, Carman suggested that the value of c' should fall in the range of 2.0–2.5, and favored the higher value, 2.5. From his observations in flow visualization experiments in unconsolidated beds of particles, Carman found that average streamlines flowed at an angle of 45° to the macroscopic flow direction and therefore, suggested a value of $\sqrt{2}$ for τ_{ck} or 2 for τ_{ck}^2. Other values suggested for τ_{ck}^2 fall in the range of 1.5 to 3.25 (Bear, 1972).

Scheidegger (1974) has given a review of the experimental studies performed to test the Carman-Kozeny equation. Most of these studies have been conducted on unconsolidated porous media and substantial amounts of disagreement have been reported between the predictions and experimental observations. A severe criticism of the Carman-Kozeny equation was put forward by Childs and Collis-George (1950). They stated that because the Carman-Kozeny equation does not involve any directed quantities, it is not valid for anisotropic porous media. Also, they reported that the equation failed to give reasonable prediction for structured bodies like "stiff-fissured" clays. Many modifications of the Carman-Kozeny equation have been reported in the literature without any substantial improvement in its predictions (Scheidegger, 1974). Wyllie and Rose (1950) and Wyllie and Spangler (1952) postulated that tortuosity in fluid and electrical flows should be the same, and therefore the tortuosity in the Carman-Kozeny equation could be found independently from electrical measurements.

However, the expression for electric tortuosity proposed by them has some inherent shortcomings which will be discussed in Chapter 4.

Bear and Bachmat (1966, 1967) and Bear (1972) conceptualized tortuosity of a porous medium as a property which measures the deviation of a fluid particle from the macroscopic flow direction at every point inside the porous medium. Accordingly, they introduced the following quantities:

$$\tau_{ij}^{*} = \tau_{ij} \left(\frac{\mathrm{d}\sigma}{\mathrm{d}s} \right)^2 \tag{2.7}$$

with

$$\tau_{ij} = \left(\frac{\mathrm{d}\zeta_i}{\mathrm{d}\sigma} \right) \left(\frac{\mathrm{d}\zeta_j}{\mathrm{d}\sigma} \right) , \tag{2.8}$$

where s is the length measured along the axis of the channel, σ is the length measured along the streamline inside the channel, ζ_i are the local Cartesian coordinates, and τ_{ij}^{*} is the tortuosity tensor. The quantity $(\mathrm{d}\zeta_i/\mathrm{d}\sigma)\ (\mathrm{d}\zeta_j/\mathrm{d}\sigma)$ represents nine elements of a symmetrical 3×3 $(i, j = 1, 2, 3)$ matrix. These elements are the products of the cosines of the angles between the direction of a streamline at a point and the coordinate axes. The coefficient $(\mathrm{d}\sigma/\mathrm{d}s)^2$ takes the converging-diverging nature of the channels into account. For flow channels with constant cross-sectional area, $\tau_{ij}^{*} = \tau_{ij}$. The permeability model introduced by Bear and Bachmat (1966, 1967) which incorporates the above concepts of tortuosity will be discussed in Section 2.4.1.

By considering two types of capillary models, one with straight parallel tubes and the other with tortuous tubes, Whitaker (1967) showed that the term involving the area integral of the jump in the concentration, in the volume averaged two-component diffusion equation for incompressible flow in porous media, is associated with tortuosity. By using a Taylor series expansion, Whitaker (1967) presented a constitutive relation between the non-dimensionalized version of this area integral, which he called tortuosity vector, and the macroscopic concentration gradient. The present work

related to tortuosity is on the lines of Whitaker's (1967) work. By considering various idealized pore models, the integral terms in the averaged momentum conservation equations for single-phase fluid flow in porous media and averaged charge conservation equations for current flow in porous media saturated with electrically conductive fluid are studied (see Chapter 4). The direct relation of these terms with tortuosity is very clearly demonstrated. Unlike Whitaker's work (1967), the present work clearly differentiates between two types of tortuosities (discussed in Chapter 4) and identifies the integral terms responsible for each type.

Dullien (1979) discussed the limited scope of the classical definition of tortuosity in the Carman-Kozeny equation when parallel- and serial-type non-uniformities are present. Dullien argued that the concept of tortuosity should not only deal with the differences between the orientations of the microscopic and macroscopic streamlines—it should also include the "networking effect". As such, he stressed that the classical definition of tortuosity in the Carman-Kozeny equation is limited to the case of uniform, parallel, serial, and parallel-serial types of models. Citing other works (Wiggs, 1958 and Haring and Greenkorn, 1970) and his own work (Dullien, 1975), he suggested that 3 is a reasonable value for the tortuosity factor.

By considering a cubic "representative unit cell" (RUC) as a representation of porous media, Du Plessis and Masliyah (1988) derived an explicit relation between porosity and tortuosity. The cell was designed to take maximum possible connectivity and staggering into account. However, the tortuosity in their study has been introduced from the geometrical point of view. As will be demonstrated in Chapter 4, their definition of tortuosity is limited in the same sense as the classical definition in the Carman-Kozeny equation.

Spearing and Matthews (1991) simulated a sandstone sample with a three-dimensional array of cubes and cylinders representing pores and throats, respectively. The pore-size distribution of the array was calculated from the mercury porosimetry

curve of the sample and a correlation of 0.16 was maintained between the throat and cube sizes. Fifty values of the tortuosity factor of the sandstone sample were then predicted by considering weighted random walks through the array. The tortuosity was then defined as the median of these fifty values. The tortuosity predicted by the simulations increased from 2.45 to 3.55 with decreasing average coordination number (average number of throats meeting at a pore). Values of tortuosity of the sandstone sample equal to 2.42 and 2.46 were found experimentally using the equations

$$D_{\text{eff}} = \frac{D_{ab}\,\phi}{\tau_{sm}^2} \tag{2.9}$$

and

$$\tau_{sm} = (F\,\phi)^{\frac{1}{2}}\ , \tag{2.10}$$

respectively. Here τ_{sm} is the tortuosity factor, ϕ is the porosity, F is the formation factor of the medium, D_{eff} is the diffusion coefficient of the gas through the medium, and D_{ab} is the bulk diffusion coefficient. As will be shown in Chapter 4, Equation (2.10) used by them to calculate experimental tortuosity factor is not the exact one. Also, it is very difficult to verify if the method can predict correct values of hydraulic tortuosities because there are no equations for fluid flow analogous to Equations (2.9) and (2.10).

2.4 Pore Structure Properties of Porous Media

In this section, contributions toward understanding the relations of permeability, Klinkenberg permeability and formation factor of a porous medium to its pore structure are reviewed. Each of them is considered one by one.

2.4.1 Permeability

Darcy's law is a phenomenological law which introduces permeability of a porous medium as a "black box" dependent on its pore structure in a unique way. Much of

the research has been directed toward exploring this relation, either by relating the permeability to the pore structure parameters or to other properties of the porous medium. While doing so, a pore structure model of the porous medium has been assumed implicitly or explicitly.

One of the earliest attempts to relate permeability to other pore structure properties was by Kozeny (1927), who gave an equation which was later modified by Carman (1937). As described in Section 2.3, this equation is developed by idealizing a porous medium as a pipe with an arbitrary cross-sectional area and accounts for the blockages due to the solid matrix. It relates the permeability to porosity, tortuosity, shape factor and specific surface area.

Scheidegger (1953) presented three types of capillary models of pore structure which he called straight, parallel type and serial type capillary models. All the three models are based on a fundamental assumption about the relation between the pore velocity, v_1 and the filter velocity, Q_1/A_1. This assumption is called the Dupuit-Forchheimer assumption:

$$v_1 = \frac{Q_1}{\phi A_1} . \tag{2.11}$$

Here Q_1 represents the bulk flow in the macroscopic flow direction and A_1 is the bulk area normal to this direction. Scheidegger, however, argues that the Dupuit-Forchheimer assumption cannot be regarded as basic since the pore velocity in this definition has not been exactly defined. The straight capillary model is the simplest of the three; here a porous medium is represented by a bundle of straight and parallel capillaries of uniform diameter $\overline{\delta}$. By considering Hagen-Poiseuille flow in the tubes, the following expression was derived for permeability:

$$k_1 = \frac{\phi \overline{\delta}^2}{32} . \tag{2.12}$$

To achieve agreement with the experimental results, Scheidegger suggested that the factor 32 in the denominator be replaced by τ_s^2, where τ_s is the "tortuosity" factor.

$\overline{\delta}^2$ may be written in terms of S'_o to give

$$k_1 = \frac{\phi^3}{\tau_s^2 S_o'^2} , \tag{2.13}$$

where S'_o is the surface area per unit bulk volume. This equation is similar to the Carman-Kozeny equation; however, the Carman-Kozeny equation is based on an altogether different line of reasoning. In fact, the Carman-Kozeny equation is an exact equation for parallel-straight capillary tube models.

Next the parallel type model was considered. This model consists of a bundle of capillaries parallel to the macroscopic flow direction but with variable diameter. The expression for the permeability of the model is similar to Equation (2.12) with two changes: one, the factor 32 in the denominator is replaced by 96 and two, the parameter $\overline{\delta}$ is given a more specific meaning in the form

$$\overline{\delta}^2 = \int_0^\infty \delta^2 \, \alpha(\delta) \, \mathrm{d}\delta , \tag{2.14}$$

where $\alpha(\delta)$ is the capillary diameter distribution function. The incorporation of the additional factor 3 in the denominator is supposed to account for the fact that only one-third of the tubes are in the macroscopic flow direction. This type of model was first considered by Purcell (1949). In his model, the capillary diameter distribution was found from the mercury capillary pressure curve.

The serial type model, the third and the final such model considered by Scheidegger, is the opposite extreme of the first two models. This model consists of sections of capillaries of different diameters joined end-to-end. A fluid particle is imagined to travel through all the pore sizes in the porous medium. For this model, the expression for permeability is similar to Equation (2.12) with the factor 32 replaced by 96 and

$$\frac{1}{\overline{\delta}^2} = \left(\int_0^\infty \delta^2 \, \alpha(\delta) \mathrm{d}\delta \right)^2 \int \frac{\alpha(\delta)}{\delta^6} \mathrm{d}\delta . \tag{2.15}$$

According to Scheidegger (1974), the parallel and serial models when used to predict permeability with tube diameters assigned according to mercury injection capillary

pressure curve, predict very high and very low values, respectively, thereby indicating that the models are sensitive to the upper and lower portion of the pore size distribution, respectively.

Random adjacent slice models are another category of models used to relate permeability to the pore structure. These models are constructed by cutting thin slices from a bundle of parallel tubes with diameters distributed according to a given distribution and then rearranging the slices randomly. Childs and Collis-George (1950) were the first to consider these types of models. They contended that the models were more realistic than the Carman-Kozeny equation because the Carman-Kozeny equation did not consider pores of different cross sections. An expression for the permeability was derived based on the following reasoning: The faces of two adjacent slices of a porous medium of bulk area A_1 will have identical radius distribution functions $\alpha(r)$ and if these slices are randomly juxtaposed, the total pore space area in contact will be $\phi^2 A_1$. Assuming that resistance to flow at a junction is confined to the smaller pores, then

$$k_1 = c_o' \sum_{r_I=0}^{r_{max}} \sum_{r_J=0}^{r_{max}} r_I^2 \, \alpha(r_I)\delta r \, \alpha(r_J)\delta r \, , \tag{2.16}$$

where r_I is the radius of the smaller tube and r_J is the radius of the larger tube, $\alpha(r_I)\delta r$ and $\alpha(r_J)\delta r$ represent the fractional areas occupied by the tubes of radius range from r to $r + \mathrm{d}r$. The tube radius distribution is to be determined by mercury porosimetry or by other means and r_{max} is the largest tube radius encountered in such an experiment. The constant c_o' has to be experimentally determined. Wyllie and Gardener (1958) and Marshal (1958) contended that, instead of using r_I as the radius of the smaller tube at a junction, $r_I \sqrt{\phi}$ should be used as the effective radius because the fit of one tube to the next one is poor. Later improvements of this approach specified the value of c_o'. Marshal (1958) used ϕ while Millington (1959) used $\phi^{4/3}$ which was obtained by considering spherical pores. Millington and Quirk

(1961) conceptualized a porous medium as made up of interpenetrating solid spheres separated by interpenetrating spherical pores. This model gives ϕ^n as the effective area, where $0.6 < n < 0.7$ for $0.1 < \phi < 0.6$.

Haring and Greenkorn (1970) conceptualized a porous medium as a collection of randomly oriented cylindrical tubes with tube diameters distributed according to the beta function. Each tube was assumed to span from one boundary to the other boundary. By considering Hagen-Poiseuille flow in each tube and taking the orientation of the tubes into account, the value of the average velocity was calculated by integration. By invoking the Dupuit-Forchheimer assumption to relate the average velocity and the seepage velocity in Darcy's law, the following expression was found for permeability:

$$k_1 = \frac{\phi r_{max}^2}{24} \frac{(\alpha'+2)(\alpha'+1)}{(\alpha'+\beta'+3)(\alpha'+\beta'+2)} . \tag{2.17}$$

Here r_{max} is the maximum value of the radius, and α' and β' are the parameters of the beta distribution. The authors claimed that the model was a random network model with intersecting tubes; however, the manner in which average velocity was calculated, ignored intersections. This limitation is also evident from the fact that capillary pressure was evaluated by assuming all the tubes to be directly accessible from the outside.

Payatakes et al. (1973a, 1973b) presented a constricted unit cell model for monosized, or nearly monosized unconsolidated granular porous media. A unit bed element contained geometrically similar but unequal sized convergent-divergent unit cells. The geometry of the unit cells was determined from experimental information about grain size distribution, porosity and saturation versus capillary pressure data. The flow inside each cell was assumed to be similar. A finite difference scheme to solve the Navier-Stokes equation through the unit cell, retaining the inertial terms, was presented. Payatakes and Neira (1977) extended the model to account for the random

orientation of the flow channels. In this case, the predicted permeability was shown to agree well with the experimentally observed one. The way these models have been implemented, the "networking effect" has been ignored. Also, the scope of the models is very limited for polysized granular unconsolidated porous media and consolidated porous media in general.

Dullien (1975) considered the network approach for modeling permeabilities of sandstones. His model consisted of a number of cubic capillary networks of arbitrary orientation with respect to the macroscopic flow direction. Each network was built of identical capillary tubes which however, were different in the various networks. Each capillary was made of segments of different diameters. The capillaries in an individual network were characterized by two pore size parameters: the controlling pore entry diameter and the diameters of all other segments which may be penetrated through the pore entry diameter. This bivariate pore size distribution was obtained by measuring the pore entry diameters using mercury porosimetry and the larger pores by using the pore size distribution derived with the help of photomicrography. The best fit to the observed and predicted permeability data required the constant 96 in the denominator of the expression for permeability to be replaced by 106, and with this value, the predicted permeabilities matched with the experimental values within $\pm 23\%$. Dullien attributed the value 106 to a constant tortuosity factor of 3.3 instead of 3, which he argued was the theoretical value for his model. While arriving at his expression for permeability, Dullien assumed that different networks (with different individual permeabilities) in his model were independent of each other and the permeability of the model was a linear sum of the permeabilities of different networks constituting the model. Therefore, his model cannot be considered as a typical network model because the effect of intersections was ignored.

Wise (1992) used a three-dimensional cubic network of tubes for modeling permeability of water through porous media. The pore size distribution was found from

the drainage capillary pressure curve and the permeability was calculated by applying network theory (see Appendix B). A critical pore size was identified. When only tubes with diameter above the critical size were used in the network, the permeability of the network equaled the measured permeability of the medium. The evaluation of pore size distribution from the drainage capillary pressure curve was based on a parallel capillary model. As has been shown by many researchers (Dullien, 1975), this practice leads to a narrower pore size distribution than exists in reality. This is because the drainage capillary pressure curve is controlled by pore-throats (smaller pores) and the pore-bodies (larger pores) that are not directly accessible from the surface are invaded at later stages. This results in higher frequencies of smaller pores in the pore size distribution. This may be one of the reasons for the existence of a critical pore size in the model put forward by Wise (1992).

Bear and Bachmat (1966, 1967; also see Bear, 1972) conceptualized the void space of a porous medium as consisting of a spatial network of interconnected flow paths of varying length, cross-section and orientation. The average fluid flow at a point inside the passage was assumed to be along the axis of the passage. Volumes of junctions (where two or more flow passages meet) were assumed to be very small as compared to the volumes of the flow channels and junctions were assumed to offer no resistance to the fluid flow. The authors assumed the viscous force per unit volume at a point inside the flow passage resisting motion of a particle (direction of the force is opposite to the local velocity vector) to be

$$\mathbf{R} = -\frac{\mu}{B}\mathbf{V}^* , \tag{2.18}$$

where B (with the dimension of length squared) is the hydraulic conductance of a channel at a point (a function of the shape of the channel cross section and the location of the point with respect to the axis of the channel) and $\mathbf{V}^*$ is the mass-averaged velocity of the particle. Equation (2.18) was incorporated into the equation

of motion of a fluid particle inside the flow channel and the resulting equation was first averaged over the cross section of the channel and then over a representative elementary volume resulting (for laminar flow of a Newtonian fluid) in

$$k_{ij} = \phi \overline{B \tau_{ij}^*} \,, \tag{2.19}$$

where k_{ij} is the permeability tensor and τ_{ij}^* is the tortuosity tensor at a point as defined by Equation (2.7). Further development consisted of writing

$$\overline{B \tau_{ij}^*} = \overline{B}\,\overline{\tau_{ij}^*} \,, \tag{2.20}$$

where $\overline{B}$ was called the average medium conductance and $\overline{\tau_{ij}^*}$ was called the medium's tortuosity. Bear and Bachmat (1966) showed that for an isotropic medium, the tortuosity tensor reduces to a single scalar $\overline{\tau^*}$. For a porous medium consisting of straight channels of circular cross section

$$\overline{\tau^*} = \overline{\tau} = \overline{\tau_{11}} = \overline{\tau_{22}} = \frac{1}{3} \tag{2.21}$$

and

$$\overline{\tau_{12}} = \overline{\tau_{21}} = 0 \,. \tag{2.22}$$

To obtain a value of $\overline{\tau^*}$ for unconsolidated porous media, the divergence of streamlines is incorporated as (see Equations (2.7) and (2.8))

$$\overline{\tau^*} = \overline{\tau} \overline{\left(\frac{\mathrm{d}\sigma}{\mathrm{d}s}\right)^2} \,. \tag{2.23}$$

If the angle θ between a channel axis and a streamline inside it is assumed to vary between $\theta = 0°$ and $\theta = 90°$ such that $\theta = 45°$ is the representative value and

$$\overline{\left(\frac{\mathrm{d}\sigma}{\mathrm{d}s}\right)^2} = \sec\theta^2 = [\sec 45°]^2 = 2 \,, \tag{2.24}$$

then

$$\overline{\tau^*} = 2\overline{\tau} = \frac{2}{3} \,. \tag{2.25}$$

As argued by Dullien (1979), volume averaging $\mathbf{B}$ does not result in the correct conductance of a network because it does not take topology of the network into account. In other words, the contribution of an individual channel to the overall conductance of the network will depend, in addition to its conductance, on the location of the channel in the network. Also, the authors did not present a way of calculating $\overline{\mathbf{B}}$ for a general case. This was also pointed out by Van Brakel (1975).

Du Plessis and Masliyah (1988) considered a cubic representative unit cell as a model of an isotropic porous medium. The flow passage inside the cell was represented by three square duct sections, connected end-to-end and oriented mutually perpendicular to each other. This type of flow passage was considered to represent the maximum possible pore interconnectivity and staggering within the cell. From geometric considerations, the explicit relation between tortuosity and porosity

$$\phi = \frac{(3\,\tau_{dm} - 1)^2}{4\,\tau_{dm}^3} \tag{2.26}$$

was derived. Here, $\tau_{dm} = d/d_e$, is their definition of tortuosity (the inverse of the general definition used in this study), d is the external linear dimension of the cell and d_e is the total path length in the cell. The authors evaluated the various terms including the nonlinear (inertial) terms, of the volume averaged Navier-Stokes equation by assuming developing laminar flow inside the square ducts. For creeping flows they obtained the following equation for permeability:

$$k_1 = \frac{\phi^2\, d^2\, \tau_{dm}^2}{42.69\,(1 - \tau_{dm})}\,. \tag{2.27}$$

The authors have considered the tortuosity in Equations (2.26) and (2.27) as a geometric quantity. As will be demonstrated in Chapter 4, an explicit relation between porosity and tortuosity is only possible if tortuosity is considered to be a geometric quantity. If the tortuosity is considered as a kinematical property, such a relation is not possible.

In addition to the permeability models presented above, many more based on other considerations have been reported in the literature, for example, fissure models (Irmay, 1955; Snow, 1965; Parsons; 1966), resistance to flow models or models based on drag theory (Iberall, 1950; Rumer and Drinker, 1966; Rumer, 1969; Harleman et al. 1963; Happel and Brenner, 1965, Hubbert, 1956) and statistical models (Scheidegger, 1954, 1960; de Joss de Jong, 1969). These models have been reviewed by Bear (1972) and Dullien (1979).

2.4.2 Klinkenberg Permeability

Since the discovery of Darcy's law (Darcy, 1856) for fluid flow in porous media, many non-Darcian behaviors have been observed. One of these behaviors is observed when the flowing fluid is a gas. Fancher and Lewis (1933) were among the first to note that air permeabilities, as calculated from Darcy's law, were higher than liquid permeabilities in the same porous medium. This increase in permeability is attributed to the existence of a finite "slip" velocity at the solid-fluid interface inside the porous medium which results in flow augmentation. The significance of the gas slippage increases as the pore size becomes comparable to the molecular mean free path of the flowing gas. The phenomenon of slip relevant to gas flow in a capillary is theoretically well established as a consequence of the kinetic theory of gases (Present, 1958). Due to the random nature of the pore structure, a rigorous treatment of gas slippage in porous media has not yet been possible. Based on the slip theory of Kundt and Warburg (1875), Klinkenberg (1941) formed an expression for flow of a gas through porous media by introducing an "apparent" permeability, k_{a1} (called here the Klinkenberg permeability; a denotes the "apparent" nature of the permeability and 1 denotes its direction), defined as

$$v_1 = \frac{k_{a1}}{\mu} \frac{\partial p}{\partial x_1}, \tag{2.28}$$

where v_1 is the filtration velocity, μ is the viscosity and p is the pressure. Klinkenberg found the dependence of this permeability on the mean pressure, P_m in the porous medium sample, to be of the form

$$\frac{k_{a1}}{k_1} = 1 + \frac{b}{P_m}, \tag{2.29}$$

where k_1 is the true permeability and b is the Klinkenberg coefficient. Using a straight parallel capillary model of porous media, Klinkenberg showed that

$$b = \frac{8\,c\,\lambda\,P_m}{\mu_\delta}, \tag{2.30}$$

where λ is the mean free path of the flowing gas, μ_δ is the mean pore diameter and c is the coefficient of slip (Jeans, 1967). Jeans described this coefficient as the fraction of molecules which start out in random direction after colliding with the wall. He further commented that its value is close to unity.

The relation of λ to pressure and other properties of the gas, based on the elementary kinetic theory of gases (Present, 1958), can be used in Equations (2.30) and similar equations, However, if such a relation for λ is used, the developments are only valid for the cases when the pore diameters are greater than the average mean free path of the flowing gas. However, at a given pressure, the size of a pore inside a porous medium may be larger, smaller or comparable to the average mean free path of the flowing gas. For the pores with $\delta >> \lambda$, the flow is governed by the Hagen-Poiseuille law and for the pores with $\delta << \lambda$, the flow is governed by Knudsen equation (Present, 1958). According to Adzumi (1937), for the pressure range where $\delta \approx \lambda$, the Hagen-Poiseuille and Knudsen mechanisms must act simultaneously to yield the following approximate relation for gas flow in a capillary:

$$\overline{q}\,P_m = \frac{\pi\,\delta^4}{128\,\mu\,S}\,(p_a - p_b)\,p_m + \frac{c\,\delta^3}{6\,S}\sqrt{2\,\pi\,R\,T}\,(p_a - p_b)\,, \tag{2.31}$$

where $\overline{q}$ is the volumetric flow rate of the gas measured at a reference pressure, P_m, δ and S are the diameter and length of the capillary, $p_a - p_b$ is the pressure drop across

the capillary, p_m is the mean pressure in the capillary, R is the gas constant and T is the absolute temperature. The difference between P_m and p_m may be noted here: p_m is the mean pressure in the capillary whereas, P_m is a reference pressure which is usually taken to be the mean pressure in the porous medium sample. As shown by Rose (1948), if Equation (2.31) is used for flow in a capillary, then for capillary models this is equivalent to using the following expression for the average mean free path:

$$\lambda = 2.13 \frac{\mu}{p_m} \sqrt{RT}. \tag{2.32}$$

The same expression for λ was used by Ertekin et al. (1986) for studying gas slippage phenomena in porous media partially saturated with water. In the present study this expression for λ is used.

According to Klinkenberg's experimental data, b increased slowly with increasing pressure; however, it has been assumed constant in most of the studies following Klinkenberg's work. In the present study it is assumed to be constant.

2.4.3 Formation Factor

Archie (1942) defined the formation factor, F, of a porous medium as

$$F = \frac{R_o}{R_w}, \tag{2.33}$$

where R_o is the resistivity of the porous medium when saturated with an electric conductor of resistivity, R_w. Archie studied the relation of formation factor to porosity and permeability for sandstones over a wide range of porosity. The log-log plots of formation factor and porosity showed good linearity suggesting the following correlation:

$$F = \phi^{-m'}, \tag{2.34}$$

where m' is called the cementation exponent. The log-log plots of formation factor and permeability showed crude linearity; however, the slopes differed dramatically from

formation to formation and large discrepancies were noted for individual samples. Archie also studied the relation between the ratio of observed resistivity and that at 100% brine saturation, termed the resistivity index, I_r, versus fractional brine saturation, S_w, and suggested the correlation

$$I_r = S_w^{-n'} , \tag{2.35}$$

where n' is called the saturation exponent. Archie found that the value of m' ranged from 1.8 to 2.0 for consolidated porous media and equaled 1.3 for unconsolidated porous media. A value of 2 was given to n for clean consolidated and unconsolidated sandstones.

Winsauer et al. (1952) defined tortuosity in the following manner:

$$\tau_{win} = \frac{L_e}{L_1} = \left(\frac{t_e}{t}\right)^{\frac{1}{2}} , \tag{2.36}$$

where t is the transit time for ions of given mobility in a capillary of length L_e having the same cross-sectional area as a porous medium with length of L_1 flowing under the same potential gradient. These workers studied the dependence of formation factor on the ratio of effective to actual cross-sectional area for electrical conduction, ψ, tortuosity, τ_{win} and packing of sand grains. They analyzed Archie's data and additional data and found that the following correlations worked well:

$$F = \frac{\psi^{1.67}}{\tau_{\text{win}}} , \tag{2.37}$$

$$F = \frac{0.8}{\psi^{1.48}} , \tag{2.38}$$

$$F = \frac{0.62}{\phi^{2.15}} . \tag{2.39}$$

Archie's formula (Equation (2.34)) and Equation (2.39) (also known as the Humble formula) were generalized by Wyllie and Gregory (1953) as

$$F = \frac{a'}{\phi^{m'}} . \tag{2.40}$$

Parameter a' was said to be dependent on the particle shape, sorting and degree of compaction whereas parameter m' was dependent on the type of cementation. Values of m' ranging between 1 and 4, and of n' ranging between 1 and 7 have been reported in the literature. The saturation exponent depends on the paths available to current flow as the brine saturation in the sample decreases, and therefore is highly dependent on the wettability of the porous medium.

Wyllie and Rose (1950) defined tortuosity as

$$\tau_{wyl} = \left(\frac{L_e}{L_1}\right)^2 \tag{2.41}$$

and from first principles derived the following relations:

$$R_w = \frac{L_e}{L_1 \phi} R_o \,, \tag{2.42}$$

$$F = \frac{R_w}{R_o} = \frac{(L_e/L_1)}{\phi} = \frac{\tau_{wyl}{}^{\frac{1}{2}}}{\phi} \,, \tag{2.43}$$

$$F_e = \frac{\tau_e^{\frac{1}{2}} S_w^{-1}}{\phi} \,, \tag{2.44}$$

$$m' = \frac{\log\left(\phi/\tau^{\frac{1}{2}}\right)}{\log\left(\phi\right)} \,, \tag{2.45}$$

$$I_r = \frac{R_t}{R_o} = \frac{F_e}{F} = \left(\frac{\tau_e}{\tau_{wyl}}\right)^{\frac{1}{2}} S_w^{-1} \,, \tag{2.46}$$

$$n' = \frac{\log\left(S_w^2\, \tau_{wyl}/\tau_e\right)}{\log\left(S_w^2\right)} \,, \tag{2.47}$$

where R_t, F_e and τ_e are the values of resistivity, formation factor and tortuosity at partial brine saturations. Wyllie and Spangler (1952) argued that hydraulic and electrical tortuosities were equivalent and that tortuosity in the Carman-Kozeny equation

could be found from Equation (2.43). As will shown in Chapter 4, Equation (2.43) is only valid for straight parallel capillary models.

Perez-Rosales (1976) arrived at the following equation:

$$F = 1 + \frac{a''(1-\phi_s)}{\phi_f}\,, \tag{2.48}$$

where ϕ_f is the fraction of porosity occupied by the conducting fluid and ϕ_s is the fraction of porosity occupied by stagnant fluid. ϕ_f was assumed to be a linear function of porosity. The results predicted by Equation (2.48) were in good agreement with experimental observations except at low values of porosity. Perez-Rosales (1982) showed that better agreement was predicted at low porosities if the relation

$$\phi_f = \phi^{m''} \tag{2.49}$$

was used instead of the linear one. The author derived the following relations for tortuosity

$$\tau_{per} = \frac{L_e}{L_1} = \phi\,\left(a\,\phi^{-m''} + 1 - a\right) \tag{2.50}$$

and

$$\tau_{per} = \frac{L_e}{L_1} \simeq \frac{\phi}{\phi^{m''}} \simeq \frac{\phi_s}{\phi_f} + 1\,. \tag{2.51}$$

In recent years, a few attempts have been made to relate formation factor to permeability and other pore structure properties on theoretical basis. Katz and Thompson (1986) have proposed the relation

$$k_1 \propto \frac{l_c^2}{F}\,, \tag{2.52}$$

where l_c is the threshold pore size such that all the pore sizes greater or equal to l_c form a connected cluster that spans the porous medium sample. Katz and Thompson showed that the length scale l_c can be determined from the inflection point in the

mercury-intrusion capillary pressure curve. Johnson et al. (1986) have proposed the relation

$$k_1 \approx \frac{\Lambda'^2}{8\,F}\,, \tag{2.53}$$

where

$$\frac{\Lambda'}{2} = \frac{\int_{V_\beta} |E_i(r_i)|^2\, dV}{\int_{A_{\sigma\beta}} |E_i(r_i)|^2\, dA}\,. \tag{2.54}$$

$E_i(r_i)$ in the above expression is the local electric field. The parameter Λ' is the weighted pore volume to surface area in which the isolated portions of the pore space that do not contribute to the transport are eliminated. Avellaneda and Torquato (1991) have derived the following rigorous relation between permeability and formation factor:

$$k_1 = \frac{L_{AT}^2}{8\,F}\,, \tag{2.55}$$

where L_{AT} is a length scale that involves certain averages of the eigenvalues of the Stokes operator and contains information related to the electrical and momentum transport. For the straight parallel capillary models, $\Lambda' = L_{AT} = \delta/2$, where δ is the diameter of the tubes.

The length scales Λ' and L_{AT} contain information about the characteristic pore dimension (i.e., analogous to mean hydraulic radius in the Carman-Kozeny equation) and the hydraulic and electrical tortuosities in a complex manner. In order to use parameters Λ' and L_{AT} for practical purposes, detailed studies of their physical meanings and methods for determining them for realistic pore geometries are required.

2.4.4 Effective-Medium Approximation (EMA)

The effective-medium approximation (Kirkpatrick, 1973) can be employed to derive the relations of permeability and formation factor of the pore structure models of porous media (e.g., network models) to the statistical parameters characterizing their

pore space. The EMA consists of replacing an infinite random network of conductors with an effective-medium network which has the same overall conductance as the original network. The elemental conductances in the effective-medium network are identical. Nicholson et al. (1988) used the EMA with a renormalization group method to relate the elemental conductance of the effective-medium network to the parameters of the probability distribution function of the elemental conductances of the original network. Details about the EMA and a comparison of the relations that will be developed in the present work to those based on EMA, will be presented in Chapter 5.

2.5 Pore Structure Models for Capillary Pressure Curves

In this section, the literature related to the application of pore structure models for studying the capillary pressure curves of porous media is reviewed with an emphasis on network type models. For the background on physics and terminology related to the capillary phenomena in porous media (e.g., wetting phase, non-wetting phase; drainage, imbibition and secondary drainage capillary pressure curves; mercury intrusion capillary pressure curve; irreducible wetting phase saturation, residual non-wetting phase saturation; hysteresis), the reader is referred to Dullien (1979). Only literature in which capillary dominated flows have been considered, is reviewed. The viscous dominated and intermediate flows are not considered here.

The capillary pressure curves are probably the most important pore structure properties of a porous medium, for they contain most of the information about the pore structure. This information is, however, reflected in a very complex fashion. The research in this field has been directed toward interpreting this information in a meaningful manner and pore structure models have proven to be very helpful for this purpose. Pore structure models are generally used in association with mercury porosimetry. Fundamentally, mercury porosimetry consists of interpreting various

features of pore structure (e.g., pore-size distribution, pore interconnectivity, correlations in pore sizes) from the mercury intrusion and follow up capillary pressure curves. The conventional method, presented by Ritter and Drake (1945) and Drake and Ritter (1945) is based on the parallel capillary model, using the equation (relating the capillary pressure inside a cylindrical tube to its radius) originally introduced by Washburn (1921). This model is, however, incapable of accounting for the irreducible wetting and residual non-wetting phase saturations and capillary hysteresis. A stochastic method to correct some of these shortcomings was developed by Meyer (1953).

The absence of interconnections between the flow passages in parallel capillary type models is largely responsible for the deficiencies mentioned above. To model the interconnections between the flow passages, Fatt (1956) presented network models, similar to electrical networks. The tube diameters of a two-dimensional square network were assigned randomly and the tube lengths were assigned according to

$$S_I = \frac{2a}{\delta_I}\,, \tag{2.56}$$

where S_I denotes the length and δ_I denotes the diameter of the Ith tube, and a is a constant. Initially the network was assumed to be completely saturated with a wetting phase and surrounded from all sides by the non-wetting phase. The pressure difference between the wetting and the non-wetting phase, that is, the capillary pressure, was increased so that the tube (tubes) with largest diameter directly in contact with the non-wetting phase outside of the network was (were) penetrated. At this point all the tubes in the network with diameters greater or equal to and connected directly to the tubes invaded on the periphery of the network were penetrated. Keeping track of the tubes penetrated, the wetting phase saturation was calculated and this gave the first point on the drainage capillary pressure curve. By increasing the pressure in the non-wetting phase and repeating the process, other points on the capillary pressure were

obtained. Fatt found that the drainage capillary pressure curves generated in this way were in qualitative agreement with ones observed for sandstone samples. However, Fatt's method did not take the phenomena of fluid trapping into consideration, and therefore, was unable to predict irreducible wetting phase saturation.

The assumption that the network was surrounded on all sides by the non-wetting phase was criticized by Rose (1957) because it was not shown how the wetting phase, displaced by the non-wetting phase, could possibly leave the network. Rose (1957) contended that different irreducible wetting phase saturations existed for different escape routes which is not the case in real porous media.

Dodd and Kiel (1959) modified Fatt's procedure by taking the phenomena of fluid trapping into account. The non-wetting phase was allowed to penetrate from three sides and the wetting phase was allowed to leave from the fourth side. The wetting phase was trapped whenever no continuous path was available for it to exit. The authors also considered the case of intermediate wettability by assigning a probability of penetration based on the diameter. Ehrlich and Crane (1969) qualitatively showed that interconnections between various pores were responsible for hysteresis in drainage and imbibition relative permeability curves. Haring and Greenkorn (1970) used the model described in Section 2.4.1 for predicting the mercury intrusion capillary pressure curve. However, this model has the same limitations as a parallel capillary model because all the pores are assumed to be directly accessible from outside.

Mayer and Stowe (1965, 1966) used random packing of uniform spheres to study capillary pressure curves. Kwon and Pickett (1975) proposed a network model of intersecting tapered angular pores to represent the pore structure of rocks. The model was used to study the effect of pore structure parameters on the shape, plateau slope, irreducible wetting phase saturations and displacement pressures of the capillary pressure curves. The results were in qualitative agreement with the experimental observations.

Dullien (1975a) emphasized the versatility of bivariate pore size distribution (explained in Section 2.4.1) for characterizing pore structure. The bivariate pore size distribution was shown to simulate hysteresis for both independent and interacting domains. The distribution of the bigger pores was determined from mercury intrusion curve and the distribution of the smaller pores was found by photomicrography.

Androutsopoulos and Mann (1979) and Mann et al. (1981) used a regular two-dimensional network to determine the pore size distribution of real porous media samples. This was accomplished by fitting the predicted curve to the experimental data by varying the parameters of the simulated pore size distribution. They studied the effect of mercury entrapment on the resulting pore size distribution. Lin and Slattery (1981) used a random three-dimensional network model to calculate permeability, capillary pressure curves as measured under static conditions and during steady state flows, and relative permeability curves as measured during steady state flows. The model, described by seven parameters, was employed to correlate single-phase permeability, the drainage and imbibition capillary pressure curves and the drainage and imbibition relative permeability curves. The subsequent loops of the capillary pressure and relative permeability curves were predicted.

Wardlaw and Taylor (1976) and Wardlaw and McKeller (1981) used sandstone samples and network models to study the effect of various pore structure parameters on capillary pressure curves. Wardlaw and Li (1988) used two-dimensional etched glass networks to study the effect of pore sizes and fluid occupied pore topology on mechanisms of the retraction process. Lapidus et al. (1985) used three-dimensional network models of throats and chambers and developed an algorithm assuming the intrusion was controlled by throats sizes and and retraction by chamber sizes. Conner et al. (1983) and Conner and Lane (1984) found that the actual throat-and-chamber size distribution is wider than the one found by differentiating the capillary pressure curve. Li et al. (1986) used a network model to study the effect of pore structure

parameters, using the concept of throat-and-chamber-controlled domains.

Percolation theory has been used to study capillary phenomena in porous media. Larson and Morrow (1981) used a percolation model to study the effect of sample size on the capillary pressure curves. He found the accessibility of pore space increases as the sample size decreases, which, in turn decreases the sharpness of the intrusion curve knee and reduction of the residual mercury saturation. Chatzis and Dullien (1977) used a bond percolation model to study breakthrough pressure as a function of network topology, effect of dead-end pores and relative permeability to mercury for sandstones. Diaz et al. (1987) also used a bond-correlated percolation model to simulate drainage and imbibition pressure curves. Lane et al. (1986) modeled intrusion as bond percolation and retraction as site percolation. Mayagoitia (1989a, 1989b) emphasized that while constructing pore-throat models, the size of any pore must be greater or equal to the size of its delimiting throat, and size distribution of both pores and throats should try to achieve maximum randomness. Mann et al. (1986) generated a random two-dimensional network model by relocating the nodes of a regular network. The model was used to fit the porosimetry curves for an oil reservoir rock sample and to find the effect of length to diameter ratio on the capillary pressure curves. Using percolation concepts, Park and Ihm (1990) studied hysteresis by proposing hypotheses of no coalescence and no entrapment for mercury intrusion and extrusion in a two-dimensional network with different distributions for micro- and macro-pores.

Mishra and Sharma (1988) used a model of Bethe lattice of pore throats and pore bodies given by Larson and Morrow (1981), to develop a mathematical technique for deriving reliable pore size distributions from capillary pressure curves. Renault (1988) found that conventional capillary and "bubble" networks were unsuitable for determining pore size distribution for soils in which the intra-clay pores were very small as compared to the inter-clay pores (lacunar pore space). By assuming a normal

distribution of the cylindrical capillaries of a network model, Cox (1991) demonstrated a rapid way of estimating the parameters of the pore size distribution. The input to the scheme was the first two normalized moments of the raw capillary pressure data. Tsakiroglou and Payatakes (1990) developed a mercury porosimeter simulator based on a three-dimensional network of chambers and throats. The simulator modeled mechanisms by which mercury menisci move in pores and stop at entrances of throats and in certain cases chambers, mechanisms of snap-off that lead to disconnection and entrapment of mercury, and the sequence in which the mercury moves and threads break. The simulator was used to study the effect of throat size and chamber size distributions, the coordination number and contact angle on capillary pressure curves. The intrusion curve was found to depend on the pore size distribution and mean coordination number, the retraction curve on the ratio of pore size to throat size. As this ratio increased, the residual mercury saturation and the hysteresis between the intrusion and retraction curves increased. The residual mercury saturation increased as mean coordination number decreased. Portsmouth and Gladden (1991) used a three-dimensional spherical network model to study the effect of connectivity and pore size distribution on the capillary pressure curves. The emphasis was laid on determining pore connectivity (coordination number) by conducting various pressure sequences of the mercury porosimetry experiment. Soll et al. (1988) and Soll (1991) developed network models to simulate the two- and three-phase capillary pressure versus saturation relations.

With the development of the sophisticated mercury porosimetry simulators described above, recently attention has been focused on the influence of correlations between the sizes of neighboring pores on various transport properties of porous media, including the capillary pressure curves. Chatzis and Dullien (1985) used a bond-site correlated percolation model to study the mercury intrusion capillary pressure curves of networks in which sizes of the neighboring pores and throats were correlated but

no correlation existed between the sizes of neighboring pores. It was observed that as the c-t (chamber-throat) size correlation increased, breakthrough pressure decreased and the primary drainage curve spread over a wider pressure range. Wardlaw et al. (1987) used the mercury porosimetry simulator of Li et al. (1986) for comparing the theoretical capillary pressure curve with experimentally observed ones. A large correlation between the neighboring throats and pores, and no correlation between pores or throats among themselves was maintained. Their results for primary drainage curves agreed with those of Chatzis and Dullien (1985). It was observed that for c-t correlated networks, the breakthrough pressure for the second drainage curve was almost the same as that for the initial drainage curve and the imbibition curves originating from different saturation values terminated at approximately the same pressure value. The findings for networks with no correlation were exactly opposite: breakthrough pressure for second drainage was lower than that for the primary drainage and the imbibition curves originating from different saturation values ended up at different pressure values. The authors suggested that these observations may in future prove to be the tools for measuring c-t correlations.

Tsakiroglou and Payatakes (1991) used the simulator that they described previously (Tsakiroglou and Payatakes, 1990) to find the effect of chamber-chamber and chamber-throat size correlations on mercury capillary pressure curves. They found that the effect of c-t correlations on the mercury porosimetry curves was relatively small but that the effects of c-c and c-t (both simultaneously) correlations were strong. The c-c and c-t correlations were found to widen the intrusion curve and the residual mercury saturation was found to be smaller for c-c and c-t correlated networks than for uncorrelated networks.

The capillary pressure versus saturation relation is an important input to the numerical models for studying multi-phase flow in porous media at the reservoir scale. Usually, the measurements of this relationship are done in the laboratory on small core

samples of the reservoir. The work on capillary pressure versus saturation relation, described in the previous paragraphs, is relevant to this scale of study, that is, the laboratory scale. By performing statistical or volume averaging of the laboratory scale relations for different core samples of a reservoir, the "effective" capillary pressure versus saturation relation for the whole reservoir is determined (Dagan and Bresler, 1983; Mantoglou and Gelhar, 1987a, 1987b, 1987c; Polmann et al., 1988, 1991). The averaging implicitly assumes that the porous medium to some extent can be considered homogeneous at the reservoir scale. However real porous media are rarely homogeneous at the reservoir scale. Ferrand and Celia (1989, 1990a, 1990b, 1992) used three-dimensional cubic network models to study the effect of various types of heterogeneity on displacement and capillary pressure versus saturation relation. They found that the capillary pressure versus saturation curve of heterogeneous networks differed considerably from the one found by averaging the individual curves for various homogeneous sub-domains constituting the complete heterogeneous network.

2.6 Present Research in Light of the Reviewed Literature

It is clear from the review of literature related to the continuum description of transport phenomena in porous media that the research in this area has been directed toward: development of mathematical concepts related to the quantification of REV size, development of averaging rules, interpretation of the various terms in the averaged equations and derivation of the phenomenological laws from first principles. Limited effort has been directed toward studying the dependences of the transport properties, such as permeability, formation factor, Klinkenberg permeability and tortuosity on various features of the pore structure using this approach. In the present study, the volume averaging method is employed to derive integral expressions for permeability, formation factor and Klinkenberg permeability of homogeneous porous

media. These expressions are studied with the help of idealized pore structure models. This study reveals useful information about the dependence of the transport properties on the pore structure. The derivation of the integral expressions and their relevance to the works by Whitaker (1986a) and Hassanizadeh and Gray (1980), will be presented in Chapter 3.

The review of literature related to tortuosity indicates that recently more attention has been focused on this property of porous media (Du Plessis and Masliyah, 1988; Spearing and Matthews, 1991). As pointed out by Bear (1972), the effective length, L_e, in the definition of tortuosity may be interpreted in two ways. When L_e is calculated by averaging the actual lengths of the flow channels—not taking into account the fact that a fluid particle may travel through different channels at various times and with varying speeds—the tortuosity is a simple ratio of lengths. This is the classical definition of tortuosity employed in the Carman-Kozeny equation and other similar equations. In the second case, if L_e is calculated by averaging the actual distance traveled by all the fluid particles passing through a particular cross section of the porous medium at a particular instant, the tortuosity is then a kinematical property. The study related to tortuosity in the present work is based on the integral expressions for permeability and formation factor mentioned in the previous paragraph. This study clearly demonstrates the limited scope of the classical definition of tortuosity and attributes the difference between the two types of tortuosities to the availability of multiple flow paths for fluid flow. This phenomena has been termed the "networking effect" by Dullien (1979). The failure of the Carman-Kozeny equation for polysized unconsolidated porous media and consolidated porous media in general can be associated with this consideration. Most of the studies related to tortuosity, including those of Bear and Bachmat (1966, 1967), Bear (1972), and Du Plessis and Masliyah (1988) have considered tortuosity as a geometric quantity. The study by Spearing and Matthews (1991) is an exception. The random walk model used by

them to simulate the tortuosity of three-dimensional arrays accounts for the networking effect to some extent and a close agreement between the experimentally observed values and predictions in their study can be attributed to this feature of their model. It is the endeavor of the present work to clearly distinguish between the two definitions, both in the case of fluid flow and electric flow. This work also presents the exact relation between the formation factor and electric tortuosity of porous media and a discussion on the equivalence of hydraulic and electric tortuosities. As mentioned earlier (Section 2.3), the present approach for studying tortuosity is similar to that reported by Whitaker (1967), however, unlike Whitaker's work, the terms in the averaged conservation equations responsible for each type of tortuosity are clearly identified. The study related to tortuosity is carried out in Chapter 4.

On the basis of the reviewed literature, the approaches followed to study the relation of permeability to pore structure can be divided into two broad categories: Under the first category, simulations of the pore structure models are generated on computers and by inverting the mass conservation equations at the junctions (or nodes), the permeability of the model is calculated (see Appendix B). The work of Wise (1992) is an example of such an approach. These methods do not result in explicit relation of permeability to the pore structure parameters. Under the other category, the pore structure models are employed to derive explicit relations of permeability to the microscopic pore structure parameters. The works that fall under this category are: the Carman-Kozeny equation (Carman, 1937), Scheidegger's capillary models (Scheidegger, 1974), random adjacent slice models (Childs and Collis-George, 1950; Marshal, 1958; Wyllie and Gardener, 1958; Millington, 1959; Millington and Quirk, 1961), the randomly oriented cylindrical tube model (Haring and Greenkorn, 1970) and constricted unit cell models (Payatakes et al., 1973a, 1973b; Payatakes and Neira, 1977). All of these models are different variations of the capillary models and ignore intersections of the tubes. As pointed out earlier, Dullien's network model

(Dullien, 1975) also ignores intersections. The Bear and Bachmat model (Bear and Bachmat, 1966, 1967, also Bear, 1972) relates permeability to the average medium conductance and tortuosity. As indicated earlier, this average medium conductance cannot be evaluated for a general case and also, the tortuosity has been considered as a geometric quantity. The model by Du Plessis and Masliyah (1988) has also considered tortuosity as a geometric quantity. In the present study, the integral expression for permeability is evaluated for a three-dimensional cubic network model of porous media. This results in an explicit relation of the permeability to the microscopic pore structure parameters. This relation is valid over a large range of the tube diameter distribution breadth and also, does not consider tortuosity as a geometric quantity. Such a relation of permeability to the pore structure parameters can also be derived with the help of the effective-medium approximation (EMA). As will be demonstrated in Chapter 5, the relation based on the EMA is valid for tube diameter distributions with relatively smaller breadths.

Most of the work related to the formation factor has centered on finding empirical correlations between the formation factor, porosity and tortuosity (Archie, 1942, Winsauer et al. 1952, Wyllie and Rose, 1950, Perez-Rosales, 1976, 1982). Most of these correlations are based on experimental data. In the present work, the integral expression for formation factor will be evaluated for a three-dimensional cubic network model. The prediction capability of this relation will be compared to that based on the EMA.

The parallel and serial capillary models have also been considered in the present work. These models help to study the effect of the topology (the pore connectivity) on the permeability and formation factor. The development of explicit relations of the macroscopic properties of the models to the pore structure parameters will be presented in Chapter 5.

It is evident that mercury porosimetry simulators have become very sophisticated

where effects of correlations between the neighboring pores on various features of capillary pressure curves have been studied in detail. However, we are still many years away from the time when complete information of the pore structure can be retrieved from capillary pressure curves only and also, most of the studies related to the mercury porosimetry are of qualitative nature. Keeping this in mind, it is the aim of the present study to outline a methodology which can complement this effort. This methodology is based on the relations of the transport properties of the models to the pore structure parameters and can be used to simulate the pore structure of real porous media samples with any of the three models. A preliminary study based on this methodology will be conducted on real porous media samples. A comparison will be made between the drainage capillary pressure curves predicted by the methodology and those observed experimentally. This study will be reported in Chapter 6.

CHAPTER 3

MATHEMATICAL DEVELOPMENTS

In this chapter, mathematical concepts and relations which form the basis of the present work are developed. An introduction to the continuum description of transport phenomena in porous media, also known as the macroscopic level description, is presented in Section 3.1. The volume averaging method, which is the technique used in the present study for achieving transition from the microscopic to the macroscopic level description, is discussed in Section 3.2. By volume averaging the relevant microscopic conservation equations, integral expressions for permeability, Klinkenberg permeability and formation factor of a homogeneous porous medium are derived in Section 3.3. These integral expressions form the core of the present study. Their applications are studied in Chapters 4, 5 and 6.

3.1 Continuum Description of Transport Phenomena in Porous Media

As mentioned in Chapter 1, the transport of extensive quantities in porous media can be described with the familiar conservation equations. It may also be possible to state the boundary conditions in some cases (e.g., the condition of no-slip at the solid-fluid interface in the case of momentum transport). However, these equations describe the transport phenomena at the microscopic level and at that level our inability to observe and describe the complex geometry of the solid-fluid interface precludes any direct solutions to these equations. Also, in most cases of practical relevance, one

is not interested in knowing the details of the transport at the microscopic level. Instead, the knowledge about the behavior of relatively large portions of the porous medium domain suffices. This level of description of transport phenomena is called the macroscopic or continuum level description. Moreover, as it allows a comparison with the experimental observations, which are only possible at the macroscopic level, the continuum description is also desirable.

A few mathematical techniques are available to achieve transition from the microscopic level to the macroscopic level. These techniques can be broadly categorized as the averaging methods and the homogenization method. Under the class of averaging methods, two approaches are generally used: one is the volume averaging method and the other is the statistical averaging method. In the volume averaging method, the microscopic variables relevant to the transport process and the pore structure properties are averaged over a representative elementary volume (REV) (an REV is formally defined in Section 3.2.1) and the averaged values are assigned to the centroid of the REV. The averaging is conducted throughout the domain of interest which results in a continuous and differentiable spatial distribution of the transport variables and the macroscopic properties of the pore structure (e.g., permeability, formation factor, porosity). In the statistical averaging method, the transport variables and the properties of the porous medium are considered as random space functions (RSF). The actual porous medium and the transport process are considered as the ensemble of the random space functions that describe them. The statistical averaging must, in principle, be carried over a sufficiently large number of realizations. In the case of porous media, most of the times, only one realization is available. This difficulty is resolved by basing the statistical information on a unique sample that satisfies the conditions of statistical homogeneity (explained in Appendix A). These conditions are similar to those related to the concept of the REV discussed in the next section. If the fluctuations of the transport variables within the REV are ignored,

the results obtained by the two methods are the same.

The homogenization method is applied to porous media which periodically repeat themselves. Artificial porous media generally fall into this class. In this method, every property of the medium is expressed in the form $f(x_i, y_i)$. Here x_i denotes the position vector of a point in the Cartesian coordinates and y_i denotes the "stretched coordinates" given by $y_i = x_i/\varepsilon'$. ε' is a parameter given by d/D, where d is the period of the medium and D denotes the characteristic length at the macroscopic level. By introducing a double scale asymptotic expansion of the partial differential equations representing the transport phenomena of interest and identifying equal powers of ε', equations in the x_i and y_i variables are obtained. In periodic media, equations in y_i are solvable and the equations in x_i represent the "homogenized" or macroscopic equations describing the global behavior of the medium.

For porous media where macroscopic pore structure properties are constant or known functions, the macroscopic conservation equations describing various transport phenomena are the classical equations of mathematical physics, and therefore have been studied extensively. For media where macroscopic pore structure properties are random space functions, stochastic approaches are employed to solve them. One of the most widely used stochastic approaches is Monte Carlo simulation. The partial differential equations (at the macroscopic level) which describe the transport phenomena of interest are cast in numerical form and the solutions of the macroscopic variables are sought in the form of vectors at the nodes of a spatial grid. Values are assigned to the coefficients of the equations (that represent the properties of the porous medium, e.g, permeability) according to a chosen probability density function. Then the values of the macroscopic variables are found by solving the problem in a deterministic manner. The operation is repeated many times which results in a set of solutions of the vectors of the macroscopic variables. In this manner, the solution is presented in the form of realizations in which any moment of interest can be

found. For relatively accurate results, finer grids are required for high variances of the input coefficients and this requires prohibitively large computer power. Also, the usefulness of Monte Carlo simulations for a deeper insight into the flow phenomena and for drawing general conclusions is limited by the very nature of the method. Other important stochastic approaches include the small perturbation theory expansion and the renormalization technique.

The volume averaging method is of interest to the present work; therefore, it is discussed in detail. For reviews of the statistical averaging method and stochastic approaches for solving macroscopic conservation equations, the reader is referred to Beran (1968) and Dagan (1989). The details about the homogenization method are given in Ene (1990).

3.2 Volume Averaging Method

A porous medium consists of a solid matrix interspersed with a continuous void space. Here, the solid matrix is called the solid phase. The void space may be filled with one or more fluid phases (e.g., water, oil, air). The transport of various extensive quantities inside a porous medium may take place within a particular phase, between the solid phase and a fluid phase through the solid-fluid interface, and between two fluid phases through the fluid-fluid interface.

As mentioned in the previous section, the volume averaging method for deriving the macroscopic conservation equations from the microscopic conservation equations consists of associating an REV to every point inside the porous medium and averaging all the relevant transport variables and pore structure properties over it. The averaged values are then assigned to the centroid of the REV which may fall inside either the solid or the fluid phase.

Figure 3.1 illustrates a conceptual representation of a porous medium and an

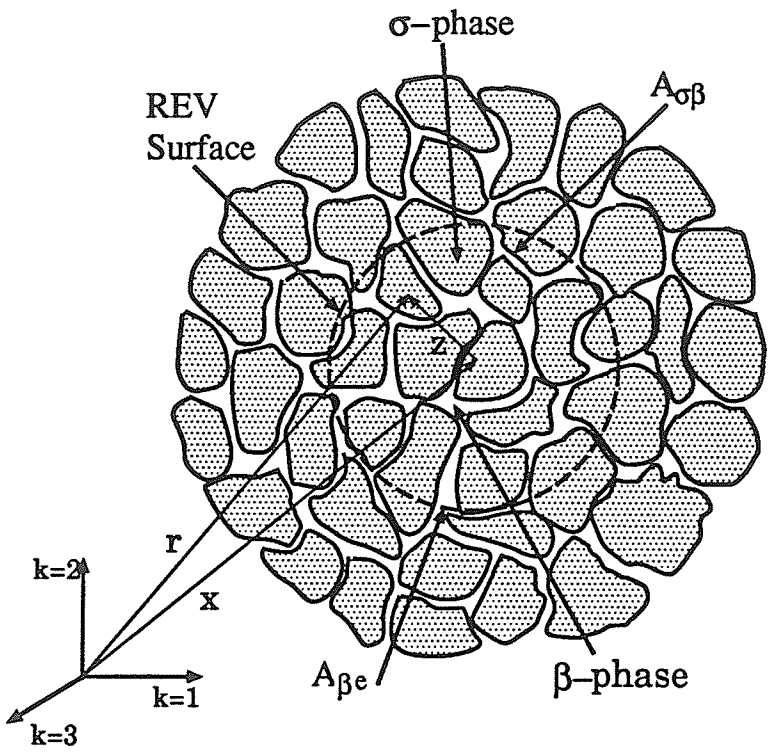

Fig. 3.1. A conceptual representation of a porous medium showing various phases, surfaces, an REV, and microscopic and macroscopic coordinate systems.

REV. Only, a single component fluid phase is considered here. A general variable is denoted by ψ. This variable may be a scalar or a component of a vector or of a tensor. The phase of which ψ represents a property is denoted by a subscript on ψ. Three subscripts are used: α to denote a general phase, β to denote the fluid phase and σ to denote the solid phase (i.e., ψ_α, ψ_β and ψ_σ). The interfacial area between solid and fluid phases in the REV is denoted by $A_{\sigma\beta}$. The part of the REV surface which constitutes the fluid-fluid interface between the fluid inside the REV and the fluid outside is denoted by $A_{\beta e}$. The time is denoted by t. Both the vector (e.g., $\mathbf{x}$) and tensor (e.g., x_i) notations are used. Throughout this monograph, the lower-case letters i, j and k, when used as subscripts, represent components of a vector or of a tensor and the upper-case letters I, J and K, when used as subscripts, represent

a tube, a flow path or a section of the pore structure models (to be considered in Chapters 4, 5 and 6) and have no vectorial or tensorial significance. The volume of the REV is denoted by V_b. It comprises the volume of the solid phase, V_σ, and the volume of the fluid phase, V_β. The porosity is denoted by ϕ and for an REV is given by $\phi = V_\beta / V_b$.

As shown in Figure 3.1, $\mathbf{x}$ represents the position vector of the centroid of the REV with respect to an inertial frame of reference. Inside the REV, $\mathbf{r}$ denotes the position vector of a point with respect to the inertial frame of reference and $\mathbf{z}$ denotes the position vector of the same point with respect to the centroid of the REV. The following relation between $\mathbf{r}$ and $\mathbf{x}$ holds:

$$\mathbf{r} = \mathbf{x} + \mathbf{z} \,. \tag{3.1}$$

In the rest of this section, the criteria for selecting the REV size, the definition of two types of averages and averaging rules are discussed. These concepts are then applied in the following section for deriving the integral expressions for permeability, Klinkenberg permeability and formation factor.

3.2.1 Selection of REV Size

As indicated a few times earlier in this chapter, the concept of an REV is the basis of the continuum description of transport phenomena in porous media. The size of an REV is related to a property representing the geometry of the void space. For an averaging volume to qualify as an REV, its size should be such that the average of the property over the volume is statistically meaningful, which in mathematical language means that the averaged property at a point inside the porous medium domain is a single valued function of the location of that point and time only and is independent of the size of the REV. Conceptually, this can be explained with the help of Figure 3.2. If, for example, at any instant, the porosity, ϕ, at a point is plotted as a function of

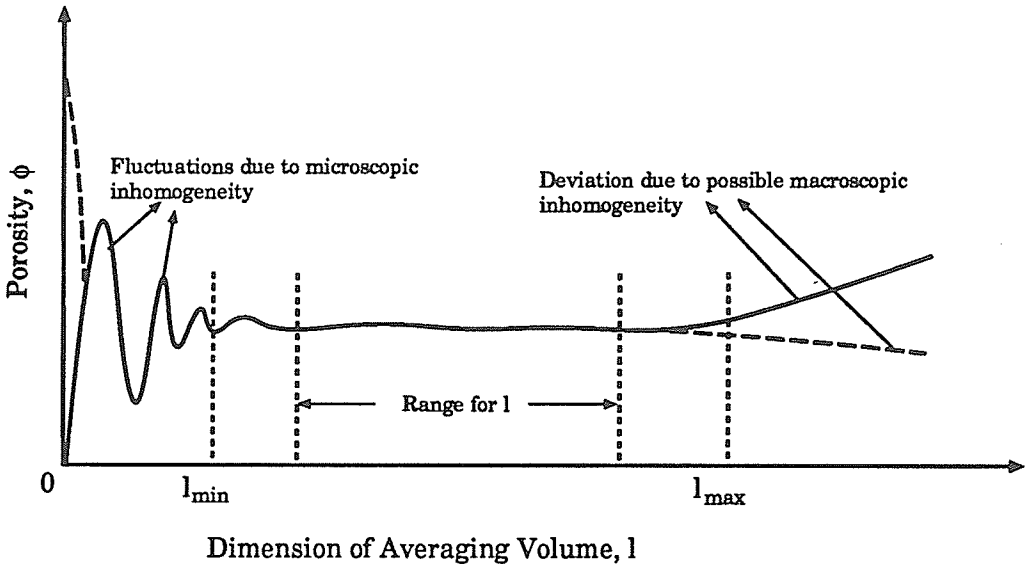

Fig. 3.2. Porosity as function of size of the averaging volume.

the size of the averaging volume (represented by its characteristic dimension) then a graph similar to the one illustrated in Figure 3.2 will result. When the size of the averaging volume is very small, the porosity will be either 1 or zero depending on whether the averaging volume lies in the void phase or in solid phase. As the size of the averaging volume is increased, the porosity fluctuates between low and high values. This is because the averaging volume contains large quantities of either the solid or the void phase. As the size of the averaging volume is further increased, the fluctuations decrease and eventually a region of sizes is obtained for which the porosity remains constant, that is, is independent of the size of the averaging volume. Further increase in the size of the averaging volume may result in deviations of porosity from the constant value. This will be due to the bulk heterogeneities in the medium. If l denotes the characteristic dimension of the averaging volume, then l has to satisfy the following constraint for the averaging volume to qualify as an REV:

$$l_{\text{min}} \ll l \ll l_{\text{max}} , \tag{3.2}$$

where $l_{\min}$ is the microscopic characteristic length and $l_{\max}$ is the macroscopic characteristic length of the porous medium. As illustrated in Figure 3.2, when the characteristic dimension of the REV is of the order of $l_{\min}$, large fluctuations of the porosity are encountered over small changes in the size of the averaging volume and when the characteristic dimension of the averaging volume is of the order $l_{\max}$, deviation of the porosity from a constant value may be encountered. The above arguments for the determination of the REV size are on the lines of the work by Whitaker (1969), Hassanizadeh and Gray (1979a) and Bachmat and Bear (1986).

In the preceding developments, the size of the REV has been based on porosity representing the geometry of the porous medium. If other properties appear in a given macroscopic model for a transport problem (e.g., permeability), a common range of REV size has to be found for all of them. If such a range cannot be determined, the macroscopic model cannot be applied. In a particular transport problem, the range of REV size should also be common to all the relevant state variables describing the problem.

3.2.2 Macroscopic Values

Two types of averages or macroscopic values are defined within an REV:

(a) A volumetric phase average

$$\langle \psi_\alpha \rangle (\mathbf{x}, t) = \frac{1}{V_b} \int_{V_\alpha} \psi_\alpha(\mathbf{r}, t)\, \mathrm{d}V\,, \tag{3.3}$$

which is evaluated over the entire REV, and

(b) a volumetric intrinsic phase average

$$\langle \psi_\alpha \rangle^\alpha (\mathbf{x}, t) = \frac{1}{V_\alpha} \int_{V_\alpha} \psi_\alpha(\mathbf{r}, t)\, \mathrm{d}V\,, \tag{3.4}$$

which is evaluated over a single phase (here denoted by α) within the REV. The $\mathbf{x}$ in the above definitions are the coordinates of the centroid of the REV to which the

averaged values are assigned at time t (Figure 3.1). From the definitions of the two averages, it follows that the two are related as

$$\langle \psi_\alpha \rangle (\mathbf{x}, t) = \phi(\mathbf{x}, t) \, \langle \psi_\alpha \rangle^\alpha (\mathbf{x}, t) \, . \tag{3.5}$$

At any point within the REV, a microscopic quantity can be expressed as (Gray, 1975; Hassanizadeh and Gray, 1979a)

$$\psi_\alpha(\mathbf{r} = \mathbf{x} + \mathbf{z}) = \langle \psi_\alpha \rangle^\alpha (\mathbf{x}, t) + \tilde{\psi}_\alpha(\mathbf{x}, \mathbf{z}, t) \, , \tag{3.6}$$

where $\tilde{\psi}_\alpha(\mathbf{x}, \mathbf{z}, t)$ is the deviation of ψ_α at a point $\mathbf{r}$ $(= \mathbf{x} + \mathbf{z})$ within the REV from its intrinsic phase average which is associated with the centroid $\mathbf{x}$ of the REV (Figure 3.1). Because a point can belong to an infinite number of REVs, it is very important to explicitly state the dependence of the deviation on $\mathbf{x}$, which denotes the centroid of the REV over which the average is calculated. The explicit dependence of $\tilde{\psi}$ on $\mathbf{x}$ and $\mathbf{z}$ in Equation (3.6) precisely does that. It states that the deviation of the microscopic quantity ψ_α at the point $\mathbf{r}$ $(= \mathbf{x} + \mathbf{z})$ is with respect to its intrinsic phase average value calculated over the REV having centroid at $\mathbf{x}$. By definition, both the phase and intrinsic phase averages of this deviation are zero. In future, the reference to the macroscopic coordinates and time inside the brackets will be omitted. If ψ_β and ψ'_β denote two variables, the average of their product is defined as

$$\left\langle \psi_\beta \, \psi'_\beta \right\rangle^\beta = \langle \psi_\beta \rangle^\beta \left\langle \psi'_\beta \right\rangle^\beta + \left\langle \tilde{\psi}_\beta \, \tilde{\psi}'_\beta \right\rangle^\beta \, , \tag{3.7}$$

which is a consequence of Equation (3.6).

The averages can, similarly, be defined with respect to a representative elementary area (abbreviated as REA). Bachmat and Bear (1986) showed that the volumetric and the areal averages of a quantity at a point are identical and the areal average at a point is independent of the orientation of the area and can be interchanged with the volume average at that point.

3.2.3 Averaging Rules

The averaging rules employed to derive the macroscopic conservation equations from the microscopic conservation equations are given below:

(a) When the macroscopic conservation equations are formed, one encounters an average of a gradient, while it is the gradient of the average that is required. These quantities are related by the spatial averaging theorem (Anderson and Jackson, 1967; Marle, 1967; Slattery, 1967; Whitaker, 1967). Mathematically this theorem can be written as

$$\left\langle \frac{\partial \psi_\beta}{\partial r_i} \right\rangle = \frac{\partial}{\partial x_i} \langle \psi_\beta \rangle + \frac{1}{V_b} \int_{A_{\sigma\beta}} \psi_\beta \, n_i \, \mathrm{d}A \,, \tag{3.8}$$

where n_i represents the unit outward normal vector on the differential area, $\mathrm{d}A$. The averaging theorem for the intrinsic phase average may be found by substituting Equation (3.5) into Equation (3.8):

$$\left\langle \frac{\partial \psi_\beta}{\partial r_i} \right\rangle^\beta = \frac{\partial}{\partial x_i} \langle \psi_\beta \rangle^\beta + \frac{1}{V_\beta} \int_{A_{\sigma\beta}} \psi_\beta \, n_i \, \mathrm{d}A + \frac{\langle \psi_\beta \rangle^\beta}{\phi} \frac{\partial \phi}{\partial x_i} \,. \tag{3.9}$$

If the porosity is constant, then the last term in Equation (3.9) vanishes. By manipulating Equations (3.5) and (3.6) and using the averaging theorem of Equation (3.8), Gray (1975) derived the following modified averaging theorem:

$$\left\langle \frac{\partial \psi_\beta}{\partial r_i} \right\rangle = \phi \frac{\partial}{\partial x_i} \langle \psi_\beta \rangle^\beta + \frac{1}{V_b} \int_{A_{\sigma\beta}} \tilde{\psi}_\beta \, n_i \, \mathrm{d}A \,. \tag{3.10}$$

(b) The average of a time derivative is evaluated using the general transport theorem in the form

$$\left\langle \frac{\partial \psi_\beta}{\partial t} \right\rangle^\beta = \frac{\partial \langle \psi_\beta \rangle^\beta}{\partial t} + \frac{\langle \psi_\beta \rangle^\beta}{\phi} \frac{\partial \phi}{\partial t} - \frac{1}{V_\beta} \int_{A_{\sigma\beta}} \psi_\beta \, (w_{\sigma\beta})_i \, n_i \, \mathrm{d}A \,, \tag{3.11}$$

where $(w_{\sigma\beta})_i$ is the velocity of the surface $A_{\sigma\beta}$. The second and third terms on the right-hand side vanish for constant porosity and stationary solid phase, respectively.

3.3 Integral Expressions for Macroscopic Transport Properties

In this section, the volume averaging method outlined in the previous sections is employed to derive integral expressions for permeability, formation factor and Klinkenberg permeability of homogeneous porous media. This is achieved by averaging the appropriate microscopic conservation equations and comparing the averaged equations to the corresponding phenomenological laws.

3.3.1 Integral Expression for Permeability

For the purposes of this section, it is assumed that the fluid is incompressible and Newtonian, and that all fluid properties (e.g., density, viscosity) and the porosity are constants in both time and space. This condition is realized in many problems and should not lead to misinterpretations. Also, it is assumed that the no-slip condition applies (i.e., Klinkenberg effects are ignored). Only porous media completely saturated with a single fluid are considered and the body force is assumed to be gravitational.

The momentum conservation equations at a point inside the fluid phase of the REV for incompressible and Newtonian microscopic flow in the microscopic Cartesian coordinate system may be written as

$$\frac{\partial(\rho\, w_i)}{\partial t} + \frac{\partial(\rho w_j\, w_i)}{\partial r_j} - \mu \frac{\partial^2 w_i}{\partial r_j\, \partial r_j} + \frac{\partial p}{\partial r_i} - \rho\, a_i = 0\,, \tag{3.12}$$

where ρ is the fluid density, w_k is the microscopic fluid velocity, μ is the fluid viscosity, p is the pressure, and a_i is the gravitational acceleration. Taking the intrinsic phase average of this equation and applying Equations (3.6) through (3.11):

$$\begin{aligned} \rho \frac{\partial \langle w_i\rangle^\beta}{\partial t} \;+\; & \rho \frac{\partial(\langle w_i\rangle^\beta \langle w_j\rangle^\beta)}{\partial x_j} + \rho \frac{\partial \langle \tilde{w}_i \tilde{w}_j\rangle^\beta}{\partial x_j} - \mu \frac{\partial^2 \langle w_i\rangle^\beta}{\partial x_j\, \partial x_j} + \frac{\partial \langle p\rangle^\beta}{\partial x_i} \\ & - \frac{\mu}{V_\beta}\int_{A_{\sigma\beta}} \frac{\partial w_i}{\partial r_j}\, n_j\, \mathrm{d}A + \frac{1}{V_\beta}\int_{A_{\sigma\beta}} p\, n_i\, \mathrm{d}A - \rho\, a_i = 0\,. \end{aligned} \tag{3.13}$$

Because all variables and properties (e.g., w_k, p, μ and ρ) relate to the fluid phase, the subscript β on all of them has been dropped. The physical meanings of the various terms are as follows: The first term is the unsteady term and has been proposed on experimental grounds by some authors (see Bear (1972) for a review). Obviously this term is zero if the macroscopic flow is steady. The second term is the macroscopic convection term and accounts for the spatial changes in the intrinsic phase average velocity. If the problem under consideration is one-dimensional and incompressible, this term is zero. The third term represents changes in average microscopic inertia (i.e., hydrodynamic dispersion of the average velocity). This term is zero for a uniform flow in a homogeneous porous medium. This term is often associated with the Forchheimer coefficient (see Dullien and Azzam, 1973); however this connection is problematic because the derivative here is macroscopic, while the Forchheimer effect is microscopic in nature. Further discussion of the Forchheimer effect is beyond the scope of this study (for more discussion on Forchheimer effects, see Ruth and Ma (1992) and the literature cited therein). The first three terms together represent macroscopic inertial effects. The fourth term is the macroscopic viscous term or the diffusion term. This term was suggested by Brinkman (1947) and is known as the Brinkman term. For a fully developed one-dimensional macroscopic flow, this term is zero. Here fully developed one-dimensional macroscopic flow means that the gradient of the intrinsic phase average velocity is zero. This is true for a homogeneous porous medium. The fifth term is the macroscopic pressure gradient term. The sixth and seventh terms contain the "hidden" information about the influence of the microstructure of the porous medium on the fluid flow. As will be shown in Chapters 4 and 5, understanding these terms requires consideration of explicit models of the porous medium. Finally, the eighth term is the gravity term. This term is zero for one-dimensional horizontal macroscopic flows.

It is well known that the Darcy's law is invalid in the presence of inertial and

Brinkman effects. Therefore, to derive an expression for permeability, the terms representing these effects in Equation (3.13) must be ignored. If we assume the macroscopic flow direction, $k = 1$ to be horizontal, then the gravity can also be ignored. It may be pointed out here that ignoring the gravity term does not limit the generality of the final expression. This is because the gravity term can be combined with the macroscopic pressure gradient term and to find the expression for permeability, the resulting equation can then be compared to the Darcy's law with the gravity effects. For the $k = 1$ direction, Equation (3.13) without macroscopic inertial, Brinkman and gravity effects then becomes:

$$\frac{\partial \langle p \rangle^{\beta}}{\partial x_1} - \frac{\mu}{V_\beta} \int_{A_{\sigma\beta}} \frac{\partial w_1}{\partial r_j} \, n_j \, \mathrm{d}A + \frac{1}{V_\beta} \int_{A_{\sigma\beta}} p \, n_1 \, \mathrm{d}A = 0 \, . \tag{3.14}$$

To visualize a typical experiment conducted for physically measuring permeability, consider a parallelepiped-shaped sample of a homogeneous porous medium with linear dimensions L_k and face areas A_k. Let the faces of the sample normal to the $k = 2, 3$ directions be sealed and let p_h and p_l denote the pressures imposed on the upstream and downstream faces (these faces are normal to the macroscopic flow direction, $k = 1$) of the sample, respectively, resulting in a bulk fluid flow rate, Q_1, in the $k = 1$ direction. If the macroscopic flow direction $k = 1$ coincides with horizontal direction, then according to the Darcy's law, the permeability k_1 of the sample in the macroscopic flow direction $k = 1$ is:

$$\frac{1}{k_1} = \frac{A_1 \, (p_h - p_l)}{Q_1 \, \mu \, L_1} \, . \tag{3.15}$$

An expression for permeability can be found by comparing Equation (3.14) to Equation (3.15). However, it may be mentioned here that Equation (3.14) is the differential form of the macroscopic momentum balance equation for $k = 1$ direction associated with the centroid of the REV, whereas Equation (3.15) is valid for a sample used in the physical experiment for the measurement of permeability. If the

characteristic dimension of the sample is very large as compared to the characteristic dimension of the REV, then the end effects in the sample can be ignored and the sample (which is assumed to be homogeneous) and the REV can be assumed to be equivalent. A comparison of Equations (3.14) and (3.15) still requires a procedure to relate $\partial \langle p \rangle^{\beta} / \partial x_1$ in Equation (3.14) to $(p_h - p_l)/L_1$ in Equation (3.15). The pressure in Equation (3.14) is an intrinsic phase average pressure, whereas the pressures in Equation (3.15) are the areal average pressures, or if the pressure measurements are made at points outside of the sample, the microscopic pressures outside of the sample. The intrinsic phase average pressure must therefore be expressed in terms of these experimental pressures. This is accomplished in the following developments.

By definition, the intrinsic phase average of the derivative of pressure within the REV is:

$$\left\langle \frac{\partial p}{\partial r_k} \right\rangle^{\beta} = \frac{1}{V_\beta} \int_{V_\beta} \frac{\partial p}{\partial r_k} \, \mathrm{d}V \, . \tag{3.16}$$

By Gauss's divergence theorem

$$\int_{V_\beta} \frac{\partial p}{\partial r_k} \, \mathrm{d}V = \int_{A_\beta} p \, n_k \, \mathrm{d}A \, , \tag{3.17}$$

where surface area A_β is equal to the sum of areas $A_{\sigma\beta}$ and $A_{\beta e}$ (see Figure 3.1). The integral can therefore be decomposed into two integrals as

$$\int_{V_\beta} \frac{\partial p}{\partial r_k} \, \mathrm{d}V = \int_{A_{\sigma\beta}} p \, n_k \, dA + \int_{A_{\beta e}} p \, n_k \, \mathrm{d}A \, . \tag{3.18}$$

Combining Equations (3.16), (3.18) and the averaging theorem for constant porosity (Equation (3.9)):

$$\frac{\partial}{\partial x_k} \langle p \rangle^{\beta} = \frac{1}{V_\beta} \int_{A_{\beta e}} p \, n_k \, \mathrm{d}A \, . \tag{3.19}$$

This equation allows the gradient of the intrinsic phase average pressure to be expressed in terms of an integral of the microscopic pressure over the fluid-fluid interface

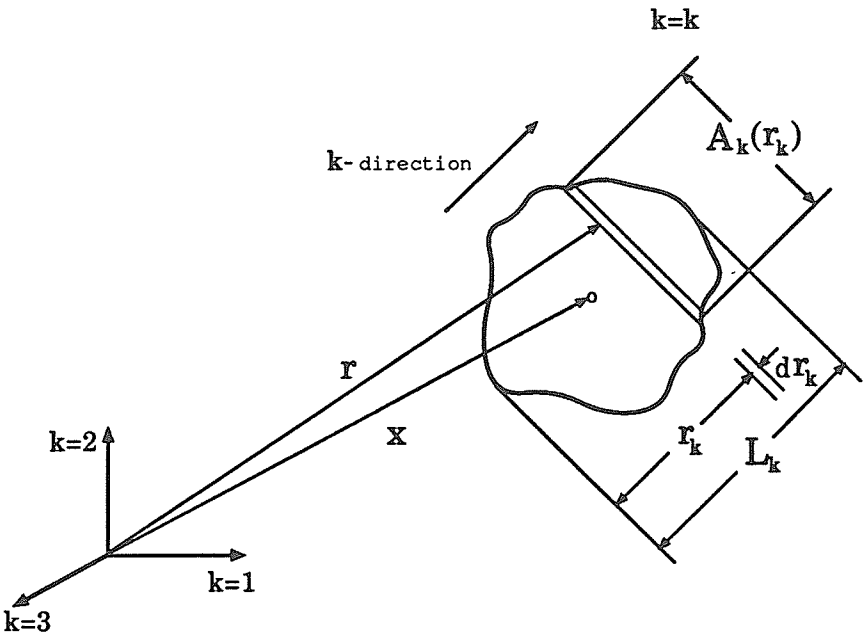

Fig. 3.3. Conceptual determination of areosity, $\xi_k(\mathbf{x})$, of an REV.

of the REV. If Equation (3.19) for $k = 1$ direction is applied to Equation (3.14), the resulting equation becomes

$$-\mu \int_{A_{\sigma\beta}} \frac{\partial w_1}{\partial r_j}\, n_j \, \mathrm{d}A + \int_{A_{\sigma\beta}} p\, n_1 \, \mathrm{d}A + \int_{A_{\beta e}} p\, n_1 \, \mathrm{d}A = 0 \,. \tag{3.20}$$

To evaluate the last term in Equation (3.20), a new parameter is defined. It is termed areosity, denoted by $\xi_k(\mathbf{x})$ and defined as

$$\xi_k(\mathbf{x}) = \frac{1}{L_k} \int_{L_k} \frac{1}{A_k(r_k)} \left[\int_{A_k(r_k)} \gamma(\mathbf{r}) \, |\cos\{\theta'(\mathbf{r})\}| \, \mathrm{d}A \right] \mathrm{d}r_k \,, \tag{3.21}$$

The various terms in the definition of areosity can be explained with help of Figure 3.3. This figure shows an arbitrary shaped REV and the microscopic and macroscopic coordinate systems. L_k is the characteristic length of the REV in the k direction and A_k is the bulk area of the REV normal to the k direction. A_k is a function of r_k, where r_k is a directed distance local to the REV as shown in Figure 3.3. γ is a function which is zero in the solid phase and 1 in the fluid phase. θ' is the angle between the direction of the microscopic flow and the k direction at a point inside the fluid phase.

The inner integral in Equation (3.21) gives the effective area open to flow in the k direction in a slice of the REV normal to the k direction. This effective open area of the slice is non-dimensionalized by the bulk area, A_k, of the slice. The outer integral sums up these non-dimensionalized effective open areas for all the slices normal to the k direction. By dividing the resulting summed up areas by L_k, an average non-dimensionalized effective area open to flow in the k direction, termed areosity here, is obtained. Therefore, areosity is a macroscopic property, defined for an REV and assigned to its centroid, $\mathbf{x}$. It is a directional property and is defined for all the points inside the porous medium domain for which an REV is defined.

For further developments we assume the effective area open to flow in the macroscopic flow direction $k = 1$ to be constant along the length of the sample. Then the expression for areosity of the sample in the $k = 1$ direction simplifies to

$$\xi_1 = \frac{1}{A_1} \int_{A_1} \gamma(\mathbf{r}) \, |\cos\{\theta'(\mathbf{r})\}| \, \mathrm{d}A. \tag{3.22}$$

With the introduction of the concept of areosity, the third integral in Equation (3.20) may be evaluated for the porous medium sample to give

$$\int_{A_{\beta e}} p \, n_1 \, \mathrm{d}A = (p_l - p_h) \, \xi_1 \, A_1 \, . \tag{3.23}$$

To show that the right-hand side in Equation (3.23) is the correct representation of the integral on the left-hand side, consider the idealized porous medium sample of Figure 3.4. This porous medium consists of a single slanted circular cylindrical tube. If we ignore the end effects, then for the laminar flow situation, the microscopic flow inside the tube is essentially in the direction of the axis of the tube. Therefore, by definition, the areosity of the sample is $A_o \cos\theta'/A_1$, where A_o is the open area, θ' is the angle between the tube axis and the macroscopic flow direction $k = 1$ and A_1 is the bulk area as shown in the figure. The areal porosity of the sample is A_o/A_1 and the porosity is given by:

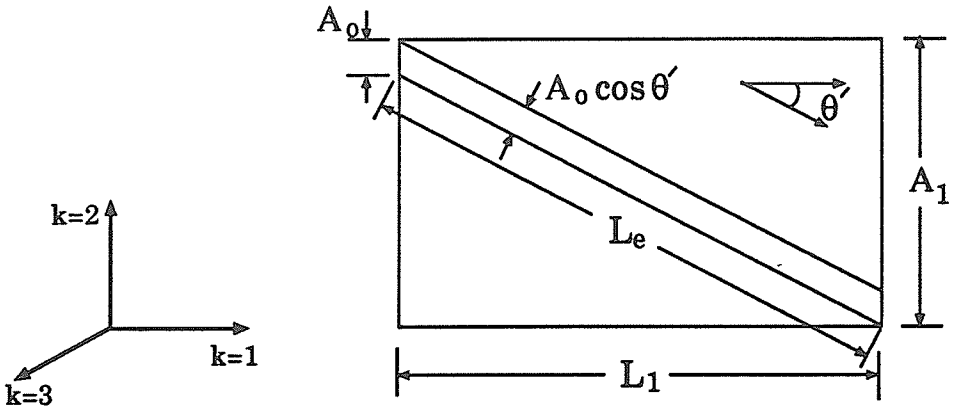

Fig. 3.4. An idealized porous medium employed to illustrate the difference between areosity, areal porosity and porosity.

$$\phi = \frac{A_o \cos\theta' L_e}{A_1 L_1} = \frac{A_o}{A_1}\,, \tag{3.24}$$

where L_e is the length of the tube. Therefore, the areal porosity and porosity are the same for this sample. However, the areosity is different from areal porosity and therefore from porosity. If porosity is used in Equation (3.23), it would mean that the microscopic pressure, for example on the upstream face of the sample, is acting on area A_o. However, Figure 3.4 clearly demonstrates that the pressure is acting on the effective area given by $A_o \cos\theta'$ and this is the area taken into account when areosity is calculated.

Application of Equation (3.23) to Equation (3.20) leads to

$$-\mu \int_{A_{\sigma\beta}} \frac{\partial w_1}{\partial r_j}\, n_j \, dA + \int_{A_{\sigma\beta}} p\, n_1 \, dA - (p_l - p_h)\, \xi_1 \, A_1 = 0\,. \tag{3.25}$$

Solving for $(p_h - p_l)\, A_1$ and substituting into Equation (3.15) gives the expression for permeability:

$$\frac{1}{k_1} = -\frac{1}{\xi_1 \, Q_1 \, L_1} \int_{A_{\sigma\beta}} \frac{\partial w_1}{\partial r_j}\, n_j \, dA + \frac{1}{\xi_1 \, Q_1 \, L_1 \, \mu} \int_{A_{\sigma\beta}} p\, n_1 \, dA\,. \tag{3.26}$$

The first term in Equation (3.26) will be referred to as the "viscous term" and denoted by T_v, the second term will be referred to as the "pressure term" and denoted by

T_p, and the complete equation will be referred to as the "integral expression for permeability".

At this point, the developments of the present section may be put in the perspective of the literature review presented in Section 2.2. Equation (3.13) is the differential form of the macroscopic momentum balance equations for flow of a single phase fluid with constant properties through a rigid homogeneous porous medium having no interaction (chemical or other) with the fluid phase. A general form of this equation for a multi-phase fluid system was derived by Hassanizadeh and Gray (1979b) which explicitly considered exchange of momentum between different phases through phase changes and mechanical interactions. Du Plessis and Masliyah (1988, 1991) and Du Plessis (1991) derived the volumetric phase averaged macroscopic momentum balance equations for a single fluid phase system. For Stokes flow of a single fluid in porous media, Whitaker (1986a) derived the following intrinsic phase averaged macroscopic momentum balance equations:

$$\frac{\partial \langle p \rangle^{\beta}}{\partial x_i} - \frac{\mu}{V_\beta} \int_{A_{\sigma\beta}} \frac{\partial \tilde{w}_i}{\partial r_j} n_j \, \mathrm{d}A + \frac{1}{V_\beta} \int_{A_{\sigma\beta}} \tilde{p} \, n_i \, \mathrm{d}A - \rho \, a_i = 0 \, . \tag{3.27}$$

In this derivation, the porosity was not assumed constant (in the present derivation, the porosity is assumed constant). In the absence of macroscopic inertial and Brinkman effects, Equation (3.27) can be derived from Equation (3.13) with the help of decomposition given by Equation (3.6) (Whitaker, 1986a).

Representations of the terms like the third, sixth and seventh terms of Equation (3.13), in terms of the average quantities $\langle w_k \rangle^{\beta}$ and $\langle p \rangle^{\beta}$, which are the dependent variables, are required for the solution of the macroscopic balance equations. This is usually called the closure problem. The constitutive theories for such terms presented by various authors have already been summarized in Section 2.2. Gray and O'Neill (1976) and Hassanizadeh and Gray (1980) showed that Darcy's law can be recovered by neglecting the inertial and macroscopic viscous effects (Brinkman

effects) in the macroscopic momentum balance equations. However, both of these studies did not associate any explicit dependence of the permeability in the Darcy's law to the micro-pore geometry. Whitaker (1986a) developed a scheme to transform the closure problem for integral terms of Equation (3.27) into a boundary value problem for the deviation quantities $\tilde{w}_i$ and $\tilde{p}$. This scheme did not require any constitutive assumptions. These developments provided for direct determination of the permeability tensor in the Darcy's law. However, explicit relation of permeability to the micro-pore geometry is not possible with this method. Also, the final solution depends on finding simpler representative pore structure cells. In the present study also, Darcy's law is recovered by neglecting the inertial and Brinkman effects. By introducing the concept of areosity, the permeability determined experimentally on a porous medium sample is related to various terms in the macroscopic balance equation valid for Darcy flow. Unlike the previous works (O'Neill and Gray, 1976; Hassanizadeh and Gray, 1980; Whitaker; 1986a), explicit interpretations will be given to the terms in this expression with the help of idealized porous media. Also, permeability will be explicitly related to the microscopic pore structure parameters of commonly used pore structure models. This will be accomplished in Chapters 4 and 5.

3.3.2 Integral Expression for Formation Factor

In this section, an integral expression is derived for the formation factor of a homogeneous porous medium saturated with a single electrically conductive fluid. This is accomplished by volume averaging the differential form of Ohm's law over an REV and comparing the averaged equation to Ohm's law for macroscopic current flow through a porous medium sample. The porous medium is assumed to be homogeneous and completely saturated with the fluid. The solid phase is assumed to be rigid and nonconductive. The electrical conduction inside the fluid phase under an electric potential gradient is assumed to be ohmic only, that is, surface-flow phenomena in

electric double-layers are ignored.

Consider a parallelepiped-shaped porous medium sample with electric potentials e_h and e_l imposed on the upstream and downstream faces (normal to the $k = 1$ direction), respectively. If the faces normal to the $k = 2, 3$ directions are insulated, then the resulting macroscopic current inside the sample, in the $k = 1$ direction, is given by Ohm's law:

$$C_1 = \frac{1}{R_o} \frac{e_h - e_l}{L_1} A_1 \,, \tag{3.28}$$

where C_1 is the macroscopic current in the $k = 1$ direction and R_o is the resistivity of the entire sample saturated with the conductive fluid. The formation factor, F, was defined by Archie (1942) as

$$F = \frac{R_o}{R_w} \,, \tag{3.29}$$

where R_w is the resistivity of the electrically conductive fluid saturating the porous medium. Therefore, the formation factor of the sample is:

$$F = \frac{A_1}{C_1 R_w} \frac{e_h - e_l}{L_1} \,. \tag{3.30}$$

At a point inside the electrically conductive fluid phase, the differential form of Ohm's law is

$$J_i = \frac{1}{R_w} E_i \,, \tag{3.31}$$

where J_i is the current density and E_i is the electric field intensity. The electric field intensity can be expressed in terms of the gradient of a scalar function e called the electric potential:

$$E_i = -\frac{\partial e}{\partial r_i} \,. \tag{3.32}$$

The minus sign is introduced by convention so that the electric field intensity points in the direction of decreasing potential. This leads to

$$J_i = -\frac{1}{R_w} \frac{\partial e}{\partial r_i} \,. \tag{3.33}$$

Taking the intrinsic phase average of Equation (3.33):

$$\langle J_i \rangle^\beta = - \left\langle \frac{1}{R_w} \frac{\partial e}{\partial r_i} \right\rangle^\beta . \tag{3.34}$$

With the application of Equation (3.9), Equation (3.34) for constant R_w and ϕ becomes

$$\frac{1}{V_\beta} \int_{V_\beta} J_i \, dV + \frac{1}{R_w} \frac{\partial}{\partial x_i} \langle e \rangle^\beta + \frac{1}{R_w V_\beta} \int_{A_{\sigma\beta}} e \, n_i \, \mathrm{d}A = 0 . \tag{3.35}$$

For $k = 1$ direction, Equation (3.35) reduces to

$$\frac{1}{V_\beta} \int_{V_\beta} J_1 \, dV + \frac{1}{R_w} \frac{\partial}{\partial x_1} \langle e \rangle^\beta + \frac{1}{R_w V_\beta} \int_{A_{\sigma\beta}} e \, n_1 \, \mathrm{d}A = 0 . \tag{3.36}$$

In order to identify an expression for the formation factor, Equation (3.36) must be compared to Equation (3.30). It may be mentioned here that Equation (3.36) is the macroscopic charge balance equation for the $k = 1$ direction associated with the centroid of the REV, whereas Equation (3.30) is valid for the laboratory sample. To make the comparison, $\partial \langle e \rangle^\beta / \partial x_1$ in Equation (3.36) must be related to $(e_h - e_l)/L_1$ in Equation (3.30). This is accomplished as follows: Based on an analogy with Equation (3.19), the following relation can be written:

$$\frac{\partial}{\partial x_1} \langle e \rangle^\beta = \frac{1}{V_\beta} \int_{A_{\beta e}} e \, n_1 \, \mathrm{d}A . \tag{3.37}$$

With the use of Equation (3.37), Equation (3.36) becomes

$$\int_{V_\beta} J_1 \, \mathrm{d}V + \frac{1}{R_w} \int_{A_{\beta e}} e \, n_1 \, dA + \frac{1}{R_w} \int_{A_{\sigma\beta}} e \, n_1 \, \mathrm{d}A = 0 . \tag{3.38}$$

The concept of areosity, introduced in the previous section, facilitates the evaluation of the second term in Equation (3.38) as follows:

$$\int_{A_{\beta e}} e \, n_1 \, \mathrm{d}A = (e_l - e_h) \, \xi_1 \, A_1 . \tag{3.39}$$

Equation (3.39) is analogous to Equation (3.23). Substitution of Equation (3.39) into Equation (3.38) leads to

$$\int_{V_\beta} J_1 \, \mathrm{d}V + \frac{1}{R_w} (e_l - e_h) \, \xi_1 \, A_1 + \frac{1}{R_w} \int_{A_{\sigma\beta}} e \, n_1 \, \mathrm{d}A = 0 . \tag{3.40}$$

Solving for $(e_l - e_h)$ and substituting in Equation (3.30):

$$F = \frac{1}{\xi_1 C_1 L_1} \int_{V_\beta} J_1 \, \mathrm{d}V + \frac{1}{\xi_1 C_1 L_1 R_w} \int_{A_{\sigma\beta}} e \, n_1 \, \mathrm{d}A \, . \tag{3.41}$$

Equation (3.41) relates the formation factor to the micro-structure of the solid-fluid interface through two integral terms. The first term involves a volume integral of the component of the current density in the macroscopic flow direction over the fluid phase; it will be called the "current term" and denoted by T_c. The second term involves a surface integral of the potential over the component of the solid-fluid interface in the macroscopic flow direction; it will be called the "potential term" and denoted by T_e; the complete equation will be referred to as the "integral expression for formation factor".

3.3.3 Integral Expression for Klinkenberg Permeability

For the purposes of this section, the fluid is assumed to be compressible and Newtonian with constant viscosity. The momentum conservation equations for such a fluid flow in a Cartesian coordinate system with gravity as the only body force are:

$$\frac{\partial(\rho \, w_i)}{\partial t} + \frac{\partial(\rho w_j \, w_i)}{\partial r_j} - \mu \frac{\partial^2 w_i}{\partial r_j \, \partial r_j} - \mu \frac{\partial^2 w_j}{\partial r_i \, \partial r_j} + \frac{2}{3} \delta_{ij} \, \mu \frac{\partial^2 w_k}{\partial r_j \, \partial r_k} + \frac{\partial p}{\partial r_i} - \rho a_i = 0, \tag{3.42}$$

where δ_{ij} is the Kronecker delta. For uniform porosity, the intrinsic phase average of Equation (3.42) is:

$$\begin{aligned}
&\frac{\partial \langle \rho \, w_i \rangle^\beta}{\partial t} + \frac{\partial}{\partial x_j} \langle \rho \, w_j \, w_i \rangle^\beta + \frac{1}{V_\beta} \int_{A_{\sigma\beta}} \rho \, w_j \, w_i \, n_j \, \mathrm{d}A \\
&-\mu \frac{\partial^2 \langle w_i \rangle^\beta}{\partial x_j \, \partial x_j} - \frac{\mu}{V_\beta} \frac{\partial}{\partial x_j} \int_{A_{\sigma\beta}} w_i \, n_j \, \mathrm{d}A - \frac{\mu}{V_\beta} \int_{A_{\sigma\beta}} \frac{\partial w_i}{\partial r_j} \, n_j \, \mathrm{d}A \\
&-\mu \frac{\partial^2 \langle w_j \rangle^\beta}{\partial x_i \, \partial x_j} - \frac{\mu}{V_\beta} \frac{\partial}{\partial x_j} \int_{A_{\sigma\beta}} w_j \, n_j \, \mathrm{d}A - \frac{\mu}{V_\beta} \int_{A_{\sigma\beta}} \frac{\partial w_j}{\partial r_j} \, n_i \, \mathrm{d}A \\
&+\frac{2}{3} \mu \, \delta_{ij} \left(\frac{\partial^2 \langle w_k \rangle^\beta}{\partial x_j \, \partial x_k} + \frac{1}{V_\beta} \frac{\partial}{\partial x_j} \int_{A_{\sigma\beta}} w_k \, n_k \, \mathrm{d}A + \frac{1}{V_\beta} \int_{A_{\sigma\beta}} \frac{\partial w_k}{\partial r_k} \, n_j \, \mathrm{d}A \right) \\
&+\frac{\partial \langle p \rangle^\beta}{\partial x_i} + \frac{1}{V_\beta} \int_{A_{\sigma\beta}} p \, n_i \, \mathrm{d}A - \langle \rho \rangle^\beta \, a_i = 0 \, .
\end{aligned} \tag{3.43}$$

A detailed discussion of various terms in the above equation has already been presented in Section 3.3.1. After ignoring the macroscopic inertial, Brinkman and gravity effects, the resulting equation for the $k = 1$ direction becomes

$$-\frac{\mu}{V_\beta}\int_{A_{\sigma\beta}}\frac{\partial w_1}{\partial r_j}\,n_j\,\mathrm{d}A-\frac{\mu}{V_\beta}\int_{A_{\sigma\beta}}\frac{\partial w_j}{\partial r_j}\,n_1\,\mathrm{d}A$$
$$+\frac{2\,\mu}{3\,V_\beta}\int_{A_{\sigma\beta}}\frac{\partial w_k}{\partial r_k}\,n_1\,\mathrm{d}A+\frac{\partial\,\langle p\rangle^\beta}{\partial x_1}+\frac{1}{V_\beta}\int_{A_{\sigma\beta}}p\,n_1\,\mathrm{d}A=0\,. \qquad (3.44)$$

The 6th, 9th and 12th terms in Equation (3.43) involve integrals of the velocity over the solid-fluid interface. For the present situation, these integrals are non-zero. However, for homogeneous porous media, these terms must vanish because they involve macroscopic gradients. Rest of the developments of this section are similar to those for the derivation of the integral expression for permeability outlined in Section 3.3.1. Here, only the important steps are presented.

Based on analogies with Equations (3.19) and (3.23), the term involving the intrinsic phase average pressure in Equation (3.44) can be expressed as

$$\frac{\partial}{\partial x_1}\,\langle p\rangle^\beta=\frac{1}{V_\beta}\int_{A_{\beta e}}p\,n_1\,\mathrm{d}A=\frac{1}{V_\beta}\,(p_l-p_h)\,\xi_1\,A_1\,. \qquad (3.45)$$

The Klinkenberg permeability, k_{a1} of a porous medium sample, in the $k = 1$ direction is defined as

$$\frac{1}{k_{a1}}=\frac{A_1\,(p_h-p_l)}{\overline{Q}_1\,\mu\,L_1}\,, \qquad (3.46)$$

where $\overline{Q}_1$ is the macroscopic gas flow rate, with finite slip at the walls, calculated at the mean pressure, $P_m = (p_h + p_l)/2$. Application of Equations (3.44) and (3.45) to Equation (3.46) yields

$$\frac{1}{k_{a1}}=-\frac{1}{\xi_1\,\overline{Q}_1\,L_1}\int_{A_{\sigma\beta}}\frac{\partial w_1}{\partial r_j}\,n_j\,\mathrm{d}A-\frac{1}{\xi_1\,\overline{Q}_1\,L_1}\int_{A_{\sigma\beta}}\frac{\partial w_j}{\partial r_j}\,n_1\,\mathrm{d}A$$
$$-\frac{2}{3\xi_1\,\overline{Q}_1\,L_1}\int_{A_{\sigma\beta}}\frac{\partial w_k}{\partial r_k}\,n_1\,\mathrm{d}A+\frac{1}{\xi_1\,\overline{Q}_1\,L_1\,\mu}\int_{A_{\sigma\beta}}p\,n_1\,\mathrm{d}A\,. \qquad (3.47)$$

The first three terms together will be called the "slip viscous term" and denoted by $\overline{T}_v$; the last term will be called the "slip pressure term" and will be denoted by $\overline{T}_p$; and the complete equation will be referred to as the "integral expression for Klinkenberg permeability". The relationship of the Klinkenberg coefficient, b, to the Klinkenberg permeability and permeability is (Klinkenberg, 1941):

$$b = P_m \left(\frac{k_{a1}}{k_1} - 1 \right) . \tag{3.48}$$

3.4 Summary

In this chapter, an introduction to the continuum description of transport phenomena in porous media has been presented. The volume averaging method, which has been used for achieving the transition from the microscopic to the macroscopic level, has been discussed in detail. The topics covered in this discussion include the criteria for selection of REV size, definition of the two type of averages and the averaging rules. All of these developments have been reproduced from the existing literature.

By averaging the appropriate microscopic conservation equations and comparing the averaged equations to the corresponding phenomenological laws, explicit integral expressions have been derived for the permeability, formation factor and Klinkenberg permeability of homogeneous porous media. The integrals in these expressions contain the information about the influence of the pore structure on the flow (fluid or electric), which is manifested at the macroscopic level in these properties.

To derive the integral expressions, a property of the pore structure, termed "areosity" in the present study, has been introduced. The areosity in a direction denotes the average of the ratios of the effective cross-sectional areas open to flow and the corresponding bulk areas along that direction, over an REV. Because the effective areas depend on the local microscopic flow direction, the areosity is different

from the areal porosity and therefore from the porosity. The integral expressions are only valid when the effective area open to flow is constant along the macroscopic flow direction. The areosity is further discussed in Chapter 4.

The derivation of the integral expression for permeability (and consequently the derivation of the integral expression for Klinkenberg permeability) has been presented in the perspective of the previously reported literature. The integral expression for formation factor is an entirely new contribution. These integral expressions form the basis of the present research. Unlike the previous works (O'Neill and Gray, 1976; Hassanizadeh and Gray, 1980; Whitaker, 1986a), explicit interpretation is given to different terms in these expressions in the following chapters. Their verification and detailed interpretation is carried out in Chapter 4. In Chapter 5, the expressions are used to derive explicit relations between the macroscopic properties and the statistical parameters characterizing the void space of parallel capillary, serial capillary and three-dimensional cubic network models of porous media. Based on the relations developed in Chapter 5, a methodology for modeling the pore structure of real porous media samples is outlined.

CHAPTER 4

DISCUSSION OF INTEGRAL EXPRESSIONS: MICROSCOPIC CROSS FLOW AND TORTUOSITY

In this chapter, idealized porous media are employed to interpret the terms in the integral expressions for permeability and formation factor. This work results in some useful concepts and relations. A better understanding of the transport property of porous media known as tortuosity is provided. Section 4.1 briefly introduces the idealized porous media used in this chapter. In Section 4.2, these media are employed to demonstrate the validity of the integral expressions for permeability and formation factor (Equations (3.26) and (3.41)) and to understand the physical meanings of the various integral terms. A detailed and clear understanding of tortuosity is given in Section 4.3. In Section 4.4, an exact relation between formation factor and tortuosity is presented. The lack of equivalence between hydraulic and electric tortuosities for general porous media is discussed in Section 4.5. Finally, areosity, the property of porous media introduced in Chapter 3, is discussed further in Section 4.6.

4.1 Idealized Porous Media and RUC's

The integral expressions for permeability, formation factor and Klinkenberg permeability (Equations (3.26), (3.41), (3.47)) are valid for any porous medium under the stated assumptions. However, demonstration of their validity for real porous media is very difficult. Their validity may instead be confirmed, in a simple manner, by applying network theory to idealized porous media. Such an exercise also provides

insight into the physical meanings of the various terms. The idealized porous media are simple enough to be amenable to mathematical analyses, yet represent some important features of real porous media, and therefore, are invaluable tools for gaining a fundamental understanding of the transport phenomena in porous media. A review of such porous media has already been presented in Chapter 2.

The porous media considered in this study consist of circular cylindrical tubes with constant cross-sectional area along their length. The point where two or more tubes meet is called a junction. A junction is assumed to possess no volume and offer no resistance to the fluid and current flows. Instead of considering an entire REV, a representative unit cell (RUC) is used. A full scale model of a porous medium may be generated by repeating the RUC in all directions. Du Plessis and Masliyah (1988) also employed the concept of RUC in their study.

In the present study, the determination of the macroscopic transport properties of idealized porous media by direct inversion of junction conservation equations is termed as network theory. The basic procedure behind network theory is presented in Appendix B.

4.2 Validity and Interpretation of Integral Expressions

In this section, a detailed study of the integral expressions for permeability and formation factor is carried out. Each of the expressions is considered separately.

4.2.1 Interpretation of the Integral Expression for Permeability

For studying the integral expression for permeability, Hagen-Poiseuille flow is assumed inside the tubes. Inertial effects are ignored and only creeping flows are considered. The RUC illustrated in Figure 4.1 (RUC 1) is studied first. It consists of three tubes (1, 2 and 3) and two junctions. All the three tubes are of the same diameter, δ, and

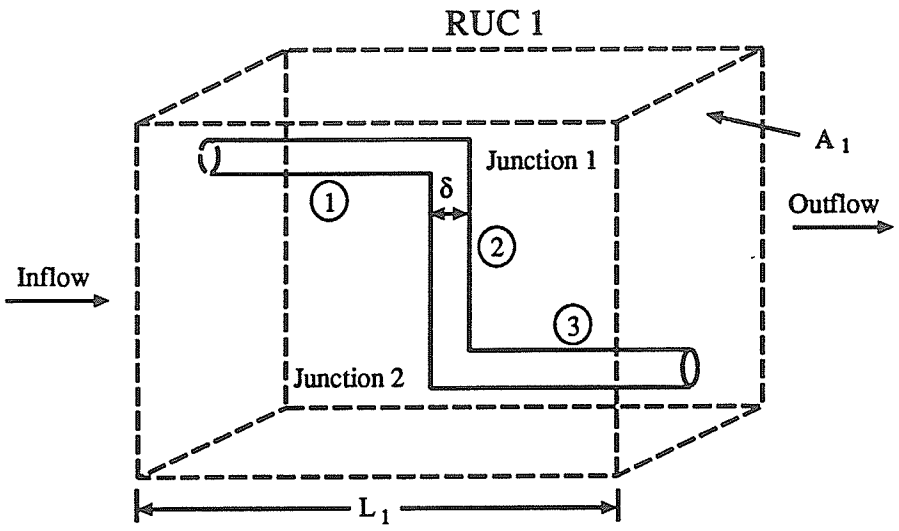

Fig. 4.1. RUC 1 showing type-a tortuosity.

therefore the assumption of constant effective area open to flow in the macroscopic flow direction, required for the application of the integral expressions, is satisfied for this RUC. The viscous and pressure terms for this RUC simplify to

$$T_v = \frac{32}{\xi_1 L_1 \delta^2} (f_1 S_1 + f_3 S_3) \tag{4.1}$$

and

$$T_p = \frac{32}{\xi_1 L_1 \delta^2} f_2 S_2 , \tag{4.2}$$

where $f_I = q_I/Q_1$ is the non-dimensionalized flow rate in the Ith tube, and S_1, S_2 and S_3 are the tube lengths. Here q_I is the volumetric flow rate in the Ith tube and Q_1 is the bulk flow rate in the macroscopic flow direction, $k = 1$. For this RUC, $f_1 = f_2 = f_3 = 1$, and therefore

$$\frac{1}{k_1} = \frac{32}{\xi_1 L_1 \delta^2} (S_1 + S_2 + S_3) . \tag{4.3}$$

If network theory (Appendix B) is applied to this RUC, then pressures p_l and p_h are related by:

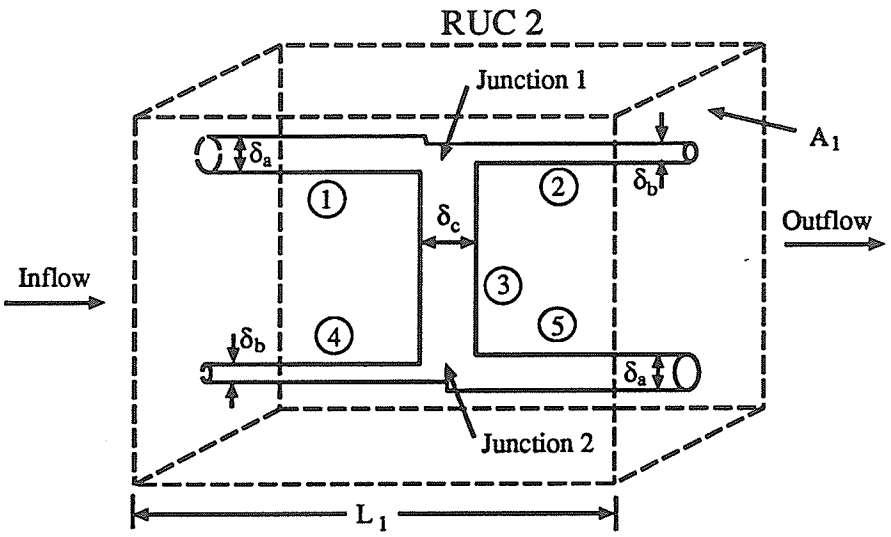

Fig. 4.2. RUC 2 showing type-b tortuosity.

$$p_l = p_h - \frac{q_1}{g_1} - \frac{q_2}{g_2} - \frac{q_3}{g_3}\,, \tag{4.4}$$

where g_I represents the conductance (in the Hagen-Poiseuille equation; Appendix B) of the Ith tube. For this RUC, $q_1 = q_2 = q_3 = Q_1$, and therefore the permeability as given by Darcy's law (Equation (3.15)) is:

$$\frac{1}{k_1} = \frac{32}{\xi_1 L_1 \delta^2}\left(S_1 + S_2 + S_3\right), \tag{4.5}$$

which is identical to Equation (4.3), thus confirming the validity of the integral expression for permeability for RUC 1.

The RUC illustrated in Figure 4.2 (RUC 2) is studied next. This RUC is fundamentally different from RUC 1 in that it offers an alternate path to the flowing fluid at each junction, through the vertical tube (Tube 3), and therefore is more representative of natural porous media. It consists of five tubes and two junctions. The diameters of Tubes 1 and 5 are denoted by δ_a, Tubes 2 and 4 by δ_b and Tube 3 by δ_c. For this arrangement of tubes the cell satisfies the assumption of constant effective area open to flow in the macroscopic flow direction required for the application of the integral

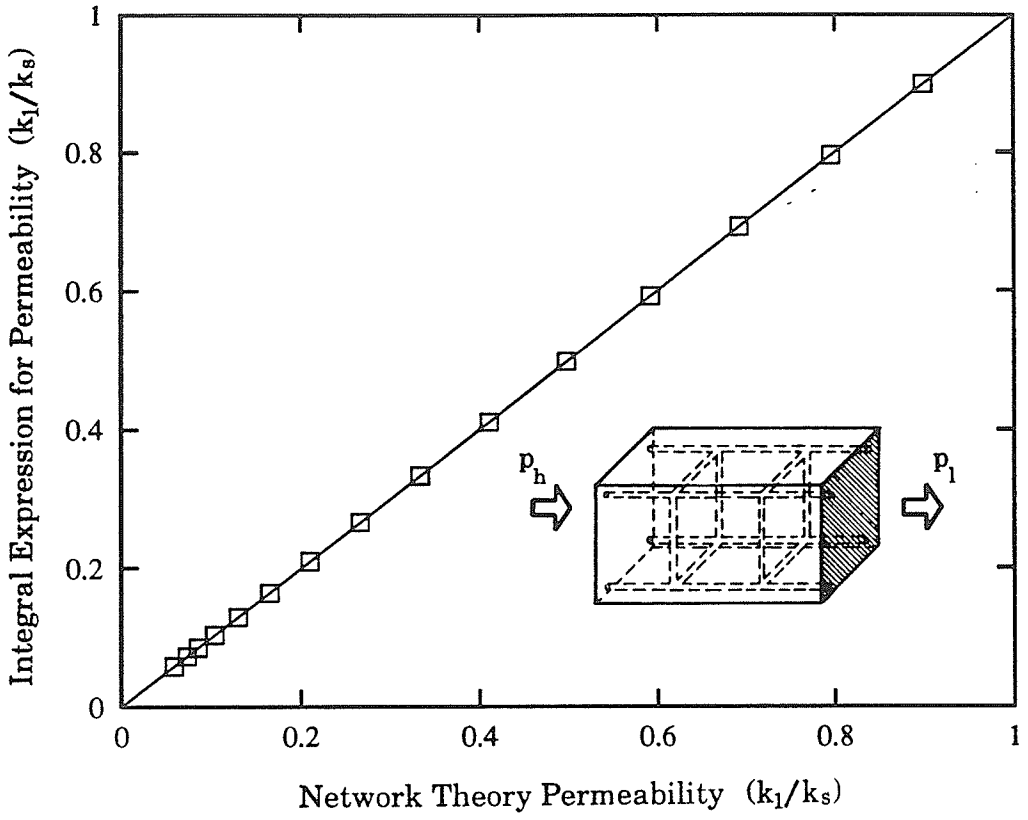

Fig. 4.3. Correlation of calculated permeabilities for a three-dimensional RUC (inscribed) with constant effective open area in the macroscopic flow direction and random cross flow tube diameters (δ_a fixed, $0 \leq \delta_b \leq \delta_a$).

expression for permeability. The tube lengths are denoted by S_1, S_2, S_3, S_4, and S_5. The viscous and pressure terms for the RUC simplify to

$$T_v = \frac{32}{\xi_1 L_1} \left(\frac{f_1 S_1 + f_5 S_5}{\delta_a^2} + \frac{f_2 S_2 + f_4 S_4}{\delta_b^2} \right) \tag{4.6}$$

and

$$T_p = \frac{32}{\xi_1 L_1} \frac{f_3 S_3}{\delta_c^2} \frac{|\delta_b^2 - \delta_a^2|}{\delta_c^2} , \tag{4.7}$$

where the absolute value sign arises from the fact that when $\delta_b < \delta_a$, the fluid flow in Tube 3 is in negative (downward) direction and vice versa. Hence the integral in T_p

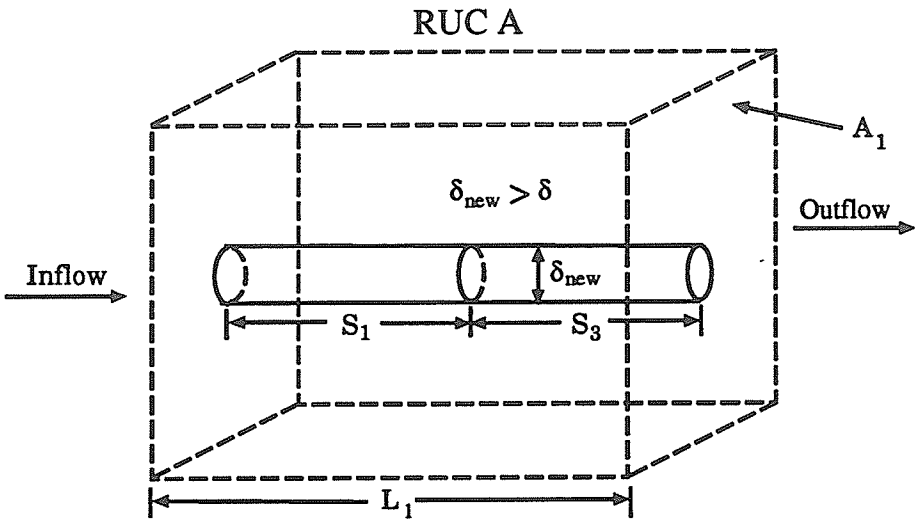

Fig. 4.4. REV A having the same external dimensions and porosity as RUC 1, with a single tube of length $S_1 + S_3$.

is always positive (no signs are associated with the f_I's). The integral expression for permeability for the RUC becomes

$$\frac{1}{k_1} = \frac{32}{\xi_1 L_1} \left(\frac{f_1 S_1 + f_5 S_5}{\delta_a^2} + \frac{f_2 S_2 + f_4 S_4}{\delta_b^2} + \frac{f_3 S_3}{\delta_c^2} \frac{|\delta_b^2 - \delta_a^2|}{\delta_c^2} \right) . \tag{4.8}$$

An identical expression results when network theory is applied to the RUC, thus confirming the validity of integral expression for permeability for RUC 2.

For large networks of tubes, it is cumbersome to validate the expression in the above manner. For such networks, the flow rates in the tubes can be calculated with the help of network theory and the viscous and pressure terms can be evaluated. With the viscous and pressure terms known, the permeability of the network can be calculated ($1/k_1 = T_v + T_p$). This permeability can then be compared to the permeability found by the direct application of network theory. Figure 4.3 shows such results for a three-dimensional RUC (inscribed in the figure). The diameters of the tubes of the RUC in the macroscopic flow direction are δ_a or δ_b and those of cross flow tubes (tubes in directions normal to the macroscopic flow direction) are

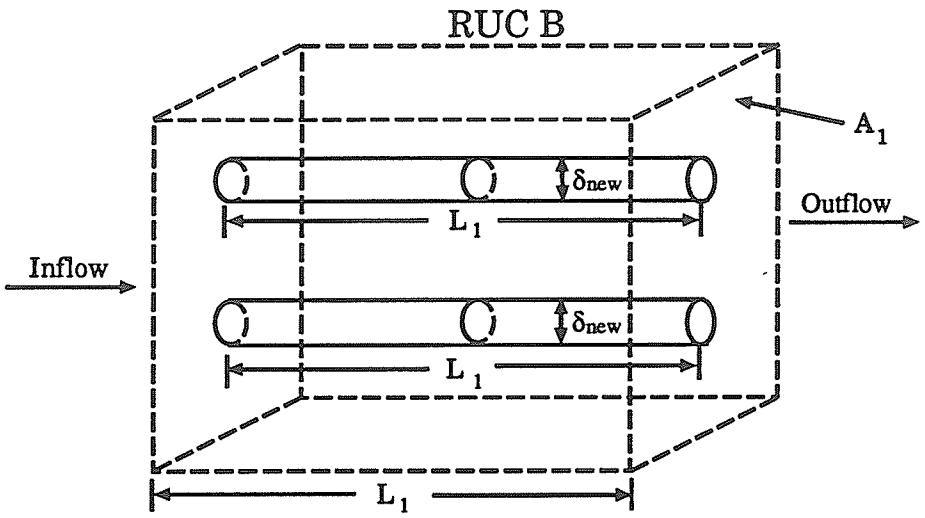

Fig. 4.5. REV B having the same external dimensions and porosity as RUC 2, with two identical tubes.

selected randomly. The diameters of cross flow tubes and δ_a are held constant whereas $0 \leq \delta_b \leq \delta_a$. The permeabilities have been scaled by k_s which is the permeability of the RUC when all tubes are of the same diameter, δ_a.

The preceding results throw some light on the physical meanings of the viscous and pressure terms. Equations (4.1) and (4.2) for RUC 1, and Equations (4.6) and (4.7) for RUC 2, show that the viscous term accounts for the fluid flow in the macroscopic flow direction and the pressure term accounts for the flow in directions normal to the macroscopic flow direction. If we compare RUC 1 to RUC A (illustrated in Figure 4.4), which has the same external dimensions and porosity as RUC 1 but consists of a single straight tube of length $S_1 + S_3$, then the decrease in permeability of RUC 1 (compared to RUC A) due to the decrease in the open cross-sectional area is taken into account by the viscous term, whereas the decrease in the permeability due to the increase in the effective length is taken into account by the pressure term. These observations are equally true when RUC 2 is compared to RUC B (illustrated in Figure 4.5), which has

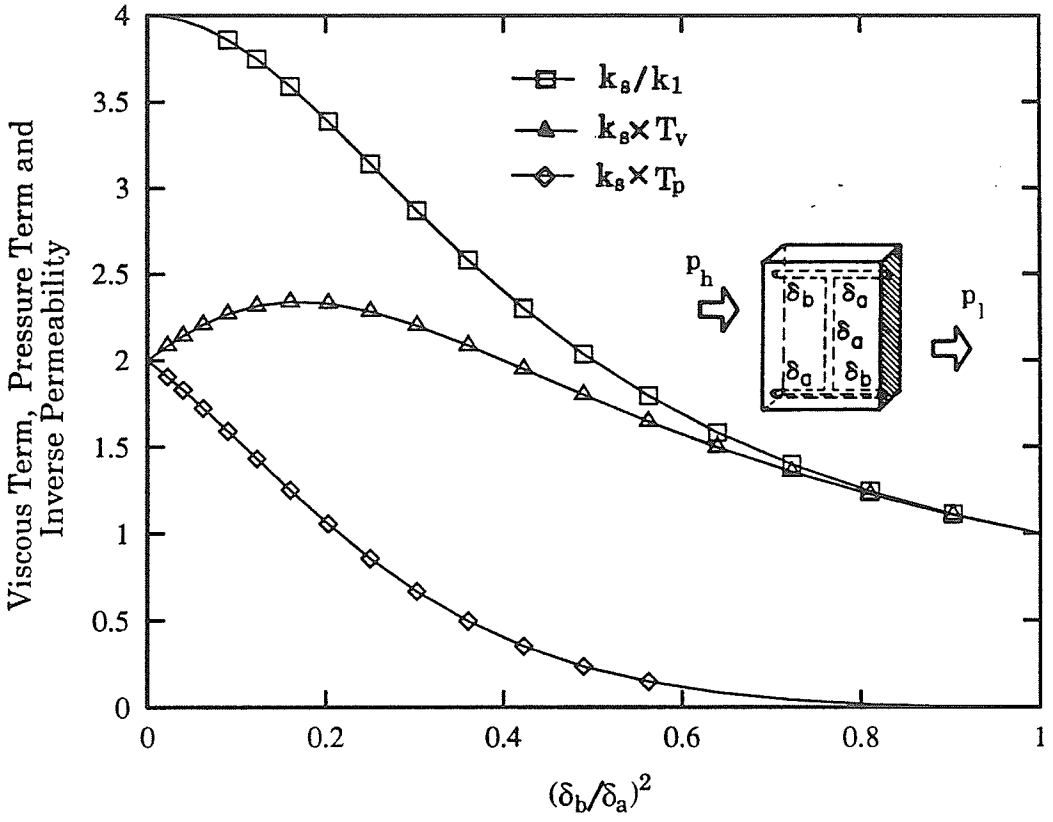

Fig. 4.6. Dependence of the viscous and pressure terms, and the inverse permeability on the ratio of tube areas (cross flow tube diameter δ_a).

the same external dimensions and porosity as RUC 2 but consists of two straight tubes with identical diameters. However, the increase in the effective length in the case of RUC 1 can be calculated from geometric considerations, but in the case of RUC 2, the increase in the effective length will depend on many factors other than physically measurable lengths. This observation is directly responsible for our inability to find an explicit expression for the macroscopic transport property of porous media known as tortuosity. This point is further discussed later in the present chapter.

For all but the limiting cases (limiting cases are when adjacent tubes in the $k = 1$ direction, that meet at a junction, have the same diameters), it may be observed from

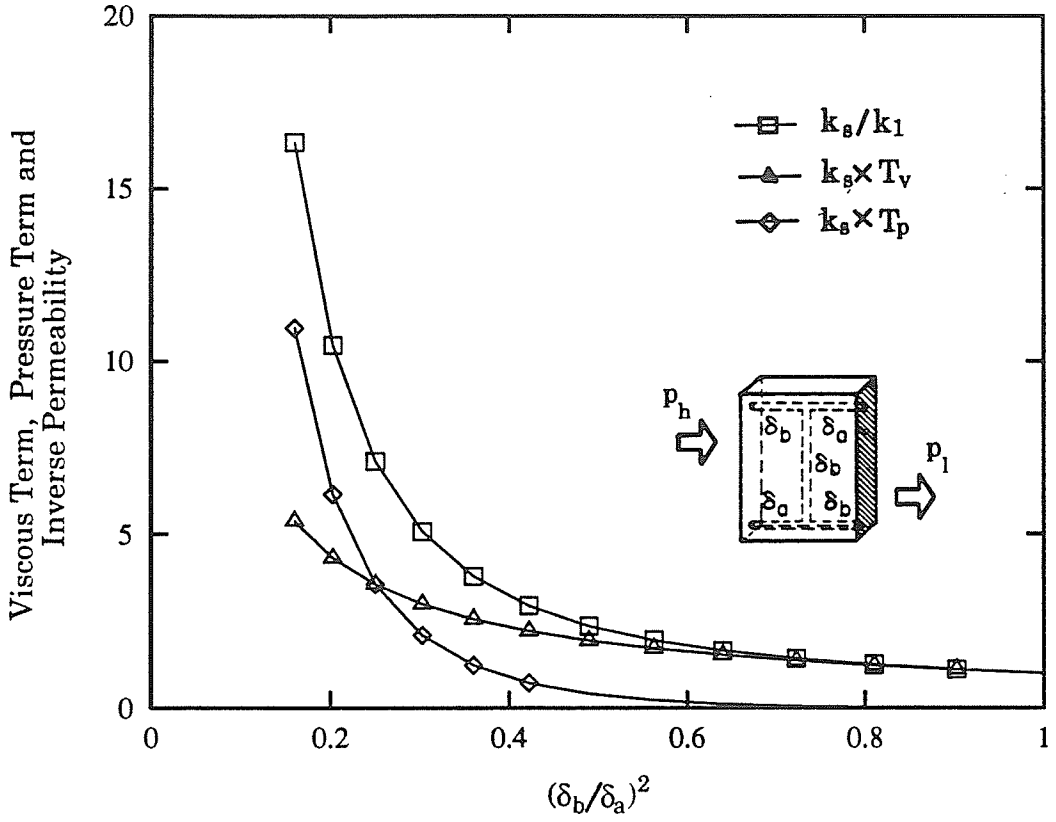

Fig. 4.7. Dependence of the viscous and pressure terms, and the inverse permeability on the ratio of tube areas (cross flow tube diameter δ_b).

Figures 4.6 through 4.8 that the diameters of the interconnecting tubes influence the permeabilities. In the limiting cases there is no cross flow; hence the diameters of the interconnecting tubes cannot have any influence. These figures also show the influence of the ratio of tube diameters on the inverse permeabilities and the terms in the integral expression for permeability. The effect of both the diameter of the interconnecting tube and the ratio of the tube areas is obvious and dramatic. In particular, it is clear from these figures that the magnitude of the pressure term is proportional to the variation of the cross-sectional areas of the tubes in the macroscopic flow direction even though it represents flow in directions normal to the macroscopic flow direction.

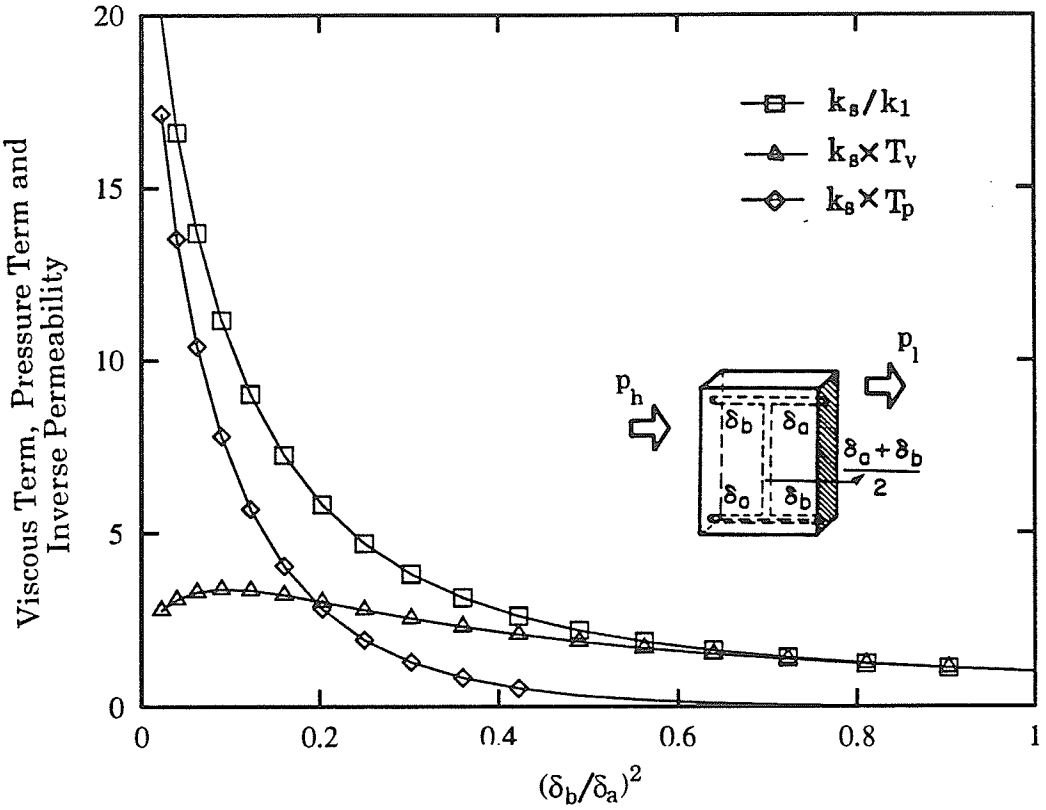

Fig. 4.8. Dependence of the viscous and pressure terms, and the inverse permeability on the ratio of tube areas (cross flow tube diameter $(\delta_a + \delta_b)/2$).

It is of interest to observe that, for $\delta_b^2 > 0.7\,\delta_a^2$, the cross flow term (pressure term) is essentially zero. This implies that the magnitude of the pressure term is very small as compared to that of the viscous term when a narrow distribution of the diameters of the tubes in the macroscopic flow direction exists.

4.2.2 Interpretation of the Integral Expression for Formation Factor

For studying the integral expression for formation factor, the current flow inside a tube saturated with an electrically conductive fluid is assumed to be governed by Ohm's law. The solid matrix is assumed to be nonconductive and the surface flow phenomena in electric double-layers are ignored.

The validity and interpretation of this expression can be carried out in a manner similar to that for the integral expression for permeability. For RUC 1, the current and potential terms simplify to

$$T_c = \frac{1}{\xi_1 L_1} \left(f_1^c S_1 + f_3^c S_3 \right), \tag{4.9}$$

$$T_e = \frac{1}{\xi_1 L_1} f_2^c S_2 \,, \tag{4.10}$$

where $f_I^c = c_I / C_1$ is the non-dimensionalized current in the Ith tube. Here c_I is the current in the Ith tube and C_1 is the bulk current in the macroscopic flow direction $k = 1$. For this RUC, $f_1^c = f_2^c = f_3^c = 1$ and therefore

$$F = \frac{1}{\xi_1 L_1} \left(S_1 + S_2 + S_3 \right). \tag{4.11}$$

If network theory is applied to this RUC, then the potentials e_h and e_l are related by

$$e_l = e_h - \frac{c_1}{g_1^c} - \frac{c_2}{g_2^c} - \frac{c_3}{g_3^c} \,, \tag{4.12}$$

where g_I^c is the electric conductance of the Ith tube saturated with an electrically conductive fluid. Because $c_1 = c_2 = c_3 = C_1$, the formation factor given by Equation (3.30) becomes

$$F = \frac{1}{\xi_1 L_1} \left(S_1 + S_2 + S_3 \right), \tag{4.13}$$

which is identical to the one given by Equation (4.11), thus confirming the validity of the integral expression for formation factor for RUC 1.

The current and potential terms for RUC 2 simplify to

$$T_c = \frac{1}{\xi_1 L_1} \left(f_1^c S_1 + f_2^c S_2 + f_4^c S_4 + f_5^c S_5 \right), \tag{4.14}$$

$$T_e = \frac{f_3^c S_3}{\xi_1 L_1} \frac{|\delta_b^2 - \delta_a^2|}{\delta_c^2} \,. \tag{4.15}$$

The reasons for the absolute sign are the same as those for the pressure term in Equation (4.7). The formation factor is given by

$$F = \frac{1}{\xi_1 L_1}(f_1^c S_1 + f_2^c S_2 + f_4^c S_4 + f_5^c S_5 + f_3^c S_3 \frac{|\delta_b^2 - \delta_a^2|}{\delta_c^2}) . \qquad (4.16)$$

An identical expression results for the formation factor if network theory is used, thereby confirming the validity of the integral expression for formation factor for RUC 2.

The validity of the expression for a three-dimensional network is demonstrated with the help of Figure 4.9. This figure compares the formation factors of the network (the same as in Figure 4.3) predicted by the integral expression for formation factor and network theory. The formation factors have been scaled by F_s which is the formation factor of the network when all the tubes are of the same diameter, δ_a. The results for the three RUC's employed in this study confirm the general validity of the integral expression for formation factor.

The physical meanings of the current and potential terms can now be discussed in the light of the preceding results. According to Equations (4.9) and (4.10) for RUC 1, the current term accounts for the current flow in the macroscopic flow direction whereas the potential term accounts for the current flow in the directions normal to the macroscopic flow direction. If we compare RUC 1 to RUC A (Figure 4.4), then for $S_1 = S_2 = S_3 = L_1/2$, the formation factor of RUC 1 is 2.25 times the formation factor of RUC A. The cross-sectional area of RUC 1 open to flow is 1/1.5 times that of RUC A and the effective length of RUC 1 is 1.5 times that of RUC A. Therefore, for the same porosity, the formation factor of RUC 1 increases by 1.5 times due to the decrease in the open cross-sectional area and by 1.5 times due to the increase in the effective flow length. The increase in the formation factor due to the decrease in the open cross-sectional area is taken into account by the current term whereas the increase due to the increase in the effective length is taken into account by the

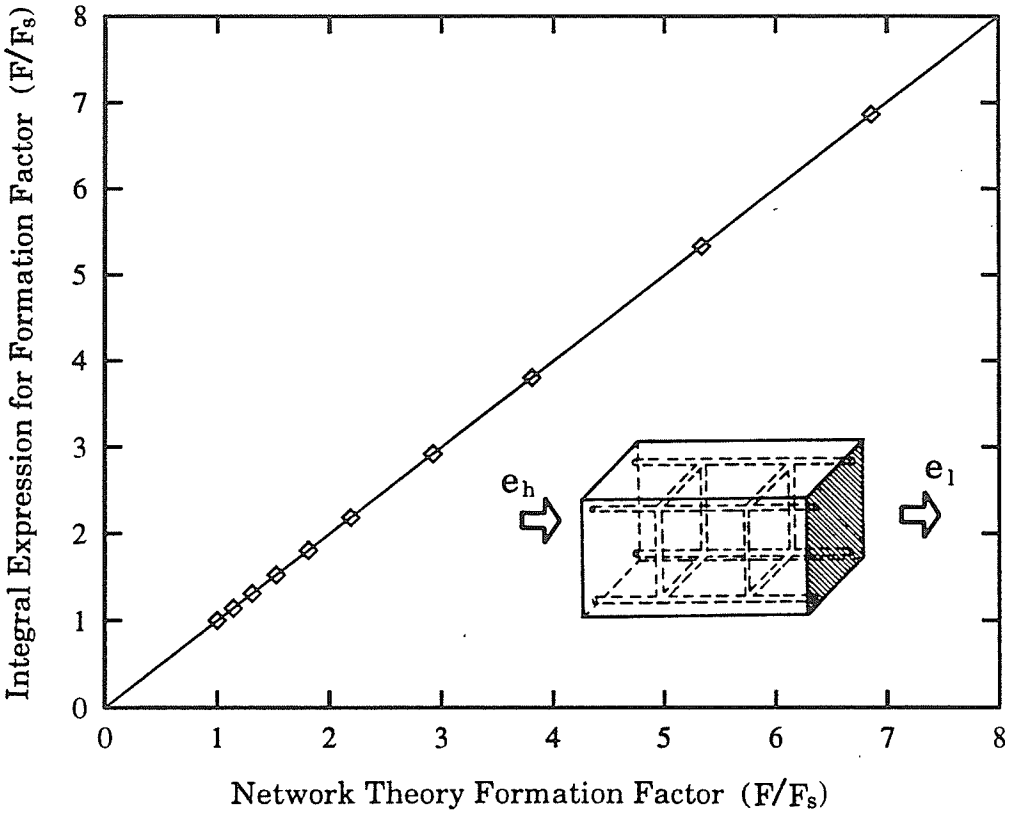

Fig. 4.9. Correlation of calculated formation factors for a three-dimensional RUC (inscribed) with constant effective open area in the macroscopic flow direction and random cross flow tube diameters (δ_a fixed, $0 \leq \delta_b \leq \delta_a$).

potential term.

In the case of RUC 2 also, the current term (Equation (4.14)) represents the current flow in the macroscopic flow direction whereas the potential term (Equation (4.15)) represents the current flow in the directions normal to the macroscopic flow direction. The increase in formation factor of RUC 2 with respect to RUC B (Figure 4.5) due to the decrease in the open cross-sectional area is taken into account by the current term and the increase due to the increase in the effective length is taken into account by the potential term. However, in this case the increase in the

effective length will depend on many factors other than the physically measurable lengths. This observation is similar to the one for fluid flow and is further discussed later in the present chapter.

As in the case of permeability, the conductances of the interconnecting tubes (tubes which are normal to the macroscopic flow direction) also have a considerable effect on the magnitudes of the formation factor, current term and potential term when the conductances of the adjacent tubes at the junctions (in the macroscopic flow direction) vary significantly.

4.2.3 Validity of Integral Expressions for Anisotropic Media

Figure 4.3 demonstrates that the integral expression for permeability predicts correct permeability even when the areosity in the other principal directions is different. For the expression to predict correct permeability, only the effective area open to flow in the macroscopic flow direction must remain constant. Therefore, the expression is also valid for anisotropic porous media. This point is further illustrated by Figures 4.10 and 4.11. These figures show correlations between the permeabilities calculated by the network theory (x-axis) and the ones predicted by the integral expression for permeability for various tube sizes (y-axis). Each figure shows two cases: one for constant effective area open to flow in the macroscopic flow direction, and the other for variable effective area open to flow in the macroscopic flow direction. Furthermore, each case has three sub-cases for δ_c ($\delta_c = \delta_a$, $\delta_c = \delta_b$ and $\delta_c = (\delta_a + \delta_b)/2$). Here also, the permeabilities have been scaled by k_s. These figures show that the expression predicts correct permeability provided the effective area open to flow in the macroscopic flow direction is constant; the results are insensitive to the values of δ_c, therefore confirming the earlier statement about anisotropic porous media. The validity of the integral expressions for formation factor and Klinkenberg permeability for anisotropic porous media can be demonstrated similarly.

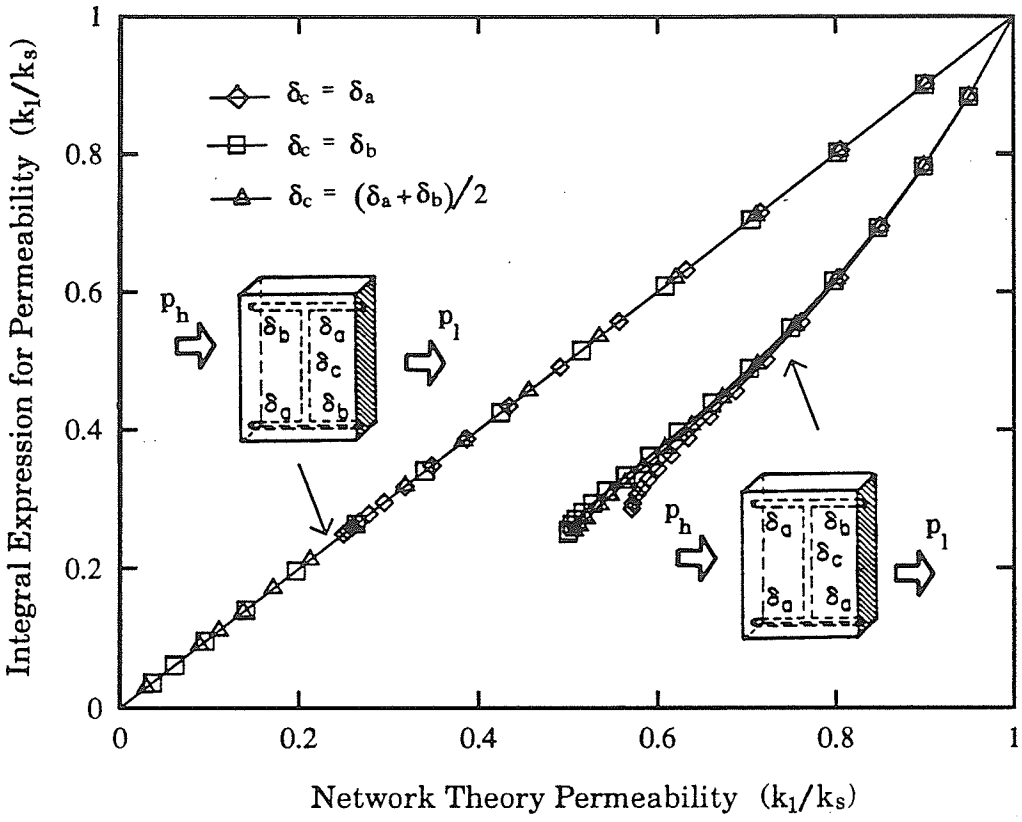

Fig. 4.10. Correlation of calculated permeabilities for equal inlet and outlet flow areas, and for total inlet flow area greater than total outlet flow area (δ_a fixed, $0 \leq \delta_b \leq \delta_a$).

4.3 Microscopic Cross Flow and Tortuosity

In this section, the relation between tortuosity and microscopic cross flow is discussed. As explained in Chapter 2, the tortuosity (hydraulic or electric) of a porous medium is defined as the ratio of "effective average path", L_e, of a fluid (or an electric) particle and the corresponding straight and shortest external distance, L_1, along the macroscopic flow direction:

$$\tau = \frac{L_e}{L_1}. \tag{4.17}$$

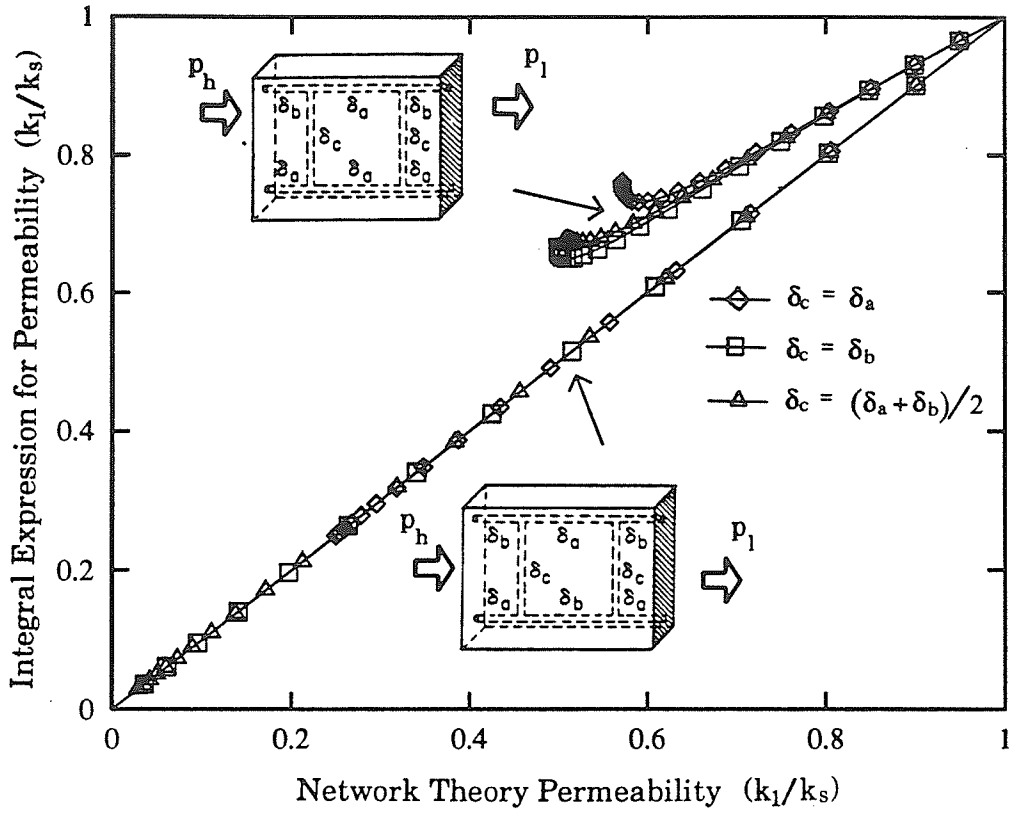

Fig. 4.11. Correlation of calculated permeabilities for constant and varying effective open area in the macroscopic flow direction (δ_a fixed, $0 \leq \delta_b \leq \delta_a$).

In some literature, tortuosity has been defined as the square of this ratio. This is just a matter of definition and the forms of the equations used to relate tortuosity to other properties such as permeability and formation factor take into account the proper power of this ratio.

Two interpretations of the effective average path are possible (Bear, 1972). When L_e is calculated by averaging the actual lengths of the flow channels — not taking into account the fact that at different times a fluid particle may travel through different channels with varying speeds — the tortuosity is a simple ratio of geometric lengths. This is the classical definition of tortuosity; in the present discussion it will be called

"type-a" tortuosity and denoted by τ_a for fluid flow and τ'_a for electric flow. In the second case, if L_e is calculated by averaging the actual distance traveled by all fluid (electric) particles passing through a particular cross section of a porous medium at a particular instant, the tortuosity is then a kinematical property. It will be called "type-b" tortuosity and denoted by τ_b for fluid flow and τ'_b for electric flow. For real porous media, the two tortuosities (type-a and type-b) are different, mainly due to the availability of multiple flow (fluid or electric) paths. This fact becomes readily evident from the following discussion.

4.3.1 Tortuosity in Fluid Flow

The classical definition of tortuosity applies to RUC 1, that is,

$$\tau_a = \frac{S_1 + S_2 + S_3}{L_1} . \tag{4.18}$$

With this substitution, Equation (4.3) for permeability reduces to

$$\frac{1}{k_1} = \frac{32}{\xi_1 \, \delta^2} \tau_a . \tag{4.19}$$

Equation (4.19) may also be expressed in terms of the flow area, $A_{\beta 1}$,

$$A_{\beta 1} = \frac{\pi \, \delta^2}{4} \tag{4.20}$$

to give

$$\frac{1}{k_1} = \frac{8\pi}{\xi_1 \, A_{\beta 1}} \tau_a . \tag{4.21}$$

For RUC 2, if the expression for permeability as given by Equation (4.8) is compared to Equation (4.21), then

$$\frac{1}{k_1} = \frac{8\pi}{\xi_1 \, A_{\beta 1}} \tau_b , \tag{4.22}$$

where

$$\tau_b = \left(\frac{f_1 \, S_1 + f_5 \, S_5}{\delta_a^2} + \frac{f_2 \, S_2 + f_4 \, S_4}{\delta_b^2} + \frac{f_3 \, S_3}{\delta_c^2} \frac{|\delta_b^2 - \delta_a^2|}{\delta_c^2} \right) \left(\frac{\delta_a^2 + \delta_b^2}{L_1} \right) . \tag{4.23}$$

The tortuosity, now of type-b, is no longer a simple ratio of lengths but depends on flow distribution (f_I), lengths of the tubes (S_I), local cross-sectional areas of the tubes (δ_I^2), and variations in the cross-sectional areas of the tubes at the junctions ($|\delta_b^2 - \delta_a^2| / \delta_c^2$).

For RUC 1, the value $\tau_a > 1$ comes from the contribution of the pressure term to permeability. The pressure term represents the microscopic cross flow (flow in Tube 2 given by Equation (4.7)), and therefore microscopic cross flow is related to the tortuosity for this RUC.

For RUC 2, the microscopic cross flow (flow in Tube 3) is also related to the tortuosity. This can be explained with the help of Figure 4.6. In this figure, non-dimensionalized permeability, viscous term and pressure term of RUC 2 (with $S_1 = S_2 = S_4 = S_5 = S_3/2 = L_1/2; \delta_c = \delta_a$) are plotted as functions of $(\delta_b/\delta_a)^2$. When $\delta_b = 0$, RUC 1 is recovered and therefore tortuosity is of type-a and is equal to 2. When $\delta_b = \delta_a$, there is no cross flow (flow in Tube 3) and the pressure term is equal to zero. For this value of δ_b, the flow is equivalent to that in straight parallel tubes and tortuosity (type-a) is equal to 1. For $0 < \delta_b < \delta_a$, the value of the tortuosity greater than 1 is due to the contribution of the pressure term to the permeability. Therefore, for RUC 2 also, microscopic cross flow is related to the tortuosity. However, there is a difference between the two cross flows. In the case of RUC 1, the fluid can take only one path, whereas, in the case of RUC 2, at each junction, the fluid can take either of the two available paths when $0 < \delta_b < \delta_a$. In the latter case, this will result in different flow rates in the two available paths. Therefore, in the presence of microscopic cross flow of the nature present in RUC 2, the classical definition of tortuosity as a simple ratio of lengths does not hold. In general, a real porous medium will possess both types of tortuosities. The type-a tortuosity will result due to the sinuousness of the individual flow channels and the type-b tortuosity will result due to the variation of the conductivities of the flow channels (in the macroscopic flow

direction) meeting at different junctions. More discussion of this point is given in Ruth and Suman (1992). The converging-diverging nature of the flow channels in real porous media will contribute to the type-a tortuosity whereas the type of pore connectivity (the average number of pores meeting at a junction) will influence the type-b tortuosity.

4.3.2 Tortuosity in Electric Flow

The observations made in Section 4.3.1 are equally true for electric flow through porous media. The classical definition applies to RUC 1, that is,

$$\tau_a' = \frac{S_1 + S_2 + S_3}{L_1}. \tag{4.24}$$

With this substitution, Equation (4.11) for formation factor reduces to

$$F = \frac{\tau_a'}{\xi_1}. \tag{4.25}$$

For RUC 2, if the expression for the formation factor given by Equation (4.16) is compared to Equation (4.25), then

$$F = \frac{\tau_b'}{\xi_1};\ \tau_b' = \frac{1}{L_1}\left(f_1 S_1 + f_2 S_2 + f_4 S_4 + f_5 S_5 + f_3 S_3 \frac{|\delta_b^2 - \delta_a^2|}{\delta_c^2}\right). \tag{4.26}$$

The tortuosity, now of type-b, is no longer a simple ratio of lengths but depends on current distribution (f_I^c), lengths (S_I) and the variations of the cross-sectional areas of the tubes at the junctions ($|\delta_b^2 - \delta_a^2|/\delta_c^2$).

For RUC 1, the value $\tau_a' > 1$ comes from the contribution of the potential term to formation factor. The potential term represents the microscopic cross flow (flow in Tube 2 given by Equation (4.10)), and therefore microscopic cross flow is related to the tortuosity for this RUC. For RUC 2 also, the microscopic cross flow (current in Tube 3) is related to the tortuosity. This can be explained with the help of Figure 4.12. In this figure T_c/F_s, T_e/F_s, F/F_s and tortuosity (Equation (4.26)) of RUC 2 (with $\delta_c = \delta_a$ and tube lengths equal to $L_1/2$) are plotted as functions of $(\delta_b/\delta_a)^2$. Here F_s

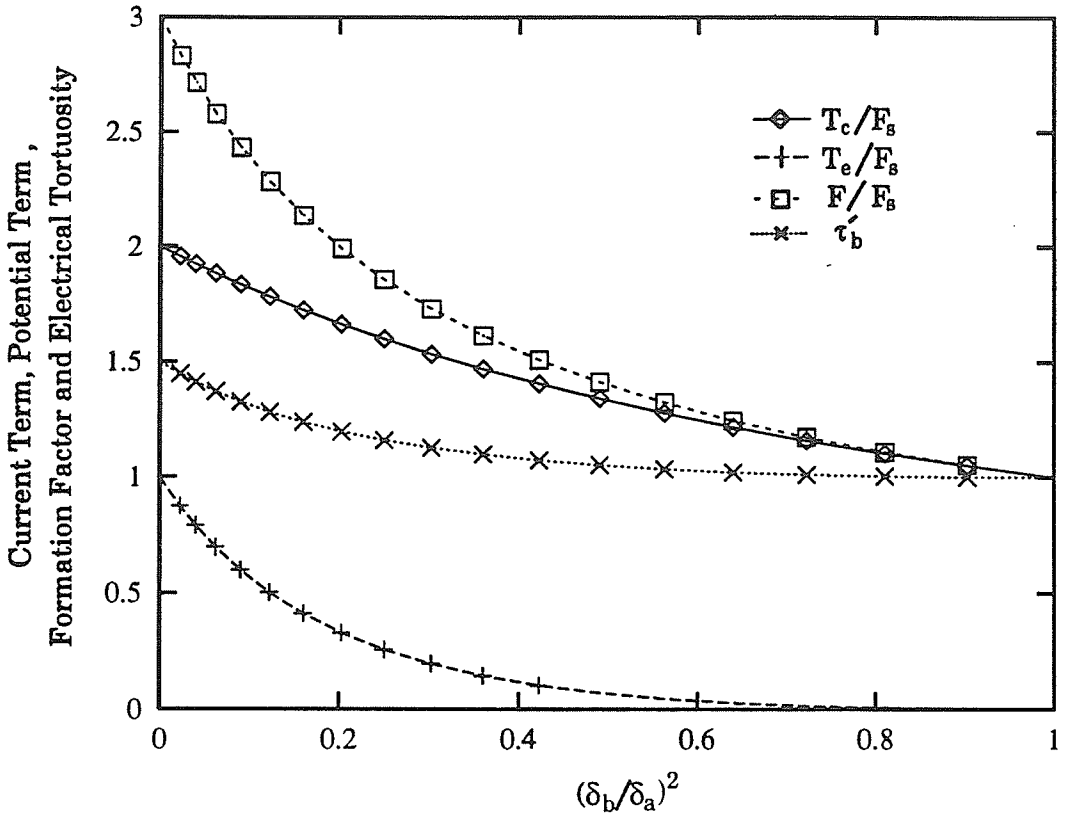

Fig. 4.12. The non-dimensionalized current term, potential term, formation factor and tortuosity ($\tau_b' = F\,\xi_1$) of RUC 2 as functions of $(\delta_b/\delta_a)^2$.

is the formation factor of RUC 2 when $\delta_b = \delta_a$. When $\delta_b = 0$, RUC 1 is recovered and the current term is twice the potential term. The tortuosity is of type-a and is equal to 1.5. When $\delta_b = \delta_a$, there is no cross flow (flow in Tube 3) and the potential term is equal to zero. For this value of δ_b, the flow is equivalent to that in straight parallel tubes and tortuosity (type-a) is equal to 1. For $0 < \delta_b < \delta_a$, the value of the tortuosity is greater than 1 due to the contribution of the potential term to the formation factor. In the case of electric flow also, there is a difference between the two cross flows. In RUC 1, the current can take only one path, whereas in RUC 2, at each junction, the current can take either of the two available paths when $0 < \delta_b < \delta_a$.

In the latter case, this will result in different magnitudes of the current in the two paths. Therefore, in the presence of microscopic cross flow of the nature present in RUC 2, the classical definition of tortuosity as a simple ratio of lengths is also not valid for electric flow.

4.4 Relation Between Formation Factor and Tortuosity

According to Wyllie and Rose (1950) and Wyllie and Spangler (1952), the resistance of a homogeneous porous medium saturated with a conductive fluid may be considered equal to the resistance of the volume of the conductive fluid of length L_e and area ϕA_1, thus relating the tortuosity and formation factor as

$$\tau'_w = F^2 \phi^2 , \tag{4.27}$$

where $\tau'_w = (L_e/L_1)^2$ represents their definition of the tortuosity. As mentioned in Section 2.4.3, Equation (4.27) is only valid for straight parallel capillary models. This inadequacy of Equation (4.27) is demonstrated below with the help of RUC 1:

The porosity of RUC 1 is

$$\phi = \frac{\pi \delta^2}{4 A_1 L_1} (S_1 + S_2 + S_3) . \tag{4.28}$$

The equation relating the resistance of the tubes to the resistance of RUC 1 is

$$\frac{R_o L_1}{A_1} = \frac{4 R_w}{\pi \delta^2} (S_1 + S_2 + S_3) , \tag{4.29}$$

and the formation factor is

$$F = \frac{R_o}{R_w} = \frac{4 A_1 (S_1 + S_2 + S_3)}{\pi L_1 \delta^2} . \tag{4.30}$$

If these values of the porosity and formation factor are substituted into Equation (4.27), one obtains

$$\tau'_w = \left(\frac{S_1 + S_2 + S_3}{L_1} \right)^4 , \tag{4.31}$$

which is only true if $S_2 = 0$, that is, the tube in RUC 1 is straight and parallel. For $S_2 > 0$, Equation (4.27) is invalid. This discrepancy has been observed by many researchers including Spearing and Matthews (1991). It can easily be traced to the value of the effective cross-sectional area open to flow in a porous medium assumed by Wyllie and co-workers while arriving at Equation (4.27). As will be shown later in this chapter, $\xi_1 A_1$ not ϕA_1, as assumed by Wyllie and co-workers, represents the effective cross-sectional area open to flow. The quantity ϕA_1 represents the average of the open areas of the planes normal to the direction $k = 1$, including those planes that intersect Tube 2. As shown in Section 3.3.1, the quantity $\xi_1 A_1$ represents the average of the effective open area of the planes normal to the direction $k = 1$ for which the flow is in the $k = 1$ direction. Tube 2 will therefore be excluded by the latter definition. The effective cross-sectional area will therefore depend on the direction of the local microscopic flow (electric or fluid). The use of the effective area, as defined in Equation (3.21), instead of the actual open area in relating the formation factor to tortuosity has also been suggested by Cornell and Katz (1953).

The equation that has generally been accepted as the right one (Barrer, 1953) relates the formation factor and tortuosity as

$$\tau'_{bar} = (F\,\phi)^{\frac{1}{2}}\,, \tag{4.32}$$

where $\tau'_{bar} = L_e/L_1$. It can be seen from Figure 4.13 that even Equation (4.32) does not predict correct results when microscopic cross of the nature present in RUC 2 exists. In this figure, the tortuosity of RUC 2 (with $\delta_c = \delta_a$ and tube lengths equal to $L_1/2$) as predicted by Equations (4.26) and (4.32) is plotted as a function of $(\delta_b/\delta_a)^2$. When $\delta_b = 0$, both the equations predict the correct value of tortuosity. For this value of δ_b, RUC 1 is recovered, and for RUC 1, Equations (4.26) and (4.32) are equivalent (e.g., one can be derived from the other by using the equation $\phi = \xi_1\,\tau'_a$, which is true for RUC 1). For $0 < \delta_b \leq \delta_a$, Equation (4.32) predicts higher values of

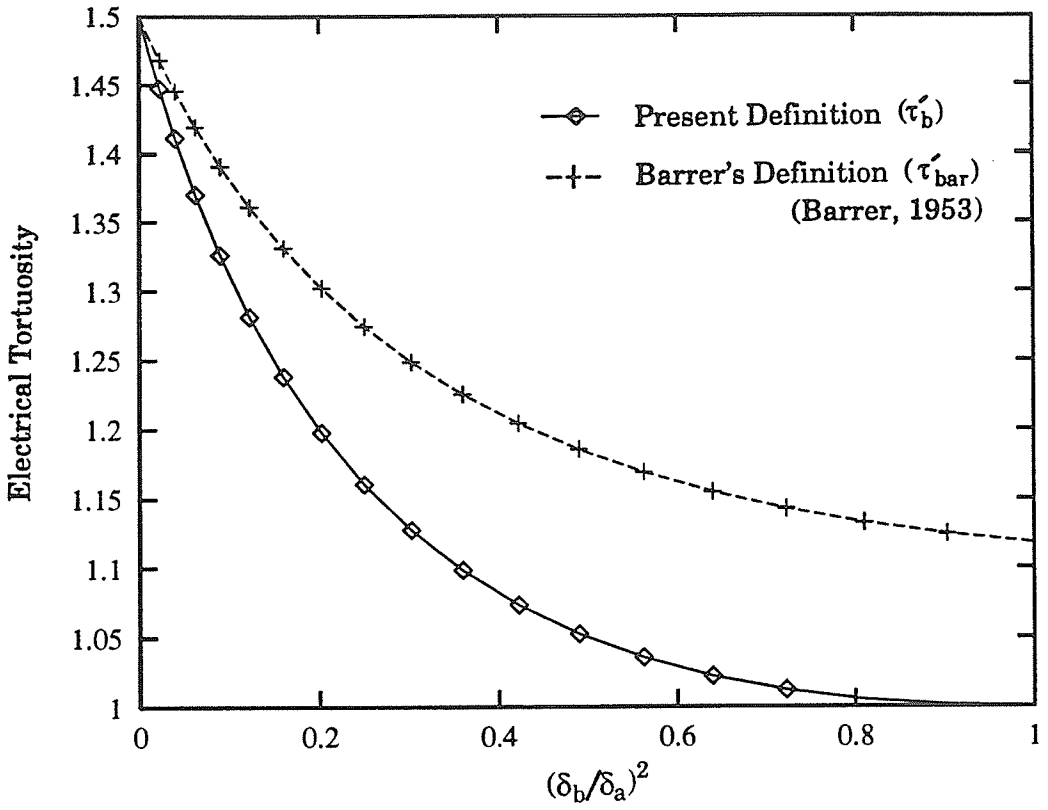

Fig. 4.13. The tortuosity of RUC 2 as a function of $(\delta_b/\delta_a)^2$, as predicted by Equation (4.26) $(\tau'_b = F\,\xi_1)$ and Equation (4.33) $(\tau'_{bar} = (F\,\phi)^{\frac{1}{2}})$.

the tortuosity than does Equation (4.26). The values predicted by Equation (4.32) for this range of δ_b are incorrect, because in the limiting case when $\delta_b = \delta_a$, the flow becomes equivalent to that in straight and parallel tubes with no cross flow (current in Tube 3), and tortuosity must be equal to 1. Equation (4.26) correctly predicts the tortuosity in this limiting case whereas Equation (4.32) does not. When $\delta_b = \delta_a$, Equation (4.32) takes Tube 3 also into account whereas in reality there is no flow through this tube for this value of δ_b. The latter fact is properly taken into account by Equation (4.26). On these grounds, Equation (4.26) in the form $\tau'_b = F\,\xi_1$ is an exact relation between the formation factor and tortuosity.

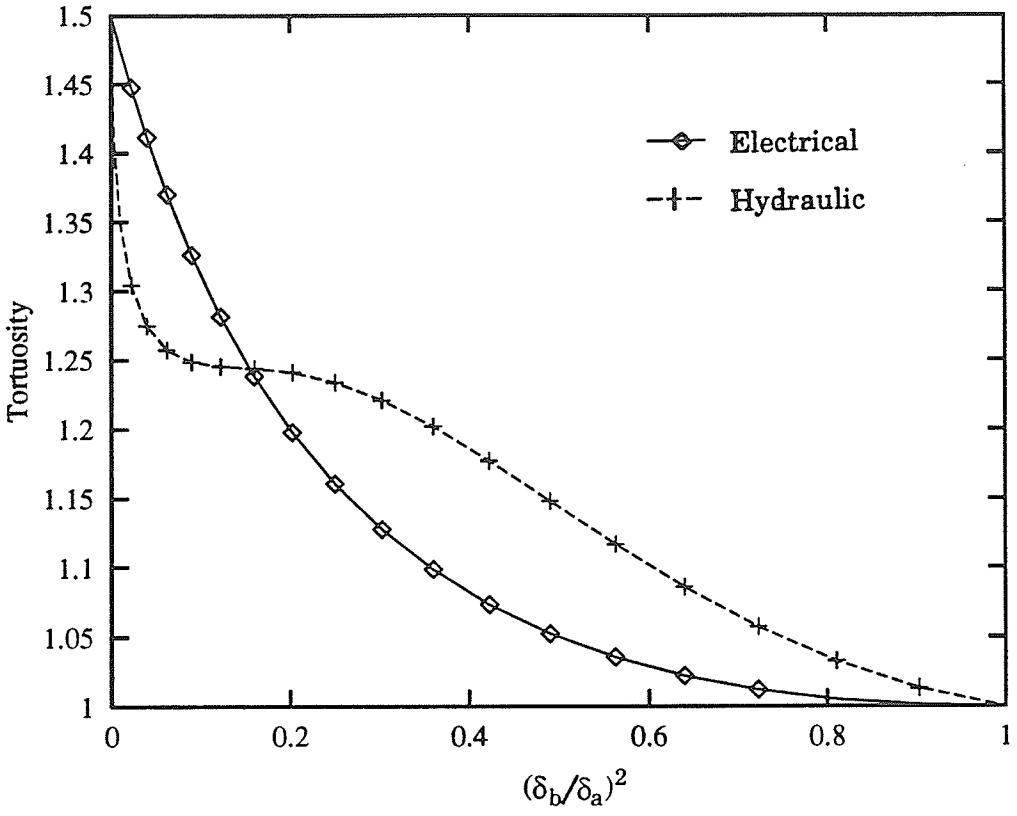

Fig. 4.14. The electric and hydraulic tortuosities of RUC 2 as predicted by $\tau_b' = F\,\xi_1$ and $\tau_h = \xi_1\, m^2/2\, k_1$, as functions of $(\delta_b/\delta_a)^2$.

4.5 Equivalence of Electric and Hydraulic Tortuosities

In the past, many attempts have been made to relate permeability and formation factor. Wyllie and Spangler (1952) proposed that the tortuosity factor in the Carman-Kozeny equation (Equation (2.5)) be determined from Equation (4.27). This argument suggests that the hydraulic and electric tortuosities are equivalent and also, that permeability and formation factor can be related. The work on this topic recently reported in the literature has been reviewed in Section 2.2.

As pointed out by Dullien (1979), the tortuosity factor in equations similar to

the Carmen-Kozeny equation will, in general, depend on the form of the equation itself. For example, tortuosity will depend on whether hydraulic mean pore radius, mean pore diameter or mean square diameter is used in Equation (2.5). Based on the discussion about areosity in the previous sections, we assume the following relation between permeability and tortuosity:

$$\frac{1}{k_1} = \frac{2}{\xi_1 m^2} \tau_h \,. \tag{4.33}$$

Equation (4.33) is equivalent to the Carman-Kozeny equation but there are some differences. Areosity has been used in place of porosity and the hydraulic tortuosity has been defined as L_e/L_1 and not $(L_e/L_1)^2$ as in the Carman-Kozeny equation. Figure 4.14 illustrates a comparison of the tortuosities predicted by Equations (4.26) and (4.33) for RUC 2 (with $\delta_c = \delta_a$ and all tube lengths equal to $L_1/2$) as functions of $(\delta_b/\delta_a)^2$. When $\delta_b = 0$, both the tortuosities are equal to 1.5 and when $\delta_b = \delta_a$ the tortuosities are equal to 1. For $0 < \delta_b < \delta_a$, the values of the two tortuosities are different. These results are to be expected. When $\delta_b = 0$, the cell equivalent to RUC 1 is recovered and only tortuosity of type-a is present. When $\delta_b = \delta_a$, the microscopic cross flow (electric or fluid) becomes zero and flow becomes equivalent to that in straight and parallel tubes. In this limiting case also, the tortuosity is of type-a. For $0 < \delta_b < \delta_a$, there is cross flow (electric and fluid in Tube 3) and tortuosity is of type-b instead of type-a. It is obvious that, in the presence of microscopic cross flow (electric or hydraulic) of the nature present in RUC 2, the previously assumed equivalence between hydraulic and electric tortuosities (Wyllie and Rose, 1950; Wyllie and Spangler, 1952) is not true. In real porous media, the equivalence is more doubtful due to the presence of other factors. For example, unlike the electric flow, the fluid flow depends on the shape of the channels, and not only on the total cross-sectional area of the channels.

4.6 Further Consideration of Areosity

As found in Chapter 3, areosity arises naturally in the expressions for permeability and formation factor. This means that average of "directed open area" represented by $\xi_1 A_1$, is more relevant in permeability and formation factor calculations than the average open area represented by ϕA_1. Areosity is a well defined property and can be readily calculated for the idealized porous media. Further discussion of this property is presented in the remainder of this section.

For RUC 1, porosity and areosity are related by:

$$\phi = \tau_a \xi_1 \ . \tag{4.34}$$

Although areosity at first appears to be the same as areal porosity, Equation (4.34) implies that there is a subtle difference. Bachmat and Bear (1986) have shown that porosity and areal porosity have the same value. Areal porosity is associated with the open area; however, as shown in Section 3.3.1, areosity is associated not only with the open area, but also with the local direction of flow, and is therefore affected by the tortuosity. It follows that constant porosity does not necessarily imply constant areosity, because tortuosity may vary in such a manner as to keep porosity constant while areosity varies. If Equation (4.34) is substituted into Equation (4.19), the result is:

$$\frac{1}{k_1} = \frac{32}{\phi \, \delta^2} \tau_a^2 \ . \tag{4.35}$$

This equation is the classic expression for permeability of a capillaric model with tortuosity (see Scheidegger, 1974). If RUC 2, illustrated in Figure 4.2 is considered, then an expression analogous to Equation (4.35) cannot be derived. However, it is of interest to consider the case when $\delta_a = \delta_b$ for this RUC. For this value of δ_b there is no cross flow and tortuosity is unity. Equation (4.19) then reduces to

$$\frac{1}{k_1} = \frac{32}{\xi_1 \, \delta^2} \ . \tag{4.36}$$

This equation disagrees with the classic expression in that areosity appears in the place of porosity. This problem has been recognized for many years, although it has never been approached before from the viewpoint of areosity. Scheidegger (1974) discusses it in the context of one-directional flow in a multi-directional porous medium. As he points out, methods of correcting the problem involve invalidation of the Dupuit-Forchheimer assumption that the mean speed of the fluid in the macroscopic flow direction, v_1, is given by

$$v_1 = \frac{Q_1}{\phi A_1} . \tag{4.37}$$

However, if areosity, defined by Equations (3.21) is used, then Dupuit-Forchheimer equation can be generalized by use of the concept of areosity to become

$$v_1 = \frac{Q_1}{\xi_1 A_1} . \tag{4.38}$$

4.7 Summary

In this chapter, validity of the integral expressions for permeability and formation factor has been demonstrated and interpretation of the terms in these expressions has been carried out with the help of three idealized porous media and network theory. In general, the expressions are valid for all porous media under the stated assumptions.

The property of the pore structure termed as "areosity", which was introduced in the previous chapter, has been further discussed. In order for the predictions of the integral expressions and the network theory to be the same, the effective area open to flow in the macroscopic flow direction must remain constant. However, it may vary in any manner in the other directions, thus confirming the validity of the expressions for anisotropic porous media also.

It has been found that the viscous and current terms represent the flow (fluid and electric) in the macroscopic flow direction whereas the pressure and potential terms

represent the flow (fluid and electric) in the directions normal to the macroscopic flow direction (microscopic cross flow). Surprisingly, the microscopic cross flow is found to depend on the variation of the conductances of the tubes in the macroscopic flow direction in addition to the conductances of the cross flow tubes themselves. The macroscopic cross flow can have a profound influence on the permeability (formation factor) in the macroscopic flow direction.

Microscopic cross flow is shown to be directly responsible for values of tortuosity exceeding one. In the presence of multiple flow paths to a fluid (electric) particle, the classical definition of tortuosity is seen to be simplistic. The study suggests two types of tortuosities, one accounting for the sinuousness of the individual flow channels and the other accounting for microscopic cross flow resulting due to the availability of multiple flow paths. The equivalence between the hydraulic and electric tortuosities is found to be invalid in the presence of microscopic cross flow in porous media with multiple flow paths.

An exact relation between formation factor, F and tortuosity, τ' of porous media, in the form $\tau' = F\,\xi_1$, has been presented. Here, ξ_1 is the areosity in the macroscopic flow direction.

CHAPTER 5

RELATIONS BETWEEN TRANSPORT PROPERTIES AND STRUCTURAL PARAMETERS OF PORE STRUCTURE MODELS

The discussion in the previous chapter was centered on very simple idealizations of pore structure. Such idealizations are very helpful for gaining a physical understanding of the transport phenomena in porous media. However, much larger and complex systems such as tube networks are required to model various flow phenomena in real porous media. Such models are considered in the present chapter. The integral expressions for permeability and formation factor are evaluated for parallel capillary, serial capillary and three-dimensional cubic network models, and the integral expression for Klinkenberg permeability is evaluated for parallel and serial capillary models. These developments result in explicit relations between the macroscopic transport properties of the models and the statistical parameters characterizing their pore space. The features of the models are discussed in Section 5.1 and the relations are developed in Section 5.2. The discussion of the results is given in Section 5.3, which also includes comparison between the predictions of the present relations and those developed by Nicholson et al. (1988), which are based on the effective-medium approximation (EMA) (Kirkpatrick, 1973).

5.1 Development of the Models

The present models are based on the conceptual model of porous media introduced by Bear and Bachmat (1966, 1967). A typical porous medium is characterized by

channels of very small cross-sectional area, and the average fluid flow and transport of other quantities through the fluid (e.g., electric charge) inside a channel is essentially in the direction of its axis. This feature is incorporated in the present models by considering a circular cylindrical tube as the basic element of pore structure. In the Bear and Bachmat model, the cross-sectional area of a channel is assumed to vary along its axis to account for the converging-diverging nature of the flow channels in real porous media. In the present models, the cross-sectional area of a tube is assumed constant along its length. This simplification makes it possible to explicitly relate the macroscopic transport properties of the models to the statistical parameters characterizing their pore space, which is not possible in the case of the Bear and Bachmat model (Van Brakel, 1975).

5.1.1 Construction of the Models

Figures 5.1 and 5.2 illustrate the important features of parallel and serial capillary models, respectively. The parallel capillary model is the simplest and consists of tubes of varying diameters and lengths running from the upstream to the downstream side of the REV. The cross-sectional area of a tube is constant along its length. In the case of the serial capillary model, a flow path running from the upstream to the downstream side of the REV consists of sections of varying diameters and lengths. However, the corresponding external macroscopic length of each section is constant, that is, the amount of tortuousness in each tube is different. Each section will be considered as a tube in this study.

The parallel and serial capillary models do not take the "networking effect" into account. The networking effect is an important feature of the pore structure that provides multiple flow paths to a fluid particle at each junction (the meeting place of two or more tubes). The importance of the networking effect can be understood in the light of the discussion of microscopic cross flow presented in the previous chap-

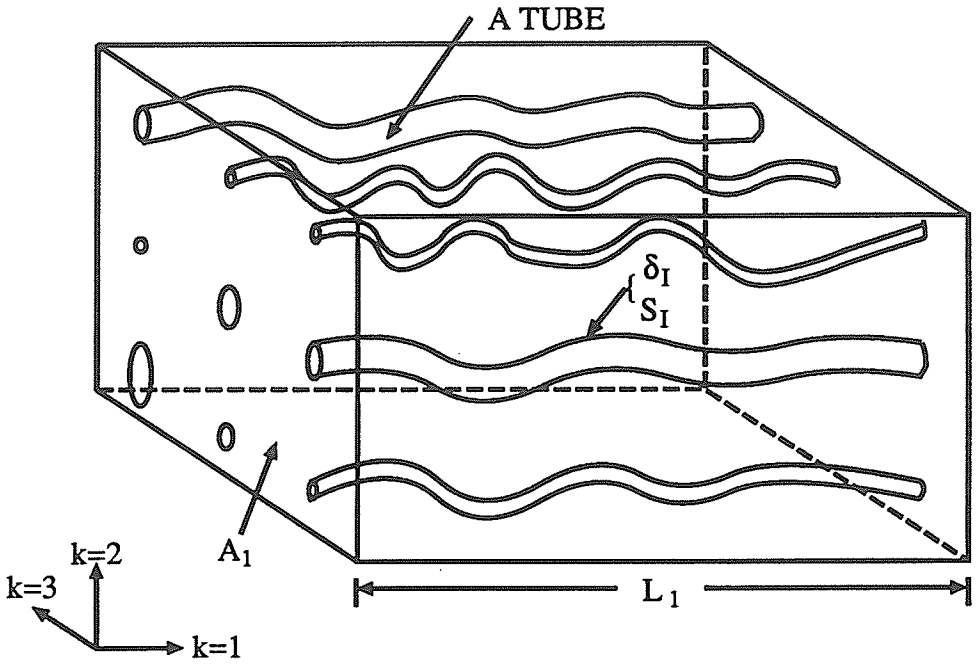

Fig. 5.1. A parallel capillary model with non-uniform tube diameters and lengths.

ter. The network models of porous media, first introduced by Fatt (1956), take such effects into account. In fact, as shown by Fatt (1956) and later commented upon by many researchers, the parallel and serial capillary models are the two extremes of the network model with coordination number equal to infinity and two, respectively. The parallel and serial capillary models, therefore, provide a valuable insight into the influence of coordination number on the properties of the models. Coordination number denotes the average number of tubes meeting at a point called the junction. It can vary between infinity and two for network models with different tube arrangements. Figure 5.3 illustrates the essential features of the three-dimensional network model considered in the present work. Such a model has a coordination number of 6.

The diameters of the tubes in the models are assumed to be distributed according to a lognormal distribution (Crow and Shimizu, 1988). The lognormal distribution has an advantage over symmetrical distributions such as uniform and normal distributions

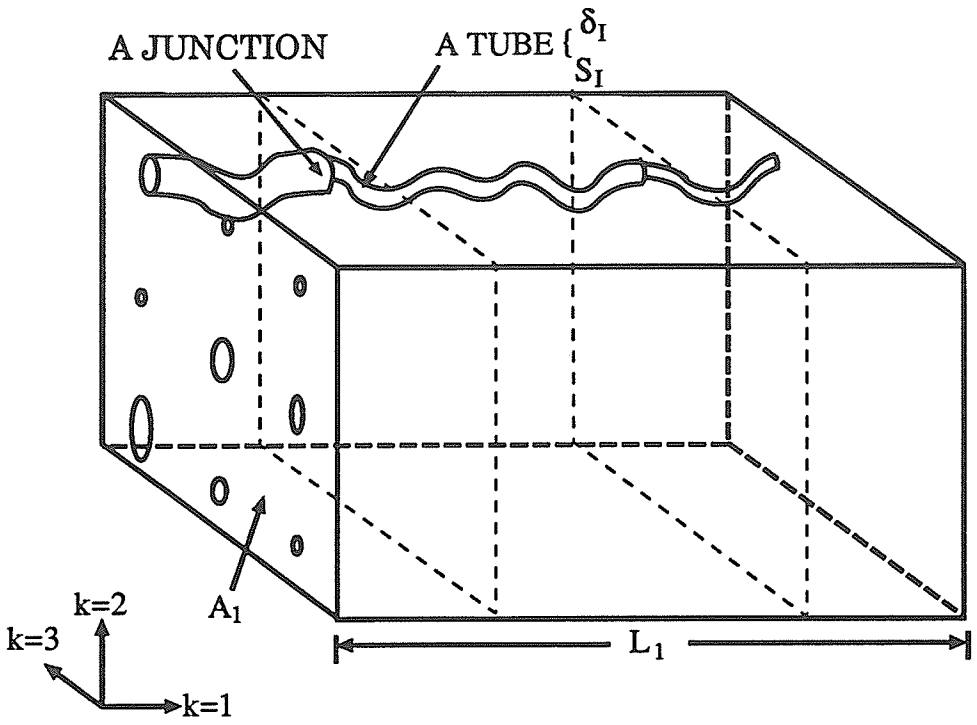

Fig. 5.2. A serial capillary model with non-uniform tube diameters and lengths. A flow path and junction are also illustrated.

because higher standard deviation to mean ratios can be employed. For example, it is known that 99.46% of the area under the normal curve lies in the range $\mu_\delta \pm 3\sigma_\delta$. Therefore, if standard deviation exceeds one-third of mean, some tube diameters will assume values less than zero, which is not acceptable. If the tubes with negative diameters are ignored or folded over to the positive side, the distribution becomes distorted. In the case of capillary models, the tube lengths are also randomly assigned according to a lognormal distribution; however, in the case of the network models, the lengths are assumed to be uniform. As commented upon by Nicholson et al. (1988), this assumption is no more arbitrary than the one by Fatt (1956) in which a relation is assumed between the tube lengths and diameters. The tubes at a junction are assumed to meet in such a manner as to not create any additional pore volume other

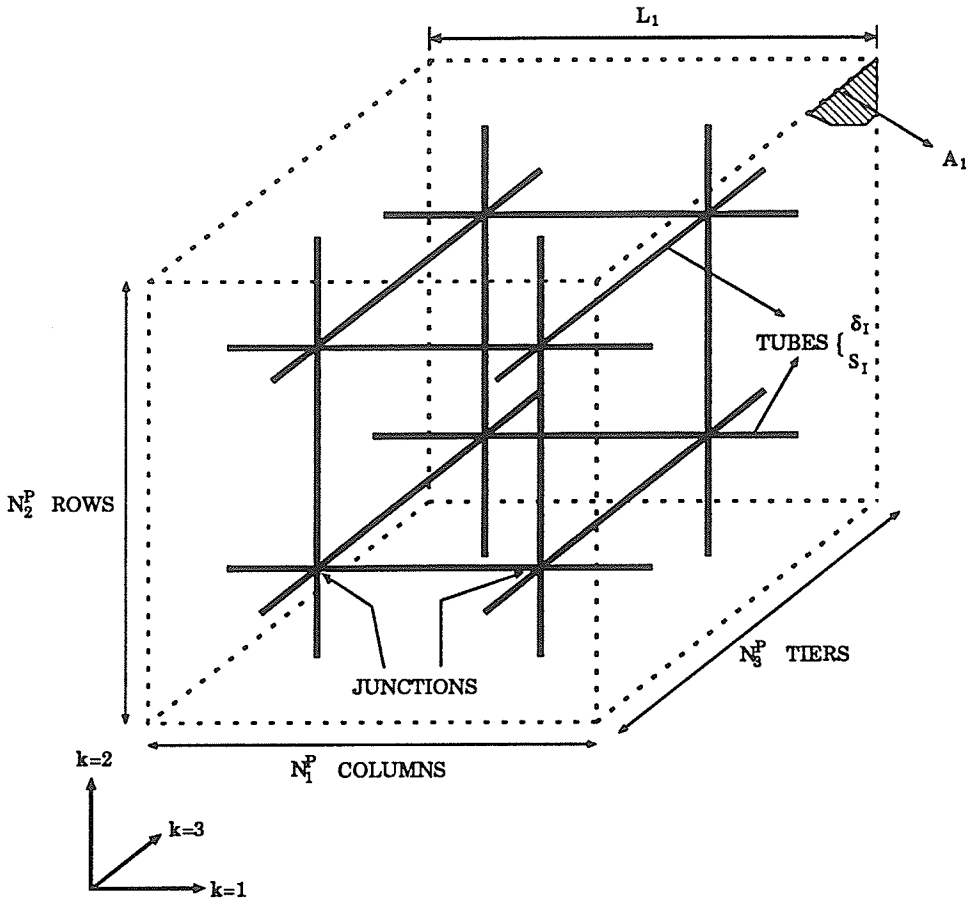

Fig. 5.3. A three-dimensional cubic network model with $N_1^P = 2$ columns, $N_2^P = 2$ rows and $N_3^P = 2$ tiers. Tubes and junctions are also shown.

than that represented by the tubes themselves, that is, the volume of the junctions is ignored.

For all the three models, $k = 1$ denotes the macroscopic flow direction, L_1 denotes the length of the REV in the $k = 1$ direction, and A_1 denotes the bulk area of the REV normal to the $k = 1$ direction. The total number of tubes in a model is denoted by N_T. The total number of flow paths in a serial capillary model running from the upstream to the downstream side is denoted by N_{ch}. Each flow path has N_P' junctions. Therefore, the total number of tubes in the serial capillary model, denoted by N_T, is equal to $N_{ch}\,(N_P' + 1)$. The sections upstream of the first junction and downstream

of the last junction are of half macroscopic length as compared to the intermediate sections (Figure 5.2). Both the parallel capillary and serial capillary models have tubes in the $k = 1$ direction only.

The network model (Figure 5.3) consists of N_3^P tiers and each tier has N_1^P columns and N_2^P rows of junctions. The total number of junctions, denoted by N_P, is equal to $N_1^P \times N_2^P \times N_3^P$ and the total number of tubes, denoted by N_T, is:

$$N_T = 3\, N_1^P\, N_2^P\, N_3^P + N_1^P\, N_2^P + N_2^P\, N_3^P + N_3^P\, N_1^P\,. \tag{5.1}$$

For given values of N_1^P, N_2^P, and N_3^P, the junctions and tubes are assigned unique global indices. As illustrated in Figure 5.3, which shows a $2 \times 2 \times 2$ network ($N_1^P = N_2^P = N_3^P = 2$), the first and last sections in all the three principal directions are of half the length of the intermediate sections. For clarity, the tubes in the figure are shown to be straight. However, the tubes used in simulations may be straight or tortuous.

All the three models in the present study are completely characterized, that is, all the macroscopic properties of the models can be expressed in terms of five pore structure parameters: N_A, τ, μ_δ, σ_δ and σ_S, where N_A is the total number of tubes in the macroscopic flow direction intersecting a plane normal to the macroscopic flow direction, per unit bulk area, and is equal to N_T/A_1 for the parallel capillary model, N_{ch}/A_1 for the serial capillary model and $N_2^P\, N_3^P/A_1$ for the network models; τ is equal to μ_S/L_1 for the parallel capillary model and $\mu_S\, N_P'/L_1$ for the serial capillary model, and $N_1^P\, \mu_S/L_1$ for the network model; μ_δ and σ_δ are the mean and standard deviation of the tube diameter distribution, respectively; and μ_S and σ_S are the mean and standard deviation of the tube length distribution, respectively.

Based on the definition given to it in Chapter 3, the areosity of the network model is defined for all the three principal directions, $k = 1, 2$ and 3. For the parallel and serial capillary models there are no tubes in the $k = 2$ and 3 directions, therefore, for

these models the areosity is not defined for these directions. For the parallel capillary model, the effective area open to flow in the macroscopic flow direction is constant, therefore the areosity in this direction may be calculated from

$$\xi_1 = \frac{\pi}{4\,A_1} \sum_{I=1}^{N_T} \delta_I^2 \,, \tag{5.2}$$

where δ_I is the diameter of the Ith tube. At any of the $(N'_P + 1)$ sections in a serial capillary model, the effective area open to flow in the macroscopic flow direction can be found from

$$A_{\beta_1}\Big|_{\text{section } I} = \frac{\pi}{4\,A_1} \sum_{J=1}^{N_{ch}} \delta_{IJ}^2 \,, \tag{5.3}$$

where δ_{IJ} is the Jth tube in the Ith section. For a network model, the effective area open to flow at any section, in any of the three principal directions, is given by

$$A_{\beta_i}\Big|_{\text{section } I} = \frac{\pi}{4\,A_i} \sum_{J=1}^{N_j^P N_k^P} \delta_{IJ}^2 \,, \tag{5.4}$$

where δ_{IJ} is the Jth tube in the Ith section in the $k = i$ direction. Here, only the cross-sectional areas of the tubes that are in the $k = i$ direction contribute to A_{β_i}. For a parallel capillary model, the effective area open to flow in the macroscopic flow direction is naturally constant. However, for the serial capillary (for the $k = 1$ direction only) and network models (for all the three directions), the number of tubes in a section has to be very large to achieve constant effective area along a particular direction. Due to the limitations on the available computer power, the following procedure was devised to achieve constant effective open area for these models.

For the serial capillary model, the area open to flow at each section, $A_{\beta 1}$, was found, and the average area open to flow was calculated by taking the mean of the open areas for all the sections. Then the diameters were reassigned according to

$$\delta_{IJ}^{\text{new}} = \sqrt{\left(\delta_{IJ}^{\text{previous}}\right)^2 A_{\beta 1}^{\text{average}} / A_{\beta 1}^{I}} \,, \tag{5.5}$$

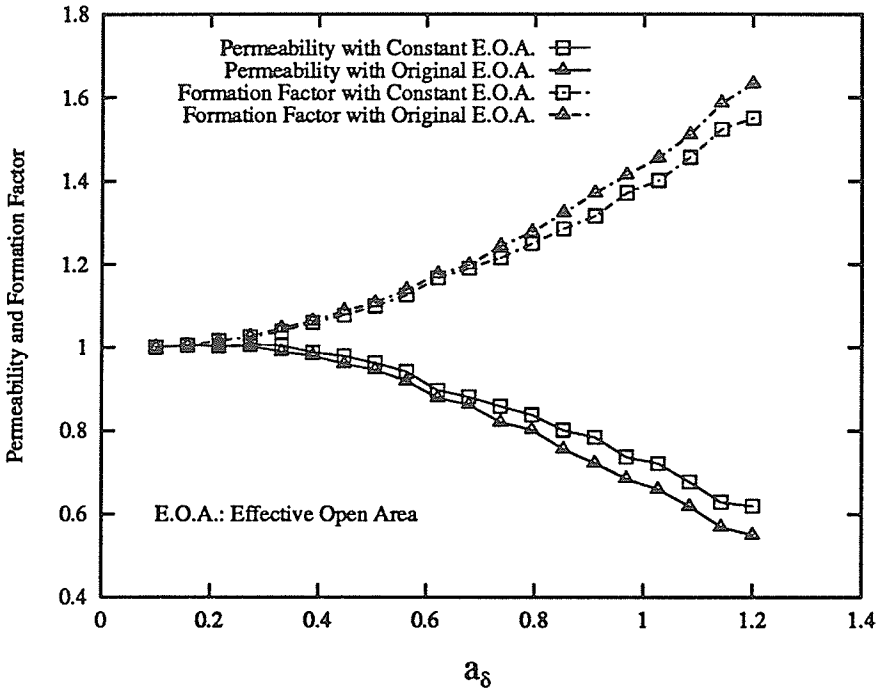

Fig. 5.4. Permeability and formation factor of network model with original effective open area at various sections and with constant effective open area (by reassigning tube diameters).

where the subscript IJ on δ denotes the Jth tube in the Ith section and the superscript I on $A_{\beta 1}$ denotes the Ith section. For network models, the same scheme was applied to achieve constant effective open area in all the three directions. However, the average open area was calculated by taking the mean of open areas in all the sections in all the three directions. This ensured constant effective open area in a particular direction as well as the same effective open area in all the three principal directions.

The effect of reassigning the tube diameters on permeability and formation factor of a $12 \times 12 \times 12$ network ($N_A = 2.4 \times 10^9\,\mathrm{m}^{-2}$, $\tau = 1.1$, $\mu_\delta = 5.32 \times 10^{-6}\,\mathrm{m}$, and $\sigma_S = 0$) as a function of $a_\delta\,(= \sigma_\delta/\mu_\delta)$ is shown in Figure 5.4. The presented data are averages of 50 realizations and are scaled by the corresponding values for a network

with reassigned tube diameters and $a_\delta = 0.1$. The permeability and formation factor were calculated by using the network theory (presented in Appendix B). The results show that the net changes in properties due to reassigning the tube diameters increase as a_δ increases. The changes are insignificant up to $a_\delta \approx 0.7$. As will be observed in Chapter 6, this is the most useful range for simulating real porous media. The maximum differences (at $a_\delta = 1.2$) between the permeabilities of the network with and without reassigning the tube diameters is 12.7%. The corresponding difference for the formation factor is 4.5%.

5.1.2 Flow Inside the Tubes of the Models

For permeability calculations, the fluid flow inside a tube is assumed to be laminar and given by Hagen-Poiseuille law. This assumption is realistic for creeping flows in which Reynolds number is $O(1)$ and inertial effects introduced by the tortuous nature of the tubes and the converging-diverging nature of the junctions are very small and therefore can be ignored. For Klinkenberg permeability calculations, the flow inside the tubes is assumed to be Hagen-Poiseuille corrected for a finite slip velocity at the solid wall. Therefore, in this case also, the inertial effects are ignored. The movement of various fluids in petroleum and water reservoirs is generally very slow, therefore these assumptions are realistic. For formation factor calculations, the solid matrix is assumed to be nonconductive and the electric conduction inside the fluid phase under a potential gradient is assumed to be ohmic only, that is, surface flow phenomena in electric double-layers are ignored. It is assumed that the junctions offer no resistance to the electric flow through the fluid in the pore space. The solid matrix is assumed to be rigid, stationary and noninteracting with the fluid which completely saturates the pore space.

5.1.3 Representativeness of the Models

For the predictions of a model to be truly representative, the size of the model should

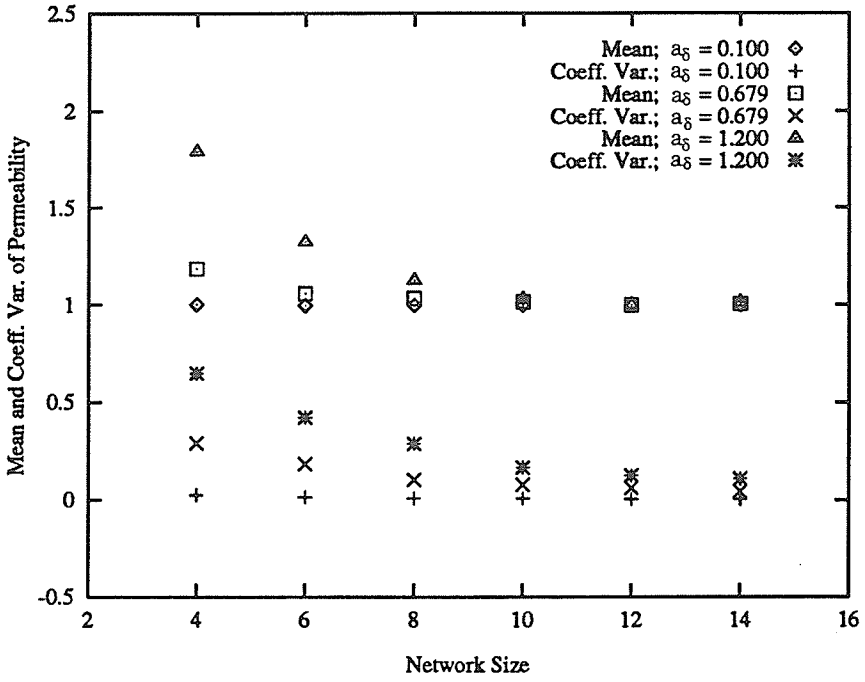

Fig. 5.5. Mean and coefficient of variation of permeability versus network size.

be sufficiently large to even out the effects introduced by the random assignment of tube diameters and lengths. In other words, the predictions of the model should be independent of its size. In terms of the concepts presented in Chapter 3, this implies that the size of the model should qualify as an REV. An REV is defined with respect to a property and its size will depend on the breadths of the tube diameter and length distributions. Therefore, an appropriate size of the model that qualifies as an REV with respect to all the properties considered and all the values of σ_δ/μ_δ and σ_S/μ_S encountered, has to be determined. In principle, an infinite size of the model will serve such a purpose. However, in practice, due to the limitations on the available computer power, the size of a model is chosen in such a way that the predictions are fairly representative for all the properties considered. The following procedure is generally adopted for this purpose: First the calculations are performed on the

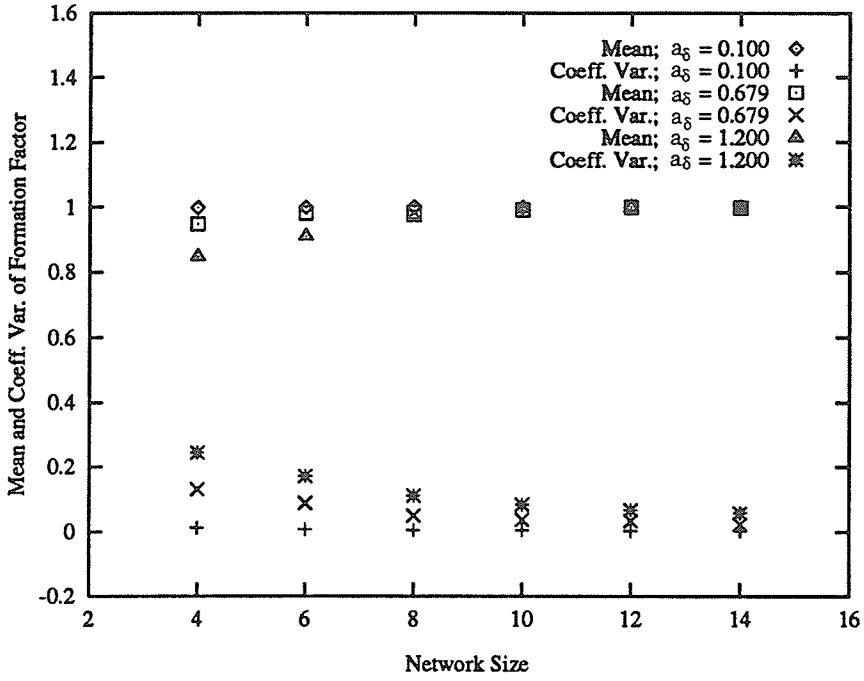

Fig. 5.6. Mean and coefficient of variation of formation factor versus network size.

model with a given number of junctions, that is, for a given size. This is called a realization. The calculations are then repeated over a large number of realizations which are generated by using different initial seeds. The final results are presented as averages of the values for the realizations. An appropriate size of the model and the number of realizations is then selected so that the errors introduced by the finite size of the model are within acceptable limits. There is a trade-off between the size of the model and the number of realizations. The property of a large network with one realization may be approximated as the mean value of a large number of realizations for a smaller network. This approximation improves as the size of the model increases (Wise, 1992).

Different combinations of the network size and the number of realizations have been reported in the literature. Bear et al. (1987) considered an $11 \times 11 \times 11$ network

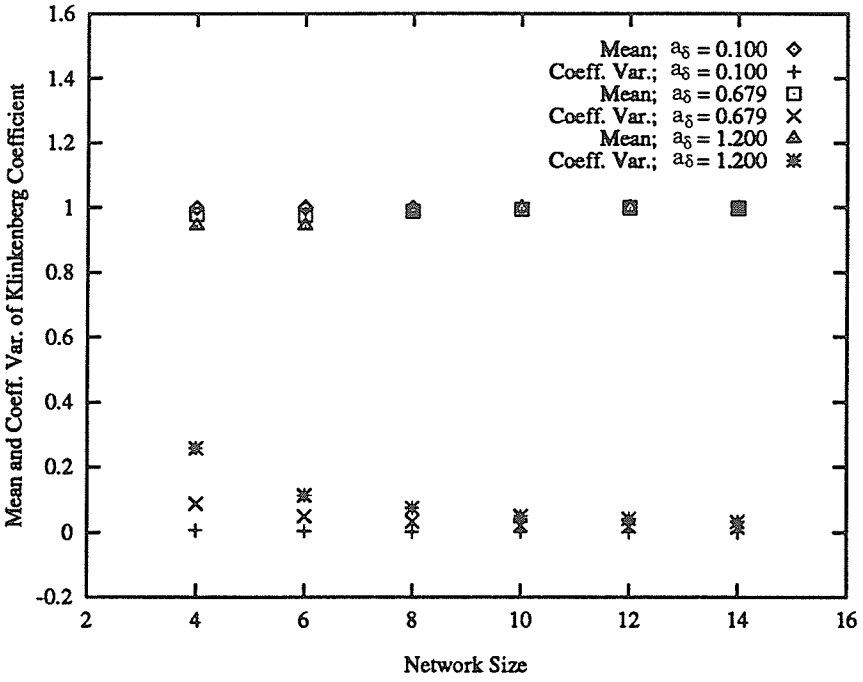

Fig. 5.7. Mean and coefficient of variation of Klinkenberg coefficient versus network size.

with 12 realizations to study the effective and relative permeabilities of anisotropic porous media. Rege and Fogler (1987) showed that a 40×40 network with one realization was satisfactory for studying straining dominated particle entrapment in porous media. Blunt and King (1991) used Delaunay triangulations for two-dimensional networks containing up to 80 000 points to study two-phase flow in porous media. Cox (1991) used $10 \times 10 \times 10$ and $20 \times 20 \times 20$ networks with 10 realizations for determining the parameters of tube diameter distribution from mercury injection measurements. Portsmouth and Gladden (1991) used a spherical network with diameter equal to 20 000 times the radius of the smallest pore for the determination of pore connectivity from mercury porosimetry. Spearing and Matthews (1991) used a $10 \times 10 \times 10$ array of cubes joined by cylinders to simulate the mercury porosimetry curve and to study tortuosity. Wise (1992) used a $15 \times 15 \times 15$ network with 1000 realizations to

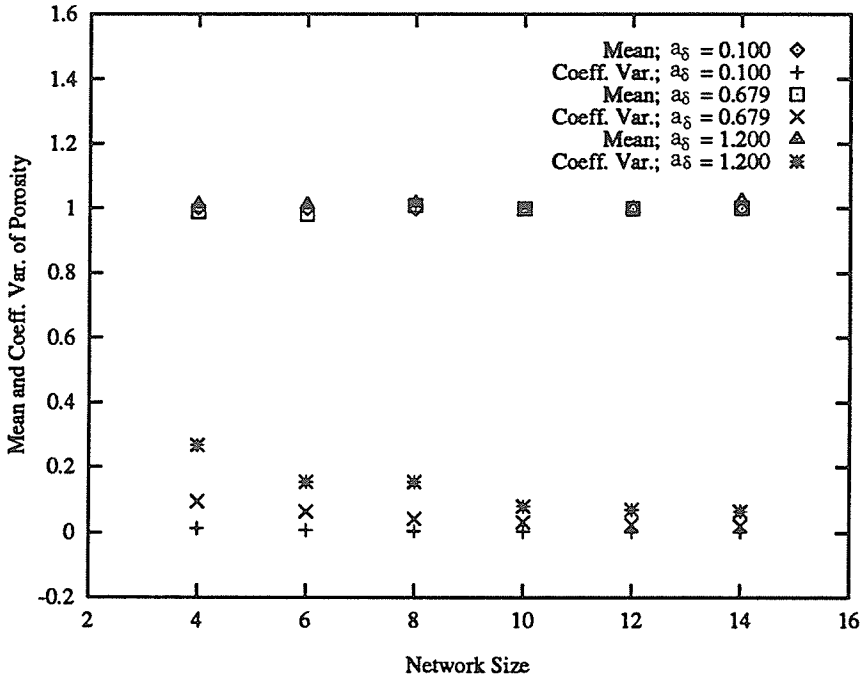

Fig. 5.8. Mean and coefficient of variation of porosity versus network size.

simulate permeability.

In the present work, the models are employed for studying permeability, formation factor, Klinkenberg permeability, porosity and drainage capillary pressure curves. Therefore, the size of a model that is a satisfactory representative with respect to all of these properties has to be found.

Figures 5.5, 5.6, 5.7 and 5.8 show the dependences of the means and coefficients of variation of permeability, formation factor, Klinkenberg coefficient and porosity of a network model ($N_A = 2.4 \times 10^9$ m^{-2}, $\tau = 1.1$, $\mu_\delta = 5.32 \times 10^{-6}$ m and $\sigma_S = 0$; lognormal distribution of tube diameters) on its size (e.g., a size of 8 denotes $8 \times 8 \times 8$ network). The means and the coefficients of variation are calculated for 50 realizations. The means for different sizes are scaled by the corresponding mean values for a $12 \times 12 \times 12$ network. For each property, the results have been presented

for three values of a_δ (= 0.1, 0.679, and 1.2). These figures illustrate that the mean values even out and the coefficients of variation decrease rapidly for all values of a_δ as the network size increases. These trends are similar to those observed by Koplik (1981, 1982), Bear et al. (1987) and Wise (1992). Therefore, using Dagan's (1989) criteria, the model is ergodic with respect to a given property if the variance of the average tends to zero. Based on these results, two more observations may be made: One, the size of the REV with respect to a given property becomes larger as a_δ increases and two, for a given value of a_δ, the size of the REV is largest for permeability followed by formation factor, Klinkenberg coefficient and porosity, in that order. Therefore, out of these four properties of a model, it is sufficient to define the size of the REV with respect to permeability only. A $12 \times 12 \times 12$ size with 50 realizations is shown to be satisfactory and in this study, this size of the network is used throughout.

A similar analysis was performed for the parallel and serial capillary models. It was found that 13 000 tubes with 100 realizations and a 750×750 size ($N_{ch} = 750$, $N'_P = 750$) with 100 realizations were satisfactory sizes for parallel and serial capillary models, respectively. The REV size of the models with respect to drainage capillary pressure curve will be determined in Chapter 6.

5.2 Development of the Relations for the Models

For the present models, the integrals in the integral expressions (Equations (3.26), (3.41) and (3.47)) can be replaced by summations. These simplifications of the expressions are performed in the next section. The simplified expressions are then evaluated for the three models in the following sections.

5.2.1 Simplification of the Integral Expressions

The integral expression for permeability is considered first. For the Hagen-Poiseuille

flow inside a cylindrical tube,

$$w_s^I = \frac{\delta_I^2}{16\,\mu}\left(1 - \frac{4\,r^2}{\delta_I^2}\right)\frac{\mathrm{d}p}{\mathrm{d}s}\,, \tag{5.6}$$

where w_s^I is the axial velocity in the Ith tube at a distance r from the axis of the tube of diameter, δ_I, p is the pressure, and s is the coordinate along the axis of the tube. Along the length of a tortuous tube, the velocity w_s^I may not be along a principal direction. However, for creeping flows, a tortuous tube with constant diameter and flow rate can be treated as a single straight tube with total length equal to the extended (straight) length (Ruth and Suman, 1992). The velocity w_s^I can therefore be taken to be along the principal direction in which the tube is aligned. The tangential and radial components of the velocity in the tube are zero for Hagen-Poiseuille flow. The radial gradient of the axial velocity inside a tube, aligned in the $k = 1$ direction, at the surface of the tube is

$$\left.\frac{\mathrm{d}w_1^I}{\mathrm{d}\,r}\right|_{\delta_I/2} = -\frac{\delta_I}{4\,\mu}\,\frac{\mathrm{d}p}{\mathrm{d}s}\,, \tag{5.7}$$

and the other gradients are zero. The viscous term, T_v, therefore, becomes

$$\begin{aligned} T_v &= -\frac{1}{\xi_1\,Q_1\,L_1}\int_{A_{\sigma\beta}}\frac{\partial w_1}{\partial\,r_j}\,n_j\,\mathrm{d}A\,, \\ &= \frac{1}{\xi_1\,Q_1\,L_1}\sum_{I=1}^{N_1^T}\int_0^{S_I}\frac{\delta_I}{4\,\mu}\frac{\mathrm{d}p}{\mathrm{d}s}\,\pi\,\delta_I\,\mathrm{d}s\,, \\ &= \frac{\pi}{4\,\xi_1\,Q_1\,L_1\,\mu}\sum_{I=1}^{N_1^T}\delta_I^2\,\Delta p_I\,, \end{aligned} \tag{5.8}$$

where Δp_I is the pressure drop across the Ith tube with length S_I, and N_1^T is the total number of tubes in the macroscopic flow direction (N_1^T is equal to N_T for the parallel and serial capillary models, and to $(N_1^P + 1)\,N_2^P\,N_3^P$ for the network model). In terms of the average flow rate, q_I, through the tube

$$T_v = \frac{32}{\xi_1\,Q_1\,L_1}\sum_{I=1}^{N_1^T}\frac{S_I}{\delta_I^2}\,q_I\,. \tag{5.9}$$

The summation in the above expression is only carried over the tubes which are aligned in the macroscopic flow direction, $k = 1$.

The pressure term, T_p, involves integration of pressure over the parts of the solid-fluid interface which are normal to the macroscopic flow direction, $k = 1$. These areas occur at the junctions where tubes of varying diameters meet. For parallel capillary models, this term is zero because there are no junctions in these models. For serial capillary and network models

$$\begin{aligned} T_p &= \frac{1}{\xi_1 Q_1 L_1 \mu} \int_{A_{\sigma\beta}} p n_1 \, \mathrm{d}A \,, \\ &= \frac{\pi}{4 \xi_1 Q_1 L_1 \mu} \sum_{I=1}^{N_P} p_I \left(\delta_{uI}^2 - \delta_{dI}^2 \right) \,, \end{aligned} \tag{5.10}$$

where p_I is the pressure at the Ith junction, and δ_{uI} and δ_{dI} are the diameters of the tubes in the $k = 1$ direction upstream and downstream of the junction. p_I is assumed to be constant over the area $\pi \left(\delta_{uI}^2 - \delta_{dI}^2 \right) / 4$. Therefore, the integral expression for permeability simplifies to

$$\frac{1}{k_1} = \frac{32}{\xi_1 Q_1 L_1} \sum_{I=1}^{N_1^T} \frac{S_I}{\delta_I^2} q_I \; + \; \frac{\pi}{4 \xi_1 Q_1 L_1 \mu} \sum_{I=1}^{N_P} p_I \left(\delta_{uI}^2 - \delta_{dI}^2 \right) \,. \tag{5.11}$$

For the Klinkenberg permeability, Hagen-Poiseuille flow corrected for a finite slip velocity, $u_\circ$, at the solid wall, is assumed inside a tube. Again, the inertial effects are ignored. The axial velocity in the Ith tube (aligned in the $k = 1$ direction) is:

$$w_1^I = \frac{\delta_I^2}{16 \mu} \left(1 - \frac{4 r^2}{\delta_I^2} \right) \frac{\mathrm{d}p}{\mathrm{d}s} + u_\circ \,. \tag{5.12}$$

For this assumption of velocity, the slip viscous term, $\overline{T_v}$, simplifies to

$$\overline{T_v} = \frac{\pi}{4 \xi_1 \overline{Q_1} L_1 \mu} \sum_{I=1}^{N_1^T} \delta_I^2 \, \Delta p_I \,. \tag{5.13}$$

The volumetric flow rate (with slip) inside a tube may be found by substituting Equation (2.32) in Equation (2.31):

$$\overline{q}_I P_m = \frac{\pi}{128 \mu} \Delta p_I p_m^I \left[\frac{\delta_I^4}{S_I} + 8 c \lambda \frac{\delta_I^3}{S_I} \right] \,, \tag{5.14}$$

where $\overline{q_I}$ is the volumetric flow rate in the tube, measured at the overall mean pressure in the REV, $P_m = (p_h + p_l)/2$, $p_m^I = (p_{Ia} + p_{Ib})/2$ (see Appendix B), c is a constant whose value is close to unity, and λ is the mean free path of the flowing gas. With the use of the above equation, the slip-viscous term becomes

$$\overline{T_v} = \frac{32}{\xi_1 \overline{Q_1} L_1} \sum_{I=1}^{N_1^T} \frac{S_I}{(\delta_I^2 + 8\, c\, \lambda\, \delta_I)} \overline{q_I} \frac{P_m}{p_m^I} \,. \tag{5.15}$$

The slip pressure term, $\overline{T_p}$, in the integral expression for Klinkenberg permeability is still given by Equation (5.10). Therefore, the final expression for the Klinkenberg permeability is:

$$\frac{1}{k_{a1}} = \frac{32}{\xi_1 \overline{Q_1} L_1} \sum_{I=1}^{N_1^T} \frac{S_I}{(\delta_I^2 + 8\, c\, \lambda\, \delta_I)} \overline{q_I} \frac{P_m}{p_m^I} + \frac{\pi}{4\, \xi_1 \overline{Q_1} L_1\, \mu} \sum_{I=1}^{N_P} p_I \left(\delta_{uI}^2 - \delta_{dI}^2\right) \,. \tag{5.16}$$

The current and potential terms in the integral expression for formation factor can be evaluated in a similar way. This leads to the following simplified expression for the formation factor:

$$F = \frac{1}{\xi_1\, C_1\, L_1} \sum_{I=1}^{N_1^T} S_I\, c_I + \frac{\pi}{4\, \xi_1\, C_1\, L_1\, R_w} \sum_{I=1}^{N_P} e_I \left(\delta_{uI}^2 - \delta_{dI}^2\right) \,. \tag{5.17}$$

Here c_I is the current in the Ith tube and e_I is the electric potential at the Ith junction.

5.2.2 Relations for the Parallel Capillary Model

For the parallel capillary model

$$Q_1 = \sum_{I=1}^{N_1^T} q_I \,, \tag{5.18}$$

$$\overline{Q_1} = \sum_{I=1}^{N_1^T} \overline{q_I} \,, \tag{5.19}$$

and

$$C_1 = \sum_{I=1}^{N_1^T} c_I \,. \tag{5.20}$$

As explained earlier, the pressure, slip-pressure and potential terms are zero for this model. With the substitution of the above equations, the expressions for permeability, Klinkenberg permeability and formation factor (Equations (5.11), (5.16) and (5.17)) reduce to

$$\frac{1}{k_1} = \frac{32}{\xi_1 L_1} \sum_{I=1}^{N_1^T} \delta_I^2 \Big/ \sum_{I=1}^{N_1^T} \frac{\delta_I^4}{S_I}\,, \tag{5.21}$$

$$\frac{1}{k_{a1}} = \frac{32}{\xi_1 L_1} \sum_{I=1}^{N_1^T} \delta_I^2 \Big/ \left[\sum_{I=1}^{N_1^T} \frac{\delta_I^4}{S_I} + 8\,c\,\lambda \sum_{I=1}^{N_1^T} \frac{\delta_I^3}{S_I}\right] \tag{5.22}$$

and

$$F = \frac{1}{\xi_1 L_1} \sum_{I=1}^{N_1^T} \delta_I^2 \Big/ \sum_{I=1}^{N_1^T} \frac{\delta_I^2}{S_I}\,. \tag{5.23}$$

For the lognormal tube diameter and length distributions, the above expressions result in the following relations:

$$\frac{1}{k_1} = \frac{32\,\tau}{\xi_1\,\mu_\delta^2} \frac{1+a_\delta^2}{B^p\,D^p}\,, \tag{5.24}$$

$$\frac{1}{k_{a1}} = \frac{32\,\tau}{\xi_1\,\mu_\delta^2} \frac{1+a_\delta^2}{(B^p + 8\,c\,\lambda/\mu_\delta\,C^p)\,D^p}\,, \tag{5.25}$$

$$b = \frac{8\,c\,\lambda\,P_m}{\mu_\delta} \frac{C^p}{B^p} \tag{5.26}$$

and

$$F = \frac{\tau}{\xi_1} \frac{1}{D^p}\,, \tag{5.27}$$

where

$$B^p = 1 + 6\,a_\delta^2 + 15\,a_\delta^4 + 20\,a_\delta^6 + 15\,a_\delta^8 + 6\,a_\delta^{10} + a_\delta^{12}\,, \tag{5.28}$$

$$C^p = 1 + 3\,a_\delta^2 + 3\,a_\delta^4 + a_\delta^6\,, \tag{5.29}$$

$$D^p = 1 + a_S^2 - \frac{3\,\tau}{\tau - 1}\, a_S^4 . \tag{5.30}$$

The detailed evaluation of the summations in Equations (5.21), (5.22) and (5.23) is presented in Appendix C. The expression for the Klinkenberg coefficient, b, has been obtained with the help of Equations (5.24), (5.25) and (2.29). The only difference between Equation (5.26) and the expression for b given by Klinkenberg (1941) (Equation (2.30)) is the factors B^p and C^p in Equation (5.26) which involve a_δ's. This is because Klinkenberg used a parallel capillary model in which all the tubes were of the same diameter and a_δ was equal to zero.

The results for three symmetrical distributions of tube diameters and lengths (uniform, normal and logistic) are also included in Appendix C.

5.2.3 Relations for the Serial Capillary Model

For the serial capillary model, Equation (5.11) for permeability may be written as

$$\frac{1}{k_1} = \frac{32}{\xi_1\, Q_1\, L_1} \sum_{I=1}^{N_{ch}} \sum_{J=1}^{N'_P+1} \frac{S_{IJ}}{\delta_{IJ}^2}\, q_{IJ} + \frac{\pi}{4\,\xi_1\, Q_1\, L_1\, \mu} \sum_{I=1}^{N_{ch}} \sum_{J=1}^{N'_P} p_{IJ} \left(\delta_{u,IJ}^2 - \delta_{d,IJ}^2\right) , \tag{5.31}$$

where N_{ch} is the total number of flow paths running from the upstream to the downstream side of the REV, $N'_P + 1$ is the number of tubes and N'_P is the number of junctions in each path. The Hagen-Poiseuille law for fluid flow inside a tube of the model is

$$q_{IJ} = \frac{\pi\, \delta_{IJ}^4}{128\, \mu\, S_{IJ}} \left(p_{IJ,a} - p_{IJ,b}\right) , \tag{5.32}$$

where $p_{IJ,a}$ and $p_{IJ,b}$ are the pressures at the upstream and downstream junctions of the Jth tube in the Ith flow path. If Equation (5.32) is substituted in Equation (5.31), then

$$\frac{1}{k_1} = \frac{\pi}{4\,\xi_1\, Q_1\, L_1\, \mu} \sum_{I=1}^{N_{ch}} \left(\delta_{I1}^2\, p_h - \delta_{I(N'_P+1)}^2\, p_l\right) , \tag{5.33}$$

where δ_{I1} and $\delta_{I(N'_P+1)}$ are the first and last tubes of the Ith flow path, respectively. If the number of flow paths in the REV is sufficiently large, the above equation simplifies to

$$\frac{1}{k_1} = \frac{\pi N_{ch} (\mu_\delta^2 + \sigma_\delta^2)}{4 \xi_1 Q_1 L_1 \mu} (p_h - p_l) . \tag{5.34}$$

The macroscopic flow rate, Q_1, can be related to the bulk pressure drop, $p_h - p_l$, by making an analogy to the flow of current in a series of conductors. The equivalent of electric resistance to the fluid flow in a tube can be found from Equation (5.32) and is given by

$$\text{Res/tube} = \frac{128 \mu S_{IJ}}{\pi \delta_{IJ}^4} , \tag{5.35}$$

and, therefore the resistance of the complete path to flow is

$$\text{Res/path} = \frac{128 \mu}{\pi} \sum_{J=1}^{N'_P+1} \frac{S_{IJ}}{\delta_{IJ}^4} . \tag{5.36}$$

If the diameters and lengths of the tubes in various paths are randomly assigned according to chosen distributions with given means and variances and also, if the number of tubes in a path is sufficiently large, then each path will tend to have the same resistance. The total resistance of the REV to the flow will therefore be

$$\text{Res/REV} = \frac{128 \mu}{\pi N_{ch}} \sum_{I=1}^{N'_P+1} \frac{S_I}{\delta_I^4} . \tag{5.37}$$

This gives the following expression for Q_1:

$$Q_1 = \frac{\pi N_{ch}}{128 \mu} (p_h - p_l) \Big/ \sum_{I=1}^{N'_P+1} \frac{S_I}{\delta_I^4} . \tag{5.38}$$

The permeability of the serial capillary model can now be found from Equations (5.34) and (5.38), and is

$$\frac{1}{k_1} = \frac{32 (\mu_\delta^2 + \sigma_\delta^2)}{\xi_1 L_1} \sum_{I=1}^{N'_P+1} \frac{S_I}{\delta_I^4} . \tag{5.39}$$

The expressions for the Klinkenberg permeability and formation factor may be found similarly. Here, only the final expressions are included:

$$\frac{1}{k_{a1}} = \frac{32\,(\mu_\delta^2 + \sigma_\delta^2)}{\xi_1\, L_1} \sum_{I=1}^{N_P'+1} \frac{S_I}{\delta_I^4 + 8\,c\,\lambda\,\delta_I^3} \frac{p_m^I}{P_m}\,, \tag{5.40}$$

$$F = \frac{(\mu_\delta^2 + \sigma_\delta^2)}{\xi_1\, L_1} \sum_{I=1}^{N_P'+1} \frac{S_I}{\delta_I^2}\,. \tag{5.41}$$

The detailed evaluation of the summations in Equations (5.39), (5.40) and (5.41) for various distributions of tube diameters and lengths is presented in Appendix D, which also includes the final results for uniform, normal and logistic distributions of tube diameters and lengths. The final results for the lognormal distributions of tube diameters and lengths are presented below:

$$\begin{aligned}\frac{1}{k_1} = \frac{32\,\tau}{\xi_1\,\mu_\delta^2} \left(1 + a_\delta^2\right) \Big(1 + 10\,a_\delta^2 + 45\,a_\delta^4 + 120\,a_\delta^6 + 210\,a_\delta^8 \\ + 252\,a_\delta^{10} + 210\,a_\delta^{12} + 120\,a_\delta^{14} + 45\,a_\delta^{16} + 10\,a_\delta^{18} + a_\delta^{20}\Big)\,,\end{aligned} \tag{5.42}$$

$$\frac{1}{k_{a1}} = \frac{32\,\tau}{\xi_1\,\mu_\delta^2} \left(1 + a_\delta^2\right) \left[\frac{1}{1 + A^s} + \frac{B^s\,C^s}{(1 + A^s)^3} - \frac{D^s\,E^s}{(1 + A^s)^4} + \frac{G^s\,H^s}{(1 + A^s)^5}\right] \tag{5.43}$$

and

$$F = \frac{\tau}{\xi_1} \left(1 + a_\delta^2\right) \left(1 + 3\,a_\delta^2 + 3\,a_\delta^4 + a_\delta^6\right)\,, \tag{5.44}$$

where

$$A^s = \frac{8\,c\,\lambda\,\mu}{\mu_\delta}\,, \tag{5.45}$$

$$B^s = a_\delta^2\,, \tag{5.46}$$

$$C^s = 10 + 15\,A^s + 6\,(A^s)^2\,, \tag{5.47}$$

$$D^s = a_\delta^6 + 3\,a_\delta^4\,, \tag{5.48}$$

$$E^s = 20 + 45\,A^s + 36\,(A^s)^2 + 10\,(A^s)^3\,, \tag{5.49}$$

$$G^s = a_\delta^{12} + 6\,a_\delta^{10} + 15\,a_\delta^8 + 16\,a_\delta^6 + 3\,a_\delta^4 \tag{5.50}$$

and

$$H^s = 35 + 105\,A^s + 126\,(A^s)^2 + 70\,(A^s)^3 + 15\,(A^s)^4\,. \tag{5.51}$$

5.2.4 Relations for the Network Model

Unlike the parallel and serial capillary models, the summations in Equations (5.11), (5.16) and (5.17) cannot be determined in closed forms for the network model. The reason for this is the availability of multiple paths for fluid and current flow at each junction in the network model. In this section, a semi-analytical approach in combination with nonlinear regression analysis is employed to evaluate the summations in Equation (5.11) for the permeability and Equation (5.17) for the formation factor of the network model.

Evaluation of the Summations in Equation (5.11) for Permeability

The viscous term, T_v, in Equation (5.11) can be re-organized as

$$T_v = \frac{32}{\xi_1\,L_1\,N_2^P\,N_3^P} \sum_{I=1}^{N_1^T} \frac{S_I}{\delta_I^2}\,f_I'\,, \tag{5.52}$$

where

$$f_I' = N_2^P\,N_3^P\,\frac{q_I}{Q_1}\,. \tag{5.53}$$

Here, f_I' is the non-dimensionalized volumetric flow rate through the Ith tube in the macroscopic flow direction, $k = 1$. Its value is equal to 1 if all the tubes in the macroscopic flow direction are of the same diameter and length, that is, possess the same hydraulic conductance.

As indicated earlier, the summation in Equation (5.52) cannot be evaluated in a closed form. This is because the flow rate f'_I in a tube depends on the position of the tube in the network in addition to its hydraulic conductance. To evaluate the summation, the following assumption, based on the Hagen-Poiseuille law, is made:

$$f'_I = A_v \frac{\delta_I^4}{S_I} , \tag{5.54}$$

where the coefficient, A_v, is assumed constant for a sufficiently large random network. With the application of Equation (5.54), Equation (5.52) becomes:

$$T_v = \frac{32\, A_v}{\xi_1\, L_1\, N_2^P\, N_3^P} \sum_{I=1}^{N_1^T} \delta_I^2 . \tag{5.55}$$

Evaluation of the summation in the above equation gives

$$T_v = \frac{32\, A_v\, N_1^T}{\xi_1\, L_1\, N_2^P\, N_3^P} \left(\mu_\delta^2 + \sigma_\delta^2\right) , \tag{5.56}$$

where N_1^T is the total number of tubes in the macroscopic flow direction, $k = 1$.

The pressure term, T_p, in Equation (5.11) is reorganized as

$$T_p = \frac{\pi}{4\,\xi_1\, L_1\, N_2^P\, N_3^P} \sum_{I=1}^{N_P} p'_I \left(\delta_{uI}^2 - \delta_{dI}^2\right) , \tag{5.57}$$

where

$$p'_I = \frac{p_I}{\mu\, Q_1 \Big/ \left(N_2^P\, N_3^P\right)} . \tag{5.58}$$

The advantages of the above reorganization are: p'_I is independent of the network size (because Q_1 has been divided by $N_2^P\, N_3^P$), pressure drop across the REV (because p_I and Q_1 are linear functions of pressure drop and the overall dependence cancels out because one is in the numerator and the other is in the denominator), and viscosity of the flowing fluid (because Q_1 is inversely proportional to μ).

p'_I can be expressed as sum of the mean pressure at the junction and a fluctuation component. The value of the fluctuation component at a junction is influenced by the

diameters and lengths of all the tubes in the network. However, the farther a tube is from a given junction, the lesser is its effect on the value of the fluctuation component at the junction. With these observations in mind, the following assumption is made:

$$p'_I = A_p \left(\delta_{uI}^2 - \delta_{dI}^2\right) + B_p\,, \tag{5.59}$$

where the coefficients A_p and B_p are assumed constant for a sufficiently large random network. Application of Equation (5.59) to Equation (5.57) leads to

$$T_p = \frac{\pi}{4\,\xi_1\,L_1\,N_2^P\,N_3^P} \sum_{I=1}^{N_P} \left[A_p \left(\delta_{uI}^2 - \delta_{dI}^2\right) + B_p\right] \left(\delta_{uI}^2 - \delta_{dI}^2\right). \tag{5.60}$$

The summation in the above equation can be replaced by a double integration to give

$$T_p = \frac{\pi}{4\,\xi_1\,L_1\,N_2^P\,N_3^P} \int_0^\infty \int_0^\infty \left[A_p \left(\delta_u^2 - \delta_d^2\right) + B_p\right] \left(\delta_u^2 - \delta_d^2\right) F_u(\delta_u)\,F_d(\delta_d)\,N_P\,\mathrm{d}\delta_u\,\mathrm{d}\delta_d\,, \tag{5.61}$$

where F_u and F_d are the probability density functions of the distributions of the tube diameters upstream and downstream of the junctions, respectively, and δ_u and δ_d are the corresponding variables of the double integration. Reorganization of Equation (5.61) leads to

$$\begin{aligned} T_p \;=\; & \frac{\pi\,N_P}{4\,\xi_1\,L_1\,N_2^P\,N_3^P} \left[\int_0^\infty \left\{\left(A_p\,\delta_u^4 + B_p\,\delta_u^2\right) F(\delta_u) \int_0^\infty F(\delta_d)\,\mathrm{d}\delta_d\right\} \mathrm{d}\delta_u \right. \\ & - \int_0^\infty \left\{\left(2\,A_p\,\delta_u^2 + B_p\right) F(\delta_u) \int_0^\infty \delta_d^2\,F(\delta_d)\,\mathrm{d}\delta_d\right\} \mathrm{d}\delta_u \\ & \left. + \int_0^\infty \left\{A_p\,F(\delta_u) \int_0^\infty \delta_d^4\,F(\delta_d)\,\mathrm{d}\delta_d\right\} \mathrm{d}\delta_u\right]. \end{aligned} \tag{5.62}$$

In the above equation the limits on the inner integrals are not functions of the variables of the corresponding outer integrals, therefore

$$\begin{aligned} T_p \;=\; & \frac{\pi\,N_P}{4\,\xi_1\,L_1\,N_2^P\,N_3^P} \left[I_{d1} \int_0^\infty \left(A_p\,\delta_u^4 + B_p\,\delta_u^2\right) F(\delta_u)\,\mathrm{d}\delta_u \right. \\ & - I_{d2} \int_0^\infty \left(2\,A_p\,\delta_u^2 + B_p\right) F(\delta_u)\,\mathrm{d}\delta_u \\ & \left. + I_{d3} \int_0^\infty A_p\,F(\delta_u)\,\mathrm{d}\delta_u\right], \end{aligned} \tag{5.63}$$

where

$$I_{d1} = \int_0^\infty F(\delta_d)\, \mathrm{d}\delta_d\,, \tag{5.64}$$

$$I_{d2} = \int_0^\infty \delta_d^2\, F(\delta_d)\, \mathrm{d}\delta_d\,, \tag{5.65}$$

$$I_{d3} = \int_0^\infty \delta_d^4\, F(\delta_d)\, \mathrm{d}\delta_d\,. \tag{5.66}$$

Equation (5.63) may be rearranged to give

$$\begin{aligned} T_p \;=\; & \frac{\pi\, N_P}{4\,\xi_1\, L_1\, N_2^P\, N_3^P} \Big[\big(A_p\, I_{d3} \,-\, B_p\, I_{d2}\big)\, I_{u1} \\ & + \big(B_p\, I_{d1} \,-\, 2\, A_p\, I_{d2}\big)\, I_{u2} \,+\, A_p\, I_{d1}\, I_{u3} \Big]\,, \end{aligned} \tag{5.67}$$

where

$$I_{u1} = \int_0^\infty F(\delta_u)\, \mathrm{d}\delta_u\,, \tag{5.68}$$

$$I_{u2} = \int_0^\infty \delta_u^2\, F(\delta_u)\, \mathrm{d}\delta_u\,, \tag{5.69}$$

$$I_{u3} = \int_0^\infty \delta_u^4\, F(\delta_u)\, \mathrm{d}\delta_u\,. \tag{5.70}$$

The tubes upstream and downstream of the junctions possess the same distribution, therefore

$$I_{u1} = I_{d1} = I_1\,; \quad I_{u2} = I_{d2} = I_2\,; \quad I_{u3} = I_{d3} = I_3\,, \tag{5.71}$$

and

$$T_p = \frac{\pi\, N_P\, A_p}{2\,\xi_1\, L_1\, N_2^P\, N_3^P}\, (I_3\, I_1 \,-\, I_2^2)\,. \tag{5.72}$$

Irrespective of the tube diameter distribution function, $F(\delta)$,

$$I_1 = \int_0^\infty F(\delta)\, \mathrm{d}\delta = 1\,, \tag{5.73}$$

$$I_2 = \int_0^\infty \delta^2 F(\delta)\, \mathrm{d}\delta = \mu_\delta^2 + \sigma_\delta^2 . \tag{5.74}$$

The value of I_3 is different for different tube diameter distributions. Here, only the results for the lognormal distribution are presented (Crow and Shimizu, 1988):

$$\begin{aligned} I_3 &= \int_0^\infty \delta^4 F(\delta)\, \mathrm{d}\delta \\ &= \mu_\delta^4 \left(1 + 6\,a_\delta^2 + 15\,a_\delta^4 + 20\,a_\delta^6 + 15\,a_\delta^8 + 6\,a_\delta^{10} + a_\delta^{12}\right). \end{aligned} \tag{5.75}$$

With the application of Equations (5.73), (5.74) and (5.75), Equation (5.72) becomes

$$T_p = \frac{\pi\, N_P\, A_p\, \mu_\delta^4}{2\,\xi_1\, L_1\, N_2^P\, N_3^P} \left(4\,a_\delta^2 + 14\,a_\delta^4 + 20\,a_\delta^6 + 15\,a_\delta^8 + 6\,a_\delta^{10} + a_\delta^{12}\right). \tag{5.76}$$

Evaluation of the Summations in Equation (5.17) for Formation Factor

For deriving an explicit relation between the formation factor and the statistical parameters of the network model, an approach similar to the one for the permeability is adopted. The current term, T_c, in Equation (5.17) is rearranged as

$$T_c = \frac{1}{\xi_1\, L_1\, N_2^P\, N_3^P} \sum_{I=1}^{N_1^T} S_I\, f_I^{c\prime}\,, \tag{5.77}$$

where

$$f_I^{c\prime} = N_2^P\, N_3^P\, \frac{c_I}{C_1}\,. \tag{5.78}$$

Here $f_I^{c\prime}$ is the non-dimensionalized current in the Ith tube in the macroscopic flow direction, $k = 1$. Like the non-dimensionalized flow rate f_I', its value is equal to 1 if all the tubes in the macroscopic flow direction possess the same electric conductivity. In order to evaluate the summation in Equation (5.77), the following assumption, based on Ohm's law of current flow, is made:

$$f_I^{c\prime} = A_c \frac{\delta_I^2}{S_I}\,. \tag{5.79}$$

The network is assumed to be random and sufficiently large so that A_c may be considered constant. The application of Equation (5.79) to Equation (5.77) results in

$$T_c = \frac{A_c}{\xi_1 L_1 N_2^P N_3^P} \sum_{I=1}^{N_1^T} \delta_I^2 , \tag{5.80}$$

which, irrespective of the chosen tube diameter distribution is

$$T_c = \frac{A_c N_1^T}{\xi_1 L_1 N_2^P N_3^P} \left(\mu_\delta^2 + \sigma_\delta^2\right) . \tag{5.81}$$

The potential term, T_e, in Equation (5.17) is rearranged to give

$$T_e = \frac{\pi}{4 \xi_1 C_1 L_1 R_w} \sum_{I=1}^{N_P} e'_I \left(\delta_{uI}^2 - \delta_{dI}^2\right) , \tag{5.82}$$

where

$$e'_I = \frac{e_I}{R_w C_1/(N_2^P N_3^P)} . \tag{5.83}$$

The advantages of the above substitution are the same as those for the pressure term in Equation (5.58). Based on the arguments presented for the pressure term, the following assumption is made:

$$e'_I = A_e \left(\delta_{uI}^2 - \delta_{dI}^2\right) + B_e . \tag{5.84}$$

This results in the following expression for the potential term:

$$T_e = \frac{\pi N_P A_e}{2 \xi_1 L_1 N_P^2 N_3^P} \left(I_3 I_1 - I_2^2\right) . \tag{5.85}$$

The values of the integrals I_1, I_2 and I_3 for the lognormal tube diameter distribution have already been presented in Equations (5.73), (5.74) and (5.75), respectively. Therefore for lognormal distribution of tube diameters

$$T_e = \frac{\pi N_P A_e \mu_\delta^4}{2 \xi_1 L_1 N_2^P N_3^P} \left(4 a_\delta^2 + 14 a_\delta^4 + 20 a_\delta^6 + 15 a_\delta^8 + 6 a_\delta^{10} + a_\delta^{12}\right) . \tag{5.86}$$

The relations between the coefficients A_v, A_p, A_c and A_e (in Equations (5.56), (5.76), (5.81) and (5.86), respectively) and the statistical parameters have to be determined. This is accomplished in the following section.

Determination of Expressions for the Coefficients A_v, A_p, A_c and A_e

Nonlinear regression was employed to find the expressions for the coefficients A_v, A_p, A_c and A_e in terms of the statistical parameters of the network. Simulations of a $12 \times 12 \times 12$, three-dimensional cubic network for fifty equally spaced values of σ_δ between 0 and $1.2\,\mu_\delta$ were generated on a SUN SPARC station 2 . The other parameters of the network were: $N_A = 2.4 \times 10^9$ m^{-2}, $\tau = 1.1$, and $\mu_\delta = 5.32 \times 10^{-6}$ m. The tube lengths were kept constant and the tube diameters were randomly assigned according to the lognormal distribution. The network possessed constant effective open area in a particular principal direction and the same effective open area in all the three principal directions. This was achieved by reassigning the tube diameters as explained in Section 5.1.1.

For a given value of σ_δ, the pressures and electric potentials at the junctions were calculated by using the network theory (presented in Appendix B). The fluid flow rates and electric currents in the tubes were then computed and the values of T_v, T_p, T_c and T_e were found from the following expressions (Equations (5.11) and (5.17)):

$$T_v = \frac{32}{\xi_1 \, Q_1 \, L_1} \sum_{I=1}^{N_1^T} \frac{S_I}{\delta_I^2} \, q_I \, , \tag{5.87}$$

$$T_p = \frac{\pi}{4 \, \xi_1 \, Q_1 \, L_1 \, \mu} \sum_{I=1}^{N_P} p_I \left(\delta_{uI}^2 - \delta_{dI}^2 \right) \, , \tag{5.88}$$

$$T_c = \frac{1}{\xi_1 \, C_1 \, L_1} \sum_{I=1}^{N_1^T} S_I \, c_I \tag{5.89}$$

and

$$T_e = \frac{\pi}{4 \, \xi_1 \, C_1 \, L_1 \, R_w} \sum_{I=1}^{N_P} e_I \left(\delta_{uI}^2 - \delta_{dI}^2 \right) \, . \tag{5.90}$$

For each value of σ_δ, fifty realizations were generated and the values of the terms were presented as averages of these fifty values. With the values of the four terms

corresponding to the 50 values of σ_δ known, the values of the coefficients, A_v, A_p, A_c and A_e for each value of σ_δ, were determined from Equations (5.56), (5.76), (5.81) and (5.86), respectively.

Using SAS software, nonlinear regression was employed to fit various empirical models to the values of the coefficients. The models tried for each coefficient and the corresponding fitting parameters are summarized in Appendix E. Based on the criterion of minimum residue, following are the expressions chosen for the coefficients:

$$A_v = \frac{\mu_S}{\mu_\delta^4} \frac{1}{1 + 3.07\,a_\delta^2 - 2.86\,a_\delta^4 + 3.99\,a_\delta^6 - 2.80\,a_\delta^6 + 0.729\,a_\delta^{10}}, \tag{5.91}$$

$$A_p = \frac{13.83\,\mu_S}{\mu_\delta^6} \frac{1 + a_\delta^2}{1 + 6.37\,a_\delta^2 + 16.40\,a_\delta^4 - 6.75\,a_\delta^6 + 30.46\,a_\delta^6 - 9.19\,a_\delta^{10}}, \tag{5.92}$$

$$A_c = \frac{\mu_S}{\mu_\delta^2} \frac{1}{1 + a_\delta^2} \tag{5.93}$$

and

$$A_e = \frac{0.2171\,\mu_S}{\mu_\delta^4} \frac{1 + a_\delta^2}{1 + 3.61\,a_\delta^2 + 10.96\,a_\delta^4 - 6.90\,a_\delta^6 + 19.77\,a_\delta^6 - 5.49\,a_\delta^{10}}. \tag{5.94}$$

Finally, the relations between the permeability and formation factor and the statistical parameters of the network can be expressed as

$$\frac{1}{k_1} = \frac{32\,\tau}{\xi_1 \mu_\delta^2} Z^{k_1}(a_\delta), \tag{5.95}$$

$$F = \frac{\tau}{\xi_1} Z^F(a_\delta), \tag{5.96}$$

where Z^{k_1} and Z^F are functions of a_δ and are given in Appendix E. When a_δ is equal to zero, both the functions are equal to 1 and the above relations for the permeability and the formation factor reduce to the corresponding relations for the parallel capillary model with uniform tube diameters and lengths.

5.3 Discussion of the Results

In this section, first the relations developed in the present chapter are studied and then a comparison is made between the predictions of these relations and similar relations based on the effective-medium approximation (Nicholson et al., 1988).

5.3.1 Present Results

Figures 5.9 and 5.10 show the predicted and observed permeabilities and formation factors of a parallel capillary model as functions of a_δ, respectively. Here, the observed values refer to the ones found with the help of the network theory (Appendix B) and the predicted values refer to the ones predicted by the relations developed in the present chapter (i.e., Equation (5.24) for the permeabilities and Equation (5.27) for the formation factors). The model consists of 13 000 tubes with $N_A = 6.0 \times 10^9$ m^{-2}, $\tau = 2.165$, and $\mu_\delta = 5.0 \times 10^{-6}$ m. Figures 5.11 and 5.12 show similar results for a serial capillary model. Here also, the predicted values refer to the ones predicted by the relations developed in the present chapter (i.e., Equation (5.39) for the permeabilities and Equation (5.41) for the formation factors). The model consists of 750 flow paths and each path has 750 tubes in it. The other properties of the model are: $N_A = 4.1 \times 10^9$ m^{-2}, $\tau = 2.015$, and $\mu_\delta = 5.0 \times 10^{-6}$ m. The observed values for both models are the averages of 100 realizations. For both models, the tube lengths are kept constant and lognormal distributions are employed for the tube diameters.

Figures 5.9 through 5.12 illustrate that the two models show opposite behaviors as a_δ increases, both with respect to permeability and formation factor. For parallel capillary model, the permeability increases and the formation factor decreases as a_δ increases, whereas, for the serial capillary model, the permeability decreases and the formation factor increases as a_δ increases. In the case of the parallel capillary model, the conducting capacity of a tube is independent of the conducting capacities of all the other tubes in the model, and because the conducting capacity of a tube is highly

dependent on its diameter (proportional to the 4th power of diameter for fluid flow and to the 2nd power for the electric flow), the overall conducting capacity of the model is dominated by the tubes with large diameters, even if their number is relatively small. An increase in a_δ broadens the tube diameter distribution resulting in higher values of maximum available tube diameter, therefore the permeability of the model increases rapidly and the formation factor decreases rapidly (but not as rapidly as the permeability) as a_δ increases. Opposite is the case with the serial capillary model. The conducting capacity of a flow path is controlled by the conducting capacity of the tube in the path with the smallest diameter. Therefore, the overall conducting capacity of the model is dominated by the tubes with smaller diameters which results in rapid decrease in permeability and rapid increases in formation factor as a_δ increases. The above results are in agreement with Schiedegger's observation (Schiedegger, 1957) that the behavior of parallel capillary model is sensitive to the upper portion of the tube diameter distribution, whereas, the behavior of the serial capillary model is sensitive to the lower portion of the tube diameter distribution.

The agreement between the observed and predicted values of permeability and formation factor of the parallel capillary model is good right up to $a_\delta = 1.2$. For the serial capillary model, the predicted and observed permeabilities start to diverge for $a_\delta \geq 0.60$ and the predicted and observed formation factors start to diverge for $a_\delta \geq 1.0$. It was found that the observed values come closer to the predicted ones as the size of the model is increased beyond the current size of 750×750 (750 flow paths with 750 tubes in each path). However, prohibitively large computer time is required to find the observed values for sizes exceeding 750×750 with 100 realizations.

Figures 5.13 through 5.22 compare the predictions of the relations for various coefficients, terms, and permeability and formation factor of the network model, developed in Section 5.2.4, to the corresponding observed values. Here also the observed values refer to the ones determined with the help of the network theory (Appendix B).

The size of the model is $12 \times 12 \times 12$ with $N_A = 2.4 \times 10^9$ m^{-2}, $\tau = 1.1$, and $\mu_\delta = 5.32 \times 10^{-6}$ m. The observed values are the average of 50 realizations. The tube lengths are constant and lognormal distributions are employed for the tube diameters. For all the quantities, the predictions match well with the observed values for the whole range of a_δ for which the relations were developed, reflecting proper selection of models in the regression analysis carried out in Section 5.2.4. The scatter in permeability (Figure 5.21) may seem to be larger than in the cases of viscous and pressure terms (Figures 5.15 and 5.16, respectively). This is because the range on the y-axis in Figure 5.21 is very small as compared to those in Figures 5.15 and 5.16. This observation is also true in the case of formation factor, and current and potential terms (Figures 5.22, 5.19 and 5.20, respectively).

It can be observed from Figures 5.15 and 5.16 that the viscous term decreases and the pressure term increases as a_δ increases. Because the reciprocal of permeability is equal to the sum of the viscous and pressure terms, a decrease in the viscous term results in an increase in the permeability, and an increase in the pressure term results in a decrease in the permeability. The viscous term represents viscous momentum dissipation in the tubes aligned in the macroscopic flow direction, $k = 1$. As a_δ increases, the tube diameter distribution broadens and because in a tube the momentum dissipated through viscosity is inversely proportional to the fourth power of the diameter, the overall momentum dissipation decreases and therefore, the viscous term decreases. The pressure term represents the viscous momentum dissipation in the cross flow tubes, that is, the tubes aligned in the directions normal to the macroscopic flow direction, $k = 1$. When $a_\delta = 0$ there is no flow through these tubes and therefore, the pressure term is zero. As a_δ increases, the amount of flow in the cross flow tubes increases resulting in increased momentum dissipation and correspondingly in higher magnitudes of the pressure term. When $a_\delta \approx 0.6$, the magnitude of the pressure term is equal to that of the viscous term. The combined effect of the viscous and pressure

terms on the permeability can be observed from Figure 5.21. For $0 \leq a_\delta \leq 0.3$, the contribution of the viscous term to the permeability dominates and the permeability increases slightly. However, for $a_\delta > 0.3$, the pressure term dominates and the permeability decreases as a_δ increases. The arguments presented in this paragraph are equally true in the case of the formation factor in which case the current term is equivalent to the viscous term and the potential term is equivalent to the pressure term.

It may be argued that, at higher values of a_δ, the errors introduced by the finite size of the network may also be modeled during the nonlinear regression analysis. To check this, a run was performed on a $14 \times 14 \times 14$ network (with 50 realizations). The maximum difference between the observed values of permeability for the $12 \times 12 \times 12$ and $14 \times 14 \times 14$ networks (at $a_\delta = 1.2$) was found to be 1.23%, and the corresponding value for the formation factor was found to be 0.75%. To check the behavior of the relations for $a_\delta > 1.2$, observed values were found for a $12 \times 12 \times 12$ network for $0 \leq a_\delta \leq 1.4$. It was found that the predictions of the relations diverge from the observed values for $a_\delta > 1.25$. Therefore, the predictions of the equations can be safely assumed to be correct for values of a_δ up to 1.2. However, the procedure outlined in Section 5.2.4 can be used to find such relations for any given range.

It is interesting to compare the behaviors of the parallel and serial capillary, and the network models at this stage. For the same range of a_δ, the permeabilities of the parallel and serial capillary models change through five orders of magnitude whereas, the permeability of the network model changes approximately by a factor of 2 only. As pointed out in Section 5.1.1, the absence of networking effect in the parallel and serial capillary models is responsible for such behaviors of these models. In the network model, the permeability is controlled by tubes with smaller diameters ("throats") but not to the same extent as in the serial capillary model. This is due the availability of multiple flow paths to a fluid particle at each junction which in turn traverses the

path of least resistance from the upstream to the downstream side of the REV. In the serial capillary model, the fluid particle has no choice but to travel through tubes of all sizes. The absence of networking effect in the parallel capillary models allows the domination of tubes with large diameters. These behaviors of the three models point out that the permeability of the network model will increase as the coordination number (average number of tubes meeting at a junction) increases.

5.3.2 Comparison with Effective-Medium Approximation (EMA)

The relations of permeability and formation factor to the statistical parameters of the pore structure models (parallel and serial capillary, and network) can also be derived with the help of the effective-medium approximation (EMA). The EMA was originally employed to find the electrical permittivity of binary random mixtures of continuous phases (Bruggeman, 1935). Kirkpatrick (1971, 1973) applied the EMA to random networks of conductors based on the following equation:

$$\int_{g_a}^{g_b} \frac{(g_m - g)\,\omega(g)\,\mathrm{d}g}{g + (\eta/2 - 1)\,g_m} = 0\,, \tag{5.97}$$

where η is the coordination number representing the average number of conducting elements connecting a junction to its neighbors. For example, η is 2 for a serial capillary model, 4 for a square network and 6 for a cubic network, both with no diagonal elements, and ∞ for a parallel capillary model. Equation (5.97) is valid for an infinite network in which the elemental conductances, g, are randomly distributed according to a probability density distribution $\omega(g)$ with $g_a \leq g \leq g_b$. g_m is the effective-medium approximation to g_n, where g_n is the exact value of g which yields the network conductance, G_n, when all elements of the network are replaced with elements of conductance g_n. Equation (5.97) is based on the reasoning that the average change in G_n caused by replacing an elementary conductor of an effective-medium network with a conductor randomly chosen from $\omega(g)$, must be equal to zero.

Here, an effective-medium network implies a network in which all the elementary conductors have the same conductance, g_n.

Most of the applications of the EMA have been in two areas: the calculation of conductivity or permeability of binary mixed component solids, and the study of network percolation properties (Kirkpatrick, 1971, 1973; Gurland, 1966; Ahmed and Blackman, 1979; Nagatani, 1981; Sax and Ottino, 1983). A Simple discrete form of $\omega(g)$ was used in both of these applications. Koplik (1981) used continuous $\omega(g)$ (uniform and log-uniform) distributions to determine the range of applicability of the EMA of Equation (5.97) with respect to the shape and breadth of $\omega(g)$. The main purpose of his work was to show that the direct inversion of the conductance matrix (see Appendix B) may be replaced by a less cumbersome numerical solution of Equation (5.97) within acceptable errors introduced thereby.

Nicholson et al. (1988) solved Equation (5.97) using a renormalization group method and found an explicit relation between g_m and the parameters of $\omega(g)$ and η in the form of a series expansion. In this section, a comparison is made between the predictions of the relations developed in the present study and those based on the Nicholson's solution to Equation (5.97).

A detailed derivation of Equation (5.97), based on Kirkpatrick (1973), is presented in Appendix F which also includes Nicholson's solution. To facilitate a discussion of the comparisons, the Nicholson's solution is summarized as follows: The elementary conductance of the network may be written as

$$g = \frac{B\,\delta^{\epsilon}}{S}\,, \tag{5.98}$$

where δ and S are the diameter and the length of the elementary tube, respectively; B and ϵ are constants which depend on the tube shape and flow considered. Values of ϵ and B for various flows and tube shapes are summarized in Appendix F. In the present study (and, also in Nicholson's work), δ is a random variable with probability

density function $\varepsilon(\delta)$ and S has a fixed value. The following reduced random variables are introduced:

$$\kappa = \frac{\delta}{\mu_\delta} - 1 \tag{5.99}$$

and

$$\zeta = \left(\frac{\delta}{\mu_\delta}\right)^\epsilon - 1 = (1+\kappa)^\epsilon - 1 \,, \tag{5.100}$$

where μ_δ is the mean tube diameter. If $\tilde{\varepsilon}(\kappa)$ and $\hat{\varepsilon}(\zeta)$ denote the probability density functions of κ and ζ, respectively, then the corresponding moments are given by

$$\kappa_n = \langle \kappa^n \rangle^{\mathrm{EN}} = \int_{\kappa_a}^{\kappa_b} \kappa^n \, \tilde{\varepsilon}(\kappa) \, \mathrm{d}\kappa \,, \tag{5.101}$$

$$\zeta_n = \langle \zeta^n \rangle^{\mathrm{EN}} = \int_{\zeta_a}^{\zeta_b} \zeta^n \, \hat{\varepsilon}(\zeta) \, \mathrm{d}\zeta \,. \tag{5.102}$$

The above relations result in the following general expression for ζ_n in terms of κ_n:

$$\zeta_n = (-1)^n \sum_{i=1}^{n} (-1)^i \, {}_i^n C \sum_{j=1}^{i\epsilon} {}_j^{i\epsilon} C \;\; \kappa_j \,, \tag{5.103}$$

where ${}_i^n C$ and ${}_j^{i\epsilon} C$ are the binomial coefficients. The normalized effective-medium conductance of a network, based on the Nicholson's series solution to Equation (5.97), is:

$$\begin{aligned}
\gamma_m(\Lambda, \zeta_n) = 1 \; &- \Lambda\,\zeta_2 + \Lambda^2\,\zeta_3 - \Lambda^3\,\zeta_4 + \Lambda^4\,\zeta_5 - \Lambda^5\,\zeta_6 \\
&+ \Lambda\,\zeta_1^2 + (2\Lambda - 3\Lambda^2)\,\zeta_1\,\zeta_2 + (4\Lambda^3 - 3\Lambda^2)\,\zeta_1\,\zeta_3 \\
&+ (4\Lambda^3 - 5\Lambda^4)\,\zeta_1\,\zeta_4 + (2\Lambda^3 - \Lambda^2)\,\zeta_2^2 \\
&+ (3\Lambda^3 - 5\Lambda^4)\,\zeta_2\,\zeta_3 + (6\Lambda^5 - 4\Lambda^4)\,\zeta_2\,\zeta_4 \\
&+ (3\Lambda^5 - 2\Lambda^4)\zeta_3^2 + (2\Lambda^2 + 2\Lambda)\,\zeta_1^3 \\
&+ (8\Lambda^4 - 7\Lambda^5 - 2\Lambda^3)\,\zeta_2^3 \\
&+ (13\Lambda^2 - 10\Lambda^3 - 3\Lambda)\,\zeta_1^2\,\zeta_2 \\
&+ (15\Lambda^4 - 17\Lambda^3 + 4\Lambda^2)\,\zeta_1\,\zeta_2^2 + \cdots \,,
\end{aligned} \tag{5.104}$$

where $\gamma_m(\Lambda, \zeta_n)$ is the effective-medium conductance of a network normalized by the effective-medium conductance of the equivalent parallel capillary model, and $\Lambda = \eta/2$. Λ varies between 0 and 1 for parallel and serial capillary models, respectively. Here the equivalent parallel capillary model is one with the same external dimensions and distribution of elementary conductances as the network model, with a coordination number of ∞. Values of ζ_n $(n = 1, \ldots, 6)$ in terms of κ_n $(n = 1, \ldots, 6)$ for four values of ϵ $(= 1, \ldots, 4)$ are included in Appendix F. This appendix also includes the values of κ_n $(n = 1, \ldots, 6)$ in terms of a_δ $(= \sigma_\delta/\mu_\delta)$ for lognormal distribution of tube diameters. Here σ_δ is the standard deviation of the distribution. a_δ is the coefficient of variation and is a measure of the breadth of the tube diameter distribution.

The relation between the permeability and the normalized effective-medium conductance (for fluid flow) of the network model is

$$\gamma_m(\epsilon = 4) = \frac{k_1^n}{k_1^p}\,, \tag{5.105}$$

where k_1^n and k_1^p denote the permeabilities of the network model and the equivalent parallel capillary model, respectively. Similarly, the relation between the formation factor and the normalized effective-medium conductance (for electric flow) of the network model is

$$\gamma_m(\epsilon = 2) = \frac{F^p}{F^n}\,, \tag{5.106}$$

where F^n and F^p denote the formation factors of the network model and the equivalent parallel capillary model, respectively. Detailed derivations of Equations (5.105) and (5.106) are given in Appendix F.

Figure 5.23 illustrates a comparison of the normalized effective-medium conductances predicted by Equation (5.104) (with $\epsilon = 4$ and $\Lambda = 0.33$) and the normalized effective-medium conductances predicted by Equation (5.105), as functions of a_δ. k_1^p and k_1^n in Equation (5.105) are found from Equations (5.24) and (5.95), respectively.

The observed values in this figure correspond to the values of the normalized effective-medium conductances given by Equation (5.105) in which k_1^n and k_1^p are determined with the help of the network theory (Appendix B).

Similarly, the normalized effective-medium conductances predicted by Equation (5.104) (with $\epsilon = 2$ and $\Lambda = 0.33$) is compared to the normalized effective-medium conductances predicted by Equation (5.106). F^p and F^n in Equation (5.106) are found from Equations (5.27) and (5.96), respectively. The comparison is illustrated in Figure 5.24. The observed values in this figure correspond to the values of the normalized effective-medium conductances given by Equation (5.106) in which F^n and F^p are determined with the help of the network theory (Appendix B).

A $12 \times 12 \times 12$ network with constant effective open area in the three principal directions is employed in the above comparisons. The tube lengths are fixed and the tube diameters are randomly assigned according to a lognormal distribution. The statistical parameters of the network are: $N_A = 2.4 \times 10^9 \mathrm{m}^{-2}$, $\tau = 1.1$, $\mu_\delta = 5.32 \times 10^{-6}\mathrm{m}$ and a_δ varies between 0 and 1.2. The observed values are the average of 50 realizations.

The results illustrated in Figures 5.23 and 5.24 show that the EMA predictions deteriorate as a_δ increases beyond certain limit. For the present network, the maximum values of a_δ up to which the EMA predicts accurate results are approximately 0.25 for the fluid flow ($\epsilon = 4$) and 0.3 for the current flow ($\epsilon = 2$). These results are in agreement with those of Koplik (1981, 1982) and Nicholson et al. (1988). The maximum value of a_δ up to which the EMA predicts accurate results depends on ϵ, Λ, and the employed tube diameter distribution. This maximum value decreases as Λ and ϵ increase. The EMA markedly deteriorates for networks dominated by very low conductances, that is, conductances with positively skewed distributions such as the lognormal distribution at high a_δ (Figure 5.25). For positively skewed distributions, the network contains regions of very low conductivity and these regions contribute

significantly to the effective-medium conductance because $\omega(g)$ emphasizes the low conductance range in the averaging in Equation (5.97). But in reality, regions of very low conductances are most likely to be by-passed by the main fluid (current) flow (Koplik, 1981). The range of applicability of the EMA for symmetrical tube diameter distributions such as uniform and normal distributions, is larger than that for the log-normal distribution (Nicholson et al., 1988). However, as explained in Section 5.1.1, the maximum values of a_δ that can be generated with the symmetrical distributions are very low, and therefore, such distributions are of limited scope.

In the present work, the relations of permeability and formation factor to the statistical parameters of the network model (Equations (5.95) and (5.96)) have been developed for values of a_δ up to 1.2, and therefore, are much more useful than those based on the EMA. However, the EMA has an advantage in that it explicitly shows the dependence of the network conductance on η, the coordination number, whereas such dependence is embedded in the coefficients of Equations (5.95) and (5.96).

5.4 Summary

In this chapter, parallel and serial capillary, and three-dimensional cubic network models of porous media have been considered. These models are based on the conceptual model of porous media due to Bear and Bachmat (1966,1967). For permeability and Klinkenberg permeability calculations, laminar flow has been assumed inside the tubes. For formation factor calculations, the electric flow inside a tube saturated with an electric conductor has been assumed to be given by Ohm's law. The tube diameters of the models are distributed according to the lognormal distribution and the tube lengths are constant.

An analysis has been performed to determine the sizes of the models that qualify as REVs with respect to permeability, formation factor, Klinkenberg coefficient and porosity. It has been shown that out of these four properties, it is sufficient to find

the REV size of a model with respect to permeability only. A $12 \times 12 \times 12$ size with 50 realizations has been shown to be a satisfactory representative size for the network model. Such sizes have also been determined for the parallel and serial capillary models.

Based on the integral expressions developed in Chapter 3 (Equations (3.26), (3.41) and (3.47)), closed form explicit relations between the permeability, Klinkenberg permeability and formation factor of the parallel and serial capillary models and the statistical parameters characterizing their pore space have been derived. With the help of nonlinear regression, similar relations, based on the integral expressions, have been developed for the permeability and formation factor of the three-dimensional cubic network model. It is observed that the absence of the networking effect results in opposite behaviors of the parallel and serial capillary models, whereas, its presence in the network model results in an intermediate behavior representative of the real porous media.

The relations of permeability and formation factor of network model to the statistical parameters characterizing its pore structure, have been developed for values of a_δ up to 1.2. The predictions of similar relations based on the effective-medium theory (Nicholson et al., 1988) are found to deteriorate for $a_\delta > 0.25$ in the case of permeability and for $a_\delta > 0.3$ in the case of formation factor.

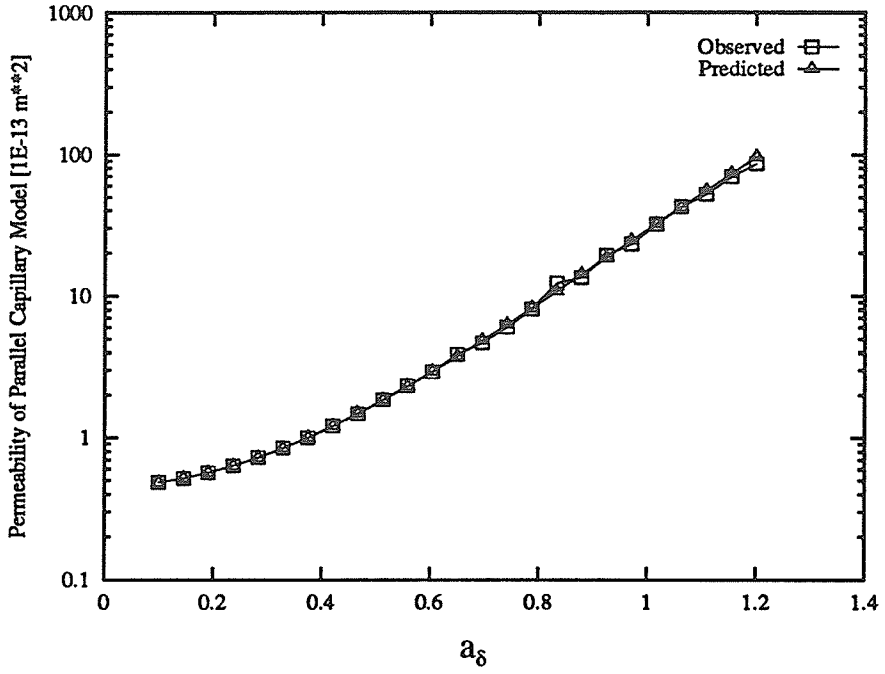

Fig. 5.9. Predicted and observed permeabilities of a parallel capillary model as functions of a_δ.

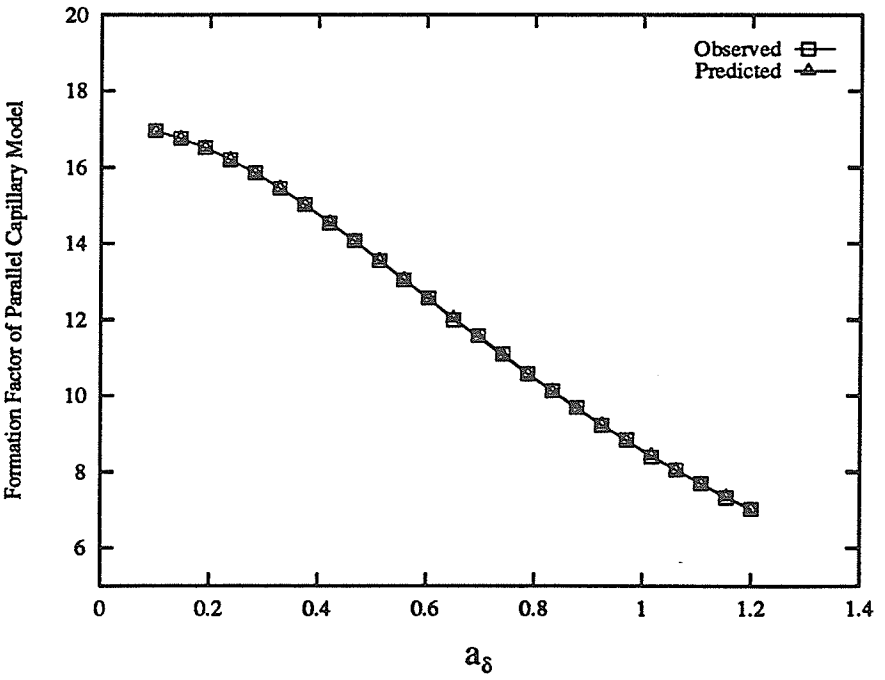

Fig. 5.10. Predicted and observed formation factors of a parallel capillary model as functions of a_δ.

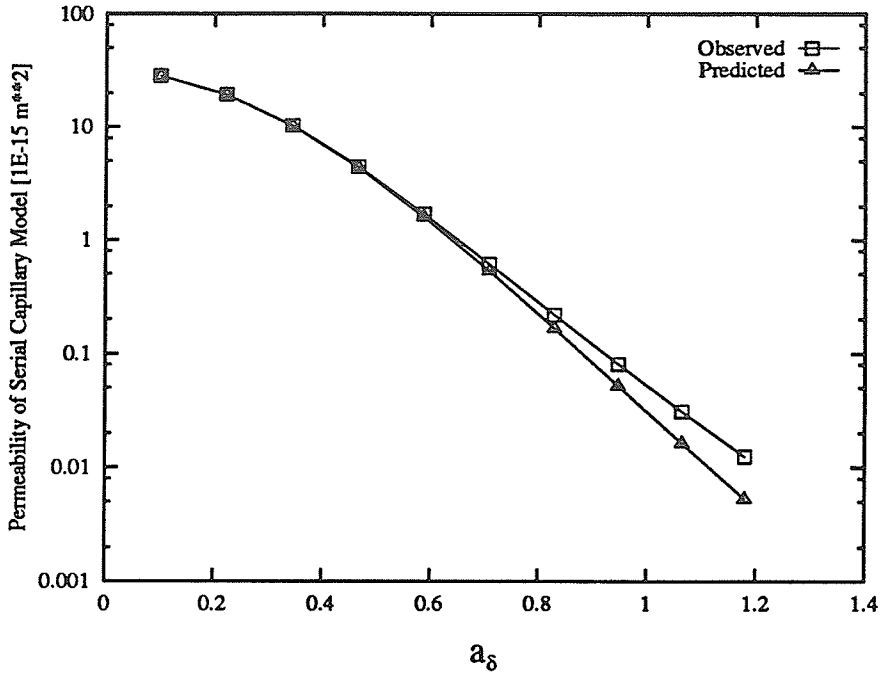

Fig. 5.11. Predicted and observed permeabilities of a serial capillary model as functions of a_δ.

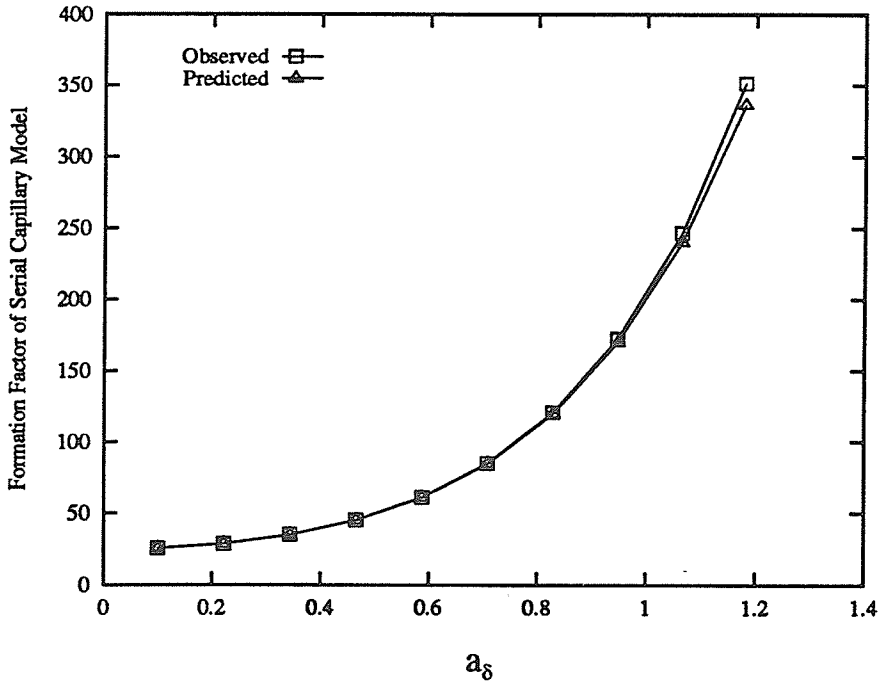

Fig. 5.12. Predicted and observed formation factors of a serial capillary model as functions of a_δ.

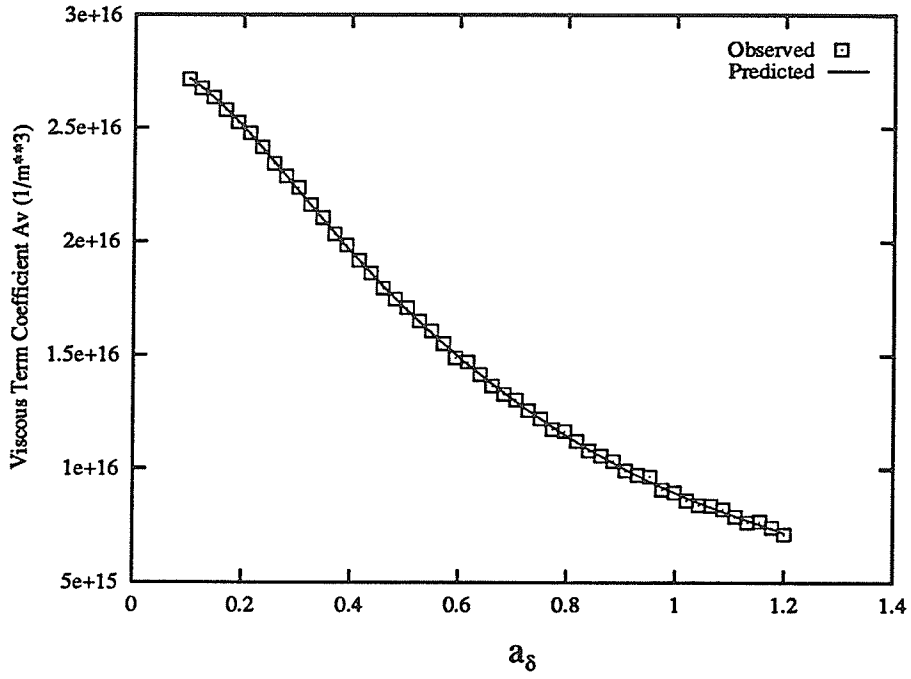

Fig. 5.13. Predicted and observed values of coefficient, A_v, as functions of a_δ.

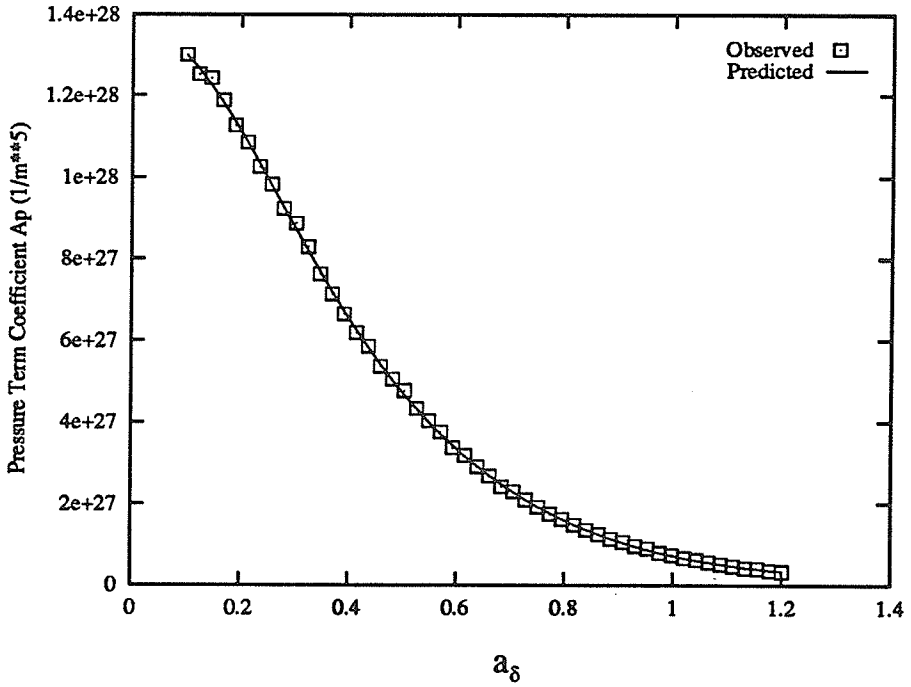

Fig. 5.14. Predicted and observed values of coefficient, A_p, as functions of a_δ.

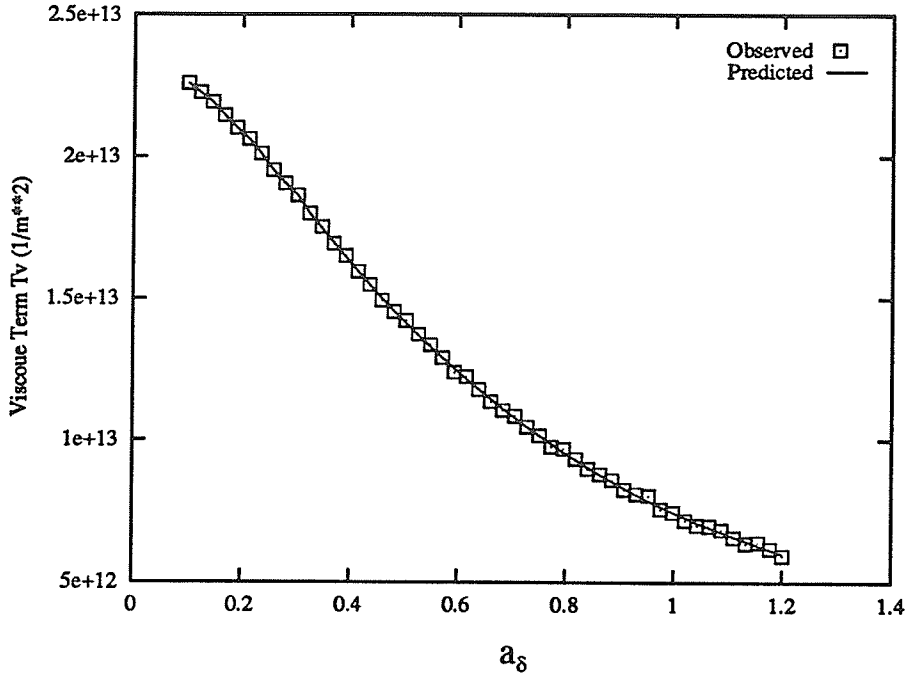

Fig. 5.15. Predicted and observed viscous terms of a network model as functions of a_δ.

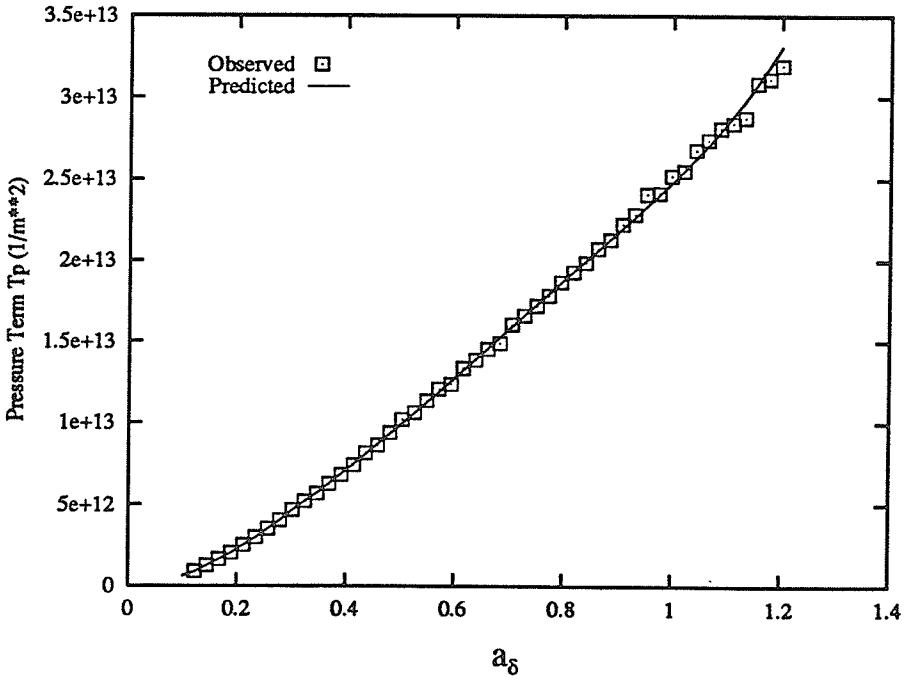

Fig. 5.16. Predicted and observed pressure term of a network model as functions of a_δ.

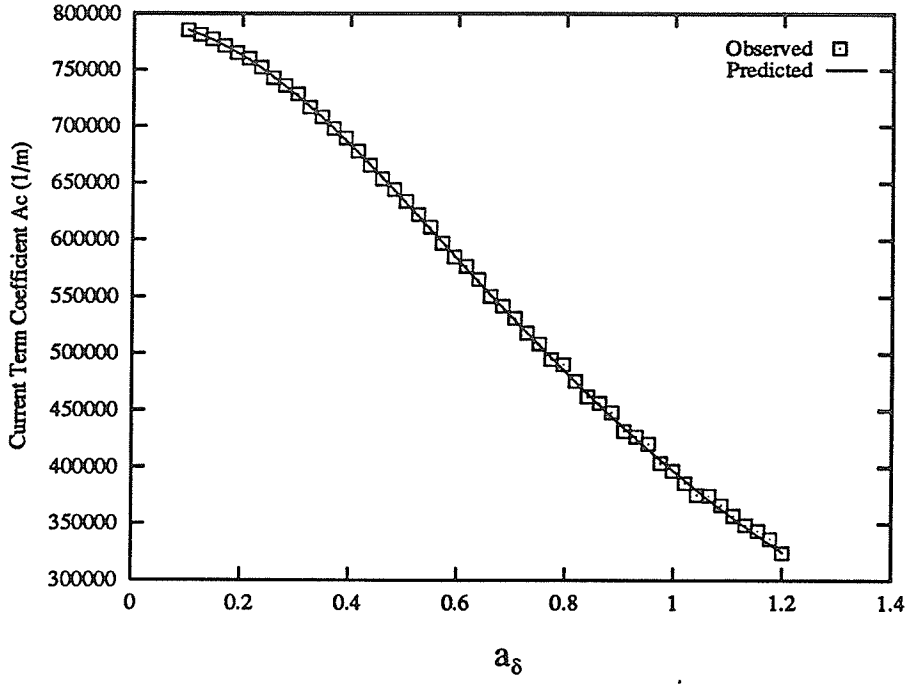

Fig. 5.17. Predicted and observed values of coefficient, A_c, as functions of a_δ.

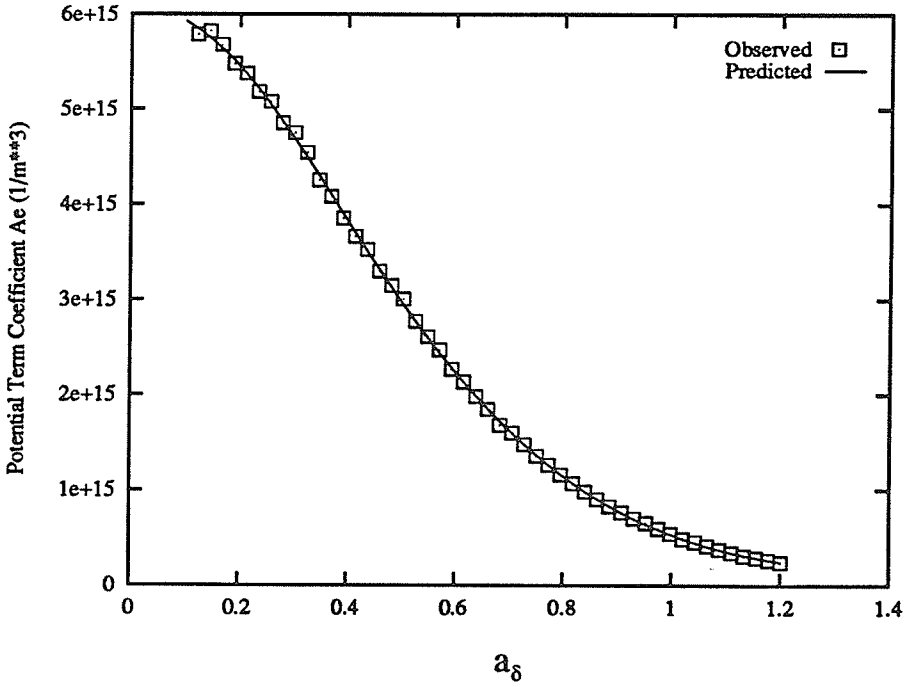

Fig. 5.18. Predicted and observed values of coefficient, A_e, as functions of a_δ.

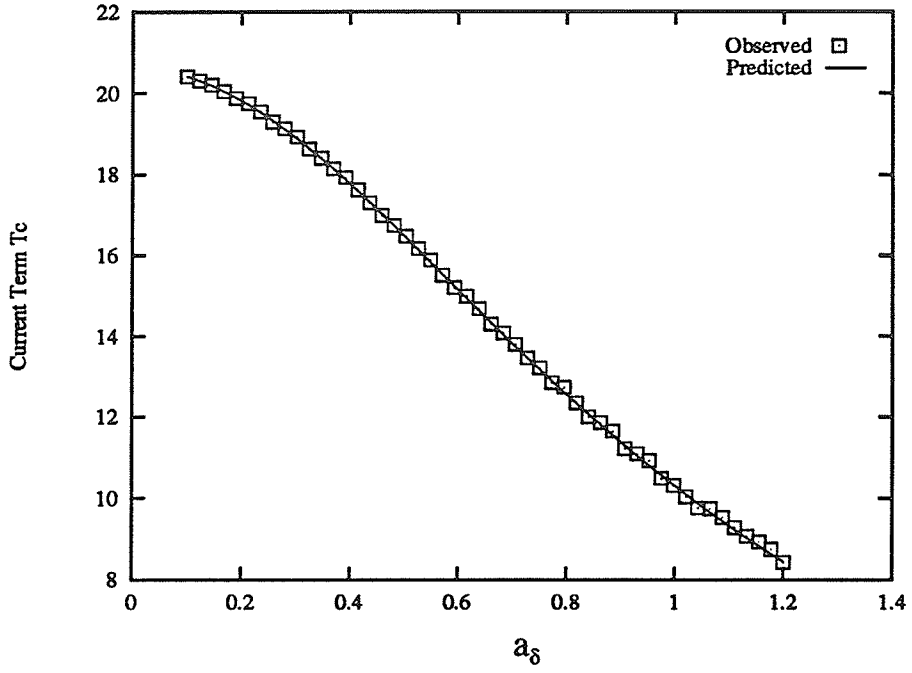

Fig. 5.19. Predicted and observed current terms of a network model as functions of a_δ.

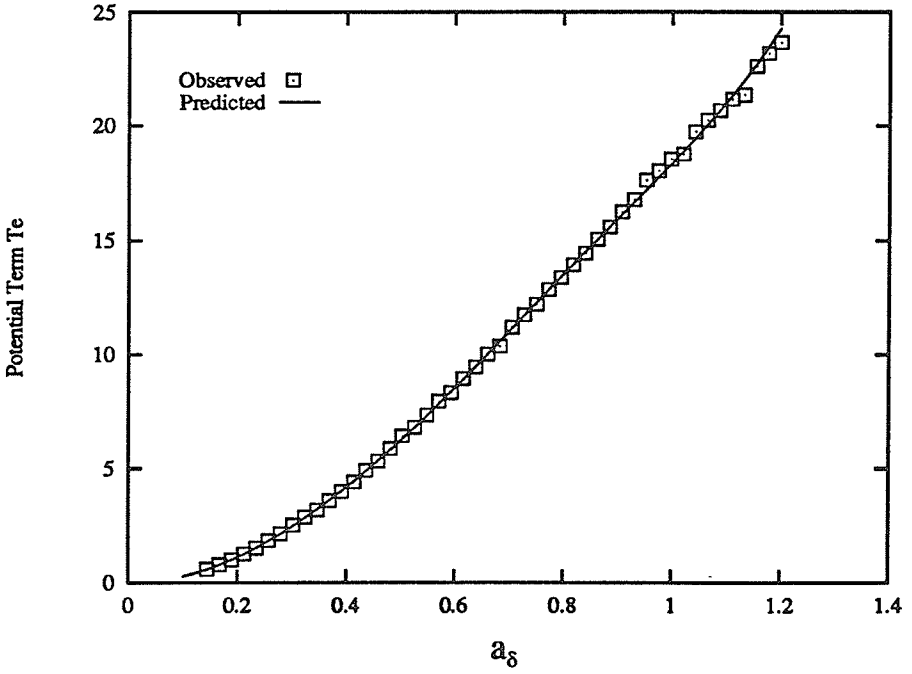

Fig. 5.20. Predicted and observed potential terms of a network model as functions of a_δ.

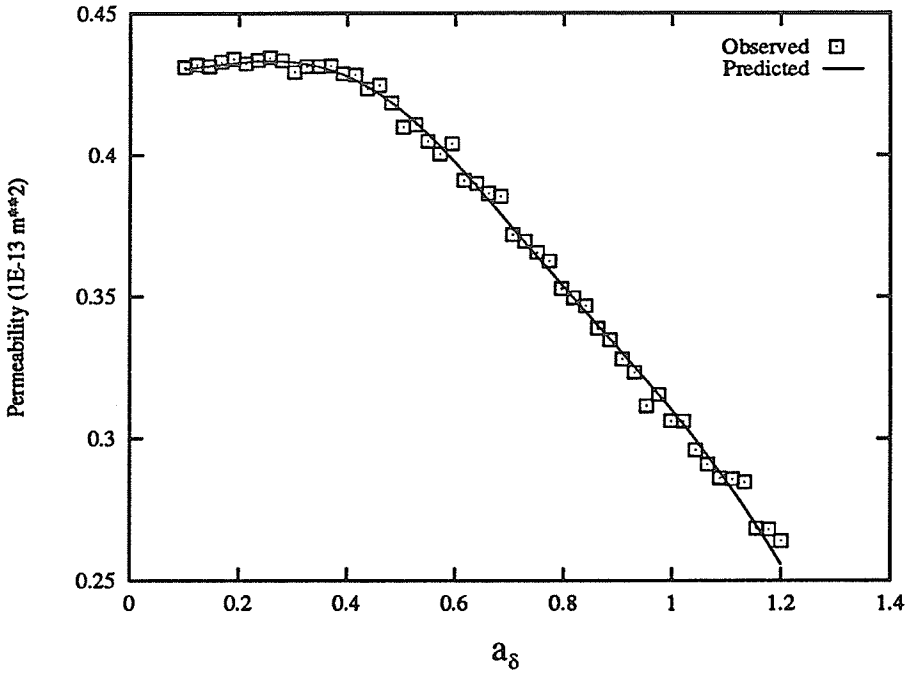

Fig. 5.21. Predicted and observed permeabilities of a network model as functions of a_δ.

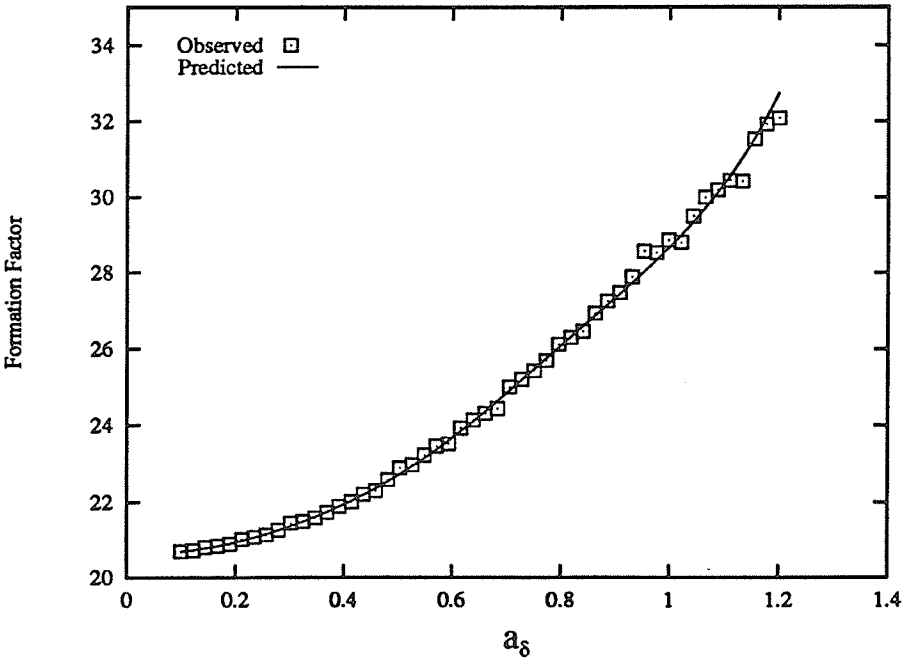

Fig. 5.22. Predicted and observed formation factors of a network model, as functions of a_δ.

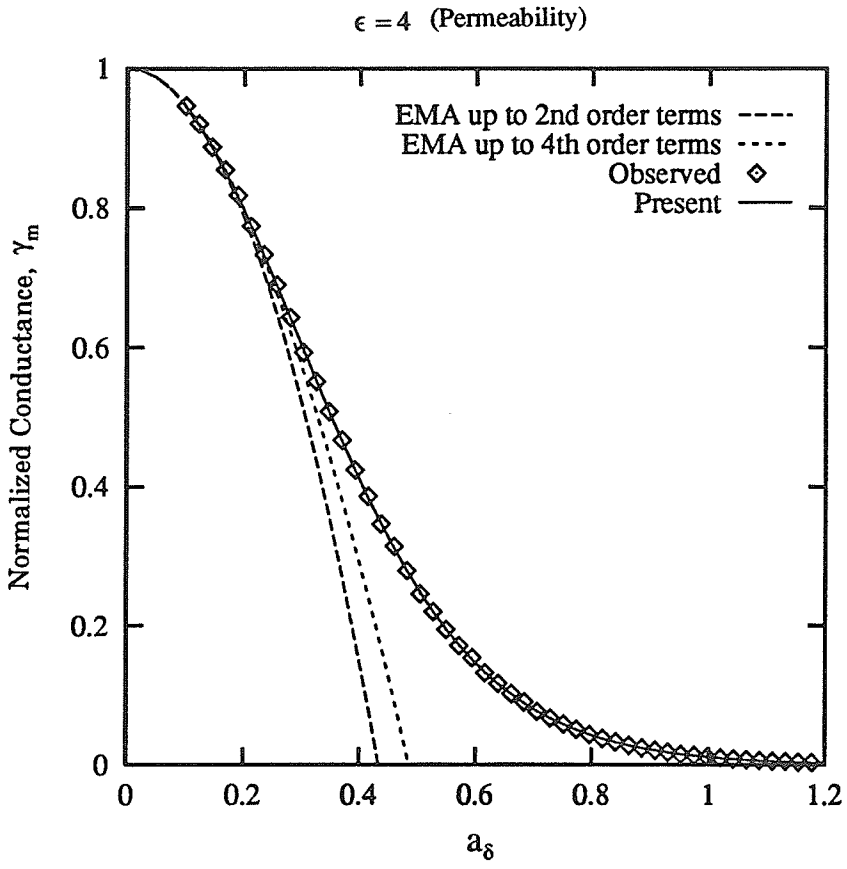

Fig. 5.23. Comparison of normalized conductances for Hagen-Poiseuille flow ($\epsilon = 4$; same as in permeability calculations) calculated from the EMA by Nicholson et al. (1988) and the present method, with the observed values.

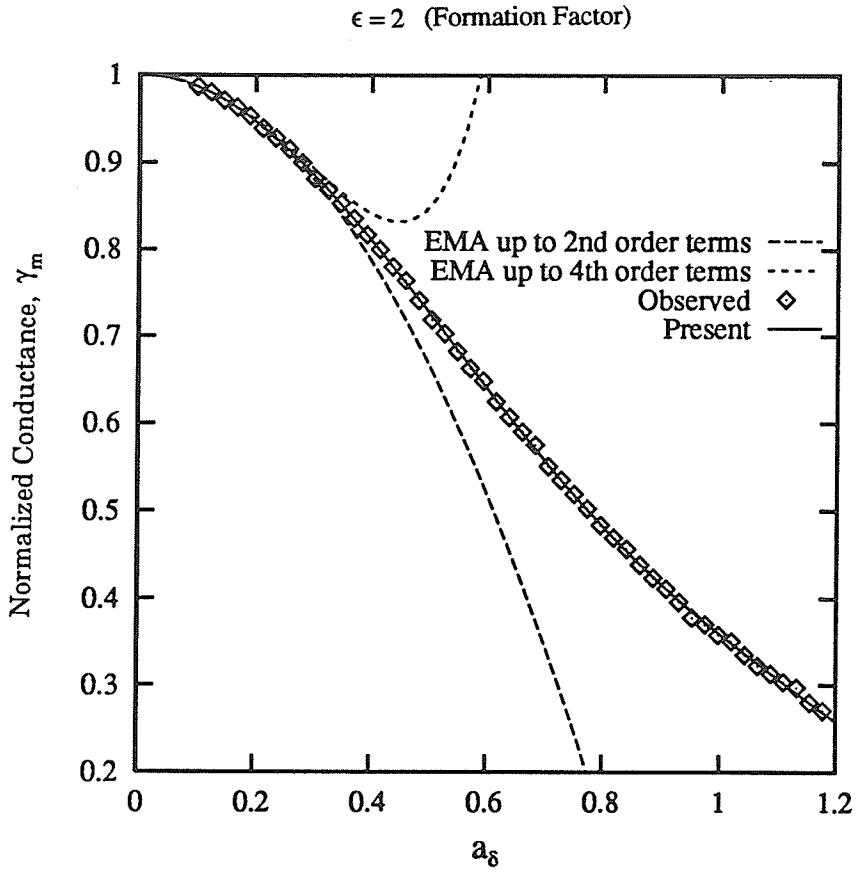

Fig. 5.24. Comparison of normalized conductances for electric flow ($\epsilon = 2$; same as in formation factor calculations) calculated from the EMA by Nicholson et al. (1988) and the present method, with the observed values.

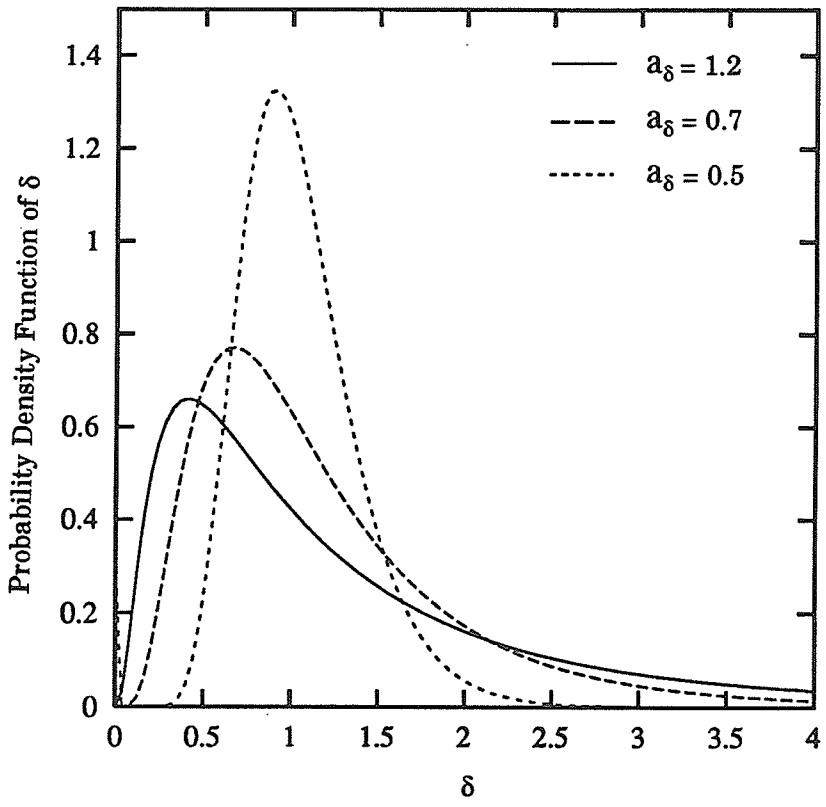

Fig. 5.25. Effect of increasing a_δ on the skewness of lognormal distribution.

CHAPTER 6

AN OUTLINE OF A METHODOLOGY FOR MODELING PORE STRUCTURE

In this chapter, a methodology to model the pore structure of homogeneous porous media, based on the explicit relations of the transport properties of the models to their statistical parameters derived in Chapter 5, is outlined. The main aim of this chapter is to explain the philosophy behind this methodology. A preliminary study based on this methodology is conducted on five sandstone and one limestone rock samples, all of which are selected from the existing literature. The methodology is used to predict the mercury drainage capillary pressure curves of five of the samples and the oil-brine drainage capillary pressure curve of one sample. All the three pore structure models are considered and a comparison is made between their predictions and the experimentally observed curves. The limitations of the models are identified and recommendations for improving the accuracy of their predictions are presented. Section 6.1 briefly explains the philosophy behind the methodology. The outline of the methodology is presented in Section 6.2. Section 6.3 summarizes the algorithm employed for determining the drainage capillary pressure curve of the models. Finally, the results are discussed in Section 6.4.

6.1 Philosophy

As mentioned in Chapter 1, if N statistical parameters are required to describe a porous medium according to a given pore structure model and if N transport properties can be experimentally determined on a sample of the porous medium, then based

on the explicit relations of the transport properties of the model to the statistical parameters, N simultaneous nonlinear algebraic equations involving the statistical parameters can be written. These equations can then be inverted to determine the values of the N statistical parameters. Once the statistical parameters are known, complex properties such as capillary pressure curves can be predicted explicitly or with the help of computer simulations. Such an exercise can serve two broad purposes. One, the experiments for measuring transport properties (e.g., permeability, formation factor) which are input to the method are simple and less time consuming as compared to those for the complex properties such as capillary pressure curves; therefore the method can provide a means for quick evaluation of such properties. The method can also be employed for the purpose of confirming the experimentally measured values of the complex properties. Two, the exercise may throw some light on the dependence of the properties on pore structure and their relation to one another.

6.2 Outline of the Methodology

6.2.1 Problem Formulation

The relations of the transport properties of the parallel capillary, serial capillary and network models to the statistical parameters characterizing their pore space, derived in the previous chapter, may be represented as follows:

$$k_1 = k_1\left(\mu_\delta,\, \sigma_\delta,\, \tau,\, \xi_1\right), \tag{6.1}$$

$$F = F\left(\mu_\delta,\, \sigma_\delta,\, \tau,\, \xi_1\right) \tag{6.2}$$

and

$$b = b\left(\mu_\delta,\, \sigma_\delta,\, \tau, \xi_1\right), \tag{6.3}$$

where k_1, F and b are the permeability, formation factor and Klinkenberg coefficient, respectively, which are the macroscopic transport properties of the models, and μ_δ,

σ_δ, τ and ξ_1 are the mean tube diameter, standard deviation of the tube diameter distribution, non-dimensionalized mean tube length (defined in Section 5.1.1) and areosity (also defined in Section 5.1.1), respectively, which are the statistical parameters characterizing the void space of the models. It may be pointed out here that an explicit relation between the Klinkenberg coefficient and the statistical parameters of the network model, in the form of Equation (6.3), has not been found. The procedure used in place of this relation for the network model is discussed in the next section.

The above relations may be recast using a relation between the areosity and other parameters. For the network model this relation is determined as follows: The areosity,

$$\xi_1 = \frac{\pi}{4\,A_1} \sum_{I=1}^{N_2^P\,N_3^P} \delta_I^2 \,. \tag{6.4}$$

With the evaluation of the summation

$$\xi_1 = \frac{\pi\,N_A}{4} \left(\mu_\delta^2 + \sigma_\delta^2\right) \,, \tag{6.5}$$

where $N_A = N_2^P\,N_3^P/A_1$, for the network model. Equation (6.5) is also true for the parallel and serial capillary models. However, for the parallel capillary model, N_A is equal to N_T/A_1, and for the serial capillary model, N_A is equal to N_{ch}/A_1. Here N_T is the total number of the tubes in the parallel capillary model (Figure 5.1) and N_{ch} is the total number of flow paths in the serial capillary model (Figure 5.2). With the introduction of Equation (6.5), the functional forms represented by Equations (6.1), (6.2) and (6.3) modify to

$$k_1 = k_1\left(\mu_\delta,\, \sigma_\delta,\, \tau, N_A\right) \,, \tag{6.6}$$

$$F = F\left(\mu_\delta,\, \sigma_\delta,\, \tau, N_A\right) \tag{6.7}$$

and

$$b = b\left(\mu_\delta,\, \sigma_\delta,\, \tau, N_A\right) \,. \tag{6.8}$$

If k_1, F and b are known, then the above relations reduce to three simultaneous algebraic equations with μ_δ, σ_δ, τ and N_A as the unknowns. To achieve closure, one more equation is required. The relation between porosity and the statistical parameters of a model can be used for this purpose. For the network model, this relation can be found from the following expression for porosity:

$$\phi = \frac{\pi}{4\,A_1\,L_1}\sum_{I=1}^{N_1^T}\delta_I^2\,S_I \;+\; \frac{\pi}{4\,A_2\,L_2}\sum_{I=1}^{N_2^T}\delta_I^2\,S_I \;+\; \frac{\pi}{4\,A_3\,L_3}\sum_{I=1}^{N_3^T}\delta_I^2\,S_I\,, \tag{6.9}$$

where N_1^T, N_2^T and N_3^T are the number of tubes in the $k = 1, 2, 3$ directions, respectively, given by

$$N_1^T = (N_1^P + 1)\,N_2^P\,N_3^P\,, \tag{6.10}$$

$$N_2^T = (N_2^P + 1)\,N_3^P\,N_1^P \tag{6.11}$$

and

$$N_3^T = (N_3^P + 1)\,N_1^P\,N_2^P\,. \tag{6.12}$$

Here N_1^P, N_2^P and N_3^P are the number of columns, rows and tiers in the network model (Figure 5.3). Because all the tubes are of the same length and the diameters of the tubes in the three principal directions possess the same distribution, Equation (6.9) reduces to

$$\phi = \frac{3\,\pi\,\tau\,N_A}{4}\,(\mu_\delta^2 \;+\; \sigma_\delta^2)\,, \tag{6.13}$$

where

$$N_A = \frac{N_2^P\,N_3^P}{A_1} = \frac{N_3^P\,N_1^P}{A_2} = \frac{N_1^P\,N_2^P}{A_3} \tag{6.14}$$

and

$$\tau = \frac{(N_1^P + 1)\,\mu_S}{L_1} = \frac{(N_2^P + 1)\,\mu_S}{L_2} = \frac{(N_3^P + 1)\,\mu_S}{L_3}\,. \tag{6.15}$$

The parallel and serial capillary models have no tubes in the directions $k = 2$ and 3, therefore the relation between the porosity and the statistical parameters for these models is:

$$\phi = \frac{\pi \tau N_A}{4} (\mu_\delta^2 + \sigma_\delta^2) . \tag{6.16}$$

If the experimental values of k_1, F, b and ϕ of a porous medium are known, then Equations (6.6), (6.7), (6.8) and (6.13) (Equations (6.6), (6.7), (6.8) and (6.16) for the parallel and serial capillary models) can be solved and μ_δ, σ_δ, τ and N_A can be found.

6.2.2 Solution of the Nonlinear Algebraic Equations

Ordinarily, an iterative scheme based on the Newton-Raphson method (Press et al., 1986, pp. 269) can be used to solve a set of nonlinear algebraic equations in which the number of unknowns is equal to the number of equations. In the present study two major difficulties were encountered when this scheme was employed to solve the sets of nonlinear equations relating the transport properties of the models to their statistical parameters. One, because the equations involve higher order terms (up to twelfth power), the solutions only converged when proper initial guesses were provided, and two, for some samples the solutions did not converge within a satisfactory tolerance. Keeping in view the simplicity of the pore structure of the models as compared to the complex pore structure of the real porous media, the second difficulty can be expected and should not lead to misinterpretations. It is expected that it may not be possible to find a network model which can exactly reproduce all the properties of a real porous medium sample. The usefulness of the methodology can only be judged if real porous media can be realistically simulated with the help of pore structure models.

To overcome the above mentioned difficulties, a modified solution scheme based on the Newton-Raphson method was used. This solution scheme although not exact,

provides a means for inverting the equations in a meaningful manner. For the parallel capillary model with symmetrical tube diameter distributions (e.g, uniform, normal and logistic), the set of nonlinear algebraic equations represented by Equations (6.6), (6.7) and (6.16) can be solved analytically if one of the four unknown parameters is treated as a constant. If N_A is treated as constant, the solution possesses definite upper and lower bounds on N_A for real and positive values of μ_δ, σ_δ and τ. These bounds are given in Table 6.1. A value of N_A was selected from this range and Equations (6.6), (6.7) and (6.16) were solved. The values of μ_δ, σ_δ, τ and N_A (the selected value of N_A) found in this way were substituted in Equation (6.8) for b and the corresponding residue was found. By an iterative procedure, an appropriate value of N_A was found which resulted in minimum residue in Equation (6.8) and lay in the range of N_A for real and positive values of μ_δ, σ_δ and τ.

For all the three models with lognormal tube diameter distributions, an iterative scheme based on the Newton-Raphson method (Press et al., 1988, pp 269) was employed to solve the equations. The values of the statistical parameters for the parallel capillary model with symmetrical tube diameter distributions (the analytical solutions discussed in the previous paragraph) were used as initial guesses in this scheme. This scheme may be summarized as follows: For a given value of N_A, Equations (6.6), (6.7) and (6.13) (Equations (6.6), (6.7) and (6.16)) for the parallel and serial capillary models) were solved using the Newton-Raphson method. The values of μ_δ σ_δ, τ and N_A (the selected value of N_A) found in this way were then substituted in Equation (6.8) for b and the corresponding residue was found. This procedure was repeated until such a value of N_A was found which resulted in minimum residue in Equation (6.8) and real and positive values of μ_δ, σ_δ and τ. As pointed out earlier, an explicit relation between the Klinkenberg coefficient b and the statistical parameters of the network model, in the form of Equation (6.3) has not been found. For this model, b in the above scheme was found with the help of the network theory.

6.2.3 Computer Simulations of the Models

For given values of the transport properties k_1, F, b and ϕ of a sample of porous medium, the corresponding values of the statistical parameters μ_δ, σ_δ, τ and ϕ were determined employing the procedure explained in the previous section. With the statistical parameters known, computer simulations of the models were generated on a SUN SPARC station 2. The physical features of the models have already been discussed in Section 5.1. The diameters of the tubes in the models were distributed according to a lognormal distribution and the tube lengths were kept constant.

The computer simulations of the models were employed for predicting the mercury drainage capillary pressure curves for four sandstone and one limestone samples, and the oil-brine drainage capillary pressure curve of one sandstone sample. All the six samples have been selected from the existing literature. In the experimental mercury drainage capillary pressure curves vacuum is the wetting phase, therefore for these samples vacuum is assumed to be the wetting phase in the simulations.

To find the size of a model so that the predicted capillary pressure curve is a satisfactory representative, the procedure explained in Section 5.1.2 was followed. The corresponding results for the network model are illustrated in Figure 6.1. This figure show that a $12 \times 12 \times 12$ network is a satisfactory size for predicting the capillary pressure curves. Similarly, 13000 tubes for the parallel capillary model and 750 channels with 750 tubes in each channel for the serial capillary model were found to be the representative sizes for these models. A single realization was employed for all the three models. The procedure employed for evaluating the drainage capillary pressure curves of the models is presented next.

6.3 Drainage Capillary Pressure Curve Modeling

To evaluate the drainage mercury capillary pressure curve of a model, complete vacuum is assumed to exist inside the parallelepiped-shaped REV. The mercury is

allowed to penetrate the REV from the face normal to the negative $k = 1$ direction and the remaining five faces are assumed to be sealed. Two conditions must be met before mercury can enter a tube in a model: one, the Washburn criterion (Washburn, 1921) must be satisfied and, two, the tube must be in contact with the bulk mercury. The Washburn condition relates the capillary pressure, p_c, to the diameter of the tube, δ, in the form

$$p_c = - \frac{4 \varrho \cos \theta}{\delta} , \tag{6.17}$$

where ϱ is the surface tension of the mercury and θ is the contact angle. The Washburn criterion assumes a piston-type displacement. Initially, the tube (tubes) with the largest diameter in the face in direct contact with the mercury is (are) found and filled with mercury. The freshly filled junctions at the ends of the invaded tubes are stored as potential penetration sites. All the tubes connected to a filled junction which satisfy the Washburn criterion at the given mercury pressure are then filled with mercury. If a junction has already been filled with mercury, then the advancing meniscus is assumed to immediately coalesce with the mercury in the junction. The process of filling the junctions and the tubes is continued until the mercury front is incapable of advancing at the given capillary pressure. The pore volume invaded by the mercury is calculated and this gives the first point on the predicted capillary pressure curve. The pressure is raised in small increments and the process is repeated to determine the other points on the curve.

For evaluating the oil-brine drainage capillary pressure curve of a model, the parallelepiped-shaped REV of the model is assumed to be completely saturated with the brine. The oil is allowed to penetrate from the face normal to the negative $k = 1$ direction and the brine is allowed to leave from the face normal to the positive $k = 1$ direction, and the remaining four faces are sealed. Initially, the brine inside the REV is assumed to be in continuous contact with a brine sink at the downstream side

of the REV. This assumption is equivalent to the presence of a porous plate in the conventional methods for measuring the oil-brine capillary pressure curve of a real porous medium sample. The function of the porous plate in such tests is to allow only the brine out of the sample and restrict the oil to the sample. For oil to invade a tube, one condition in addition to the two conditions mentioned for mercury invasion above, must be met. This condition is that the brine inside a tube to be invaded by the oil, must be in continuous contact with the brine sink downstream of the REV. The brine in the tubes which is not in continuous contact with the brine sink, becomes isolated and contributes to the irreducible wetting phase (or the brine) saturation. A junction filled with oil is assumed to disallow continuity (through the junction) between the brine in different tubes meeting at the junction.

6.4 Results and Discussion

In this section, the properties of the selected samples are summarized and results of the methodology for these sample are discussed.

6.4.1 Selected Samples and Their Properties

Six rock samples covering a wide range of permeability were selected from the existing literature. As indicated earlier, five of them are sandstone samples and one is a limestone sample. For five of the samples, the properties permeability, formation factor and porosity were provided in the source. The values of the Klinkenberg coefficient for these samples were determined from two correlations between k_l and b existing in the literature. These correlations are: $b = 0.777\, k_l^{-0.39}$, given in Heid et al. (1950) and reported in API RP27 (1956), and $b = 0.697\, k_l^{-0.38}$, found by McPhee and Arthur (1991). In both of these correlations, air is the flowing gas (viscosity, μ = 0.1817 Pa·s; gas constant, R = 8.3143 J/kg-k; molecular weight, M=0.02897 kg/mol), b is measured in psi, and k_l in darcys. For one sandstone sample, only two

properties (k_1 and ϕ) were provided in the source. For this sample b was found as explained above, and F was determined from the correlation $F = 0.62\,\phi^{-2.15}$, given by Winsauer et al. (1952). This correlation was preferred over the correlation given by Archie (1942) ($F = \phi^{-2}$), because as shown by Winsauer et al. (1952), their correlation is a better representation of the experimental data from different sources including Archie's data. Table 6.2 summarizes the properties of the samples and their source. The values of b determined from the two correlations mentioned above are summarized in Table 6.3.

Ideally, complete sets of experimental data for the samples would have been more helpful in critically examining the present methodology. However, such extensive data for the same sample of a porous medium are rare in the literature. The correlations used for finding the missing data have been shown to give satisfactory predictions (McPhee and Arthur, 1991 for b; Winsauer et al., 1952 for F) and also, keeping in view the preliminary nature of this investigation, use of such data in place of the missing experimental data should be satisfactory.

For five samples, the drainage mercury capillary pressure curve data were available from their sources in the literature. For these data, vacuum is the wetting phase and mercury (surface tension 485 mN/m and contact angle 130° for samples from Thompson et al., 1987; surface tension 480 mN/m and contact angle 140° for the sample from Brown, 1951) is the non-wetting or invading phase. For one sample, oil-brine drainage capillary pressure curve was available (surface tension of oil 27.4 mN/m; oil-brine contact angle 0°; oil as the non-wetting phase and brine as the wetting phase).

In the present work, the maximum mercury capillary pressure of the samples from Thompson et al. (1987) is assumed to be at zero vacuum saturation. In practice, there is always a small vacuum saturation (of the order 0.05) which cannot be accessed by the mercury even at very high pressures. The main reasons for this phenomenon are:

One, it is very difficult to achieve 100% vacuum inside the sample before mercury is forced into it, and therefore, the compressed air occupies a very small fraction of the pore space even at very high mercury pressures; two, a few pores with extremely small sizes are generally present. For example, the sizes of the majority of the pores in the present samples are of the order of 1×10^{-6}m, whereas the size of the "small" pores are of the order of 1×10^{-9}m. However, the contribution of these "small" pores to the overall porosity of a sample is negligible.

6.4.2 Pore Structure Modeling of the Samples

Tables 6.4, 6.5 and 6.6 contain the values of the statistical parameters N_A, μ_δ, σ_δ and τ predicted by the network, serial capillary and parallel capillary models for the six samples, respectively. Based on the data in these tables, two observations can be made: One, the values of the parameters simulated by all the three models for each sample (lower numbers in braces) are almost identical to the values of the parameters found by inverting the equations (upper numbers). Based on this observation, it can be concluded that the change in pore structure of the models due to the reassignment of tube diameters to achieve constant areosity (details already presented in Section 5.1.1) is negligible. Two, the values of the parameters predicted by the three models for the same sample vary greatly. This observation is true for all the six samples. The values of μ_δ for all the six samples predicted by the network model are intermediate between those predicted by the parallel and serial capillary models, the values predicted by the parallel capillary model being the lowest and those predicted by the serial capillary model being the highest. As discussed in the previous chapter, the behavior of the parallel capillary model is sensitive to the upper portion of the tube diameter distribution because a fluid (electrical) particle travels through the same tube from the upstream to the downstream side of the REV. The model, therefore, predicts lower values of μ_δ. Opposite is the case with the serial capillary model in

which a fluid (electrical) particle is assumed to traverse all tube diameter sizes when traveling from the upstream to the downstream side of the REV, and therefore, the conducting capacity of a flow path inside the model determined by the tube with smallest diameter in the path. This makes the serial capillary model sensitive to the lower portion of the tube diameter distribution, thus predicting higher values of μ_δ. Due to the availability of multiple flow paths to a fluid (electrical) particle at each junction, the network model depicts an intermediate behavior.

The values of τ predicted by the network model are close to one for all the six samples whereas its values predicted by the serial capillary model lie between 1.44 and 1.85, and those predicted by the parallel capillary model lie between 1.63 and 2.2. Because the parallel and serial capillary models have no tubes in the $k = 2, 3$ directions, the values of τ predicted by these models are considerably higher than one. To model the porosity of a sample correctly, the value of τ predicted by the parallel capillary model is greater than that predicted by the serial capillary model because the value of μ_δ predicted by the parallel capillary model is lower than that predicted by the serial capillary model.

Tables 6.7, 6.8 and 6.9 contain the values of k_1, F, ϕ and b simulated by the three models corresponding to the six samples (the upper numbers). These tables also include the percent errors of the simulated values with respect to the experimental values (or values given by correlations) given in Tables 6.2 and 6.3 (the lower numbers). The errors in simulated values of the k_1, F and ϕ are very small thus confirming the earlier statement about the reassignment of tube diameters to achieve constant areosity. The errors in the simulated values of b with respect to the values given in Table 6.3 are relatively higher than those for k_1, F and ϕ, the maximum being for the limestone sample. Keeping in view the complexity of the pore structure of real porous media as compared to that of the idealized models, for the sandstone samples these errors are within satisfactory limits. The results for the limestone sample indicate

that the present procedure for modeling the pore structure is not appropriate for vuggy porous media such as limestones. This is because the present models ignore the vugs present in limestones.

It is appropriate at this point to mention about the robustness and uniqueness of the solution scheme presented in Section 6.2.2. It was found that for all the samples with given values of k_1, F, b and ϕ, the final solutions were independent of the initial guesses. Keeping in view the preliminary nature of this methodology at the present stage, it is sufficient to show that the solution scheme is robust and unique. However, for general application, the uniqueness and robustness of the solution has be checked more stringently. One approximate way to accomplish this objective is: For a given sample the value of one of the input properties (k_1, F, b and ϕ) may be changed by a small fraction and if the final solutions do not change significantly, the scheme can be said to be approximately unique and robust.

6.4.3 Drainage Capillary Pressure Curve of the Samples

Figures 6.2 through 6.6 illustrate the comparisons between the experimentally observed mercury drainage capillary pressure curves and the ones predicted by the models for four sandstone samples and the limestone sample. Except for the Berea sandstone and Austin Chalk limestone samples, all the three models satisfactorily predict the plateau portions of the capillary pressure curves.

For the limestone sample, a physical reason is available for the shape of the predicted curves. As shown by Wardlaw et al. (1987), the shape of the capillary pressure curves is influenced by the existence of pores (of larger size, also called vugs) and throats (of smaller size) and correlations between the sizes of the neighboring pores and throats, in addition to the pore and throat size distributions. It was shown by these workers that a high degree of pore-throat size correlation is present in the limestones, and consequently the slope of the drainage capillary pressure curve for

such rock samples may change very significantly near the zero mercury saturation point (or 100 percent vacuum saturation). As mentioned earlier, the present models ignore vugs. Also, the diameters are randomly assigned to the tubes of the models in which case no correlation exists between the neighboring tubes. These are the prime reasons for the inability of the present models to accurately reproduce the behavior of the limestones. These conclusions can also be corroborated with the work of Ferrand and Celia (1992) who studied the effect of different types of heterogeneity on the drainage capillary pressure curves of three-dimensional network models. The authors have shown that random network models are only suitable for homogeneous porous media and the shape of the drainage capillary pressure curves of such models is flat in the plateau portion. However, when heterogeneities are introduced in the network model, the effective drainage capillary pressure curve has a plateau region very similar the one in the experimentally determined curve on the limestone sample of Figure 6.6.

Wardlaw et al. (1987) found that the pore-throat size correlation was very small for the sandstone samples. However, at high capillary pressure, this correlation increases. This explains the good agreement between the experimentally observed and predicted capillary pressure curves in the plateau region and disagreement around zero vacuum saturation for the other sandstone samples. Berea being a sandstone sample, one would have expected results similar to those for the other sandstone samples. The probable reasons for such a behavior could either be the presence of non-uniformities in the pore structure which the models are unable to capture, or imperfect measurements of the properties of the sample.

Figure 6.7 illustrates the comparison between the experimentally observed oil-brine drainage capillary pressure curve and the similar curves predicted by the models for the sandstone sample from Longeron et al. (1989). As can be observed from the figure, all the three models satisfactorily predict the plateau portion of the curve.

Due to the absence of the "networking effect", the parallel and serial capillary models cannot account for the trapping of the wetting phase. The irreducible brine saturation predicted by the network model is 0.20, whereas 0.28 is the experimentally observed value. The influence of the pore-throat size correlations on the predicted capillary pressure curve, discussed in the previous paragraph, is accentuated when oil and water is used in place of mercury and vacuum. This is due to the isolation of the wetting phase mentioned earlier. This explains the larger disagreement between the experimentally observed and predicted oil-brine capillary pressure curve for this sample as compared to the disagreements between the observed and predicted mercury drainage capillary pressure curves for other sandstone samples near the irreducible wetting phase saturation (zero vacuum saturation for the mercury capillary pressure curves).

It is interesting to note that although the three models predict significantly different values of the pore structure parameters for the same sample, still the capillary pressure curves predicted by the models for the same sample do not vary appreciably. This indicates that all the three models are capable of qualitatively modeling the pore structure of a sample. However, as can be observed from the figures, the network model gives the best predictions out of the three models. Also, as indicated earlier, only the network model can account for the irreducible wetting phase saturations in oil-brine capillary pressure curves.

The above results indicate that the present methodology to model the pore structure is fundamentally correct. However, the models used in this methodology are not appropriate for modeling the pore structure of nonhomogeneous porous media such as limestones. Also, for homogeneous porous media encountered in practice such as sandstones, additional features need to be incorporated in the models so that their predictions of the capillary pressure curve are accurate for the complete saturation range. Some of these features are the assignment of volume to the junctions (in the

present models, no volume is assigned to the junctions) and the incorporation of pore-throat size correlations. A detailed discussion of these and other recommendations is presented in Chapter 7.

6.5 Summary

In this chapter, a methodology for modeling the pore structure of homogeneous porous media has been outlined. This methodology is based on the explicit relations of the transport properties (e.g., permeability, formation factor Klinkenberg coefficient and porosity) of the parallel capillary, serial capillary and network models to the statistical parameters describing their pore space, developed in Chapter 5. A preliminary study of this methodology has been conducted with the help of five sandstone samples and one limestone sample. For these samples, the drainage capillary pressure curves predicted by the methodology have been compared to the experimentally observed ones. The limitations of the models have been identified and recommendation to improve their predictions have been suggested.

For the same sample, the statistical parameters predicted by the three models vary significantly. The parallel and serial capillary models predict the lowest and highest values of the mean tube diameter, respectively, whereas the network model predicts an intermediate value for this parameter. All the three models satisfactorily simulated the permeability, formation factor, Klinkenberg coefficient and porosity of the sandstone samples. However, the errors in the simulated value of the Klinkenberg coefficient were significantly larger for the limestone sample.

The present models are found to be incapable of accurately predicting the capillary pressure curves for non-uniform porous media such as limestones. Except for one sandstone sample, all three models satisfactorily predicted the plateau portion of the drainage capillary pressure curves of the remaining sandstone samples, the predictions of the network model being the best. However, the models do not

accurately predict the capillary pressure curve of these samples near the irreducible wetting phase saturation. Incorporation of features such as the assignment of volume to the junctions and size correlations between the neighboring tubes are suggested to improve the predictions of the models near the irreducible wetting phase saturation for the sandstone samples.

Table 6.1. The bounds on N_A for real and positive roots of the set of nonlinear equations for the parallel capillary model with symmetrical tube diameter distributions.

Tube Diameter Distribution	Lower Bound on N_A	Upper Bound on N_A
Uniform	$\frac{0.125\,\phi^{0.5}}{\pi F^{1.5} k_1}$	$\frac{0.28125\,\phi^{0.5}}{\pi F^{1.5} k_1}$
Normal	$\frac{0.125\,\phi^{0.5}}{\pi F^{1.5} k_1}$	$\frac{0.375\,\phi^{0.5}}{\pi F^{1.5} k_1}$
Logistic	$\frac{0.125\,\phi^{0.5}}{\pi F^{1.5} k_1}$	$\frac{0.75\,\phi^{0.5}}{\pi F^{1.5} k_1}$

Table 6.2. Properties of the rock samples employed in the present work together with their sources in the literature.

#	Sample	Source	k_1 (m^2)	F	ϕ	b (Pa)
1	Sandstone	Longeron et al. (1989)	0.040×10^{-12}	22.100	0.184	NP+
2	Berea Sandstone	Thompson et al. (1987)	0.121×10^{-12}	16.129	0.205	NP+
3	Red Navajo Sandstone	Thompson et al. (1987)	1.123×10^{-12}	14.080	0.230	NP+
4	Boise Marsing 1 Sandstone	Thompson et al. (1987)	1.259×10^{-12}	20.325	0.239	NP+
5	Sandstone	Brown (1951)	1.411×10^{-12}	9.500++	0.281	NP+
6	Austin Chalk Limestone	Thompson et al. (1987)	3.109×10^{-15}	15.873	0.288	NP+

+NP–Not Provided.

++Experimental value not provided; found from Winsauer et al. (1952) correlation.

Table 6.3. The values of the Klinkenberg coefficient, b, of the samples, determined from Heid et al. (1950) and McPhee and Arthur (1991) regressions.

#	Sample	Source	b (Pa)	
			Heid et al. (1950)	McPhee & Arthur (1991)
1	Sandstone	Longeron et al. (1989)	18700	16248
2	Berea Sandstone	Thompson et al. (1987)	12127	10649
3	Red Navajo Sandstone	Thompson et al. (1987)	5092	4574
4	Boise Marsing 1 Sandstone	Thompson et al. (1987)	4870	4379
5	Sandstone	Brown (1951)	4658	4194
6	Austin Chalk Limestone	Thompson et al. (1987)	50759	42880

Table 6.4. The statistical parameters of the samples predicted by the network model.

#	Sample	Source	Statistical Parameters			
			N_A (1/m^2)	μ_δ (μm)	σ_δ (μm)	τ
1	Sandstone	Longeron et al. (1989)	2.400×10^9	5.1553$^+$ (5.1932)†	2.2470 (2.2772)	1.029 (1.029)
2	Berea Sandstone	Thompson et al. (87)	1.340×10^9	7.8125 (7.8382)	1.6507 (1.6481)	1.018 (1.018)
3	Red Navajo Sandstone	Thompson et al. (1987)	1.891×10^8	21.8963 (22.0250)	7.8716 (7.8551)	0.953 (0.953)
4	Boise Marsing 1 Sandstone	Thompson et al. (1987)	9.500×10^7	27.7536 (28.0805)	16.77120 (16.6955)	1.015 1.015
5	Sandstone	Brown (1951)	3.000×10^8	20.2192 (20.3249)	6.5540 (6.5414)	0.879 (0.879)
6	Austin Chalk Limestone	Thompson et al. (1987)	6.200×10^{10}	1.2170 (1.2296)	0.6790 (0.6763)	1.016 (1.016)

$^+$ Values determined by inverting the equations (upper values).

† Values present in the computer simulations of the model (lower values in the braces).

Table 6.5. The statistical parameters of the samples predicted by the serial capillary model.

#	Sample	Source	Statistical Parameters			
			N_A (1/m^2)	μ_δ (μm)	σ_δ (μm)	τ
1	Sandstone	Longeron et al. (1989)	2.000×10^9	8.0887$^+$ (8.1425)†	2.8872 (2.8895)	1.586 (1.586)
2	Berea Sandstone	Thompson et al. (1987)	1.500×10^9	10.1331 (10.1697)	2.74071 (2.7493)	1.579 (1.579)
3	Red Navajo Sandstone	Thompson et al. (1987)	2.000×10^8	29.6687 (29.8088)	8.5155 (8.5390)	1.536 (1.536)
4	Boise Marsing 1 Sandstone	Thompson et al. (1987)	1.000×10^8	38.8236 (39.0212)	11.7075 (11.7353)	1.852 (1.852)
5	Sandstone	Brown (1951)	3.500×10^8	25.8149 (25.9179)	6.5767 (6.6002)	1.441 (1.441)
6	Austin Chalk Limestone	Thompson et al. (1987)	6.000×10^{10}	1.7771 (1.7836)	0.5733 (0.5742)	1.754 (1.754)

$^+$ Values determined by inverting the equations (upper values).

† Values present in the computer simulations of the model (lower values in the braces).

Table 6.6. The statistical parameters of the samples predicted by the parallel capillary model.

#	Sample	Source	Statistical Parameters			
			N_A (1/m^2)	μ_δ (μm)	σ_δ (μm)	τ
1	Sandstone	Longeron et al. (1989)	6.000×10^9	4.1950$^+$ (4.2033)†	1.3226 (1.328)	2.016 (2.016)
2	Berea Sandstone	Thompson et al. (1987)	2.500×10^9	7.4963 (7.5032)	1.1130 (1.1158)	1.818 (1.818)
3	Red Navajo Sandstone	Thompson et al. (1987)	5.000×10^8	17.0760 (17.1129)	5.8319 (5.8583)	1.800 (1.800)
4	Boise Marsing 1 Sandstone	Thompson et al. (1987)	2.000×10^8	25.7099 (25.7431)	5.3718 (5.3877)	2.204 (2.204)
5	Sandstone	Brown (1951)	6.300×10^8	18.1527 (18.1789)	4.2194 (4.2330)	1.634 (1.634)
6	Austin Chalk Limestone	Thompson et al. (1987)	2.000×10^{11}	0.8573 (0.8601)	0.3482 (0.3501)	2.138 (2.138)

$^+$ Values determined by inverting the equations (upper values).

† Values present in the computer simulations of the model (lower values in the braces).

Table 6.7. The transport properties of the computer simulations of the network model for the various samples.

#	Sample	Source	Properties of the Model			
			k_1 (m^2)	F	ϕ	b (N/m^2)
1	Sandstone	Longeron et al. (1989)	0.418×10^{-13}*	21.58	0.186	16517.2
			4.6**	-2.3	2.1	$-11.7; 1.2^{\dagger}$
2	Berea Sandstone	Thompson et al. (1987)	0.124×10^{-12}	15.99	0.206	11224.8
			2.0	-2.0	0.6	-7.4; 5.1
3	Red Navajo Sandstone	Thompson et al. (1987)	0.116×10^{-11}	13.83	0.232	3924.2
			-3.6	-1.8	1.0	-22.9; -14.2
4	B. Marsing 1 Sandstone	Thompson et al. (1987)	0.136×10^{-11}	19.53	0.243	3041.8
			7.9	-8.1	1.5	-37.5; -30.5
5	Sandstone	Brown (1951)	0.146×10^{-11}	9.35	0.2834	4268.0
			3.2	-1.5	0.9	-8.4; 1.8
6	Austin Chalk Limestone	Thompson et al. (1987)	0.332×10^{-14}	15.32	0.292	69318.5
			6.9	3.4	1.4	36.6; 61.7

*Values of the properties of the computer simulations of the model (upper numbers).

**Percent errors in the properties of the model with respect to the experimentally observed values given in Tables 6.2 and 6.3 (lower numbers).

†Percent errors in b with respect to the values predicted by the Heid et al. and McPhee and Arthur regressions given in Table 6.3.

Table 6.8. The transport properties of the computer simulations of the serial capillary model for the various samples.

#	Sample	Source	Properties of the Model			
			k_1 (m^2)	F	ϕ	b (N/m^2)
1	Sandstone	Longeron et al. (1989)	0.425×10^{-13}*	21.82	0.186	18128.1
			6.2**	-1.3	1.1	-3.1; 11.6†
2	Berea Sandstone	Thompson et al. (1987)	0.122×10^{-12}	16.35	0.202	12037.8
			-0.7	0.0	-1.5	-0.7;11.5
3	Red Navajo Sandstone	Thompson et al. (1987)	0.116×10^{-11}	13.94	0.232	4322.1
			3.6	-1.0	0.9	-15.1;-5.5
4	B. Marsing 1 Sandstone	Thompson et al. (1987)	0.131×10^{-11}	20.86	0.241	3422.1
			4.1	-1.2	1.0	-29.7;-21.8
5	Sandstone	Brown (1951)	0.145×10^{-11}	9.41	0.283	4629.53
			2.7	2.7	0.8	-0.6;10.4
6	Austin Chalk Limestone	Thompson et al. (1987)	0.319×10^{-14}	15.16	0.285	74447.4
			2.5	0.9	-1.1	46.7;73.6

*Values of the properties of the computer simulations of the model (upper numbers).

**Percent errors in the properties of the model with respect to the experimentally observed values given in Tables 6.2 and 6.3 (lower numbers).

†Percent errors in b with respect to the values predicted by the Heid et al. and McPhee and Arthur regressions given in Table 6.3.

Table 6.9. The transport properties of the computer simulations of the parallel capillary model for the various samples.

#	Sample	Source	Properties of the Model			
			k_1 (m^2)	F	ϕ	b (N/m^2)
1	Sandstone	Longeron et al. (1989)	0.404×10^{-13}*	22.02	0.185	16055.5
			−0.9**	-0.4	0.4	-14.1; −1.2†
2	Berea Sandstone	Thompson et al. (1987)	0.122×10^{-12}	16.09	0.205	11206.5
			-0.5	0.2	0.2	-7.6; 5.23
3	Red Navajo Sandstone	Thompson et al. (1987)	0.114×10^{-11}	14.07	0.231	3750.2
			1.2	-0.5	0.5	-26.3; -18.0
4	B. Marsing 1 Sandstone	Thompson et al. (1987)	0.126×10^{-11}	20.28	0.240	3065.8
			0.5	-0.2	0.2	-37.03; -29.18
5	Sandstone	Brown (1951)	0.142×10^{-11}	9.48	0.2816	4212.8
			0.6	-0.2	0.3	-9.6; 0.4
6	Austin Chalk Limestone	Thompson et al. (1987)	0.315×10^{-14}	15.78	0.290	65470.0
			1.4	-0.5	0.5	29.0; 52.7

*Values of the properties of the computer simulations of the model (upper numbers).

**Percent errors in the properties of the model with respect to the experimentally observed values given in Tables 6.2 and 6.3 (lower numbers).

†Percent errors in b with respect to the values predicted by the Heid et al. and McPhee and Arthur regressions given in Table 6.3.

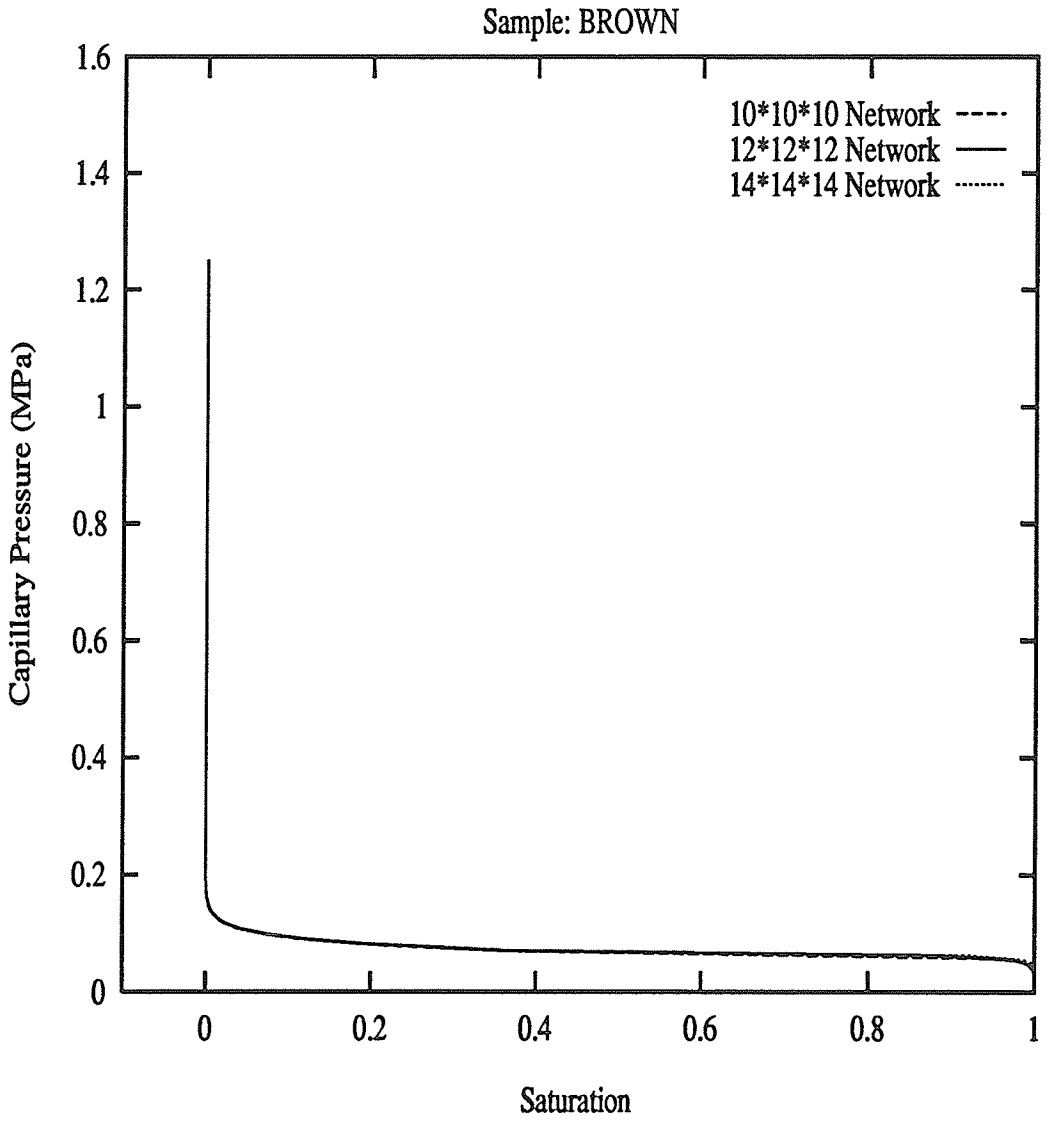

Fig. 6.1. The dependence of the shape of the mercury drainage capillary pressure curve on the size of the network. These are the predicted curves for the Brown (1951) sample.

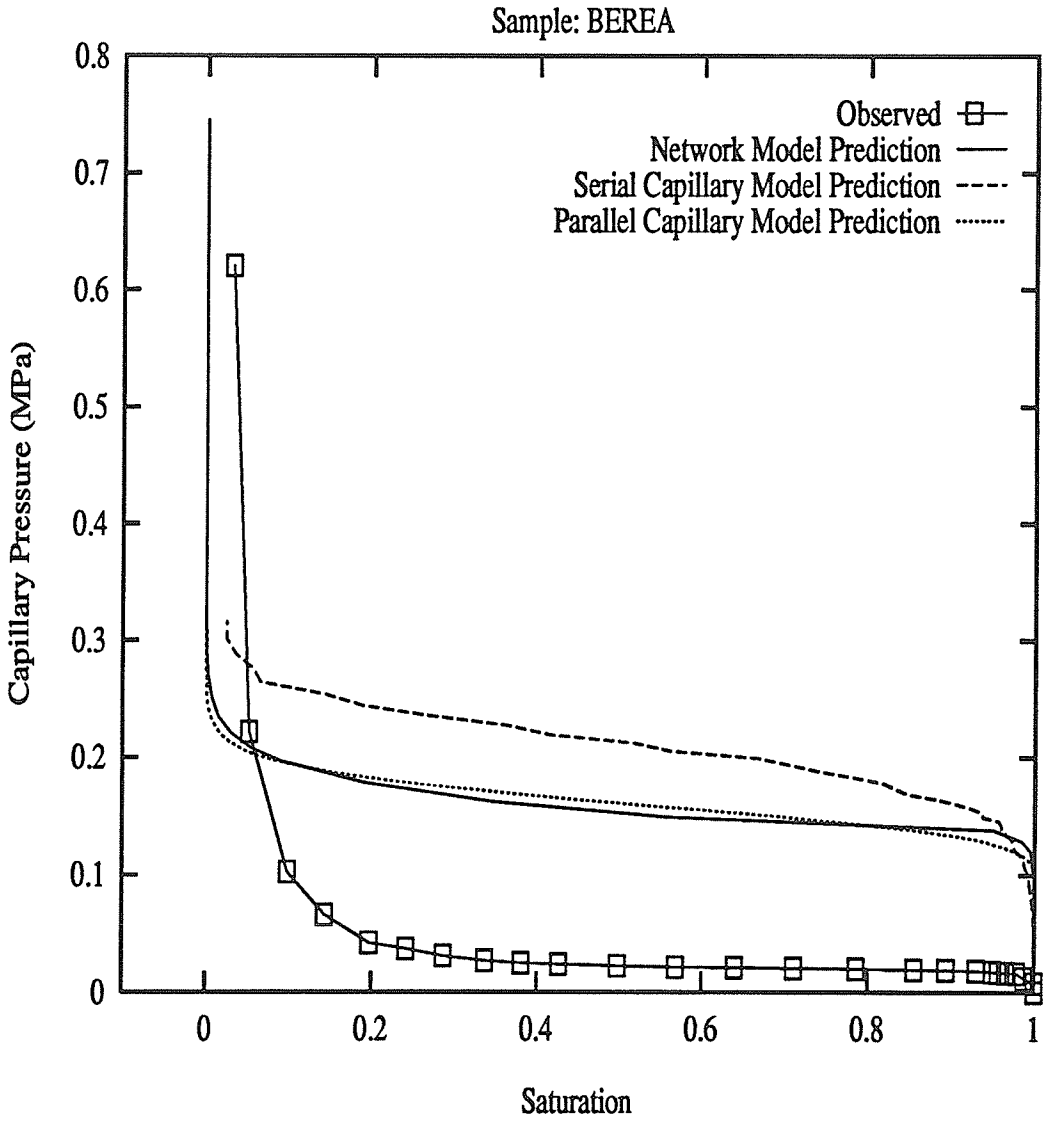

Fig. 6.2. Predicted and observed drainage mercury capillary pressure curves of the Berea sandstone sample from Thompson et al. (1987). Vacuum is the wetting phase.

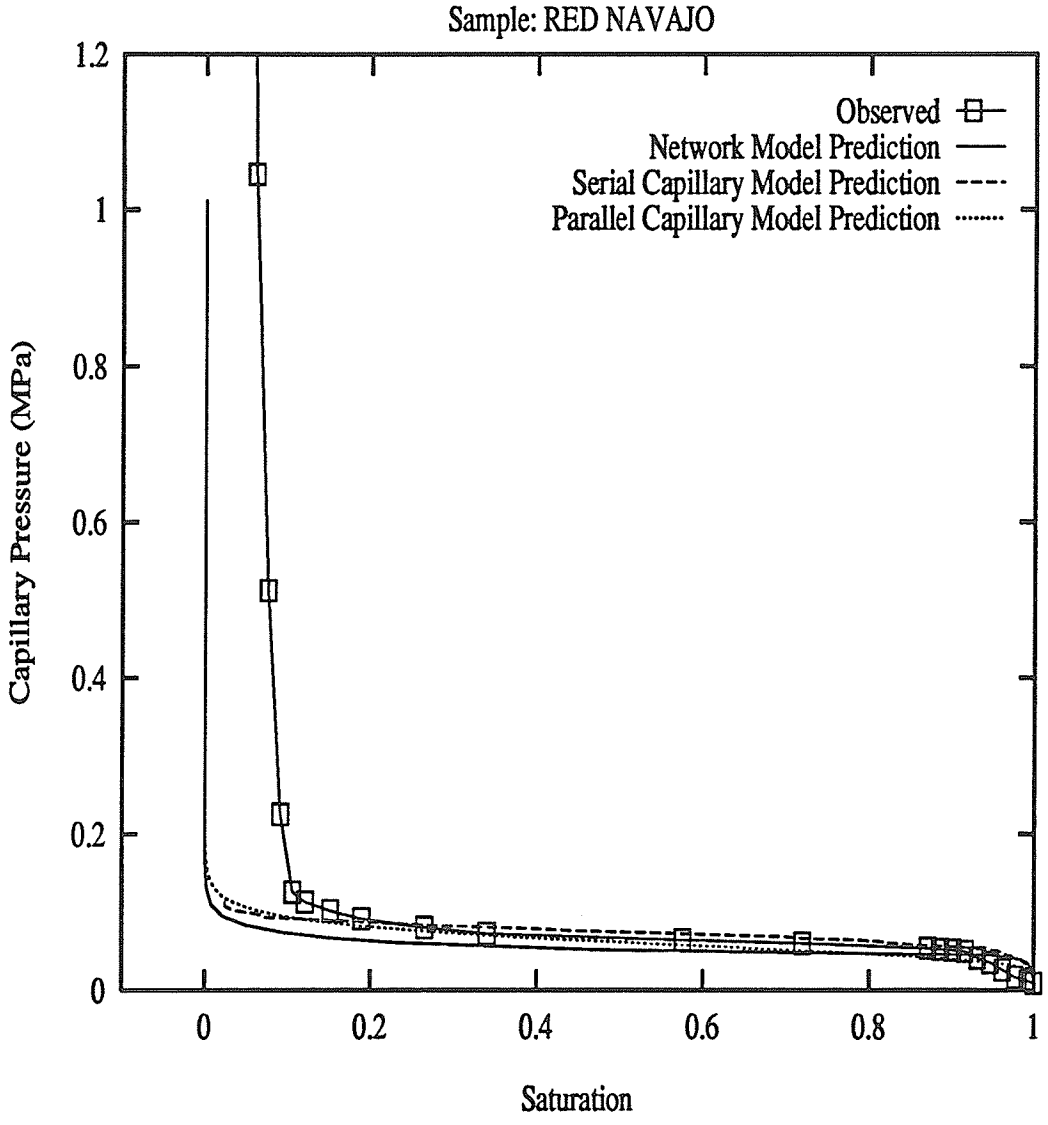

Fig. 6.3. Predicted and observed drainage mercury capillary pressure curves of the Red Navajo sandstone sample from Thompson et al. (1987). Vacuum is the wetting phase.

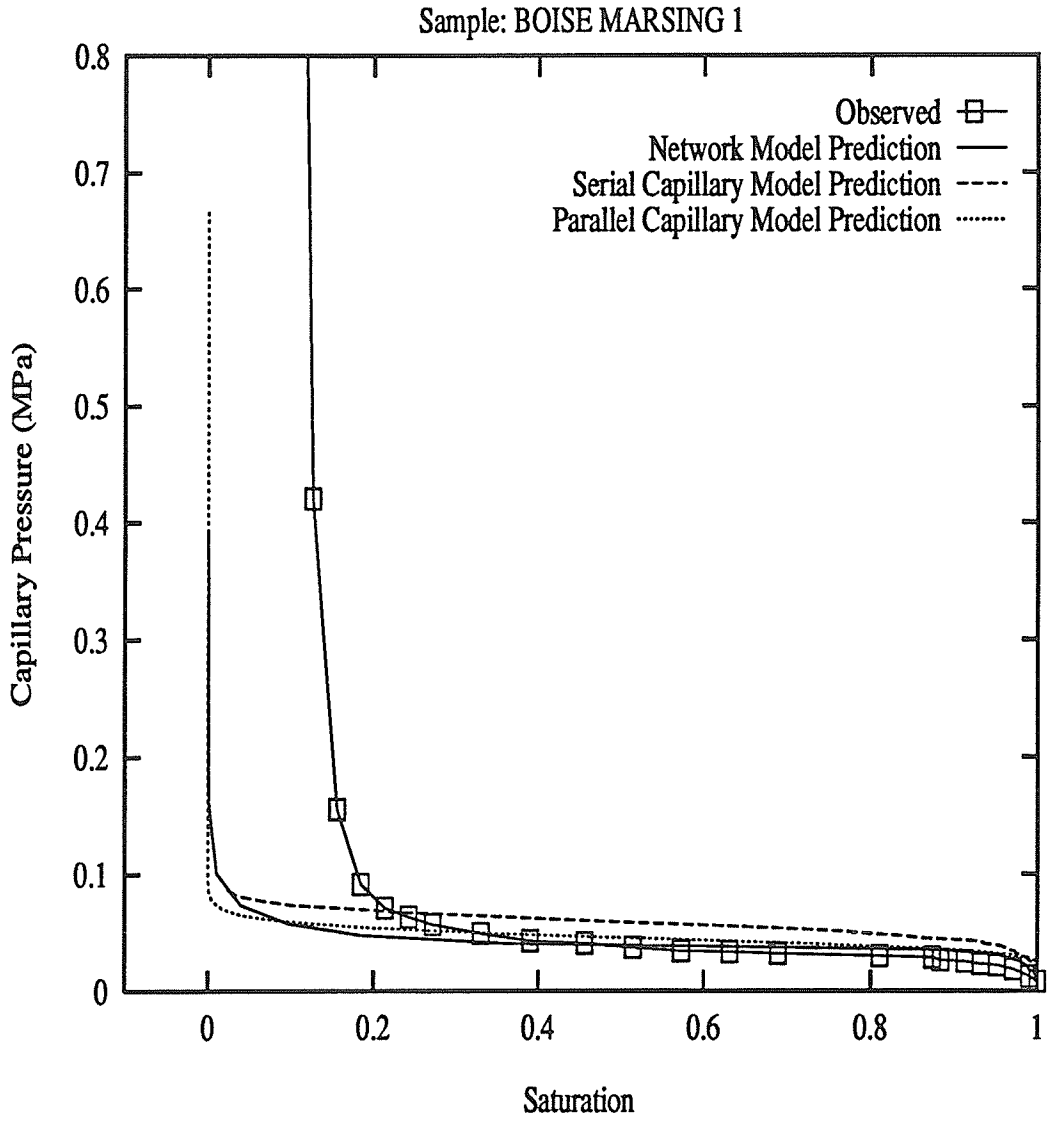

Fig. 6.4. Predicted and observed drainage mercury capillary pressure curves of the Boise Marsing 1 sandstone sample from Thompson et al. (1987). Vacuum is the wetting phase.

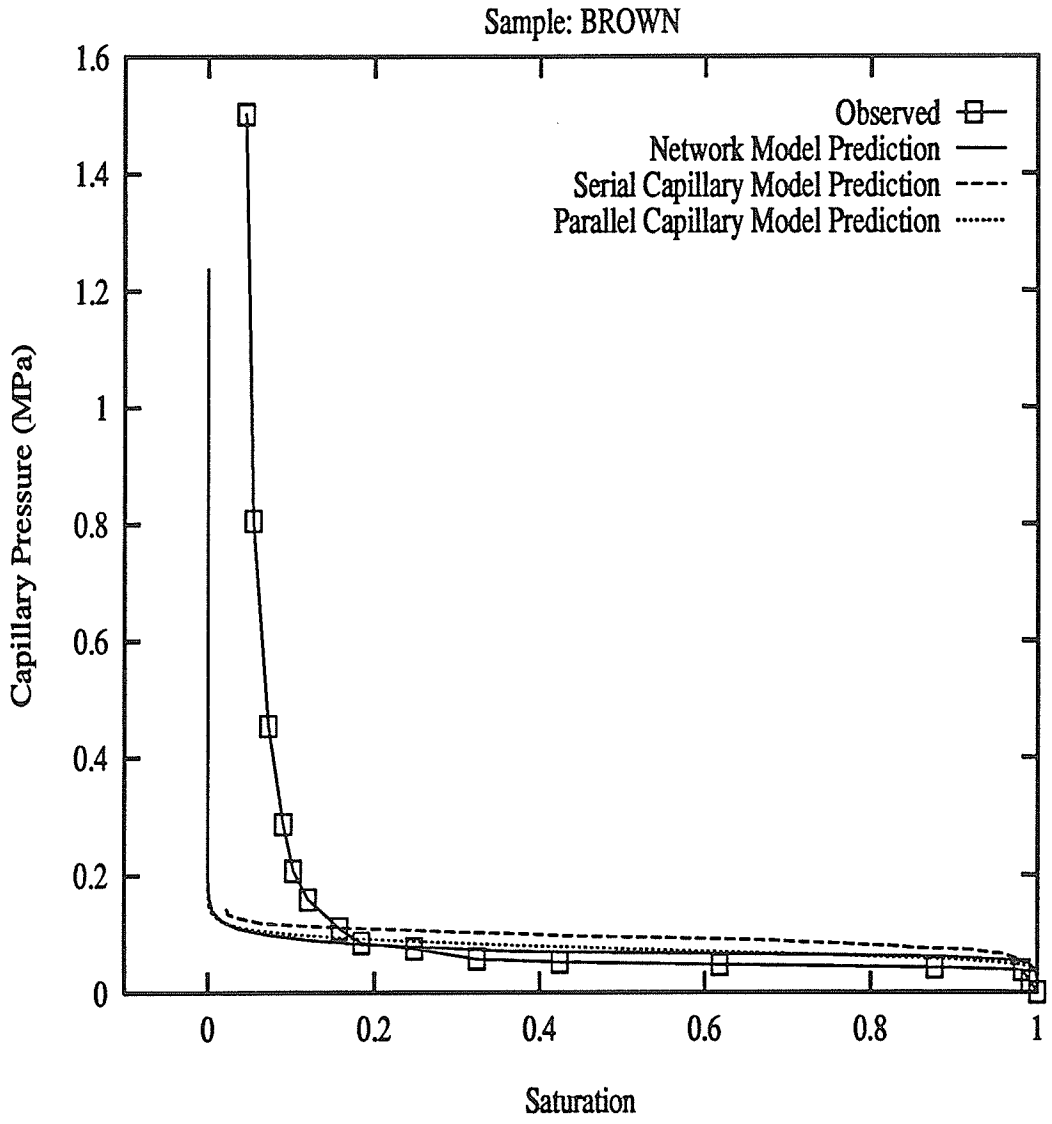

Fig. 6.5. Predicted and observed drainage mercury capillary pressure curves of the sandstone sample from Brown (1951). Vacuum is the wetting phase.

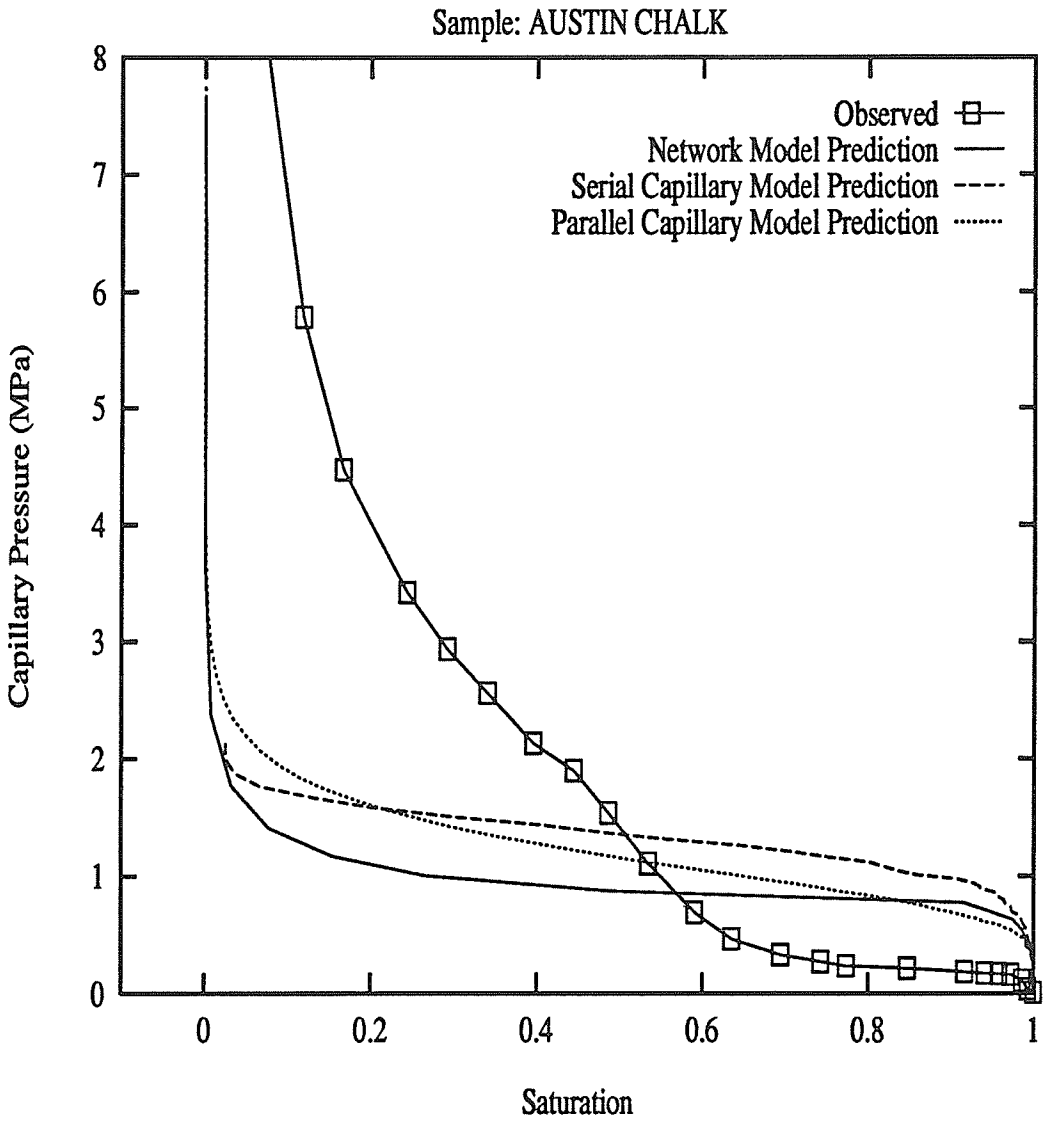

Fig. 6.6. Predicted and observed drainage mercury capillary pressure curves of the Austin Chalk limestone sample from Thompson et al. (1987). Vacuum is the wetting phase.

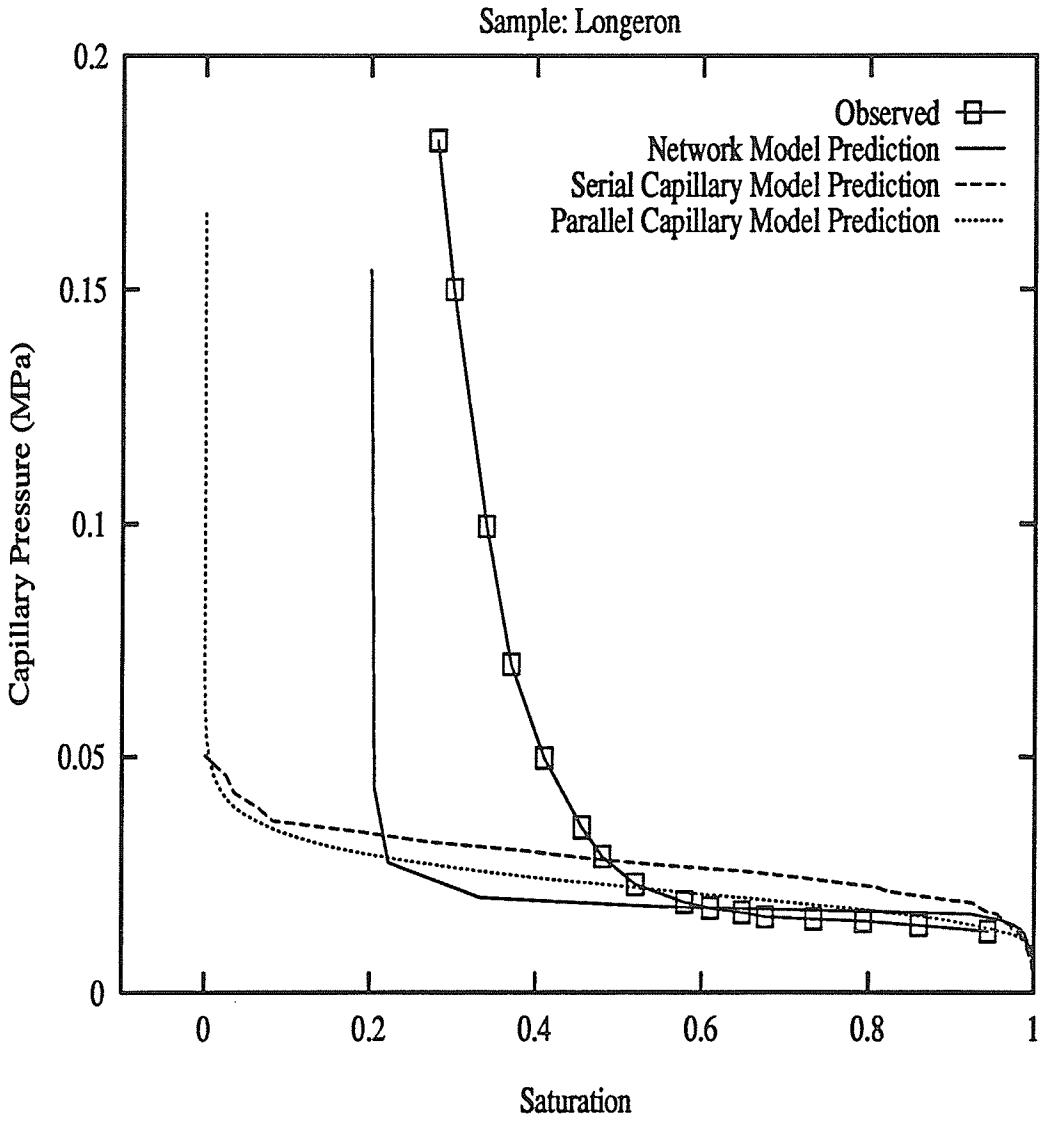

Fig. 6.7. Predicted and observed drainage oil-brine capillary pressure curve of the sandstone sample from Longeron et al. (1989). The trapping of the wetting phase (brine) is taken into account.

CHAPTER 7

CONCLUSIONS

In this chapter, the accomplishments of the present research are summarized and recommendations are given for future research.

7.1 Accomplishments of the Present Research

In the present research, the volume averaging method has been employed to study the relations of the macroscopic transport properties permeability, formation factor and Klinkenberg permeability to various features of pore structure. Explicit relations between these properties and the microscopic pore structure parameters of parallel capillary, serial capillary and three-dimensional cubic network models of porous media have been derived. The dependence of the tortuosity of porous media on various terms in the averaged conservation equations has been studied. A methodology to model the pore structure and to predict the drainage capillary pressure curves of homogeneous porous media has been outlined. A preliminary study based on this methodology has been conducted on real porous media samples. The present research, briefly outlined above, can be divided into four major parts. The main accomplishments of each part and the conclusions supported by it, are presented below:

7.1.1 Development of Integral Expressions for Macroscopic Transport Properties

Explicit integral expressions have been derived for the macroscopic transport properties permeability, formation factor and Klinkenberg permeability of homogeneous porous media. This has been accomplished by comparing the appropriate volume

averaged microscopic conservation equations (mass and momentum for permeability and Klinkenberg permeability, and electric charge for formation factor) to the corresponding phenomenological laws (Darcy's law for permeability and Klinkenberg permeability, and Ohm's law at macroscopic level for the formation factor). The expression for each property consists of two terms which involve integrals of the related microscopic field variables. These integrals contain the information about the influence of the pore structure on flow, "hidden" in the macroscopic properties.

The derivation of the integral expression for permeability (and consequently the derivation of the integral expression for Klinkenberg permeability) has been presented in the perspective of the previously reported literature. The integral expression for formation factor is an entirely new contribution. These integral expressions form the basis of the present research. Unlike the previous works (O'Neill and Gray, 1976; Hassanizadeh and Gray, 1980; Whitaker, 1986a), explicit interpretations is given to different terms in these expressions.

To derive the integral expressions, a property of the pore structure, termed "areosity" in the present study, has been introduced. The areosity in a direction denotes the average of the ratios of the effective cross-sectional areas open to flow and the corresponding bulk areas along that direction, over an REV. Because the effective areas depend on the local microscopic flow direction, the areosity is different from the areal porosity and therefore from the porosity. The integral expressions are only valid when the effective area open to flow is constant along the macroscopic flow direction.

7.1.2 Validation and Interpretation of the Integral Expressions

The validity of the integral expressions has been confirmed with the help of three idealized porous media and network theory (details about network theory have been presented in Appendix B). In general, the expressions are valid for any homogeneous

porous medium when the assumptions concerning the flow (fluid and electric) through it, stated in the previous section, are satisfied. The physical meanings of the viscous and pressure terms in the integral expression for permeability, and the current and potential terms in the integral expression for formation factor have been discussed. A general and exact relation between the formation factor, F, and the tortuosity, τ', of a porous medium, in the form $\tau' = F\,\xi_1$ has been presented. Here, ξ_1 is the areosity. The main conclusions of this part of the present research are given below:

1. The effective area open to flow in the macroscopic flow direction must remain constant in order for the predictions of the integral expressions and the network theory to be the same. However, the effective open area may vary in any manner in the other principal directions. Therefore the expressions are also valid for anisotropic porous media.
2. The viscous and current terms represent the flow (fluid and electric) in the macroscopic flow direction whereas the pressure and potential terms represent the flow (fluid and electric) in the directions normal to the macroscopic flow direction. The microscopic flow in the directions normal to the macroscopic flow direction is termed "microscopic cross flow" in the present study.
3. The magnitude of the microscopic cross flow in porous media depends on the variation of the conductances of the tubes in the macroscopic flow direction, and the conductances of the cross flow tubes themselves.
4. The microscopic cross flow can have a profound influence on the permeability (formation factor) in the macroscopic flow direction.
5. The microscopic cross flow in porous media is directly related to tortuosity.
6. In the presence of the microscopic cross flow in porous media in which multiple flow paths are available to the flowing fluid (electric) particles at

intersections of the flow channels, the classical definition of tortuosity as a ratio of geometric lengths is simplistic. This study suggests two types of tortuosities, one accounting for the sinuousness of the individual flow channels (classic definition of tortuosity) and the other accounting for the microscopic cross flow resulting due to the availability of multiple flow paths.

7. In the presence of microscopic cross flow in porous media with multiple flow (electric or fluid) paths, the equivalence of hydraulic and electric tortuosities is not valid.

7.1.3 Development of Relations Between the Macroscopic Transport Properties and Microscopic Pore Structure Parameters

Based on the integral expressions, closed form explicit relations between the permeability, Klinkenberg permeability and formation factor, and the statistical parameters characterizing the pore space of parallel and serial capillary models of porous media have been derived. With the help of nonlinear regression, similar relations, based on the integral expressions, have also been developed for the permeability and formation factor of a three-dimensional cubic network model. In these models, the diameters of the tubes are assigned according to the lognormal distribution and the lengths are kept fixed. For permeability and Klinkenberg permeability calculations, fully developed laminar flow has been assumed inside the tubes. For formation factor calculations, the electric flow inside a tube saturated with an electric conductor has been assumed to be given by the Ohm's law. A comparison has been made between the predictions of the present relations and those developed by Nicholson et al. (1988), which are based on the effective-medium approximation (EMA) (Kirkpatrick, 1973). An analysis has been performed to determine the size of a model that qualifies as an REV with respect to permeability, formation factor, Klinkenberg coefficient, porosity

and capillary pressure. The main conclusions of this part of the present research are given below:

1. The permeability of the parallel capillary model increases by approximately five orders of magnitude when a_δ changes from 0 to 1.2. Here a_δ is the coefficient of variation of the tube diameter distribution and represents the breadth of the distribution. For the serial capillary model, the permeability decreases by the same order of magnitude when a_δ goes from 0 to 1.2. These results are in conformity with the Scheidegger's observation (Scheidegger, 1974) according to which the parallel capillary model is sensitive to the upper portion of the tube diameter distribution and the serial capillary model is sensitive to the lower portion of the tube diameter distribution.

2. The permeability of the network model decreases as a_δ decreases. However, the decrease between the values of a_δ equal to 0 and 1.2 is of the same order of magnitude. This relatively small change for the network model, in comparison with the capillary models, is more representative of the real porous media and is due to the presence of the networking effect in the network model. Similar results have also been found for the formation factor of the models.

3. In the present study, the relations of permeability and formation factor of network model to the statistical parameters characterizing its pore structure, have been developed for values of a_δ up to 1.2. The predictions of similar relations based on the effective-medium theory (Nicholson et al., 1988) are found to deteriorate for $a_\delta > 0.25$ in the case of permeability and for $a_\delta > 0.3$ in the case of formation factor.

4. Out of the properties permeability, formation factor, Klinkenberg coefficient and porosity, it is sufficient to find the REV size of a model with

respect to permeability only. A $12 \times 12 \times 12$ size with 50 realizations is a satisfactory representative size for the network model. Such size for the parallel capillary model is 13 000 tubes with 100 realizations. For the serial capillary model, the representative size is 750×750 (750 flow paths with 750 tubes in each path) with 100 realizations.

7.1.4 Development of a Methodology for Modeling Pore Structure

A methodology for modeling the pore structure of homogeneous porous media has been outlined. This methodology is based on the explicit relations of the transport properties (e.g., permeability, formation factor and Klinkenberg coefficient) of the parallel capillary, serial capillary and network models to the statistical parameters describing their pore space, discussed in the previous section, and a similar relation for porosity. A preliminary study of this methodology has been conducted with the help of five sandstone samples and one limestone sample. For these samples, the drainage capillary pressure curves predicted by the methodology have been compared to the experimentally observed ones. The limitations of the models have been identified and recommendations to improve their predictions have been suggested. The main conclusions of this part of the present research are given below:

1. For the same sample, the statistical parameters predicted by the three models vary significantly. The parallel and serial capillary models predict the lowest and highest values of the mean tube diameter, respectively, whereas the network model predicts an intermediate value for this parameter.

2. All the three models satisfactorily simulated the permeability, formation factor, Klinkenberg coefficient and porosity of the sandstone samples. However, the errors in the simulated value of the Klinkenberg coefficient

were significantly larger for the limestone sample.

3. The present models are unable to accurately predict the capillary pressure curves of non-uniform porous media such as limestones.

4. Except for one sandstone sample, all three models satisfactorily predicted the plateau portion of the drainage capillary pressure curves of the remaining sandstone samples, the predictions of the network model being the best. However, the models did not accurately predict the capillary pressure curves of these samples near the irreducible wetting phase saturation.

5. Incorporation of features such as the assignment of volume to the junctions and size correlations between the neighboring tubes has been suggested to improve the predictions of the models near the irreducible wetting phase saturation for the sandstone samples. These and other recommendations are discussed in the following section.

7.2 Recommendations

1. In the present study, the junctions in the network model (the confluence of two or more tubes) are assumed to possess no volume. It is recommended that a given pore volume be assigned to the junctions (in which case they will be called the pores). In order to carry out this effectively, the following issues have to be addressed:

   - What percentage of the total pore volume should be assigned to the pores ?
   - Should the sizes of pores be distributed according to a probability density distribution or should they be fixed ?

- Should the resistance offered by the pores to the flow (fluid and current) be considered or ignored ? If it is considered, then how should it be incorporated ?
- How would the additional lengths introduced by the pores in the flow paths affect the tortuosity of the model ?

2. The effects of correlations between the sizes of the neighboring pores and tubes, neighboring tubes and tubes, and neighboring pores and pores on permeability, formation factor, Klinkenberg coefficient and shape of the drainage capillary pressure curves should be studied in detail. This study may help in the incorporation of these correlations in the structure of the network model in a meaningful way.
3. The algorithm used in the present study for calculating the drainage capillary pressure curve of the network model considers the mercury intrusion (oil in oil-brine curves) in one tube at a time. It is recommended that an algorithm be developed which can simultaneously track the mercury fronts at different locations inside the network. It is expected that the incorporation of this suggestion will improve the accuracy of the irreducible wetting phase saturation predicted by the model.
4. It is recommended that algorithms be developed for calculating the relative permeabilities and resistivity index of the models and incorporated in the present methodology.
5. The relations of the permeability and formation factor of the network model to its pore structure parameters, developed in the present study, are valid for a coordination number of 6. It is recommended that similar relations be developed for other coordination numbers.

REFERENCES

Adzumi, H., "On the flow of gases through a porous wall," *Bull. Chem. Soc. Japan*, **12**, 304–312 (1937).

Ahmed, G., and J. A. Blackman, "On theories of transport in disordered media," *J. Phys. C*, **12**, 837–853 (1979).

Aitchison, J., and J. A. C. Brown, *The Lognormal Distribution*, Cambridge University Press, Cambridge (1969).

American Petroleum Institute, *Recommended Practice for Determining Permeability of Porous Media*, Report RP 27, 3rd edn, Washington DC: API (1956).

Anderson, T. B., and R. Jackson, "A fluid mechanical description of fluidized beds," *Ind. Engng. Chem. Fundam.*, **6**, 527–538 (1967).

Androutsopoulos, G. P., and R. Mann, "Evaluation of mercury porosimetry experiments using a network pore structure model," *Chem. Engng. Sci.*, **34**, 1203–1212 (1979).

Archie, G. E., "The electric resistivity log as an aid in determining some reservoir characteristics," *Petroleum Trans. AIME*, **146**, 54–61 (1942).

Avellaneda, M., and S. Torquato, "Rigorous link between fluid permeability, electrical conductivity, and relaxation times for transport in porous media," *Phys. Fluids A*, **3**, 2529–2540 (1991).

Bachmat, Y., and J. Bear, "Macroscopic modelling of transport phenomena in porous media. I: the continuum approach," *Transport in Porous Media*, **1**, 213–240 (1986).

Barak, A. Z., "Comments on 'High velocity flow in porous media' by Hassanizadeh and Gray," *Transport in Porous Media*, **2**, 533–535 (1987).

Barak, A. Z., and J. Bear, "Flow at high Reynolds number through anisotropic porous media," *Adv. Water Resour.*, **4**, 54–66 (1981).

Barrer, R. M., "The measurement of surface area of finely divided solids by the flow of gases through them," *Brit. J. Appl. Phys.* Paper B.1, s41–s49 (1953).

Barrere, J., O. Gipouloux, and S. Whitaker, "On the closure problem for Darcy's law," *Transport in Porous Media*, **7**, 209–222 (1992).

Bathe, K. J., *Finite Element Procedures in Engineering Analysis*, Prentice-Hall, Inc., Englewood Cliffs, New Jersey (1982).

Bear, J., *Dynamics of Fluids in Porous Media*, Elsevier, New York (1972).

Bear, J., and Y. Bachmat, "Hydrodynamic dispersion in non-uniform flow through porous media, taking into account viscosity differences," (in Hebrew with English summary), Hydraulic Lab., Technion, Haifa, Israel, IASH, P.N. 4/66 (1966).

Bear, J., and Y. Bachmat, "A generalized theory on hydrodynamic dispersion in porous media," *I.A.S.H. Symp. Artificial Recharge and Management of Aquifers, Haifa*, Israel, IASH, P.N. 72, 7–16 (1967).

Bear, J., and Y. Bachmat, "Macroscopic modelling of transport phenomena in porous media. II: Application to mass, momentum and energy transport," *Transport in Porous Media*, **1**, 241–269 (1986).

Bear, J., and Y. Bachmat, *Introduction to Modeling of Transport Phenomena in Porous Media*, Kluwer Academic Publishers, Dordrecht, The Netherlands (1991).

Bear J., B. Carol, and P. C. Menier, "Effective and relative permeabilities of anisotropic porous media," *Transport in Porous Media*, **2**, 301–316 (1987).

Beran, M. J., *Statistical Continuum Theories*, Interscience, New York (1968).

Bertin, H., M. Quintard, P. V. Corpel, and S. Whitaker, "Two-phase flow in heterogeneous porous media III: laboratory experiments for flow parallel to a stratified system," *Transport in Porous Media*, **5**, 543–590 (1990).

Blunt, M., and P. King, "Relative permeabilities from two- and three-dimensional pore-scale network modelling," *Transport in Porous Media*, **6**, 407–433 (1991).

Brinkman, H. C., "A calculation of viscous force exerted by a flowing fluid on a dense swarm of particles," *Appl. Sci. Res.*, **A1**, 27–34 (1947).

Brown, H. W., "Capillary pressure investigations," *Petroleum Trans. AIME*, **192**, 67–74 (1951).

Bruggeman, D. A. G., "Calculation of various physical constants of heterogeneous substances. 1. Dielectric constant and conductivity of isotropic substances," *Ann. Phys. (Leipzig)*, **24**, 636–644, 665–679 (1935).

Carbonell, R. G., and S. Whitaker, "Heat and mass transfer in porous media," in *Fundamentals of Transport in Porous Media* (edited by J. Bear and Y. Corapcioglu), Martinus Nijhoff, Brussels (1984).

Carman, P. C., "Fluid flow through granular beds," *Trans. Inst. Chem. Engng. London*, **15**, 150–156 (1937).

Carman, P. C., "Determination of specific surface of powders I," *J. Soc. Chem. Indus.*, **57**, 225–234 (1938).

Chatzis, I, and F. A. L. Dullien, "Modelling pore structure by 2-D and 3-D networks with application to sandstones," *J. Canadian Petrol. Technol.*, **16**, 97–108 (1977).

Chatzis, I., and F. A. L. Dullien, "The modeling of mercury porosimetry and the relative permeability of mercury in sandstones using percolation theory," *Int. Chem. Engng.*, **25**, 47–66 (1985).

Childs, E. C., and N. Collis-George, "The permeability of porous materials," *Proc. Royal Soc. London, Ser. A*, **201**, 392–405 (1950).

Conner, W. C., A. M. Lane, K. M. Ng, and M. Goldblatt, "Measurement of the morphology of high surface area solids: porosimetry of agglomerated particles," *J. Catal.*, **83**, 336–345 (1983).

Conner, W. C., A. M. Lane, "Measurement of the morphology of high surface area solids: effects of network structure on the simulation of the porosimetry," *J. Catal.*, **89**, 217–225 (1984).

Cornell, D., and D. L. Katz, "Flow of gases through consolidated porous media," *Ind. Engng. Chem.*, **45**, 2145–2152 (1953).

Coulaud, O., P. Morel, and J. P. Caltagirone, "Numerical modelling of nonlinear effects in laminar flow through a porous medium," *J. Fluid Mech.*, **190**, 393–407 (1988).

Cox, M. A. A., "Mercury injection measurements used in the prediction of rock pore dimensions employing a crystalline lattice of capillaries," *Chem. Engng. Sci.*, **46**, 167–172 (1991).

Crow, E. L., and K. Shimizu, *Lognormal Distributions Theory and Applications*, Marcel Dekker Inc., New York (1988).

Cvetkovič, V. D., "A continuum approach to high velocity flow in porous media," *Transport in Porous Media,* **1**, 63–97 (1986).

Dagan, G., *Flow and Transport in Porous Formations*, Springer-Verlag, Berlin (1989).

Dagan, G., and E. Bresler, "Unsaturated flow in spatially variable fields, 1, Derivation of models of infiltration and redistribution," *Water Resour. Res.*, **19**(2), 413–420 (1983).

Darcy, H., *Les Fontaines publiques de la ville de Dijon*, Dalmont, Paris (1856).

De Josselin De Jong, G., "The tensor character of dispersion coefficient in anisotropic porous media," *1st IAHR Symp. Fundamentals of Transport Phenomena in Porous Media*, Haifa (1969).

Diaz, C. E., I. Chatzis, and F. A. L. Dullien, "Simulation of capillary pressure curves using bond correlated site percolation on a simple cubic network," *Transport in Porous Media*, **2**, 215–240 (1987).

Dodd, C. G., and O. G. Kiel, "Evaluation of Monte-Carlo methods in studying displacement and wettability in porous rocks," *J. Phys. Chem.*, **63**, 1646–1652 (1959).

Drake, L. C., and H. L. Ritter, "Macroscopic-size distributions in some typical porous substances," *Ind. Engng. Chem. Anal. Ed.*, **17**, 787–791 (1945).

Dullien, F. A. L., "New network permeability model of porous media," *AIChE J.*, **21**, 299–307 (1975).

Dullien, F. A. L., "Effects of pore structure on capillary and flow phenomena in sandstones," *J. Canadian Petrol. Technol.*, **July–September**, 48–55 (1975a).

Dullien, F. A. L., *Porous Media: Fluid Transport and Pore Structure*, Academic Press, New York (1979).

Dullien, F. A. L., and M. I. S. Azzam, "Flow rate-pressure gradient measurements of periodically non-uniform capillary tubes," *AIChE J.*, **19**, 222–229 (1973).

Du Plessis, J. P., "Saturated crossflow through a two-dimensional porous medium," *Adv. Water Resour.*, **14**(3), 131–137 (1991).

Du Plessis, J. P., and J. H. Masliyah, "Mathematical modelling of flow through consolidated isotropic porous media," *Transport in Porous Media*, **3**, 145–161 (1988).

Du Plessis, J. P., and J. H. Masliyah, "Flow through isotropic granular porous media," *Transport in Porous Media*, **6**, 207–221 (1991).

Ehrlich, R., and F. E. Crane, "A model for two-phase flow in consolidated materials," *Soc. Pet. Engng. J.*, **June**, 221–231 (1969).

Ene, H. I., "Application of the homogenization method to transport in porous media," in J. H. Cushman (ed.), *Dynamics of Fluids in Hierarchical Porous Media*, Academic Press, New York, 223–241 (1990).

Ertekin, T., G. R. King, and F. C. Schwerer, "Dynamic gas slippage: a unique dual-mechanism approach to the flow of gases in tight formations," *SPE Formation Evaluation*, **1**, 43–52 (1986).

Fancher, G. H., and J. A. Lewis, "Flow of simple fluids through porous materials," *Ind. Engng. Chem.*, **25**, 1139–1147 (1933).

Fatt, I., "The network model of porous media," in 3 parts, *Petroleum Trans. AIME*, **207**, 144–181 (1956).

Ferrand, L. A., and M. A. Celia, "Development of three-dimensional network model for quasi-static immiscible displacement," in Proceedings of the International Symposium on Contaminant Transport in Groundwater (Stuttgart), edited by H. E. Kobus and W. Kinzelbach, pp. 394–403, Balkema, Rotterdam, The Netherlands (1989).

Ferrand, L. A., and M. A. Celia, "A percolation-based model for drainage in porous media," *Water Resour. Rep. WR-90-2*, Princeton University, Princeton, New Jersy (1990a).

Ferrand, L. A., and M. A. Celia, "A computational investigation of the effects of heterogeneity on the capillary pressure-saturation relation," in Computational Methods in Subsurface Flow (Proceedings of the 8th International Conference on Computational Methods in Water Resources), edited by G. Gambolati et al., Computational Mechanics, Southampton, U. K. (1990b).

Ferrand, L. A., and M. A. Celia, "The effect of heterogeneity on the drainage capillary pressure-saturation relation," *Water Resour. Res.*, **28**(3), 859–870 (1992).

Forchheimer, P., "Wasserbewegung durch boden," *Zeit. Ver. Deutsch. Ing.*, **45** (1901).

Gray, W. G., "A derivation of the equations for multi-phase transport," *Chem. Engng. Sci.*, **30**, 229–233 (1975).

Gray, W. G., and K. O'Neill, "On the general equations for flow in porous media and their reduction to Darcy's law," *Water Resour. Res.*, **12**, 148–154 (1976).

Gray, W. G., and P. C. Y. Lee, "On the theorems for local averaging of multiphase systems," *Int. J. Multiphase Flow*, **3**, 333–340 (1977).

Gray, W. G., and S. M. Hassanizadeh, "Averaging theorems and averaged equations for transport of interface properties in multiphase systems," *Int. J. Multiphase Flow*, **15**, 81–95 (1989).

Gray, W. G., and S. M. Hassanizadeh, "Paradoxes and realities in unsaturated flow theory," *Water Resour. Res.*, **27**(8), 1847–1854 (1991a).

Gray, W. G., and S. M. Hassanizadeh, "Unsaturated flow theory including interfacial phenomena," *Water Resour. Res.*, **27**(8), 1855–1863 (1991b).

Gurland, J., "An estimate of contact and continuity of dispersions in opaque samples," *Trans. Metall. Soc. AIME*, **236**, 642–646 (1966).

Happel, J. and H. Brenner, *Low Reynolds Number Hydrodynamics, with Special Applications to Particulate Media*, Prentice-Hall, Englewood Cliffs, New Jersey (1965).

Haring, R. E., and R. A. Greenkorn, "A statistical model of a porous medium with nonuniform pores," *AIChE J.*, **16**, 477–483 (1970).

Harleman, D. R. E., P. F. Mehlhorn, and R. R. Rumer, "Dispersion-permeability correlation in porous media," *J. Hydraul. Div. Amer. Soc. Civil. Engng.* No. HY2, **89**, 67–85 (1963).

Hassanizadeh, S. M., "Macroscopic description of multi-phase systems—a thermodynamic theory of flow in porous media," Ph.D. Thesis, Princeton University, New Jersey (1979).

Hassanizadeh, M., and W. G. Gray, "General conservation equations for multi-phase systems: 1. Averaging procedure," *Adv. Water Resour.*, **2**, 131–144 (1979a).

Hassanizadeh, M., and W. G. Gray, "General conservation equations for multi-phase systems: 2. Mass, momenta, energy, and entropy equations," *Adv. Water Resour.*, **2**, 191–203 (1979b).

Hassanizadeh, M., and W. G. Gray, "General conservation equations for multi-phase systems: 3. Constitutive theory for porous media flow," *Adv. Water Resour.*, **3**, 25–40 (1980).

Hassanizadeh, S. M., and W. G. Gray, "High velocity flow in porous media," *Transport in Porous Media*, **2**, 521–531 (1987).

Hassanizadeh, S. M., and W. G. Gray, "Reply to comments by Barak on 'High velocity flow in porous media' by Hassanizadeh and Gray," *Transport in Porous Media*, **3**, 319–321 (1988).

Hassanizadeh, S. M., and W. G. Gray, "Derivation of conditions describing transport across zones of reduced dynamics within multiphase systems," *Water Resour. Res.*, **25**(3), 529–539 (1989a).

Hassanizadeh, S. M., and W. G. Gray, "Boundary and interface conditions in porous media," *Water Resour. Res.*, **25**(7), 1705–1715 (1989b).

Hassanizadeh, S. M., and W. G. Gray, "Mechanics and thermodynamics of multiphase flow in porous media including interphase boundaries," *Adv. Water Resour.*, **13**(4), 169–186 (1990).

Heid, J. G., J. J. McMahon, R. F. Neilson, and S. T. Yuster, "Study of permeability of rocks to homogeneous fluids," *API Drill. Prod. Prac.*, 230–246 (1950).

Howes, F. A., and S. Whitaker, "The spatial averaging theorem revisited," *Chem. Engng. Sci.*, **40**, 1387–1392 (1985).

Hirschfelder, J. O., C. F. Curtiss, and R. B. Bird, *Molecular Theory of Gases and Liquids*, Wiley, New York (1954).

Hubbert, M. K., "Darcy law and the field equations of the flow of underground fluids," *Trans. AIME*, **207**, 222–239 (1956).

Iberall, A. S., "Permeability of glass wool and other highly porous media," *J. Res. Nat. Bur. Stand.*, **45**, 398–406 (1950).

Irmay, S., "Flow of liquid through cracked media," *Bull. Res. Council of Israel* No. 1, **5A**, 84 (1955).

Jeans, J., *An Introduction to the Kinetic Theory of Gases*, Cambridge University Press, Cambridge (1967).

Jerauld, G. R., and S. J. Salter, "The effect of pore-structure on hysteresis in relative permeability and capillary pressure: pore-level modeling," *Transport in Porous Media*, **5**, 103–151 (1990).

Johnson, D. L., J. Koplik, and L. M. Schwartz, 1986, "New pore-size parameter characterizing transport in porous media," *Physical Review Letters*, **57**, 2564–2567 (1986).

Johnston, N. I., and S. Kotz, *Distributions in Statistics Continuous Univariate Distributions - 1 & 2*, Houghton Mifflin Company, Boston (1970).

Kalaydjian, F., "A macroscopic description of multiphase flow in porous media involving spacetime evolution of fluid/fluid interface," *Transport in Porous Media*, **2**, 537–552 (1987).

Kalaydjian, F., and B. Legait, "Ecoulement lent à contre-courant de deux fluides non miscibles dans un capillaire présentant un rétrécissement," *C. R. Acad. Sc. Paris Ser. II*, **304**, 869–872 (1987a).

Kalaydjian, F., and B. Legait, "Perméabilités relatives couplées dans des écoulements en capillaire et en milieu poreux," *C. R. Acad. Sc. Paris Ser. II*, **304**, 1035–1038 (1987b).

Kalaydjian, F., "Origin and quantification of coupling between relative permeabilities for two-phase flow in porous media," *Transport in Porous Media*, **5**, 215–229 (1990).

Katz, A. J., and A. H. Thompson, "Quantitative prediction of permeability in porous rock," *Physical Review B*, **34**, 8179–8181 (1986).

Kirkpatrick, S., "Classical transport in disordered media: scaling and effective medium theory," *Phys. Rev. Lett.*, **27**, 1722–1725 (1971).

Kirkpatrick, S., "Percolation and conduction," *Rev. Mod. Phys.*, **45**, 574–588 (1973).

Klinkenberg, L. J., " The permeability of porous media to liquids and gases," *API Drill. Prod. Prac.*, 200–213 (1941).

Koplik, J., "On the effective medium theory of random linear networks," *J. Phys. C.*, **14**, 4821–4837 (1981).

Koplik, J., "Creeping flow in two-dimensional networks," *J. Fluid Mech.*, **119**, 219–247 (1982).

Kozeny, J., "Ober kapillare leitung das wassers im boden," *S. Ber. Weiner Akad. Abt.* iia, **136**, 271–306 (1927).

Kundt, A., and E. Warburg, "Ueber reibung und waermeleitung verduennter gase," *Ann. Physik, Poggendorf*, **155**, 337–365 (1875).

Kwon, B. S., and G. R. Pickett, "A new pore structure model and pore structure interrelations," *Society of Petroleum Well Logging Analysts (SPWLA), 16th Annual Logging Symposium, June 4–7* (1975).

Lane, A., N. Shah, and W. C. Conner, "Measurement of morphology of high-surface-area solids: porosimetry as a percolation problem," *J. Colloid Interface Sci.*, **109**, 235–242 (1986).

Lapidus, G. R., A. M. Lane, K. M. Ng, and W. C. Conner, "Interpretation of mercury porosimetry data using pore-throat network model," *Chem. Engng. Commun.*, **38**, 33–56 (1985).

Larson, R. G., and N. R. Morrow, "Effects of sample size on capillary pressures in porous media," *Powder Technol.*, **30**, 123–138 (1981).

Li, Y., W. G. Laidlaw, and N. C. Wardlaw, "Sensitivity of drainage and imbibition to pore structures as revealed by computer simulation of displacement process," *Adv. Colloid Interface Sci.*, **26**, 1–68 (1986).

Lin Cheng-Yuan, and J. C. Slattery, "Three-dimensional, randomized, network model for two-phase flow through porous media," *SPE/DOE (9803) 2nd Joint Symposium on Enhanced Oil Recovery of the Society of Petroleum Engineers, Tulsa, Oklahoma, April, 5–8* (1981).

Longeron, D. G., M. J. Argaud, and J. -P. Feraud, "Effect of overburden pressure and the nature of the microscopic distribution of fluids on electrical properties of rock samples," *SPE Formation Evaluation*, **4**, 194–202 (1989).

Mann, M., J. J. Almeida, and M. N. Mugerwa, "A random pattern extension to the stochastic network pore model," *Chem. Engng. Sci.*, **41**, 2663–2671 (1986).

Mann, R., G. P. Androutsopoulos, and H. Golshan, "Application of stochastic network model to oil-bearing rock with observations relevant to oil recovery," *Chem. Engng. Sci.*, **36**, 337–346 (1981).

Mantoglou, A., and L. W. Gelhar, "Stochastic modeling of large-scale transient unsaturated flow systems," *Water Resour. Res.*, **23**(1), 37–46 (1987a).

Mantoglou, A., and L. W. Gelhar, "Capillary tension head variance, mean soil moisture content and effective specific soil moisture capacity of transient unsaturated flow in stratified soils," *Water Resour. Res.*, **23**(1), 47–56 (1987b).

Mantoglou, A., and L. W. Gelhar, "Effective hydraulic conductivity of transient unsaturated flow in stratified soils," *Water Resour. Res.*, **23**(1), 57–68 (1987c).

Marle, C. M.," Ecoulements monophasiques en milieu poreux," *Revue de L'Institut Français Pétrol*, **22**, 1471–1505 (1967).

Marshal, T. J., "A relation between permeability and size distribution of pores," *J. Soil Sci.*, **9**, 1–8 (1958).

Mayagoitia, V., M. Javier Cruz, and F. Rozas, "Mechanistic studies of capillary processes in porous media Part 1–probabilistic description of porous media," *J. Chem. Soc. Faraday Trans.*, **85**, 2071–2078 (1989a).

Mayagoitia, V., M. Javier Cruz, and F. Rozas, "Mechanistic studies of capillary processes in porous media Part 2–construction of porous networks by Monte-Carlo methods," *J. Chem. Soc. Faraday Trans.*, **85**, 2079–2086 (1989b).

Mayer, R. P., and R. A. Stowe, " Mercury porosimetry—breakthrough pressure for penetration between packed spheres," *J. Colloid Sci.*, **20**, 893–911 (1953).

Mayer, R. P., and R. A. Stowe, "Mercury porosimetry: filling of toroidal void volume following breakthrough between packed spheres," *J. Phys. Chem.*, **70**, 3867–3873 (1966).

McPhee, C. A., and K. G. Arthur, "Klinkenberg permeability measurements: problems and practical solutions," *Reviewed Proceedings of the Second Society of Core Analysts European Core Analysis Symposium London, UK, 20–22 May*, 371–391 (1991).

Meyer, H. I., "Pore distribution in porous media," *J. Appl. Phys.*, **24**, 510–512 (1953).

Millington, R. J., "Gas diffusion in porous media," *Science*, **130**, 100–102 (1959).

Millington, R. J., and J. P. Quirk, "Permeability of porous solids," *Trans. Faraday Soc.*, **57**, 1200–1206 (1961).

Mishra, B. K., and M. M. Sharma, "Measurement of pore distributions from capillary pressure curves," *AIChE J.*, **34**, 684–687 (1988).

Mls, R., "On the existence of the derivative of the volume average," *Transport in Porous Media*, **2**, 615–621 (1987).

Mood, A. M., F. A. Graybill, and D. C. Boes, *Introduction to the Theory of Statistics*, (3rd edn.) McGraw-Hill, New York (1974).

Nagatani, T., "Multi-bond expansions for effective conductivity in bond-disordered resistor networks," *J. Phys. C.*, **14**, 4839–4847 (1981).

Nicholson, D., J. K. Petrou, and J. H. Petropoulos, "Relation between macroscopic conductance and microscopic structural parameters of stochastic networks with application to fluid transport in porous materials," *Chem. Engng. Sci.*, **43**, 1385–1393 (1988).

Park C., and S. Ihm, "New hypotheses for mercury porosimetry with percolation approach," *AIChE J.*, **36**, 1641–1648 (1990).

Parsons, R. W., "Permeability of idealized fractured rock," *Soc. Petrol. Engng. J.*, **6**, 126–136 (1966).

Payatakes, A. C., C. Tien, and R. M. Turian, "A new model for granular porous media: Part I. Model formulation," *AIChE J.*, **19**, 58–67 (1973a).

Payatakes, A. C., C. Tien, and R. M. Turian, "A new model for granular porous media: Part II. Numerical solution of steady state incompressible Newtonian flow through periodically constricted tubes," *AIChE J.*, **19**, 67–76 (1973b).

Payatakes, A. C., and M. A. Neira, "Model of the constricted unit cell type for isotropic granular porous media," *AIChE J.*, **23**, 922–930 (1977).

Perez-Rosales, C., "Generalization of the Maxwell equation for formation resistivity factors," *J. Pet. Tech.*, **July**, 819–824 (1976).

Perez-Rosales, C., "On the relationship between formation resistivity factor and porosity," *Soc. Pet. Engng. J.*, **August**, 531–536 (1982).

Polmann, D. J., E. G. Vomvoris, D. McLaughlin, E. M. Hammick, and L. W. Gelhar, "Application of stochastic methods to the simulation of large-scale unsaturated flow and transport," *Rep. NUREG/CR-5094*, Nucl. Regul. Comm., Washington, D. C. (1988).

Polmann, D. J., D. McLaughlin, S. Luis, L. W. Gelhar, and R. Ababou, "Stochastic modeling of large-scale flow in heterogeneous unsaturated soils," *Water Resour. Res.*, **27**(7), 1447–1458 (1991).

Portsmouth, R. L., and L. F. Gladden, "Determination of pore connectivity by mercury porosimetry," *Chem. Engng. Sci.*, **46**, 3023–3036 (1991).

Present, R. D., *The Kinetic Theory of Gases*, McGraw-Hill, New York (1958).

Press, W. H., B. P. Flannery, S. A. Teukolsky, and W. T. Vetterling, *Numerical Recipes The Art of Scientific Computing*, Cambridge University Press, Cambridge (1986).

Purcell, W. R., "Capillary pressures—their measurement using mercury and the calculation of permeability their from," *Trans. AIME*, **186**, 39–46 (1949).

Quintard, M., and S. Whitaker, "Ecoulements monophasiques en milieu poreux: effet des hétérogénéités locales," *J. Méca. Théo. et Appl.*, **6**, 691–726 (1987).

Quintard, M., and S. Whitaker, "Two-phase flow in heterogeneous porous media: the method of large scale averaging," *Transport in Porous Media*, **3**, 357–413 (1988).

Quintard, M., and S. Whitaker, "Two-phase flow in heterogeneous porous media I: the influence of large spatial and temporal gradients," *Transport in Porous Media*, **5**, 341–379 (1990a).

Quintard, M., and S. Whitaker, "Two-phase flow in heterogeneous porous media II: numerical experiments for flow perpendicular to a stratified system," *Transport in Porous Media*, **5**, 429–472 (1990b).

Rege, S. D., and H. S. Fogler, "Network model for straining dominated particle entrapment in porous media," *Chem. Engng. Sci.*, **42**, 1553–1564 (1987).

Renault, P., "Theoretical studies of mercury intrusion in some networks: testing the applicability of mercury intrusion in the size characterisation of the lacunar pore space of soil samples," *Transport in Porous Media*, **3**, 529–547 (1988).

Ritter, H. L., and L. C. Drake, "Pore-size distribution in porous materials," *Ind. Engng. Chem. Anal. Ed.*, **17**, 782–786 (1945).

Rose, W. D., "Permeability and gas-slippage phenomenon," *API Drill. Prod. Prac.*, 209–217 (1948).

Rose, W., "Studies of waterflood performance III. Use of network models," Illinois State Geol. Survey, Circ. No. 237, Urbana, Illinois (1957).

Rumer, R. R., "Resistance to flow through porous media," in *Flow through Porous Media* (R. J. M. de Wiest, Ed.), Academic Press, New York (1969).

Rumer, R. R., and P. A. Drinker, "Resistance to laminar flow through porous media," *Proc. Amer. Soc. Civil Engng.* No. HY5, **92**, 155–164 (1966).

Ruth, D. and R. Suman, "The rôle of microscopic cross flow in idealized porous media," *Transport in Porous Media*, **7**, 103–125 (1992).

Ruth, D. W. and H. Ma, "On the derivation of the Forchheimer equation by volume averaging theorem," *Transport in Porous Media*, **7**, 255–264 (1992).

Sax, J., and J. M. Ottino, "Modeling of transport of small molecules in polymer blends: application of effective medium theory," *Polym. Engng. Sci.*, **23**, 165–176 (1983).

Scheidegger, A. E., "Theoretical models of porous media," *Producers Monthly* No. 10, **17**, 17–23 (1953).

Scheidegger, A. E., "Statistical hydrodynamics in porous media," *J. Appl. Phys.* **25**, 994–1001 (1954).

Scheidegger, A. E., "On theory of flow of miscible phases in porous media," *Proc. IUGG General Assembly, Toronto*, **2**, 236–242 (1957).

Scheidegger, A. E., *The Physics of Flow Through Porous Media*, 2nd edn, University of Toronto Press, Toronto (1960).

Scheidegger, A. E., *The Physics of Flow Through Porous Media*, 3rd edn, University of Toronto Press, Toronto (1974).

Shapiro, A. M., "Fractured Porous Media: Equation Development and Parameter Identification," Ph.D. Thesis, Princeton University, New Jersey (1981).

Slattery, J. C., "Flow of viscoelastic fluids through porous media," *AIChE J.*, **13**, 1066–1071 (1967).

Slattery, J. C., "Single-phase flow through porous media," *AIChE J.*, **15**, 866–872 (1969).

Slattery, J. C., *Momentum, energy and mass transfer in continua*, Robert E. Krieger Publishing Company, Huntington, N. Y. (1981).

Snow D. T., "A Parallel Plate Model of Fractured Permeable Media," Ph.D. Thesis, University of California, Berkeley, California (1965).

Soll, W. E., "Development of a pore-scale model for simulating two and three phase capillary pressure-saturation relationships," Ph.D. dissertation, Mass. Inst. of Technol., Cambridge (1991).

Soll, W. E., L. A. Ferrand and M. A. Celia, "An enhanced percolation model for the capillary pressure-saturation relation," in Proceedings of the 7th International Conference on Computational Methods in Water Resources, edited by M. A. Celia et al., Elsevier, New York (1988).

Spearing, M., and G. P. Matthews, "Modelling characteristic properties of sandstones," *Transport in Porous Media*, **6**, 71–90 (1991).

Suman, R., and D. Ruth, "Formation factor and tortuosity of homogeneous porous media," to be published in *Transport in Porous Media* (1993).

Thompson, A. H., A. J. Katz, and C. E. Krohn, "The microgeometry and transport properties of sedimentary rocks," *Adv. in Phys.*, **36**, 625–694 (1987).

Tsakiroglou, C. D., and A. C. Payatakes, "A new simulator of mercury porosimetry for the characterization of porous materials," *J. Colloid Interface Sci.*, **137**, 315–339 (1990).

Tsakiroglou, C. D., and A. C. Payatakes, "Effects of pore-size correlations on mercury porosimetry curves," *J. Colloid Interface Sci.*, **146**, 479–494 (1991).

Van Brakel, J., "Pore space models for transport phenomena in porous media. Review and evaluation with special emphasis on capillary transport," *Powder Technol.*, **11**, 205–236 (1975).

Veverka, V., "Theorem for the local average of a gradient revised," *Chem. Engng. Sci.*, 833–838 (1981).

Wardlaw, N. C., and M. McKeller, "Mercury porosimetry and the interpretation of pore geometry in sedimentary rocks and artificial models," *Powder Technol.*, **29**, 127–143 (1981).

Wardlaw, N. C., and R. P. Taylor, "Mercury capillary pressure curves and the interpretation of pore-structure and capillary behavior in reservoir rocks," *Bull. Canadian Petroleum Geology*, **24**, 225–262 (1976).

Wardlaw, N. C., Y. Li, and D. Forbes, "Pore-throat size correlation from capillary pressure curves," *Transport in Porous Media*, **2**, 597–614 (1987).

Wardlaw, N. C., and Y. Li, "Fluid topology, pore size and aspect ratio during imbibition," *Transport in Porous Media*, **3**, 17–34 (1988).

Washburn, E. W., "The dynamics of capillary flow," *Phys. Rev.*, **17**, 273–283 (1921).

Whitaker, S., "Diffusion and dispersion in porous media," *AIChE J.*, **13**, 420–427 (1967).

Whitaker, S., "Advances in theory of fluid motion in porous media," *Ind. Engng. Chem.*, **61**, 14–28 (1969).

Whitaker, S., "Flow in porous media I: a derivation of Darcy's law," *Transport in Porous Media*, **1**, 14–28 (1986a).

Whitaker, S., "Flow in porous media II: the governing equations for immiscible, two-phase flow," *Transport in Porous Media*, **1**, 105–125 (1986b).

Whitaker, S., "Flow in porous media III: deformable media," *Transport in Porous Media*, **1**, 127–154 (1986c).

Wiggs, P. K. C., *The structure and properties of porous materials*, (D. H. Everett and F. S. Stone Eds.) Academic Press, New York (1958).

Winsauer, W. O., H. M. Shearing Jr., P. H. Mason, and M. Williams, "Resistivity of brine-saturated sands in relation to pore geometry," *Bull. Amer. Assoc. Petrol. Geol.*, **36**, 253–277 (1952).

Wise, W. R., "A new insight on pore structure and permeability," *Water Resour. Res.*, **28**, 189–198 (1992).

Wyllie, M. R. J., and G. H. F. Gardner, "The generalized Kozeny-Carman equation II. A novel approach to problems of fluid flow," *World Oil Prod. Sect.*, **146**, 210–228 (1958).

Wyllie, M. R. J., and A. R. Gregory, "Formation factors of unconsolidated porous media: influence of particle shape and effect of cementation," *Trans. AIME*, **198**, 103–110 (1953).

Wyllie, M. R. J., and W. D. Rose, "Some theoretical considerations related to the quantitative evaluation of the physical characteristics of reservoir rock from electrical log data," *Petroleum Trans. AIME*, **189**, 105–118 (1950).

Wyllie, M. R. J., and M. B. Spangler, "Application of electric resistivity measurements to problems of fluid flow in porous media," *Bull. Amer. Assoc. Petrol. Geol.*, **36**, 359–403 (1952).

APPENDICES

APPENDIX A

EXPLANATIONS OF SOME STATISTICAL CONCEPTS

The following explanations are based on Dagan (1989). For detailed descriptions of these concepts, the reader is referred to Dagan (1989).

Stationary Random Function

If the random space function, $\gamma(\mathbf{r})$, is defined in the domain under consideration, that is, the joint probability density function, $T(\gamma_1, \gamma_2, \ldots, \gamma_N)$, is known for any set of arbitrary, but finite number of N points, $\mathbf{r}_1, \mathbf{r}_2, \ldots, \mathbf{r}_N$ in the domain, then it is considered stationary (or homogeneous) if it satisfies the requirement (Dagan, 1989)

$$T\left[\gamma(\mathbf{r}_1+\mathbf{h}), \gamma(\mathbf{r}_2+\mathbf{h}), \ldots, \gamma(\mathbf{r}_N+\mathbf{h})\right] = T\left[\gamma(\mathbf{r}_1), \gamma(\mathbf{r}_2), \ldots, \gamma(\mathbf{r}_N)\right] \ , \qquad \text{(A.1)}$$

where $\mathbf{h}$ is a constant but arbitrary vector and γ_I is the value of γ at a point, $\mathbf{r} = \mathbf{r}_I$. This means that T is invariant to a translation of the points $\mathbf{r}_I$ and depends only on their relative positions. When $\gamma(\mathbf{r})$ is a stationary random function in the domain under consideration, then the domain is said to be statistically homogeneous with respect to the function γ. This physically implies that γ in some sense repeats itself in the entire space.

The Ergodic Hypothesis

As explained at the beginning of Section 3.1, most of the times only a single realization is available when applications related to fluid flow are considered. Therefore, the statistical characterization of the random structure has to be based on the given single realization. In other words, the moments such as the expected value and variance, have to be found from space averages rather than ensemble averages. This is only possible if the ergodic hypothesis is satisfied. Stated in a simple way, the

ergodic hypothesis for a system means that all states of the ensemble are available in each realization. As most of the times, only a single realization is available, it is impossible to rigorously validate this hypothesis. The approach generally followed is to assume ergodicity and derive the moments of interest by space averaging and subsequently check the validity of the ergodic assumption. As explained by Dagan (1989), it is generally assumed that the ergodic hypothesis holds if the variance of the space average tends to zero. This point is further explained in Chapter 5 in which representativeness of the pore structure models of porous media is considered .

APPENDIX B

NETWORK THEORY

A two-dimensional square network model is illustrated in Figure B.1. The coordinate system is chosen to be positive up and to the right. If δ_I and S_I denote the diameter and tortuous length of a tube in the network, respectively, then the volumetric flow rate inside the tube can be calculated from the Hagen-Poiseuille law:

$$q_I = g_I \, (p_{Ia} - p_{Ib}) \ , \tag{B.1}$$

where g_I is the hydraulic conductance of the tube given by

$$g_I = \frac{\pi \, \delta_I^4}{128 \, \mu \, S_I} \ . \tag{B.2}$$

The subscript I on pressure p denotes the tube number, and the subscripts a and b give the location (i.e., a for the left/bottom end and b for the right/upper end, depending on the direction of the tube). The assumption of Hagen-Poiseuille flow implies that all inertial effects are ignored and that only creeping flows are considered.

The boundary conditions applied to the network are: a pressure p_h at the left-hand boundary; a pressure p_l at the right-hand boundary; and zero-flow at all other boundaries. For incompressible flow, a mass balance at each junction requires

$$\sum_I q_{IJ} = 0 \qquad\qquad J = 1, 2, \ldots, N_P \ , \tag{B.3}$$

where the subscript J denotes the junction, the subscript I denotes the tubes meeting at this junction, and N_P is the total number of junctions in the network. The system of linear algebraic equations represented by Equation (B.3) can be translated into a

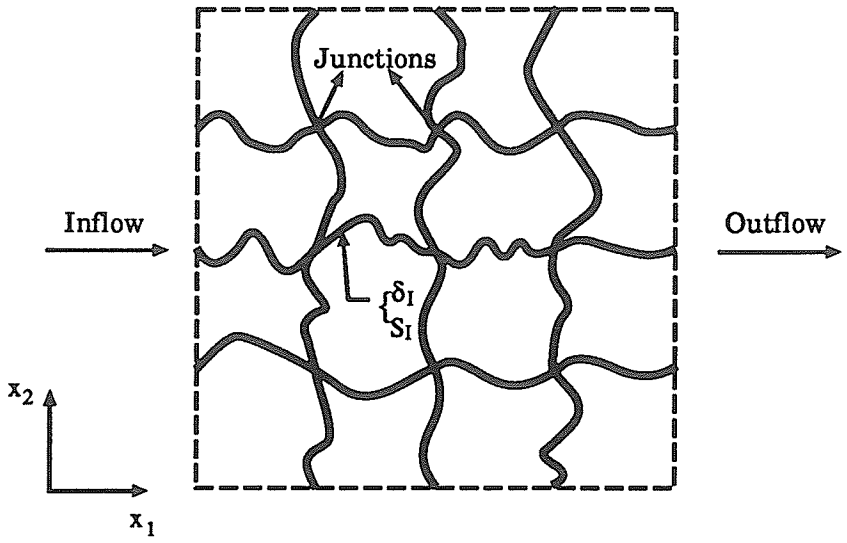

Fig. B.1. A regularly spaced two-dimensional network model.

matrix notation:

$$[G_{ij}]\{p_j\} = \{y_i\}\,, \tag{B.4}$$

where p_j is the vector of junction pressures, y_i is the forcing vector representing the imposed pressures at the left-hand and right-hand boundaries of the network, and G_{ij} is the conductance matrix. G_{ij} is a symmetric and banded matrix of order $N_P \times N_P$. For a three-dimensional cubic network model, the bands correspond to: $I - N_1^P \times N_2^P$, $I - N_1^P$, $I-1$, $I+1$, $I+N_1^P$, and $I+N_1^P \times N_2^P$. Here, I denotes the diagonal elements of G_{ij} and N_1^P, N_2^P and N_3^P denote the number of columns, rows and tiers in the network (see Figure 5.3). For computation purposes, only elements of the diagonal and upper three bands are stored and algorithm based on Gauss elimination for such matrices is used for inverting the equations. The details of the algorithm are given in Bathe (1982) (pp. 434). Once the pressures at the junctions are known, the flow rate in each tube can be calculated. A permeability for the network can then be calculated from Darcy's law given by Equation (3.15).

For the formation factor calculations, the same approach is followed for calculating the electric potentials at the junctions. The current flow inside a tube filled with a conductive fluid is calculated from Ohm's law in the form

$$c_I = g_I^c \, (e_{Ia} - e_{Ib}) \ , \tag{B.5}$$

where g_I^c is the electric conductance of the tube given by

$$g_I^c = \frac{\pi \, \delta_I^2}{4 \, R_w \, S_I} \ , \tag{B.6}$$

and $e_{Ia} - e_{Ib}$ denotes the electric potential drop across the Ith tube. Once, potentials at the junctions are known, the currents in the tubes can be calculated and the formation factor of the network can be calculated from Equation (3.30).

For the Klinkenberg permeability calculations, the Hagen-Poiseuille equation corrected for slip (Equation (2.31)) is employed for calculating the volumetric flow rate of a gas through a tube in the network. For the sake of completeness, this equation is again presented here:

$$\overline{q}_I \, P_m = \frac{\pi \, \delta_I^4}{128 \, \mu \, S_I} \, (p_{Ia} - p_{Ib}) \, p_m^I + \frac{c \, \delta_I^3}{6 \, S_I} \sqrt{2 \, \pi \, R \, T} \, (p_{Ia} - p_{Ib}) \ , \tag{B.7}$$

where $\overline{q}_I$ is the volumetric flow rate measured at $P_m (= (p_h + p_l)/2)$, c is a constant whose value is close to unity, p_m^I is the mean pressure in the capillary, R is the gas constant, and T is the absolute temperature. Because the gas flow rates in all the tubes of the network are calculated at the same pressure, P_m, the mass conservation at the junctions requires

$$\sum_I \overline{q}_{IJ} = 0 \qquad\qquad J = 1, 2, \ldots, N_P \ . \tag{B.8}$$

The system of nonlinear algebraic equations represented by Equation (B.8) can be translated into the matrix notation:

$$[G'_{ij}] \, \{p_j\} \{p_i^{\mathrm{T}}\} + [G''_{ij}] \, \{p_j\} = \{y_i\} \ , \tag{B.9}$$

where G'_{ij} and G''_{ij} are the conductance matrices, p_j is the vector of junction pressures, p_i^{T} is transpose of p_j, and y_i is the forcing vector representing the imposed pressures at the left-hand and right-hand boundaries of the network. The matrices, G'_{ij} and G''_{ij}, have the same properties as the matrix G_{ij} of Equation (B.4) and therefore are stored likewise. An iterative scheme based on the Newton-Raphson method is employed to solve the system of nonlinear equations represented by Equation (B.9). Details of the Newton-Raphson method are given in Press et al. (1986). The linear algebraic equations arising in the Newton-Raphson method are solved by the Gauss elimination scheme for symmetric banded matrices (Bathe, 1982; pp. 434). Once the junction pressures are known, the flow rates in the tubes can be computed and the Klinkenberg permeability of the network can be found from Darcy's law given by Equation (3.46).

The values of the permeability and Klinkenberg permeability found with the help of network theory (explained above) can be substituted in the following relation, given by Klinkenberg (1941), to find the Klinkenberg coefficient, b:

$$b = P_m \left(\frac{k_{a1}}{k_1} - 1 \right) , \tag{B.10}$$

where k_{a1} and k_1 are the Klinkenberg permeability and permeability, respectively and P_m is the mean pressure given by

$$P_m = \frac{p_h + p_l}{2} . \tag{B.11}$$

APPENDIX C

SUMMATIONS: PARALLEL CAPILLARY MODEL

In this appendix, the different summations arising in the case of the parallel capillary model are evaluated, and the final results for the uniform, normal and logistic distributions of tube diameters and lengths are summarized.

Irrespective of the chosen tube diameter distribution,

$$\sum_{I=1}^{N_1^T} \delta_I^2 = N_1^T \, \mu_\delta^2 \left(1 + a_\delta^2\right) , \tag{C.1}$$

where $a_\delta = \sigma_\delta / \mu_\delta$.

If δ and S are continuous random variables representing the tube diameters and lengths respectively, then regardless of their distributions, for large N_1^T, the distribution of $\sum \delta^4/S$ can be closely approximated by the normal distribution $\mathrm{N}(N_1^T \mu', N_1^T \sigma^2)$, where

$$\mu' = E\left[\frac{\delta^4}{S}\right] \qquad \text{and} \qquad \sigma^2 = Var\left[\frac{\delta^4}{S}\right] . \tag{C.2}$$

Here, E and Var denote the expected value and variance, respectively. If δ and S have independent distributions, then

$$\sum_{I=1}^{N_1^T} \frac{\delta^4}{S} = N_1^T \, E\left[\delta^4\right] \, E\left[\frac{1}{S}\right] . \tag{C.3}$$

For symmetrical distributions of tube diameters (Mood et al., 1974)

$$E\left[\delta^4\right] = \mu_\delta^4 + 6\,\mu_\delta^2\,\sigma_\delta^2 + A^p\,\sigma_\delta^4 , \tag{C.4}$$

where the value of A^p depends on the distribution. For evaluating $E\left[1/S\right]$, a Taylor's series expansion must be used. If $f(S) = 1/S$, then the Taylor's series expansion of

$f(S)$ about μ_S is:

$$f(S) = f(\mu_S) + \frac{(S-\mu_S)}{1!}\frac{d\,f}{dS}\Big|_{S=\mu_S} + \frac{(S-\mu_S)^2}{2!}\frac{d^2 f}{dS^2}\Big|_{S=\mu_S} + \cdots . \tag{C.5}$$

For symmetrical distributions of tube lengths, $E[f(S)]$ is:

$$E[f(S)] = \frac{1}{\mu_S} + \frac{\sigma_S^2}{\mu_S^3} + A^p \frac{\sigma_S^4}{\mu_S^5} + \cdots . \tag{C.6}$$

If the higher order terms in Equation (C.6) are neglected, then Equation (C.3) becomes

$$\sum_{I=1}^{N_1^T} \frac{\delta_I^4}{S_I} = \frac{N_1^T \mu_\delta^4}{\mu_S} \left(1 + 6\,a_\delta^2 + A^p\,a_\delta^4\right) \left(1 + a_S^2 + A^p\,a_S^4\right) , \tag{C.7}$$

where $a_S = \sigma_S/\mu_S$. The other summations may be evaluated in a similar fashion and for the symmetrical tube diameter and length distributions are:

$$\sum_{I=1}^{N_1^T} \frac{\delta_I^3}{S_I} = \frac{N_1^T \mu_\delta^3}{\mu_S} \left(1 + 3\,a_\delta^2\right) \left(1 + a_S^2 + A^p\,a_S^4\right) , \tag{C.8}$$

$$\sum_{I=1}^{N_1^T} \frac{\delta_I^2}{S_I} = \frac{N_1^T \mu_\delta^2}{\mu_S} \left(1 + a_\delta^2\right) \left(1 + a_S^2 + A^p\,a_S^4\right) . \tag{C.9}$$

For lognormal distributions (Crow and Shimizu, 1988; Aitchison and Brown, 1969) of tube diameters and lengths, $\sum_{I=1}^{N_1^T} \delta_I^2/S_I$ is also given by Equation (C.9) and the other summations are:

$$\sum_{I=1}^{N_1^T} \frac{\delta_I^4}{S_I} = \frac{N_1^T \mu_\delta^4}{\mu_S} \Big(1 + 6\,a_\delta^2 + 15\,a_\delta^4 + 20\,a_\delta^6 + 15\,a_\delta^8 + 6\,a_\delta^{10} + a_\delta^{12}\Big) \left(1 + a_S^2 - \frac{3\,\tau}{\tau - 1}\,a_S^4\right) , \tag{C.10}$$

$$\sum_{I=1}^{N_1^T} \frac{\delta_I^3}{S_I} = \frac{N_1^T \mu_\delta^3}{\mu_S} \left(1 + 3\,a_\delta^2 + 3\,a_\delta^4 + a_\delta^6\right) \left(1 + a_S^2 - \frac{3\,\tau}{\tau - 1}\,a_S^4\right) . \tag{C.11}$$

For the symmetrical tube diameter and length distributions, the final relations for permeability, Klinkenberg permeability and formation factor are:

$$\frac{1}{k_1} = \frac{32\,\tau}{\xi_1\,\mu_\delta^2} \frac{1 + a_\delta^2}{(1 + 6\,a_\delta^2 + A^p\,a_\delta^4)\,(1 + a_S^2 + A^p\,a_S^4)} , \tag{C.12}$$

$$\frac{1}{k_{a1}} = \frac{32\,\tau}{\xi_1\,\mu_\delta^2\,(1+6\,a_\delta^2+A^p\,a_\delta^4+8\,c\,\lambda/\mu_\delta\,(1+3\,a_\delta^2))\,(1+a_S^2+A^p\,a_S^4)}\,, \tag{C.13}$$

$$F = \frac{\tau}{\xi_1}\frac{1}{(1+a_S^2+A^p\,a_S^4)}\,, \tag{C.14}$$

where μ_δ and σ_δ , and μ_S and σ_S denote the means and standard deviations of the tube diameter and length distributions, respectively, $\tau = \mu_S/L_1$, $a_\delta = \sigma_\delta/\mu_\delta$, $a_S = \sigma_S/\mu_S$, c is a constant, and λ is the average mean free path of the flowing gas. The value of A^p is 1.8 for the uniform distribution (Mood et al., 1974), 3 for the normal distribution (Mood et al., 1974), and 4.2 for the logistic distribution (Johnson and Kotz, 1970) of tube diameters and lengths.

The expression for the Klinkenberg coefficient, b, can be obtained from Equations (C.12), (C.13) and (2.27), and is:

$$b = \frac{8\,c\,\lambda\,P_m}{\mu_\delta}\frac{1+3\,a_\delta^2}{1+6\,a_\delta^2+A^p\,a_\delta^4}\,. \tag{C.15}$$

APPENDIX D

SUMMATIONS: SERIAL CAPILLARY MODEL

In this appendix, the summations arising in the serial capillary model calculations are evaluated, and the final results for the symmetrical tube diameter and length distributions are presented.

A detailed derivation of the summation in Equation (5.40) for lognormal tube diameter and length distributions (Aitchison and Brown, 1969; Crow and Shimizu, 1988) is presented. The other summations may be evaluated similarly. For independent tube diameter and length distributions, the summation in Equation (5.40) can be expressed as

$$\sum_{I=1}^{N'_P+1} \frac{S_I}{\delta_I^4 + A'\,\delta^3} = (N'_P + 1)\, E[S]\; E\left[\frac{1}{\delta_I^4 + A'\,\delta^3}\right] , \tag{D.1}$$

where $A' = 8\,c\,\lambda$, and E represents the expected value. Here, it is assumed that the effect of ignoring the factor p_m^I/P_m in the summation is negligible. This is true for models with relatively small values of a_δ. The expected value,

$$E[S] = \mu_S\,. \tag{D.2}$$

For evaluating $E[1/(\delta_I^4 + A'\,\delta^3)]$, a Taylor's series expansion is used. If

$$f(\delta) = \frac{1}{\delta_I^4 + A'\,\delta^3}\,, \tag{D.3}$$

then, the Taylor's series expansion of $f(\delta)$ about μ_δ is:

$$f(\delta) = f(\mu_\delta) \;+\; \frac{(\delta - \mu_\delta)}{1\,!}\,\frac{d\,f}{d\delta}\Big|_{\delta=\mu_\delta} \;+\; \frac{(\delta - \mu_\delta)^2}{2\,!}\,\frac{d^2 f}{d\delta^2}\Big|_{\delta=\mu_\delta} \;+\; \cdots\,, \tag{D.4}$$

which gives

$$E[f(\delta)] = f(\mu_\delta) \;+\; \frac{E[(\delta - \mu_\delta)]}{1\,!}\,\frac{d\,f}{d\delta}\Big|_{\delta=\mu_\delta} \;+\; \frac{E[(\delta - \mu_\delta)^2]}{2\,!}\,\frac{d^2 f}{d\delta^2}\Big|_{\delta=\mu_\delta} \;+\; \cdots\,. \tag{D.5}$$

The various factors in the above equation are:

$$\left.\frac{d\,f}{d\,\delta}\right|_{\delta=\mu_\delta} = -\frac{4\,\mu_\delta^3 + 3\,A'\,\mu_\delta^2}{\left(\mu_\delta^4 + A'\,\mu_\delta^3\right)^2}\,, \tag{D.6}$$

$$\left.\frac{d^2 f}{d\delta^2}\right|_{\delta=\mu_\delta} = \frac{20\,\mu_\delta^6 + 30\,A'\,\mu_\delta^5 + 12\,A'^2\,\mu_\delta^4}{\left(\mu_\delta^4 + A'\,\mu_\delta^3\right)^3}\,, \tag{D.7}$$

$$\left.\frac{d^3 f}{d\delta^3}\right|_{\delta=\mu_\delta} = -\frac{120\,\mu_\delta^9 + 270\,A'\,\mu_\delta^8 + 216\,A'^2\,\mu_\delta^7 + 60\,A'^3\,\mu_\delta^5}{\left(\mu_\delta^4 + A'\,\mu_\delta^3\right)^4}\,, \tag{D.8}$$

$$\left.\frac{d^4 f}{d\delta^4}\right|_{\delta=\mu_\delta} = \frac{840\,\mu_\delta^{12} + 2520\,A'\,\mu_\delta^{11} + 3024\,A'^2\,\mu_\delta^{10} + 1680\,A'^3\,\mu_\delta^9 + 360\,A'^4\,\mu_\delta^8}{\left(\mu_\delta^4 + A'\,\mu_\delta^3\right)^5}\,, \tag{D.9}$$

$$E\left[(\delta - \mu_\delta)\right] = 0\,, \tag{D.10}$$

$$E\left[(\delta - \mu_\delta)^2\right] = \sigma_\delta^2 = \mu_\delta^2\,a_\delta^2\,, \tag{D.11}$$

$$E\left[(\delta - \mu_\delta)^3\right] = \mu_\delta^3\left(a_\delta^6 + 3\,a_\delta^4\right)\,, \tag{D.12}$$

$$E\left[(\delta - \mu_\delta)^4\right] = \mu_\delta^4\left(a_\delta^{12} + 6\,a_\delta^{10} + 15\,a_\delta^8 + 16\,a_\delta^6 + 3\,a_\delta^4\right)\,. \tag{D.13}$$

If the higher order terms in Equation (D.5) are ignored, then

$$E\left[\frac{1}{\delta^4 + A'\,\delta^3}\right] = \frac{(N_P' + 1)\,\mu_S}{\mu_\delta^4}\left[\frac{1}{1 + A^s} + \frac{B^s\,C^s}{(1 + A^s)^3} + \frac{D^s\,E^s}{(1 + A^s)^4} + \frac{G^s\,H^s}{(1 + A^s)^5}\right] \tag{D.14}$$

where

$$A^s = \frac{8\,c\,\lambda\,\mu}{\mu_\delta}\,, \tag{D.15}$$

$$B^s = a_\delta^2\,, \tag{D.16}$$

$$C^s = 10 + 15\,A^s + 6\,(A^s)^2\,, \tag{D.17}$$

$$D^s = a_\delta^6 + 3\,a_\delta^4\,, \tag{D.18}$$

$$E^s = 20 + 45\,A^s + 36\,(A^s)^2 + 10\,(A^s)^3\,, \tag{D.19}$$

$$G^s = a_\delta^{12} + 6\,a_\delta^{10} + 15\,a_\delta^8 + 16\,a_\delta^6 + 3\,a_\delta^4\,, \tag{D.20}$$

and

$$H^s = 35 + 105\,A^s + 126\,(A^s)^2 + 70\,(A^s)^3 + 15\,(A^s)^4\,. \tag{D.21}$$

Therefore, the Klinkenberg permeability is:

$$\frac{1}{k_{a1}} = \frac{32\,\tau}{\xi_1\,\mu_\delta^2}\left(1 + a_\delta^2\right)\left[\frac{1}{1+A^s} + \frac{B^s\,C^s}{(1+A^s)^3} - \frac{D^s\,E^s}{(1+A^s)^4} + \frac{G^s\,H^s}{(1+A^s)^5}\right]\,, \tag{D.22}$$

The summations in Equations (5.39) and (5.41) can be evaluated similarly. They are not included here.

The final results for the uniform tube diameter and length distributions (Mood et al., 1974) are:

$$\frac{1}{k_1} = \frac{32\,\tau}{\xi_1\,\mu_\delta^2}\left(1 + a_\delta^2\right)\left(1 + 10\,a_\delta^2 + 63\,a_\delta^4 + 324\,a_\delta^6 + 1485\,a_\delta^8\right)\,, \tag{D.23}$$

$$\frac{1}{k_{a1}} = \frac{32\,\tau}{\xi_1\,\mu_\delta^2}\left(1 + a_\delta^2\right)\left[\frac{1}{1+A^s} + \frac{B^s\,C^s}{(1+A^s)^3} + \frac{D^s\,E^s}{(1+A^s)^5}\right]\,, \tag{D.24}$$

$$F = \frac{1}{\xi_1}\left(1 + a_\delta^2\right)\left(1 + 3\,a_\delta^2 + 9\,a_\delta^4 + 27\,a_\delta^6 + 81\,a_\delta^8\right)\,, \tag{D.25}$$

where

$$A^s = \frac{8\,c\,\lambda\,\mu}{\mu_\delta}\,, \tag{D.26}$$

$$B^s = a_\delta^2\,, \tag{D.27}$$

$$C^s = 10 + 15\,A^s + 6\,(A^s)^2\,, \tag{D.28}$$

$$D^s = a_\delta^4 \,, \tag{D.29}$$

$$E^s = 63 + 189\,A^s + 226.8\,(A^s)^2 + 126\,(A^s)^3 + 27\,(A^s)^4 \,. \tag{D.30}$$

The final results for the normal tube diameter and length distributions (Mood et al., 1974) are:

$$\frac{1}{k_1} = \frac{32\,\tau}{\xi_1\,\mu_\delta^2}\left(1 + a_\delta^2\right)\left(1 + 10\,a_\delta^2 + 105\,a_\delta^4 + 1260\,a_\delta^6 + 17325\,a_\delta^8\right) , \tag{D.31}$$

$$\frac{1}{k_{a1}} = \frac{32\,\tau}{\xi_1\,\mu_\delta^2}\left(1 + a_\delta^2\right)\left[\frac{1}{1+A^s} + \frac{B^s\,C^s}{(1+A^s)^3} + \frac{D^s\,E^s}{(1+A^s)^5}\right] , \tag{D.32}$$

$$F = \frac{1}{\xi_1}\left(1 + a_\delta^2\right)\left(1 + 3\,a_\delta^2 + 15\,a_\delta^4 + 105\,a_\delta^6 + 945\,a_\delta^8\right) , \tag{D.33}$$

where

$$A^s = \frac{8\,c\,\lambda\,\mu}{\mu_\delta} \,, \tag{D.34}$$

$$B^s = a_\delta^2 \,, \tag{D.35}$$

$$C^s = 10 + 15\,A^s + 6\,(A^s)^2 \,, \tag{D.36}$$

$$D^s = a_\delta^4 \,, \tag{D.37}$$

$$E^s = 105 + 315\,A^s + 378\,(A^s)^2 + 210\,(A^s)^3 + 45\,(A^s)^4 \,. \tag{D.38}$$

The final results for the logistic tube diameter and length distributions (Johnson and Kotz, 1970) are:

$$\frac{1}{k_1} = \frac{32\,\tau}{\xi_1\,\mu_\delta^2}\left(1 + a_\delta^2\right)\left(1 + 10\,a_\delta^2 + 147\,a_\delta^4 + 3348\,a_\delta^6 + 113157\,a_\delta^8\right) , \tag{D.39}$$

$$\frac{1}{k_{a1}} = \frac{32\,\tau}{\xi_1\,\mu_\delta^2}\left(1+a_\delta^2\right)\left[\frac{1}{1+A^s}+\frac{B^s\,C^s}{(1+A^s)^3}+\frac{D^s\,E^s}{(1+A^s)^5}\right], \tag{D.40}$$

$$F = \frac{1}{\xi_1}\left(1+a_\delta^2\right)\left(1+3\,a_\delta^2+21\,a_\delta^4+279\,a_\delta^6+6172.2\,a_\delta^8\right), \tag{D.41}$$

where

$$A^s = \frac{8\,c\,\lambda\,\mu}{\mu_\delta}, \tag{D.42}$$

$$B^s = a_\delta^2, \tag{D.43}$$

$$C^s = 10+15\,A^s+6\,(A^s)^2, \tag{D.44}$$

$$D^s = a_\delta^4, \tag{D.45}$$

$$E^s = 147+441\,A^s+529.2\,(A^s)^2+294\,(A^s)^3+63\,(A^s)^4. \tag{D.46}$$

The final results for the lognormal tube diameter and length distributions are given in Chapter 5.

APPENDIX E

RESULTS OF NONLINEAR REGRESSION ANALYSIS FOR THE NETWORK MODEL

In this appendix, the results for the various nonlinear models tried for finding relations of the coefficients A_v, A_p, A_c and A_e to the statistical parameters of the network are summarized and complete expressions for functions $Z^{k_1}(a_\delta)$ and $Z^F(a_\delta)$ are given.

E.1 Models for A_v

MODEL 1

$$A_v = \frac{\mu_S}{\mu_\delta^4} \frac{1}{1 + m_1 a_\delta^2 + m_2 a_\delta^4 + m_3 a_\delta^6 + m_4 a_\delta^8 + m_5 a_\delta^{10}} \tag{E.1}$$

MODEL 2

$$A_v = \frac{\mu_S}{\mu_\delta^4} \frac{1}{1 + m_1 a_\delta^2 + m_2 a_\delta^4 + m_3 a_\delta^6 + m_4 a_\delta^8} \tag{E.2}$$

MODEL 3

$$A_v = \frac{\mu_S}{\mu_\delta^4} \frac{1}{1 + m_1 a_\delta^2 + m_2 a_\delta^4 + m_3 a_\delta^6} \tag{E.3}$$

MODEL 4

$$A_v = \frac{\mu_S}{\mu_\delta^4} \frac{1}{1 + m_1 a_\delta^2 + m_2 a_\delta^4} \tag{E.4}$$

MODEL 5

$$A_v = \frac{\mu_S}{\mu_\delta^4} \frac{1}{1 + m_1 a_\delta^2} \tag{E.5}$$

MODEL 6

$$A_v = \frac{\mu_S}{\mu_\delta^4} \frac{1}{1 + m_1 a_\delta + m_2 a_\delta^2 + m_3 a_\delta^3 + m_4 a_\delta^4 + m_5 a_\delta^5} \tag{E.6}$$

MODEL 7

$$A_v = \frac{\mu_S}{\mu_\delta^4} \frac{1}{1 + m_1 a_\delta + m_2 a_\delta^2 + m_3 a_\delta^3 + m_4 a_\delta^4} \tag{E.7}$$

MODEL 8

$$A_v = \frac{\mu_S}{\mu_\delta^4} \frac{1}{1 + m_1 a_\delta + m_2 a_\delta^2 + m_3 a_\delta^3} \tag{E.8}$$

MODEL 9

$$A_v = \frac{\mu_S}{\mu_\delta^4} \frac{1}{1 + m_1 a_\delta + m_2 a_\delta^2} \tag{E.9}$$

MODEL 10

$$A_v = \frac{\mu_S}{\mu_\delta^4} \frac{1}{1 + m_1 a_\delta} \tag{E.10}$$

The values of $m_1, m_2, \ldots$, mean square residue and mean of the sum of the squares of the observed values for each model are given in Table E.1. In all the tables of this appendix, the mean square residue (M.S.R.) refers to the mean of the sum of the squares of the differences between the observed values (found with the help of network theory presented in Appendix B) and the corresponding values predicted by the regression model.

E.2 Models for A_p

MODEL 1

$$A_p = m_6 \frac{\mu_S}{\mu_\delta^6} \frac{1 + a_\delta^2}{1 + m_1 a_\delta^2 + m_2 a_\delta^4 + m_3 a_\delta^6 + m_4 a_\delta^8 + m_5 a_\delta^{10}} \tag{E.11}$$

MODEL 2

$$A_p = m_6 \frac{\mu_S}{\mu_\delta^6} \frac{1 + a_\delta^2}{1 + m_1 a_\delta^2 + m_2 a_\delta^4 + m_3 a_\delta^6 + m_4 a_\delta^8} \tag{E.12}$$

MODEL 3

$$A_p = m_6 \frac{\mu_S}{\mu_\delta^6} \frac{1 + a_\delta^2}{1 + m_1 a_\delta^2 + m_2 a_\delta^4 + m_3 a_\delta^6} \tag{E.13}$$

MODEL 4

$$A_p = m_6 \frac{\mu_S}{\mu_\delta^6} \frac{1 + a_\delta^2}{1 + m_1 a_\delta^2 + m_2 a_\delta^4} \tag{E.14}$$

MODEL 5

$$A_p = m_6 \frac{\mu_S}{\mu_\delta^6} \frac{1 + a_\delta^2}{1 + m_1 a_\delta^2} \tag{E.15}$$

MODEL 6

$$A_p = m_6 \frac{\mu_S}{\mu_\delta^6} \frac{1 + a_\delta^2}{1 + m_1 a_\delta + m_2 a_\delta^2 + m_3 a_\delta^3 + m_4 a_\delta^4 + m_5 a_\delta^5} \tag{E.16}$$

MODEL 7

$$A_p = m_6 \frac{\mu_S}{\mu_\delta^6} \frac{1 + a_\delta^2}{1 + m_1 a_\delta + m_2 a_\delta^2 + m_3 a_\delta^3 + m_4 a_\delta^4} \tag{E.17}$$

MODEL 8

$$A_p = m_6 \frac{\mu_S}{\mu_\delta^6} \frac{1 + a_\delta^2}{1 + m_1 a_\delta + m_2 a_\delta^2 + m_3 a_\delta^3} \tag{E.18}$$

MODEL 9

$$A_p = m_6 \frac{\mu_S}{\mu_\delta^6} \frac{1 + a_\delta^2}{1 + m_1 a_\delta + m_2 a_\delta^2} \tag{E.19}$$

MODEL 10

$$A_p = m_6 \frac{\mu_S}{\mu_\delta^6} \frac{1 + a_\delta^2}{1 + m_1 a_\delta} \tag{E.20}$$

The values of $m_1, m_2, \ldots$, mean square residue and mean of the sum of the squares of the observed values for each model are given in Table E.2.

E.3 Models for A_c

MODEL 1

$$A_c = \frac{\mu_S}{\mu_\delta^2} \frac{1}{1 + m_1 a_\delta^2 + m_2 a_\delta^4 + m_3 a_\delta^6 + m_4 a_\delta^8 + m_5 a_\delta^{10}} \tag{E.21}$$

MODEL 2

$$A_c = \frac{\mu_S}{\mu_\delta^2} \frac{1}{1 + m_1 a_\delta^2 + m_2 a_\delta^4 + m_3 a_\delta^6 + m_4 a_\delta^8} \tag{E.22}$$

MODEL 3

$$A_c = \frac{\mu_S}{\mu_\delta^2} \frac{1}{1 + m_1 a_\delta^2 + m_2 a_\delta^4 + m_3 a_\delta^6} \tag{E.23}$$

MODEL 4

$$A_c = \frac{\mu_S}{\mu_\delta^2} \frac{1}{1 + m_1 a_\delta^2 + m_2 a_\delta^4} \tag{E.24}$$

MODEL 5

$$A_c = \frac{\mu_S}{\mu_\delta^2} \frac{1}{1 + m_1 a_\delta^2} \tag{E.25}$$

MODEL 6

$$A_c = \frac{\mu_S}{\mu_\delta^2} \frac{1}{1 + m_1 a_\delta + m_2 a_\delta^2 + m_3 a_\delta^3 + m_4 a_\delta^4 + m_5 a_\delta^5} \tag{E.26}$$

MODEL 7

$$A_c = \frac{\mu_S}{\mu_\delta^2} \frac{1}{1 + m_1 a_\delta + m_2 a_\delta^2 + m_3 a_\delta^3 + m_4 a_\delta^4} \tag{E.27}$$

MODEL 8

$$A_c = \frac{\mu_S}{\mu_\delta^2} \frac{1}{1 + m_1 a_\delta + m_2 a_\delta^2 + m_3 a_\delta^3} \tag{E.28}$$

MODEL 9

$$A_c = \frac{\mu_S}{\mu_\delta^2} \frac{1}{1 + m_1 a_\delta + m_2 a_\delta^2} \tag{E.29}$$

MODEL 10

$$A_c = \frac{\mu_S}{\mu_\delta^2} \frac{1}{1 + m_1 a_\delta} \tag{E.30}$$

The values of $m_1, m_2, \ldots$, mean square residue and mean of the sum of the squares of the observed values for each model are given in Table E.3.

E.4 Models for A_e

MODEL 1

$$A_e = m_6 \frac{\mu_S}{\mu_\delta^4} \frac{1 + a_\delta^2}{1 + m_1 a_\delta^2 + m_2 a_\delta^4 + m_3 a_\delta^6 + m_4 a_\delta^8 + m_5 a_\delta^{10}} \tag{E.31}$$

MODEL 2

$$A_e = m_6 \frac{\mu_S}{\mu_\delta^4} \frac{1 + a_\delta^2}{1 + m_1 a_\delta^2 + m_2 a_\delta^4 + m_3 a_\delta^6 + m_4 a_\delta^8} \tag{E.32}$$

MODEL 3

$$A_e = m_6 \frac{\mu_S}{\mu_\delta^4} \frac{1 + a_\delta^2}{1 + m_1 a_\delta^2 + m_2 a_\delta^4 + m_3 a_\delta^6} \tag{E.33}$$

MODEL 4

$$A_e = m_6 \frac{\mu_S}{\mu_\delta^4} \frac{1 + a_\delta^2}{1 + m_1 a_\delta^2 + m_2 a_\delta^4} \tag{E.34}$$

MODEL 5

$$A_e = m_6 \frac{\mu_S}{\mu_\delta^4} \frac{1 + a_\delta^2}{1 + m_1 a_\delta^2} \tag{E.35}$$

MODEL 6

$$A_e = m_6 \frac{\mu_S}{\mu_\delta^4} \frac{1 + a_\delta^2}{1 + m_1 a_\delta + m_2 a_\delta^2 + m_3 a_\delta^3 + m_4 a_\delta^4 + m_5 a_\delta^5} \tag{E.36}$$

MODEL 7

$$A_e = m_6 \frac{\mu_S}{\mu_\delta^4} \frac{1 + a_\delta^2}{1 + m_1 a_\delta + m_2 a_\delta^2 + m_3 a_\delta^3 + m_4 a_\delta^4} \tag{E.37}$$

MODEL 8

$$A_e = m_6 \frac{\mu_S}{\mu_\delta^4} \frac{1 + a_\delta^2}{1 + m_1 a_\delta + m_2 a_\delta^2 + m_3 a_\delta^3} \tag{E.38}$$

MODEL 9

$$A_e = m_6 \frac{\mu_S}{\mu_\delta^4} \frac{1 + a_\delta^2}{1 + m_1 a_\delta + m_2 a_\delta^2} \tag{E.39}$$

MODEL 10

$$A_e = m_6 \frac{\mu_S}{\mu_\delta^4} \frac{1 + a_\delta^2}{1 + m_1 a_\delta} \tag{E.40}$$

The values of $m_1, m_2, \ldots$, mean square residue and mean of the sum of the squares of the observed values for each model are given in Table E.4.

E.5 Functions $Z^{k_1}(a_\delta)$ and $Z^F(a_\delta)$

$$Z^{k_1}(a_\delta) = \frac{1 + a_\delta^2}{1 + 3.07\, a_\delta^2 - 2.86\, a_\delta^4 + 3.99\, a_\delta^6 - 2.80\, a_\delta^8 + 0.729\, a_\delta^{10}} + \frac{0.681(1 + a_\delta^2)(4\, a_\delta^2 + 14\, a_\delta^4 + 20\, a_\delta^6 + 15\, a_\delta^8 + 6\, a_\delta^{10} + a_\delta^{12})}{1 + 6.37\, a_\delta^2 + 16.40\, a_\delta^4 - 6.75\, a_\delta^6 + 30.46\, a_\delta^8 - 9.19\, a_\delta^{10}} \tag{E.41}$$

$$Z^F(a_\delta) = 1 \quad + \quad \frac{0.341(1 + a_\delta^2)(4\, a_\delta^2 + 14\, a_\delta^4 + 20\, a_\delta^6 + 15\, a_\delta^8 + 6\, a_\delta^{10} + a_\delta^{12})}{1 + 3.61\, a_\delta^2 + 10.96\, a_\delta^4 - 6.89\, a_\delta^6 + 19.77\, a_\delta^8 - 5.49\, a_\delta^{10}} \tag{E.42}$$

Table E.1. The models tried for A_v with the corresponding fitting parameters. The mean of the sum of the squares of the observed values for A_v is 2.71×10^{32}.

Model	m_1	m_2	m_3	m_4	m_5	M.S.R.†
Model 1††	3.07	−2.86	3.99	−2.80	0.729	6.99×10^{27}
Model 2	3.00	−2.13	1.92	−0.644	–	8.11×10^{27}
Model 3	2.87	−1.27	0.493	–	–	1.53×10^{28}
Model 4	2.69	−0.55	–	–	–	4.71×10^{28}
Model 5	2.35	–	–	–	–	3.32×10^{29}
Model 6	−0.026	3.65	−2.99	2.14	−0.65	7.00×10^{27}
Model 7	0.020	3.18	−1.57	0.49	–	7.15×10^{27}
Model 8	0.09	2.67	−0.65	–	–	9.13×10^{27}
Model 9	0.29	1.88	–	–	–	5.26×10^{28}
Model 10	1.51	–	–	–	–	4.88×10^{30}

†Mean Square Residue

††The selected model

Table E.2. The models tried for A_p with the corresponding fitting parameters. The mean of the sum of the squares of the observed values for A_p is 3.45×10^{55}.

Model	m_1	m_2	m_3	m_4	m_5	m_6	M.S.R.†
Model 1††	6.37	16.40	−6.75	30.46	−9.19	13.83	3.04×10^{51}
Model 2	6.55	13.96	4.71	11.82	–	13.87	3.04×10^{51}
Model 3	7.05	8.98	20.21	–	–	13.97	3.78×10^{51}
Model 4	4.97	22.49	–	–	–	13.44	2.96×10^{52}
Model 5	15.73	–	–	–	–	16.78	1.02×10^{54}
Model 6	2.00	−10.72	70.78	−114.26	92.33	14.97	3.07×10^{51}
Model 7	−3.50	26.67	−52.90	57.57	–	11.19	6.06×10^{51}
Model 8	8.82	−31.26	66.34	–	–	21.75	4.33×10^{52}
Model 9	−4.18	14.47	–	–	–	8.61	3.69×10^{53}
Model 10	−21568	–	–	–	–	−34792	4.54×10^{54}

†Mean Square Residue

††The selected model

Table E.3. The models tried for A_c with the corresponding parameters. The mean of the sum of the squares of the observed values for A_c is 3.36×10^{11}.

Model	m_1	m_2	m_3	m_4	m_5	M.S.R.†
Model 1	1.14	−0.95	1.97	−1.62	0.46	9.11×10^6
Model 2	1.00	−0.02	0.05	−0.03	–	4.15×10^6
Model 3	0.99	0.01	−0.01	–	–	4.12×10^6
Model 4	1.00	0.00	–	–	–	4.11×10^6
Model 5††	1.00	–	–	–	–	4.07×10^6
Model 6	−0.01	1.10	−0.34	0.43	−0.185	4.24×10^6
Model 7	0.00	0.94	0.10	−0.05	–	4.21×10^6
Model 8	0.00	1.00	−0.01	–	–	4.20×10^6
Model 9	0.00	0.99	–	–	–	4.14×10^6
Model 10	0.74	–	–	–	–	3.52×10^9

†Mean Square Residue

††The selected model

Table E.4. The models tried for A_e with the corresponding fitting parameters. The mean of the sum of the squares of the observed values for A_e is 9.50×10^{30}.

Model	m_1	m_2	m_3	m_4	m_5	m_6	M.S.R.†
Model 1††	3.61	10.96	−6.89	19.77	−5.49	0.217	7.65×10^{26}
Model 2	3.77	9.03	1.12	7.90	–	0.217	7.89×10^{26}
Model 3	4.27	4.78	12.57	–	–	0.219	1.12×10^{27}
Model 4	2.49	14.54	–	–	–	0.210	1.03×10^{28}
Model 5	10.83	–	–	–	–	0.263	3.27×10^{29}
Model 6	0.91	−5.97	42.66	−71.01	56.29	0.223	8.13×10^{26}
Model 7	−3.26	21.37	−41.37	40.02	–	0.175	1.74×10^{27}
Model 8	7.01	−24.65	44.00	–	–	0.323	1.46×10^{28}
Model 9	−3.67	10.79	–	–	–	0.137	1.16×10^{29}
Model 10	57.13	–	–	–	–	1.85	1.26×10^{30}

†Mean Square Residue

††The selected model

APPENDIX F

EFFECTIVE-MEDIUM APPROXIMATION (EMA)

In this appendix, a derivation of effective-medium approximation (EMA), given by Equation (5.97), is presented. It is reproduced from Kirkpatrick (1973) with some changes in nomenclature. Based on this equation, an explicit relation between the overall network conductance and the statistical parameters characterizing the distribution of the elementary conductors in the network is reproduced from Nicholson et al. (1988). Finally, the relations of the permeability and formation factor of the network to the corresponding normalized effective-medium conductances are found. Electrical terminology is used for these derivations; however, similar statements apply to fluid flow in networks of tubes.

F.1 Effective-Medium Approximation (EMA)

Consider an infinite network of electric resistors in which the conductances of the individual resistors are randomly assigned according to probability density function $\omega(g)$ such that $g_a \leq g \leq g_b$. The coordination number of the network, that is, the average number of resistors meeting at a junction, is denoted by η. For example, η is 2 for a serial capillary model, 4 for a square network and 6 for a cubic network, both with no diagonal elements, and ∞ for a parallel capillary model. The EMA seeks to replace all the resistors of the network with identical resistors of conductances g_m such that the total conductance, G_n, of the effective-medium network is the same as that of the original network.

Consider an effective-medium network illustrated in Figure F.1. Here e_m is the

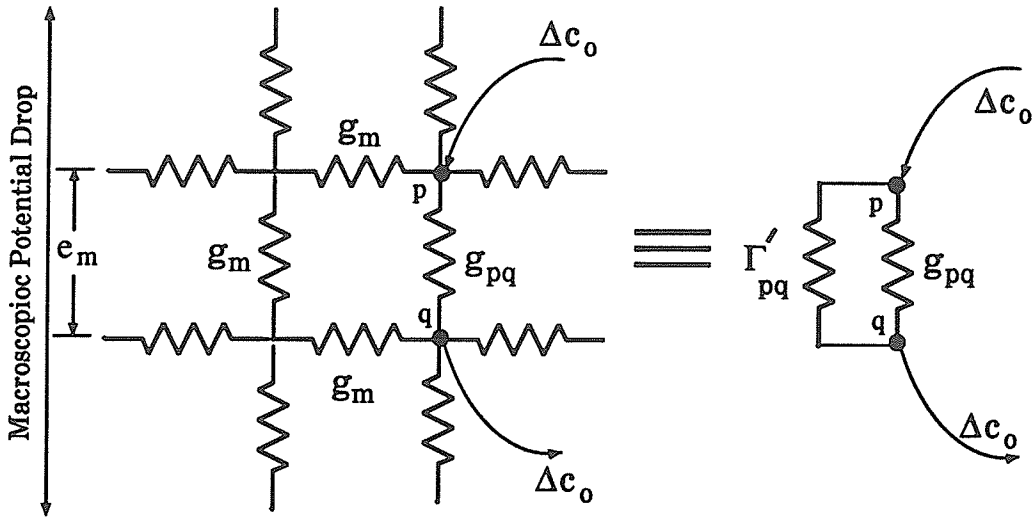

Fig. F.1. Determining EMT conductance (from Kirkpatrick, 1973).

potential drop per row in the direction of the macroscopic potential drop. If, in the effective-medium network, one conductor is reverted back to its original value, g_{pq}, then the potential drop across pq will be different from e_m. A fictitious current, Δc_o may be introduced at p and extracted at q such that the potential drop across pq reverts back to e_m. In that case

$$\Delta c_o = (g_m - g_{pq})\, e_m \ . \tag{F.1}$$

The current Δc_o produces an additional voltage

$$\Delta e_{pq} = \frac{\Delta c_o}{g_{pq} + \Gamma'_{pq}} \ , \tag{F.2}$$

where Γ'_{pq} is the conductance of the rest of the network between junctions p and q. For the effective-medium network, the total conductance, Γ'_{pq}, between the junctions p and q is

$$\Gamma_{pq} = \Gamma'_{pq} + g_m \ . \tag{F.3}$$

Γ_{pq} can be calculated from the definition: if current c_o enters junction p and leaves junction q producing a potential difference of e_{pq}, then $\Gamma_{pq} = c_o/e_{pq}$. However, this

situation is the linear superposition of the current c_o entering junction p and leaking out at infinity, and the current c_o leaking in at infinity and exiting at junction q. In the former case, current c_o/η is present in all resistors leading out of p, including pq, so $e_{pq} = c_o/\eta\, g_m$. In the latter case, the same current and the same voltage drop occur in pq, so adding we have

$$e_{pq} = \frac{1}{g_m}\,\frac{2\,c_o}{\eta}\,. \tag{F.4}$$

Therefore

$$\Gamma_{pq} = \frac{\eta}{2}\,g_m\,, \tag{F.5}$$

and from Equation (F.3),

$$\Gamma'_{pq} = (\frac{\eta}{2} - 1)\,g_m\,. \tag{F.6}$$

If Equations (F.1) and (F.6) are used in (F.2), then

$$\Delta e_{pq} = e_m\,\frac{g_m - g_{pq}}{g_{pq} + (\eta/2 - 1)\,g_m}\,. \tag{F.7}$$

The value of g_{pq} and hence of Δe_{pq} is a random variable, and it is required that the average of Δe_{pq} with respect to the probability density function $\omega(g_{pq})$ be zero:

$$\int_{g_a}^{g_b} \frac{(g_m - g)\;\omega(g)\,\mathrm{d}g}{g + (\eta/2 - 1)\;g_m} = 0. \tag{F.8}$$

The effective-medium conductance is chosen such that Equation (F.8) is satisfied.

F.2 Nicholson's Solution to EMA

Nicholson et al. (1988) presented a solution to EMA, given in Equation (F.8), using a renormalization group method. This resulted in an explicit relation between the overall conductance, G_n, of the network and the statistical parameters charac-

terizing g. In this section, these development are reproduced. Nomenclature consistent with the present work is employed.

The assumptions regarding the construction of the network and flow (fluid or electric) inside the elementary tubes (conductors of fluid or electricity) are the same as presented in Section 5.1.1. The elementary conductance may be written as

$$g = \frac{B\,\delta^{\epsilon}}{S}\,, \tag{F.9}$$

where δ and S are the diameter and the length of the elementary tube, respectively; B and ϵ are constants which depend on the tube shape and flow considered. For example, B is equal to $\pi/128\mu$ for the Hagen-Poiseuille flow and $\pi/4R_{\mathrm{w}}$ for electric flow in a cylindrical tube of constant cross-sectional area, where μ is the viscosity of the flowing fluid and R_{w} is the resistivity of electric conductor saturating the tube; $\epsilon = 2, 3, 4$ for diffusion and electric flow, dilute gas flow (Knudson), and Hagen-Poiseuille flow, respectively. The corresponding values of ϵ for slit-shaped tubes are $1, 2$, and 3, respectively. δ is assumed to be distributed randomly according to the probability density function $\varepsilon(\delta)$ and S is assigned a fixed value. Therefore,

$$g = \overline{B}\,\delta^{\epsilon}\,, \tag{F.10}$$

where $\overline{B} = B/S$. $\omega(g)$ is completely determined by $\varepsilon(\delta)$.

The following reduced random variable may be introduced in order to facilitate the characterization of the shape and breadth of $\varepsilon(\delta)$ by the first few moments about the mean, μ_{δ}:

$$\kappa = \frac{\delta}{\mu_{\delta}} - 1\,, \tag{F.11}$$

which varies between $\kappa_a = \delta_a/\mu_{\delta} - 1$ and $\kappa_b = \delta_b/\mu_{\delta} - 1$, and another variable $\zeta_a \leq \zeta \leq \zeta_b$ given by

$$\zeta = \left(\frac{\delta}{\mu_{\delta}}\right)^{\epsilon} - 1 = (1+\kappa)^{\epsilon} - 1\,. \tag{F.12}$$

The corresponding probability density functions are denoted by $\tilde{\varepsilon}(\kappa)$ and $\hat{\varepsilon}(\zeta)$, respectively, and the related moments are given by

$$\kappa_n = \langle \kappa^n \rangle^{\mathrm{EN}} = \int_{\kappa_a}^{\kappa_b} \kappa^n \, \tilde{\varepsilon}(\kappa) \, \mathrm{d}\kappa \,, \tag{F.13}$$

$$\zeta_n = \langle \zeta^n \rangle^{\mathrm{EN}} = \int_{\zeta_a}^{\zeta_b} \zeta^n \, \hat{\varepsilon}(\zeta) \, \mathrm{d}\zeta \,. \tag{F.14}$$

Equations (F.11) through (F.14) give the following expression for ζ_n:

$$\zeta_n = (-1)^n \sum_{i=1}^{n} (-1)^i \, {}_i^n C \sum_{j=1}^{i\epsilon} {}_j^{i\epsilon} C \;\; \kappa_j \,, \tag{F.15}$$

where ${}_i^n C$ and ${}_j^{i\epsilon} C$ are the binomial coefficients. The effective-medium conductance and reciprocal connectivity factor are normalized as

$$\overline{g}_m = \frac{g_m}{\overline{B} \mu_\delta^\epsilon} - 1 \,, \tag{F.16}$$

$$\Lambda = \frac{2}{\eta} \qquad (0 \leq \Lambda \leq 1) \,. \tag{F.17}$$

With the help of Equations (F.10), (F.12), (F.16) and (F.17), Equation (F.8) transforms into

$$\int_{\zeta_a}^{\zeta_b} \frac{\Lambda(\overline{g}_m - \zeta) \, \hat{\varepsilon}(\zeta) \, \mathrm{d}\zeta}{1 + \Lambda\zeta + (1 - \Lambda)\overline{g}_m} = 0. \tag{F.18}$$

If $\overline{g}_m$ is assumed to be small with respect to 1 (see Equation (F.16)), then the denominator of the integrand in Equation (F.18) may be expanded and the term-by-term integration yields

$$K_o(\Lambda, \zeta_n) + K_1(\Lambda, \zeta_n) \, \overline{g}_m + K_2(\Lambda, \zeta_n) \, \overline{g}_m^2 + \ldots = 0 \,, \tag{F.19}$$

where

$$K_o = \sum_{n=1}^{\infty} (-1)^n \, \Lambda^{n-1} \, \zeta_n \,, \tag{F.20}$$

$$K_1 = \sum_{n=1}^{\infty}(-1)^{n+1}\, n\, \Lambda^{n-1}\, (\zeta_{n-1} + \zeta_n)\ , \tag{F.21}$$

$$K_2 = \sum_{n=1}^{\infty}(-1)^{n}\, n(n+1)\, \Lambda^{n-1}\, (\zeta_{n-1} + \zeta_n)\, /2\ , \tag{F.22}$$

$$K_3 = \sum_{n=1}^{\infty}(-1)^{n+1}\, n(n+1)(n+2)\ \Lambda^{n-1}\, (\zeta_{n-1} + \zeta_n)\, /6\ . \tag{F.23}$$

Here, the binomial coefficients have been written explicitly. Equation (F.19) in combination with Equations (F.20) through (F.23), gives an explicit solution for $\overline{g}_m$, in the form of an infinite series in ascending moments of ζ_n and powers of Λ:

$$\begin{aligned}\overline{g}_m(\Lambda, \zeta_n) \;=\; & -K_o\, K_1^{-1} - (1-\Lambda)\, K_0^2\, K_1^{-3}\, K_2 \\ & -(1-\Lambda)^2\, K_0^3\, K_1^{-5}\, (2\, K_2^2 - K_1\, K_3)\ .\end{aligned} \tag{F.24}$$

The limiting cases of $\Lambda = 0$ and $\Lambda = 1$ correspond to parallel and serial capillary models, respectively (Koplik, 1981). The corresponding solutions for these cases are

$$\overline{g}_m(\Lambda = 0) = \zeta_1\ , \tag{F.25}$$

$$\overline{g}_m(\Lambda = 1) = \sum_{n=1}^{\infty}(-1)^{n}\, \zeta_n \Big/ \sum_{n=1}^{\infty}(-1)^{n+1}\, n\, (\zeta_{n-1} + \zeta_n)\ . \tag{F.26}$$

From Equations (F.16), (F.25) and (F.26),

$$g_m(\Lambda = 0) \equiv g_p\ , \tag{F.27}$$

$$g_m(\Lambda = 1) \equiv g_s\ , \tag{F.28}$$

where g_p and g_s are the effective-medium conductances of the parallel and serial capillary models, respectively. From Equations (F.16) and (F.27)

$$g_p = (1 + \overline{g}_p)\overline{B}\, \mu_\delta^\epsilon\ , \tag{F.29}$$

and from Equation (F.16)

$$g_m(\Lambda, \zeta_n) = [1 + \overline{g}_m(\Lambda, \zeta_n)]\, \overline{B}\, \mu_\delta^\epsilon\ . \tag{F.30}$$

The normalized $g_m(\Lambda, \zeta_n)$ with respect to g_p may be obtained from

$$\gamma_m(\Lambda, \zeta_n) = g_m(\Lambda, \zeta_n)/g_p = [1 + \overline{g}_m(\Lambda, \zeta_n)]\,/(1 + \zeta_1)\,. \tag{F.31}$$

The expression for $\gamma(\Lambda, \zeta_n)$ can be obtained by substitution of Equations (F.20) through (F.24) into Equation (F.31) and is (up to sixth order terms):

$$\begin{aligned}
\gamma_m(\Lambda, \zeta_n) = 1 &- \Lambda\,\zeta_2 + \Lambda^2\,\zeta_3 - \Lambda^3\,\zeta_4 + \Lambda^4\,\zeta_5 - \Lambda^5\,\zeta_6 \\
&+ \Lambda\,\zeta_1^2 + (2\,\Lambda - 3\,\Lambda^2)\,\zeta_1\,\zeta_2 + (4\,\Lambda^3 - 3\,\Lambda^2)\,\zeta_1\,\zeta_3 \\
&+ (4\,\Lambda^3 - 5\,\Lambda^4)\,\zeta_1\,\zeta_4 + (2\,\Lambda^3 - \Lambda^2)\,\zeta_2^2 \\
&+ (3\,\Lambda^3 - 5\,\Lambda^4)\,\zeta_2\,\zeta_3 + (6\,\Lambda^5 - 4\,\Lambda^4)\,\zeta_2\,\zeta_4 \\
&+ (3\,\Lambda^5 - 2\,\Lambda^4)\zeta_3^2 + (2\,\Lambda^2 + 2\Lambda)\,\zeta_1^3 \\
&+ (8\,\Lambda^4 - 7\,\Lambda^5 - 2\,\Lambda^3)\,\zeta_2^3 \\
&+ (13\,\Lambda^2 - 10\,\Lambda^3 - 3\,\Lambda)\,\zeta_1^2\,\zeta_2 \\
&+ (15\,\Lambda^4 - 17\,\Lambda^3 + 4\,\Lambda^2)\,\zeta_1\,\zeta_2^2 + \cdots\,.
\end{aligned} \tag{F.32}$$

The values of $\zeta_n (n = 1,6)$ in terms of $\kappa_n (n = 1,6)$ for various values of ϵ can be calculated from Equation (F.15). The expressions (containing terms up to sixth order) for $\epsilon = 1,4$ are summarized below. As mentioned in the beginning of this section, different values of ϵ correspond to different kinds of flows in the network.

(a) Values of ζ_n in terms of κ_n $(n = 1,6)$ for $\epsilon = 1$

$$\kappa \equiv \zeta\,. \tag{F.33}$$

(b) Values of ζ_n in terms of κ_n $(n = 1,6)$ for $\epsilon = 2$

$$\begin{aligned}
\zeta_1 &= 2\,\kappa_1 + \kappa_2 \\
\zeta_2 &= 4\,\kappa_2 + 4\,\kappa_3 + \kappa_4 \\
\zeta_3 &= 8\,\kappa_3 + 12\,\kappa_4 + 6\,\kappa_5 + \kappa_6 \\
\zeta_4 &= 16\,\kappa_4 + 32\,\kappa_5 + 24\,\kappa_6
\end{aligned}$$

$$\zeta_5 = 32\,\kappa_5 + 80\,\kappa_6$$

$$\zeta_6 = 64\,\kappa_6 \tag{F.34}$$

(c) Values of ζ_n in terms of $\kappa_n\,(n = 1, 6)$ for $\epsilon = 3$

$$\zeta_1 = 3\,\kappa_1 + 3\,\kappa_2 + \kappa_3$$

$$\zeta_2 = 9\,\kappa_2 + 18\,\kappa_3 + 15\kappa_4 + 6\,\kappa_5 + \kappa_6$$

$$\zeta_3 = 273\,\kappa_3 + 81\,\kappa_4 + 108\,\kappa_5 + 81\,\kappa_6$$

$$\zeta_4 = 81\,\kappa_4 + 324\,\kappa_5 + 594\,\kappa_6$$

$$\zeta_5 = 243\,\kappa_5 + 1215\,\kappa_6$$

$$\zeta_6 = 729\,\kappa_6 \tag{F.35}$$

(d) Values of ζ_n in terms of $\kappa_n\,(n = 1, 6)$ for $\epsilon = 4$

$$\zeta_1 = 2\,\kappa_1 + 6\,\kappa_2 + 4\,\kappa_3 + \kappa_4$$

$$\zeta_2 = 16\,\kappa_2 + 48\,\kappa_3 + 64\,\kappa_4 + 56\kappa_5 + 28\,\kappa_6$$

$$\zeta_3 = 64\,\kappa_3 + 288\,\kappa_4 + 624\,\kappa_5 + 840\,\kappa_6$$

$$\zeta_4 = 256\,\kappa_4 + 1536\,\kappa_5 + 4480\,\kappa_6$$

$$\zeta_5 = 1024\,\kappa_5 + 7680\,\kappa_6$$

$$\zeta_6 = 4096\,\kappa_6 \tag{F.36}$$

Values of $\kappa_n, (n = 1, 6)$ for lognormal distribution

It may be noted here that $\kappa_1 = 0$ irrespective of the probability distribution chosen for the element conductances of the network. If μ_δ and σ_δ^2 represent the mean and the variance of the employed lognormal distribution for tube diameters (tube lengths are fixed), and $a_\delta = \sigma_\delta/\mu_\delta$, then other moments are (Aitchison and Brown, 1969):

$$\kappa_2 = a_\delta^2$$

$$\kappa_3 = a_\delta^6 + 3\,a_\delta^4$$

$$\kappa_4 = a_\delta^{12} + 6\,a_\delta^{10} + 15\,a_\delta^8 + 16\,a_\delta^6 + 3\,a_\delta^4$$

$$\kappa_5 = a_\delta^{20} + 10\,a_\delta^{18} + 45\,a_\delta^{16} + 120\,a_\delta^{14} + 205\,a_\delta^{12} + 222\,a_\delta^{10} + 135\,a_\delta^8 + 30\,a_\delta^6$$

$$\begin{aligned}\kappa_6 = a_\delta^{30} &+ 15\,a_\delta^{28} + 105\,a_\delta^{26} + 445\,a_\delta^{24} + 1365\,a_\delta^{22} + 2997\,a_\delta^{20} + 4945\,a_\delta^{18} \\ &+ 6165\,a_\delta^{16} + 5715\,a_\delta^{14} + 3760\,a_\delta^{12} + 1581\,a_\delta^{10} + 330\,a_\delta^8 \\ &+ 15\,a_\delta^6 \end{aligned} \tag{F.37}$$

F.3 Relations of Network Permeability and Formation Factor to Effective-Medium Conductances

In this section, the relations of network permeability and formation factor to the corresponding effective-medium conductances (fluid and electric flow) are developed. For fluid flow, the overall network conductance is

$$G_n = \frac{Q_1}{p_h - p_l}\,, \tag{F.38}$$

where Q_1 is the bulk flow rate in the macroscopic flow direction, and p_h and p_l are the pressures at the upstream and downstream sides of the network (see Appendix B). Q_1 may be written in terms of the permeability as

$$Q_1 = \frac{k_1^n\,A_1}{\mu\,L_1}\,(p_h - p_l)\,, \tag{F.39}$$

where k_1^n denotes the permeability of the network, A_1 is the bulk area normal to and L_1 is the bulk length parallel to the macroscopic flow direction, $k = 1$, and μ is the viscosity of the flowing fluid. From Equations (F.38) and (F.39), we get

$$G_n = \frac{k_1^n\,A_1}{\mu\,L_1}\,. \tag{F.40}$$

Similarly for an equivalent parallel capillary model

$$G_p = \frac{k_1^p\,A_1}{\mu\,L_1}\,. \tag{F.41}$$

The equivalent parallel capillary model is one with the same external dimensions and distribution of elementary conductances as the network model, with a coordination number of ∞. If g_n and g_p represent the effective-medium conductances of the network and the equivalent parallel capillary models, respectively, then

$$G_n \propto g_n \tag{F.42}$$

and

$$G_p \propto g_p \ , \tag{F.43}$$

Because the elementary conductors of an effective-medium network are identical, the conductors in directions other than the macroscopic flow direction, do not contribute to the overall conductance of the network in the macroscopic flow direction. Therefore, the factors of proportionality in Equations (F.42) and (F.43) are identical. Substitutions of Equations (F.40) and (F.41) into Equations (F.42) and (F.43), respectively, leads to

$$g_n \propto \frac{k_1^n \, A_1}{\mu \, L_1} \ , \tag{F.44}$$

$$g_p \propto \frac{k_1^p \, A_1}{\mu \, L_1} \ . \tag{F.45}$$

With the help of Equations (F.44) and (F.45), Equation (F.31) becomes

$$\gamma_n(\epsilon = 4) = \frac{g_n(\epsilon = 4)}{g_p(\epsilon = 4)} = \frac{k_1^n}{k_1^p} \ . \tag{F.46}$$

The relations of k_1^p and k_1^n to the statistical parameters of the models are given in Equations (5.24) and (5.95), respectively. It may be noted here that the value of a_S is zero in Equation (5.24) because tubes with fixed length are employed. A comparison of the normalized effective-medium conductances predicted by Equations (F.32) (with $\epsilon = 4$) and (F.46) is presented in Section 5.3.2. In this comparison, k_1^p and k_1^n are

found from the relations developed in the present study (Equations (5.24) and (5.95), respectively)

The relation between the formation factors of the network model and the equivalent parallel capillary model, and the corresponding normalized effective-medium conductance of the network may be found similarly. Here, only the final result is presented:

$$\gamma_n(\epsilon = 2) = \frac{g_n(\epsilon = 2)}{g_p(\epsilon = 2)} = \frac{F^p}{F^n} \,. \tag{F.47}$$

where F^p and F^n denote the formation factors of the parallel capillary model and network model, respectively. The relations of F^p and F^n to the statistical parameters of the models are given in Equations (5.27) and (5.96), respectively. Again, a_δ is zero in Equation (5.27). A comparison of the normalized effective-medium conductances predicted by Equations (F.32) (with $\epsilon = 2$) and (F.47) is presented in Section 5.3.2. In this comparison, F^p and F^n are found from the relations developed in the present study (Equations (5.27) and (5.96), respectively)